Understanding the role of metabolic perturbation in disease condition through mathematical modelling

Thesis submitted to Jadavpur University
for the award of the degree of
Doctor of Philosophy

Submitted by
Abhijit Paul

Under the supervision of
Dr. Samrat Chatterjee

Translational Health Science and Technology Institute
Faridabad – Gurugram Expressway, Faridabad
Haryana-121001, India
January 2023

Declaration

I, Abhijit Paul, solemnly declare that this thesis represents my own work which has been done after registration for the degree of PhD at Jadavpur University and has not been previously included in any thesis or dissertation for the purpose of earning a degree, diploma, or any other credential.

Abhijit Paul
17/01/2023

Abhijit Paul

iii

thsti
ट्रांसलेशनल स्वास्थ्य विज्ञान
एवं प्रौद्योगिकी संस्थान
TRANSLATIONAL HEALTH SCIENCE
AND TECHNOLOGY INSTITUTE
An autonomous institute of the Deptt. of Biotechnology, Ministry of Science & Technology, Govt. of India

NCR Biotech Science Cluster
3rd Milestone, Faridabad-Gurgaon Expressway,
P O Box No. 04, Faridabad-121001
Haryana, India

CERTIFICATE FROM THE SUPERVISOR

This is to certify that the thesis entitled "**Understanding the role of metabolic perturbation in disease condition through mathematical modelling**" submitted by **Sri Abhijit Paul**, who got his name registered (**Ref. No.: D-7/SC/31/2018** and **Index No.: 73/18/Maths./25**) on 20/02/2018 for the award of Ph. D. (Science) Degree of Jadavpur University, is absolutely based upon his own work under the supervision of myself, and that neither this thesis nor any part of it has been submitted for either any degree / diploma or any other academic award anywhere before.

17/1/2023

Dr. Samrat Chatterjee

(Signature of the Supervisor date with official seal)

डॉ. सम्राट चटर्जी / Dr. Samrat Chatterjee
सह-आचार्य / Associate Professor
ट्रांसलेशनल स्वास्थ्य विज्ञान एवं प्रौद्योगिकी संस्थान
(भारत सरकार के जैव प्रौद्योगिकी विभाग का एक स्वायत संस्थान)
एनसीआर बायोटेक विज्ञान क्लस्टर, फरीदाबाद -१२१००१ हरियाणा, भारत
Translational Health Science and Technology Institute
(An Autonomous Institute of the Dept. of Biotechnology, Govt. of India)
NCR Biotech Science Cluster, Faridabad -121001 Haryana, India

Phone: +91-129-2876300, Fax: +91-129-2876402, Email: info@thsti.res.in, Website: www.thsti.res.in

Dedicated to my parents

and

teachers

Acknowledgement

Writing my PhD thesis is a heart-touching experience, getting close to achieving one of my big goals. The satisfaction of fulfilling a goal would always be incomplete without expressing my gratitude to everyone who encouraged, inspired, supported and helped me unconditionally throughout my journey.

First and foremost, I would like to express my sincere gratitude to my guide and advisor, Dr. Samrat Chatterjee, for continuous guidance, support and motivation throughout my PhD journey. From him, I have learnt how to multi-task and, at the same time, how to balance between personal life and professional life. After joining this lab, l always learnt something new from him. When I faced any problem in my PhD work, he always gave me suggestions and tricks to solve the problem. His guidance and advice make me passionate towards research. He also taught me how to present research work in front of an audience to make them attentive. When I felt depressed or demotivated, he encouraged me every time. His friendly nature, professional maturity and strong faith in his students are really appreciable. I am very fortunate to have him as my research supervisor.

I would like to thank my Research Advisory Committee (RAC) members, Prof. Nandadulal Bairagi and Dr. Bhabatosh Das, for their valuable feedback and suggestions during my doctoral research. I am very fortunate to have Prof. Nandadulal Bairagi sir, as my RAC member. In my college life, he inspired me to higher study and encouraged me to choose this field. His expertise and vast knowledge helps me to build and analyze mathematical models. Also, his valuable suggestions and ideas increase the quality of my research. His presence and guidance

have made me a successful researcher. I am grateful to two of my seniors and advisor, Dr. Rajat Anand and Dr. Phonindra Nath Das. They helped me to start my PhD journey and showed me the path by which I would become a successful PhD scholar. They taught me many new algorithms and codes. When I did not understand any concept clearly, they explained it to me easily. We also had a good time watching movies and having food at restaurants. I am also thankful to my collaborators Prof. Salman Azhar, Sonali Porey Karmakar and Surender Rawat, for all their support. Special thanks to Prof. Salman Azhar, Stanford University School of Medicine, for giving valuable suggestion in one of my research work and increasing the quality of the manuscript.

I am thankful to Jadavpur University for allowing me to pursue a PhD degree. I want to express my sincerest gratitude towards the Translational Health Science and Technology Institute (THSTI) for giving me an opportunity to provide the infrastructure for carrying out my research. Working in the warm and friendly environment of the Complex Analysis Group, THSTI, is a delightful experience for me. I am also grateful to the University Grants Commission (UGC), India, for providing fellowship during my PhD.

Working with my lab mates has been enjoyable for me. I felt very lucky to have such friendly labmates during my PhD days. Firstly, I want to take the name Dipanka: senior and previous roommate. We had spent a lot of good times together and crossed the toughest period of the PhD. He helped me a lot in my PhD work, developing presentation and writing skills. I am also thankful to have my other labmates Shivam, Krishna, Jay, Dev, Suvankar, Poulami and Mimansa. I learned many things from them during my PhD journey. They made my long journey more memorable. I also want to name some friends like senior Mitul, Mrituyunjay, Lovika and Anita. Thank you for the support and advice that they have given me throughout my PhD journey. We spend a lot of time together cooking, funning, and enjoying parties. From the juniors, I want to mention some persons, Shivam, Krishna, Jay, Dev and Debapriyo, for keeping such a dynamic and friendly lab environment. I have been attached to Shivam since the beginning of my PhD journey. He was always available to offer helpful advice or resolve problems whenever I encountered coding or technical issues. His helping nature is remarkable and undoubtedly unforgettable. I am grateful to Krishna for helping me and being part of my

PhD journey. Every day in my lab started with his cheerful face. I am also very fortunate to have juniors like Jay, dev and Debapriyo. Since joining the lab, they have become part of my life for their pleasant nature. They have maintained the lab's vividness, and it will be in my sweet memories whatever funny incidents they have created in the lab, hostel and at parties. I took a lot of help from them and learnt many things. I am very thankful to all of my labmate for making my PhD life sweet and memorable. I am thankful to Abhijit and Chitta from the Jadavpur University Mathematics Department for their constant help and support regarding the PhD admission and coursework.

My childhood friend also played a vital role in various aspects of my life. Especially, I want to mention Rahul (Swadaghar) and Rahul (Mahanta), who became my extended family member. I do not have enough words to express gratitude towards them. There were a lot of students in the primary class, but I don't know how we became best friends. We, the trio, explored many things from childhood, roomed in many places, and were made a lot of fun. My eyes always look for you, buddies, whenever I go to hometown. I missed you here !!! They have made a lot of contributions to me. From childhood, when I had felt hesitant, depressed and weak, they encouraged me every time. When I fell in danger, they extended their hand to rescue me. We have shared our sorrow and joyful moments. Even in the absence of my brother and me, Rahul (Swadager) helped my family every time. More than that, he is more excited about my PhD degree. Other friends I want to mention are Baidyanath, Suman, Munna, and Chandan. I am also thankful to my college and University friends Moni and Manoj for their tremendous support and contribution during my college life.

I want to mention one of my friends Sushanta. We became good friends within some day. Both of us are food lovers (mainly Bengali food). I learnt many recipes from him. From far away from home, he made me feel at home with his cooking. In addition to cooking, he addressed a lot of my doubts. Even when I faced any problem in my PhD work, he gave suggestions for solving the problem. I would like to express my thanks to my roommate Linus. We shared a lot of sad and happy moments with each other. We also spent quality time watching movies, which sometimes helped to relieve our frustration.

I would like to express my heartiest gratitude to my dearest friend, love, and my better half, Antara. Your presence makes me kind, caring, happy and complete. You entered my life when I was rudderless and upheld my hand to walk in a particular direction. You always encouraged me to pursue higher education and supported me mentally during my ups and downs. Your kind and lovely character have helped me to relieve frustration during my PhD. Your smile makes me feel less anxious during all the stressful circumstances. Without you, this journey would have been very cumbersome to pursue.

I would like to express my sincere gratitude to all of the teachers at my school, college, University and others for inspiring me from my childhood and laying the foundation of my education. Some notable names are Sujit sir, Shanti sir, Manik sir, Debkumar sir, Laltu sir, Tarachand sir, Kajal sir, Rajib sir, Suprakash sir, Paresh sir, Aloke sir, Gunodhar sir, Parbir sir and many more. I am very much grateful to Shanti sir, Manik sir and Debkumar sir, who taught me and inspired me to learn mathematics. They helped me choose the correct route for my journey as well. I do not have enough words to express gratitude towards Sujit sir. His unconditional support, faith and guidance made my journey smooth. They (sir and Jethima) held my hand when I most needed help in the early years of my life. I am very much fortunate to have their love, affection and guidance. I am also grateful to my childhood teacher and guides Bhabani kaku, Kajal kaku Partha kaku and Koshik kaku. Without their encouragement, guidance and support, l could not achieve my goal. They always insisted on the higher study and helped me immensely in various aspects of life. Even in the absence of my brother and me, they helped my family every time. I am very thankful to Titu mama for supporting me in college life and giving valuable suggestions and inspiration in higher study. I will forever be indebted to my teachers for helping me make my dream successful.

This PhD thesis is an outcome of my parents' countless efforts, sacrifices and relentless struggle. You are my strength and source of my energy. You always encourage me to reach my goal. Your hard work, care, faith, love and sacrifice for us (me & my brother) are not comparable to anything in the world. No words in the world can explain your contribution to my life. This whole PhD journey is not only mine. I know you both are always there at every step of my journey. Having their sons a few thousand miles away from home was not an easy

affair for them. They missed my physical presence every moment of the past few years and kept inspiring me despite all my shortfalls in carrying out my responsibilities towards them. I am blessed to get you as ma & baba in all aspects of my life. Your unlimited kindness, pure emotions, and respect for others have made me the person I am. No words can express my gratitude to my beloved brother Surajit for his unconditional support and love. He stood by my side whenever I needed him. In my absence, he took care of my parents very carefully. For this reason, I was able to focus freely on my work. I am also thankful to my sisters Koyel and Payel for taking care of my parents in the absence of my brother and me. Kaku, Kakima, Koyel and Payel support me throughout my entire journey. Without their support, I was not able to work freely. I am also thankful to my extended family members: Mama, Mami, Dadu, Dida, Smriti, and Govinda, for their unconditional love, support and care. I am also thankful to Didi, Dada, Mashi, Sukla, Asha, Biltu and Jhunu mama for their faith, love, affection and support and also making my journey beautiful. I am also grateful to Pompi pisi, Bhola, Koshik kaku, Kakima, Dadu, Dida and Bappa kaku for their unconditional support, love and affection.

Above all, I thank Lord Shiva for giving me strength, blessing me and helping me throughout my journey. You have assisted me in overcoming all the obstacles that came to my journey.

This list can only acknowledge a tiny fraction of the people who directly and indirectly supported me and believed in me. I want to express my sincere gratitude to everyone from the bottom of my heart. Without their support, I would not reach here.

Abhijit Paul

Abstract

Understanding metabolism is crucial for comprehending the phenotypic nature of all living things, including humans. Metabolism is essential for life and good health, any dysregulation in metabolic processes can be detrimental and involved in various diseases, including cancers, diabetes, cardiovascular diseases, etc. Therefore, exploring metabolic alterations is essential to comprehend the underlying mechanism behind disease development. Additionally, it offers a unique opportunity to identify potential drug targets and design new therapeutic strategies. Due to the complexity and high dimensionality, mathematical modelling-based approaches have been used to study metabolic perturbations in various conditions like human diseases. Although numerous mathematical modelling-based studies have been performed, there still exists a lacuna of metabolic perturbations in several diseases such as diabetes, cancer, nonalcoholic fatty liver disease, etc. The present thesis aims to explore metabolic perturbations in disease to understand the underlying mechanism and develop therapeutic strategies.

Here, we explored the application of genome-scale metabolic models (GSMM) and small-scale kinetic models in studying the role of metabolites and associated pathways in disease progression. We start by applying GSMM to identify the altered metabolic flux state of pancreatic β-cells under type 2 diabetes (T2D). We identified seven secreted metabolites from β-cell associated with cardiovascular disease (CVD) pathogenesis. Additionally, GSMMs were applied to identify critical regulatory points through *in silico* knockout approaches. In total, 13 genes were obtained whose knockout reduced the growth rate of all cancer models but were inactive across all nine normal cell models. We later validated two of these genes (SOAT1 and

CYTB) experimentally on four cancer cell-lines. Finally, the combination of these two applications of GSMM, i.e., identifying metabolic alterations and regulatory points through *in silico* gene knockout, was used to identify potential targets for nonalcoholic steatohepatitis (NASH). We elucidated the possible mechanism of action of these identified targets using GSMM. Our analysis identified three potential targets for NASH. Their inhibition attenuate hepatic steatosis by promoting higher flux rates for the altered reactions involved in fatty acid activation and mitochondrial beta-oxidation pathways.

The current thesis is not limited to the application of GSMM. We have also used small-scale kinetic models to capture the underlying disease mechanism. We have proposed and analyzed a six-dimensional model on glucose-stimulated insulin secretion (GSIS) to identify the crucial factors whose impairment can either lead to hyperglycemia or hypoglycemia. Our analysis uncovers the potential therapeutic strategies for preventing the progression of T2D during these alterations. We have also proposed another seven-dimensional model for insulin synthesis and secretion to understand the pathophysiology of T2D and hyperinsulinemic hypoglycaemia. The model analysis revealed that the defects in the insulin granules dynamics hamper first- and second-phase insulin secretion. In contrast, abnormal insulin synthesis takes a long time to exert the effect and might also be one of the reasons for fasting hypoglycemia in insulinoma patients. Our study also suggests that targeting insulin synthesis could become a potential therapeutic strategy for controlling impaired insulin secretion.

Overall, the work discussed in this thesis explores the application of GSMMs and small-scale kinetic models in understanding metabolic perturbations in human disease. The identified crucial factors responsible for impaired metabolism will enrich our understanding of disease pathogenesis. The proposed drug targets or therapeutic strategies have the potential to control the disease progression, and thus opens door for further exploration.

Abbreviations

ACACA gene:- Acetyl-Coenzyme A Carboxylase Alpha gene

ACACB gene:- Acetyl-Coenzyme A Carboxylase Beta gene

ACHR:- Artificial Centering Hit-and-Run

ACOT1 gene:- Acyl-CoA Thioesterase 1 gene

ACOT2 gene:- Acyl-CoA Thioesterase 2 gene

ACOX1 gene:- Acyl-CoA Oxidase 1 gene

ADP:- Adenosine Diphosphate

AHR gene:- Aryl Hydrocarbon Receptor gene

ALDH1A3 gene:- Aldehyde Dehydrogenase 1 Family Member A3 gene

ARNT gene:- Aryl Hydrocarbon Receptor Nuclear Translocator gene

ATP:- Adenosine Triphosphate

BAAT gene:- Bile Acid-CoA: Amino Acid-N-Acyltransferase gene

BAG6 gene:- BCL2 Associated Athanogene 6 gene

BRS:- Biomass Reduction Score

Ca^{2+}:- Calcium Ions

CASP3 gene:- Caspase 3, Apoptosis-Related Cysteine Peptidase gene

CYCS gene:- Cytochrome C gene

CEL gene:- Carboxyl Ester Lipase Gene

CH25H gene:- Cholesterol 25-Hydroxylase gene

CHDH gene:- Choline Dehydrogenase gene

CHRR:- Coordinate Hit-and-Run with Rounding

CLOCK gene:- Clock Circadian Regulator gene

COBRA Toolbox:- Constrained Based Reconstruction and Analysis

Cp:- Candidate Proteins

CPA2 gene:- Carboxypeptidase A2 gene

CVD:- Cardiovascular Disease

CYC1 gene:- Ubiquinol-Cytochrome-C Reductase Complex Cytochrome C1 Subunit gene

DEG:- Differentially expressed genes

DEMG:- Differentially Expressed Metabolic Gene

DOM:- Dual Oscillator Model

E2F1 gene:- E2F Transcrption Factor 1 gene

ELE:- Enzymatically Less Efficient

ER:- Endoplasmic Reticulum

ESR1 gene:- Estrogen Receptor 1 gene

$FADH_2$:- Flavin Adenine Dinucleotide

FBA:- Flux Balance Analysis

FCG:- Fractional Cell Growth

FDR:- False Discovery Rate

FFA:- Free Fatty Acid

FOXH1 gene:- Forkhead Box H1 gene

FOXM1 gene:- Forkhead Box M1 gene

FOXO3 gene:- Forkhead Box O3 gene

FVA:- Flux Variability Analysis

G6PD gene:- Glucose-6-phosphate Dehydrogenase gene

GATA3 gene:- GATA Binding Protein 3 gene

GIMME:- Gene Inactivity Moderated by Metabolism and Expression

GK:- Glucokinase

GLP-1:- Glucagon-like Peptide 1

GLUT-2:- Glucose Transporter 2

GPR:- Gene-Protein-Reaction

GSA:- Global Sensitivity Analysis

GSEA:- Gene Set Enrichment Analysis

GSIS:- Glucose-stimulated Insulin Secretion

GSMM:- Genome-scale Metabolic Model

HADH gene:- Hydroxyacyl-CoA Dehydrogenase gene

HNF4A gene:- Hepatocyte Nuclear Factor 4 Alpha gene

ICp:- Indispensable Candidate Protein

IDO2 gene:- Indoleamine 2,3-Dioxygenase 2 gene

IFG:- Impaired Fasting Glucose

IGT:- Impaired Glucose Tolerance

iMAT:- Integrative Metabolic Analysis Tool

INIT:- Intergrative Network Inference for Tissues

IR:- Insulin Resistance

IVGTT:- Intravenous Glucose Tolerance Test

K^+:- Potassium Ions

K_{ATP}:- ATP-sensitive Potassium Channels

LDHA gene:- Lactate Dehydrogenase A gene

LHS:- Latin Hypercube Sampling

LP:- Linear Programming

MBA:- Model-Building Algorithm

mCADRE:- metabolic Context-specificity Assessed by Deterministic Reaction Evaluation

MCG:- Metabolic Candidate Genes

ME:- Module Eigengene

MLE:- Metabolically Less Efficient

MODY-2:- Maturity-onset Diabetes of the Young type 2

MOMA:- Minimization of Metabolic Adjustment

mRNA:- Messenger Ribonucleic Acid

MTA:- Metabolic Transformation Algorithm

MT-CYB gene:- Mitochondrially Encoded Cytochrome B gene

NADH:- Nicotinamide Adenine Dinucleotide Hydride

NAFL:- Nonalcoholic Fatty Liver

NAFLD:- Nonalcoholic Fatty Liver Disease

NASH:- Nonalcoholic Steatohepatitis

NCX:- Sodium/Calcium Exchange

NR1H3 gene:- Nuclear Receptor Subfamily 1 Group H Member 3 gene

ODE:- Ordinary Differential Equation

OGTT:- Oral Glucose Test

pFBA:- Parsimonious Enzyme Usage FBA

PGM2 gene:- Phosphoglucomutase 2 gene

PMCA:- Plasma Membrane Calcium ATPase

PNLIP gene:- Pancreatic Lipase gene

PNLIPRP1 gene:- Triglyceride Lipase Inhibitor gene

PPI:- Protein-Protein Interaction

PRCC:- Partial Ranked Correlation Coefficient

PRODH gene:- Proline Dehydrogenase 1 gene

PRODH2 gene:- Proline Dehydrogenase 2 gene

PRPS1 gene:- Phosphoribosyl Pyrophosphate Synthetase gene

PSAT1 gene:- Phosphoserine Aminotransferase 1 gene

QP:- Quadratic Programming

rER:- Rough Endoplasmic Reticulum

RELA gene:- RELA Pro-Oncogenic, NF-κB Subunit gene

ROOM:- Regulatory On/Off Minimization

ROS:- Reactive Oxygen Species

RyR2:- Ryanodine Receptor 2

SERCA:- Sarco/Endoplasmic Reticulum Calcium ATPase

SGLT2:- Sodium/glucose Cotransporter 2

SGPL1 gene:- Sphingosine-1-Phosphate Lyase 1

SMAD2 gene:- SMAD Family Member 2 gene

SMAD3 gene:- SMAD Family Member 3 gene

SOAT1 :- Sterol O-Acyltransferase (Acyl-Coenzyme A: Cholesterol Acyltransferase) 1

SOX11 gene:- SRY-Box Transcription Factor 11 gene

SPI1 gene:- Spi-1 Proto-Oncogene gene

ST6GALNAC6 gene:- GalNAc α2,6-Sialyltransferase 6 gene

STAG1 (SA1) gene:- Stromal Antigen 1 gene

STAT3 gene:- Signal Transducer And Activator Of Transcription 3 gene

SUR1:- Sulfonylurea Receptor 1

T1D:- Type 1 Diabetes

T2D:- Type 2 Diabetes

TCA cycle:- Tricarboxylic Acid cycle

TCF3 (E2A) gene:- Transcription Factor 3 gene

TF:- Transcription Factor

TP63 gene:- Tumor Protein P63 gene

TPM:- Transcripts Per Kilobase Million

TS:- Transformation Score

UCP2:- Uncoupling Protein 2

UQCR10 gene:- Ubiquinol-Cytochrome C Reductase, Complex III Subunit X gene

UQCR11 gene:- Ubiquinol-Cytochrome C Reductase, Complex III Subunit XI gene

UQCRB gene:- Ubiquinol-Cytochrome C Reductase Binding Protein gene

UQCRC1 gene:- Ubiquinol-Cytochrome C Reductase Core Protein 1 gene

UQCRC2 gene:- Ubiquinol-Cytochrome C Reductase Core Protein 2 gene

UQCRFS1 gene:- Ubiquinol-Cytochrome C Reductase, Rieske Iron-Sulfur gene

UQCRH gene:- Ubiquinol-Cytochrome C Reductase Hinge Protein gene

UQCRQ gene:- Ubiquinol-Cytochrome C Reductase Complex III Subunit VII gene

VDAC:- Voltage-dependent Anion Channels

VGCC:- Voltage-gated Calcium Channels

WGCNA:- Weighted Gene Co-expression Network Analysis

Contents

List of Figures

List of Tables

1

Introduction

1.1 Metabolism

Metabolism is the set of all biochemical reactions that occur within each living cell of an organism [1]. The word “metabolism” originates from the Greek word “metabolē”, meaning “change” or from the French word “métabolisme” [2]. These chemical reactions include the biosynthesis of complex macromolecules such as proteins, lipids, carbohydrates, and nucleic acids (anabolism) and the degradation of these macromolecules into smaller molecules such as carbon dioxide, water, and ammonia with the release of energy in the form of ATP (catabolism). Catabolism can occur either in the presence of oxygen (called aerobic catabolism) or even in the absence of oxygen (called anaerobic catabolism). Although the energy yield is much lower in anaerobic catabolism, it is also crucial for organisms or cells to survive in such environments

that are temporarily or permanently devoid of oxygen. Photosynthesis, a phototrophic energy metabolism, is an essential metabolic process in which plants, algae, and some bacteria acquire light energy to synthesize food. Ultimately, almost all organisms rely on the food produced through photosynthesis for nourishment. There are three major purposes of metabolism: 1) the conversion of food into energy to perform the cellular processes, 2) the conversion of food to building blocks for carbohydrates, proteins, lipids, and nucleic acids, and 3) the elimination of metabolic wastes. These enzyme-catalyzed chemical reactions allow organisms to carry out activities such as growth, movement, development, reproduction and responding to their environments.

1.1.1 Metabolic pathways

Metabolism mainly consists of a series of enzymatic steps, also called metabolic pathways. Metabolic pathways refer to the series of enzyme-catalyzed chemical reactions connected by their intermediates, i.e., the reactants of one reaction are the products of the previous one, and so on (**Fig. 1.1**). Basically, the pathway converts one or more starting molecules into products through a series of intermediates. Each of these chemical reactions in metabolic pathways doesn't take place automatically, instead facilitated by a specific protein called an enzyme. Also, some of these enzymes need dietary vitamins, minerals, and other cofactors to catalyze their corresponding reactions. The reactants, products, and intermediates of the metabolic reactions are called metabolites, which play roles in many cellular functions such as energy conversion, cofactor activity, signalling, and epigenetic regulation [3, 4]. Metabolic pathways are distributed in various compartments of the cell and based on these, their function and significance vary [5]. For instance, the tricarboxylic acid (TCA) cycle, oxidative phosphorylation, and electron transport chain occur in the mitochondria [6]. Whereas glycolysis, fatty acid biosynthesis, and pentose phosphate pathway occur in the cytoplasm [7].

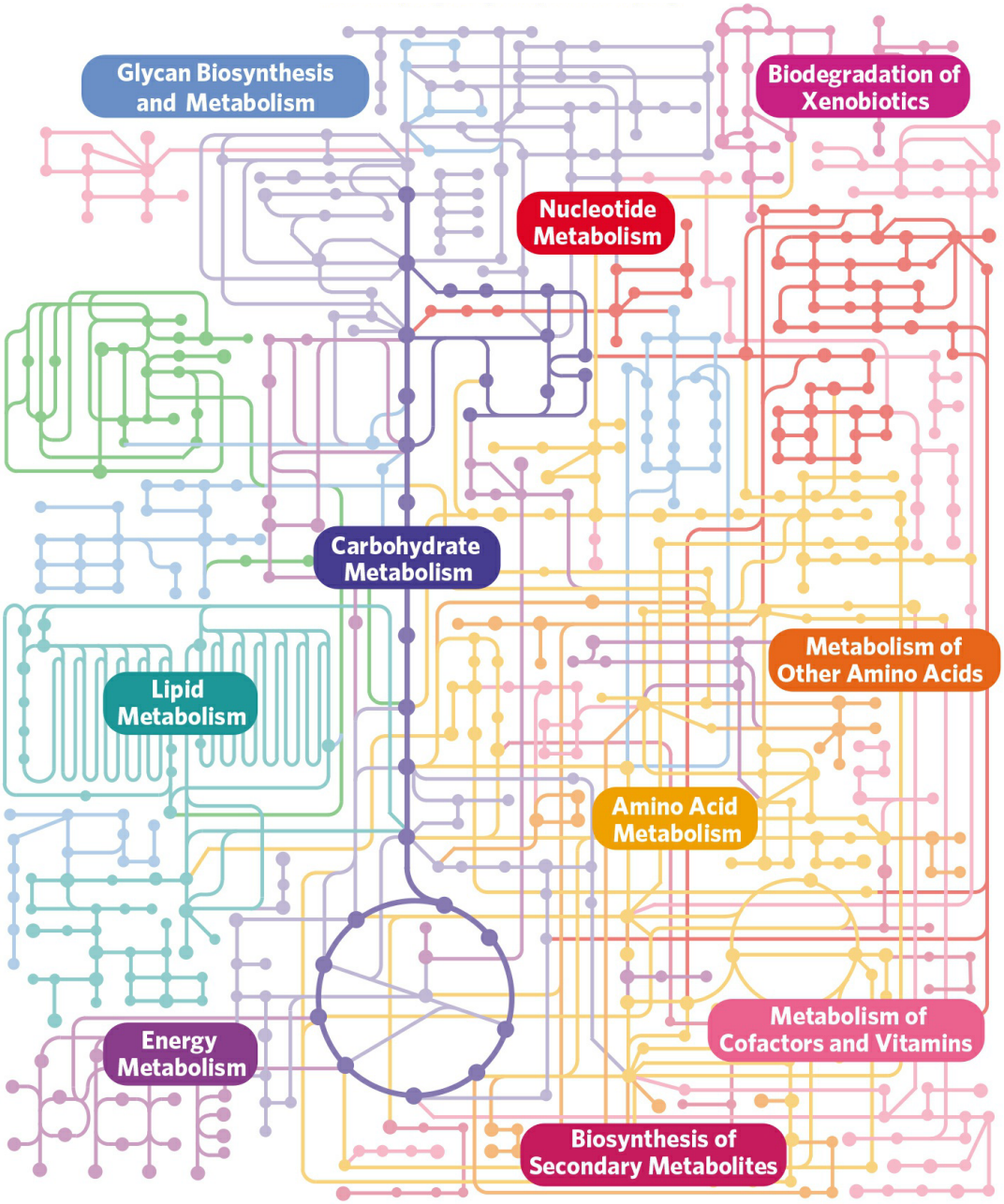

Figure 1.1: **Overview of the metabolic pathways** (Source: KEGG: Kyoto Encyclopedia of Genes and Genomes [8]). Here each dot represents the metabolites and each edges denotes an enzymatic reaction.

Metabolic pathways are broadly divided into two categories: 1) anabolic pathways and 2) catabolic pathways (**Fig. 1.2**). Anabolic pathways construct macromolecules such as carbohydrates, proteins, lipids, and nucleic acids from smaller units and typically need an energy input. Anabolic processes help to make the building blocks of the cells. Photosynthesis, pentose phosphate pathway, gluconeogenesis, glycogenesis, protein biosynthesis are fatty acid synthesis are examples of anabolic pathways. Catabolic pathways involve the breaking down of macro-

molecules and biomolecular polymers into simpler molecules such as carbon dioxide, water, and ammonia and release energy. Catabolic pathways have two major roles: they provide the small biomolecules that are the building blocks for the macromolecules and produce the energy needed to run cellular functions and synthesize the macromolecules. Glycolysis, TCA cycle, glycogenolysis, beta-oxidation of fatty acid, and urea cycle are examples of catabolic pathways.

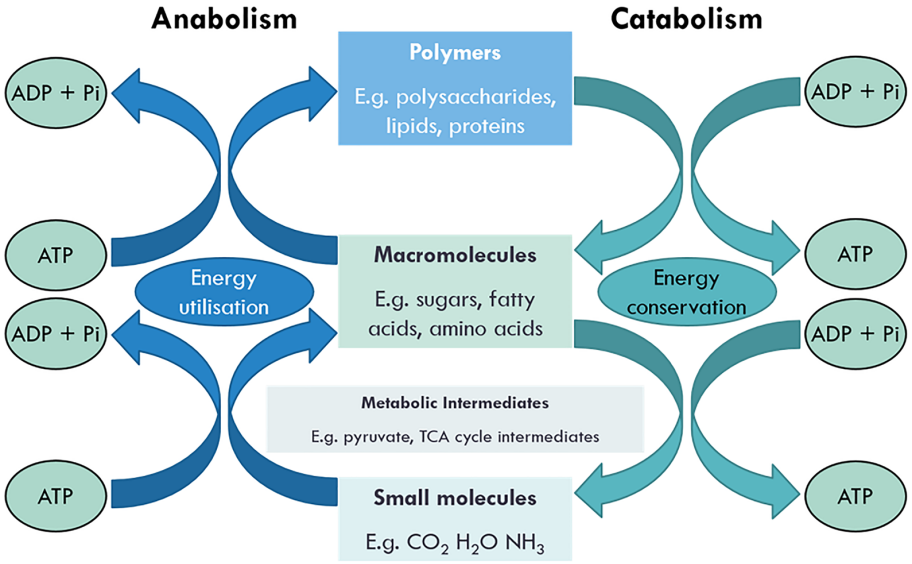

Figure 1.2: **Coupling of anabolic and catabolic pathways in cell metabolism** (Source: Judge, A. et al. *Essays Biochem* (2020) [2]; reprinted with unrestricted use under the license: CC BY-NC-ND 4.0). Catabolic pathways involve in the breakdown of macromolecules and biomolecular polymers into simpler molecules and release energy. Anabolic pathways utilize energy to build new molecules out of the products of catabolism.

1.1.2 History of metabolic research

Metabolism and metabolic pathways have been explored over the course of several centuries and now have progressed from studying whole animals in early studies to investing each reaction in modern biochemistry and molecular biology. Metabolic studies were conducted as early as the thirteenth century by Ibn al-Nafis, who stated that "the body and its parts are in a continuous state of dissolution and nourishment, so they are inevitably undergoing permanent change" in his work titled "Al-Risalah al-Kamiliyyah fil Siera al-Nabawiyyah" [9]. The more sophisticated and documented research started in the closing decades of the sixteenth century. Instrumentation enhanced direct observation by enabling quantification, allowing verification in the sciences, especially of biological systems. The first controlled experiments on humans

were published in 1614 by Santorio Santorio in his book titled "Ars de statica medecina" [10]. His efforts were devoted to understanding metabolic balance studies. In these early studies, the underlying mechanisms of the metabolic processes had not been investigated, and it was thought that a vital force was there to animate the living tissue [11]. In the 19th century, Louis Pasteur observed that sugar fermentation by yeast is catalyzed by the substances present within the yeast cells, and he called them "ferments" [12]. This discovery, along with the publication made by Friedrich Wöhler in 1828 that describes the formation of urea from two inorganic molecules [13], established the basis for organic compounds and biochemical reactions found in cells. The discovery of enzymes at the beginning of the 20th century advanced the knowledge further and also separated the study of metabolic reactions from the biological study of cells and marked the beginnings of biochemistry. The early 20th century saw rapid advancement in metabolic studies, and the most notable finding was the discovery of Kreb's cycle or citric acid cycle by Hans Krebs, who contributed a lot to the field of metabolism and obtained the Nobel Prize in Physiology or Medicine in 1953 [14]. He also discovered the urea cycle and, later, the glyoxylate cycle working with Hans Kornberg.

At least 25 prizes have been awarded for metabolism-related work: 15 times to 31 laureates in Physiology or Medicine and 10 times to 15 laureates in Chemistry. The first one came in 1902 in Chemistry and was awarded to Emil Fischer's pioneering work on sugar and purine syntheses. The most recent one was awarded for the oxygen-sensing role of HIF-1α in 2019. In mammals, two small peptide hormones: insulin and glucagon, can control metabolism. Both are secreted from the islets of Langerhans of the pancreas, where insulin is produced in β-cells and glucagon is produced in α-cells. Given the significance of insulin in the management of diabetes, Nobel prizes were awarded in 1923, 1958, and 1977 for its discovery, structural identification, and development of its radioimmunoassay. Lipids are biomolecules that are highly soluble in nonpolar solvents but insoluble in polar solvents. Most of the energy in various organisms is stored in the form of fats and oils [15]. There are two main subtypes of lipids: sterols (such as cholesterols) and those containing fatty acids (such as triglycerides). They serve as cellular messengers, assisting proteins in their functions. They also initiate several chemical reactions that aid in regulating development, immunity, reproduction, and other aspects of ba-

sic metabolism. In the years 1964 and 1985, Nobel prizes were also awarded for discoveries concerning the mechanism and regulation of cholesterol and fatty acid metabolism. Vitamins are the essential micronutrients in the diet, even though in small amounts, they cannot be synthesized by our bodies, and their deficiency leads to severe diseases [16]. Due to accumulated research on vitamins, we now apparent that 13 vitamins are necessary for human health, including nine water-soluble vitamins (C and eight B vitamins) and four fat-soluble vitamins (A, D, E, and K). In total, seven Nobel prizes were awarded in the vitamins-related work [17]. A series of catabolic reactions known as cellular respiration transform nutrients into energy in the form of ATP [1]. The nature and the mode of action of the respiratory enzyme haemoglobin were discovered by Otto Warburg, and this pioneering work was also awarded the Nobel prize in 1931. Moreover, various transporter proteins can assemble in the channels present in the cell membrane for transporting water, mineral ions, and various metabolites [1]. In 2003, the Nobel prize was awarded in chemistry for discovering water channels and for structural and mechanistic studies of ion channels. These prize-winning studies on the enzymes and membrane channels paved the way for our current understanding of how cells process and transport matter and energy. Also, the understanding of drug metabolism and xenobiotic metabolism has advanced over the last two centuries of research.

Development of new advanced techniques such as chromatography, NMR spectroscopy, X-ray diffraction, isotopic labelling, electron microscopy, etc., have tremendously advanced modern biochemical research. These methods have made it possible to identify and thoroughly examine the numerous chemicals and metabolic pathways in cells. Till now, a very large number of metabolic pathways have been discovered, and the corresponding information can be found in various online resources such as KEGG [8], BRENDA [18], BioCyc [19], MetaCyc [20], Reactome [21], etc. Among these resources, KEGG is one of the most extensively used databases and provides various information on genomes, pathways, enzymes, metabolites, and drugs. Information regarding the orthologous genes for multiple organisms can also be obtained from KEGG. In addition to KEGG, organism-specific metabolic information can be obtained from other resources, including BioCyc, MetaCyc, etc. From BRENDA, we can get information regarding the enzymes, their activity, expression, and inhibition.

1.1.3 Significance of studying metabolism

Understanding metabolism is crucial for comprehending the phenotypic nature of all living things, including humans. The studies of metabolism have been conducted in a broad range of fields, such as biotechnology, nutrition, medicine, disease diagnosis, and drug metabolism [2, 22–25]. Studies on biotechnology mainly focus on identifying techniques to synthesize valuable substances on an industrial scale in a cost-effective manner [25, 26]. The commonly used methods for performing metabolic engineering are 1) overexpressing the rate-limiting enzyme of the biosynthetic pathway of the desired compounds, 2) inhibiting the competing metabolic reactions, 3) engineering the rate-limiting enzyme, 4) gene expression in the non-native organism, i.e., heterologous host [27]. Understanding metabolism gives a unique opportunity to understand the genotype-phenotype and the environment-phenotype relationship, as the metabolome of an organism reflects the genes, diet, and lifestyle in that entity [23, 28]. Research on the discovery and breakdown of specific metabolic pathways occupied a prominent position in scientific inquiry for many years until the 1960s [2]. Since then, research on the role of metabolism has been primarily focused on recognizing metabolic perturbations and their manifestation in human diseases [2]. As metabolism is essential for life and good health, any disruptions or dysregulation in metabolic processes can be harmful and involved in most human diseases. Aberrant metabolism is one of the major causes of various diseases, including cancers, diabetes, cardiovascular diseases, nonalcoholic fatty liver disease and neuronal diseases [29–35]. So, understanding metabolic alterations in various pathophysiology conditions allow us to understand the disease mechanisms and helps to identify potential drug targets and metabolic biomarkers [36]. More importantly, targeting metabolic enzymes is much more promising since metabolism is evolutionarily more conserved than other biologic processes [37].

However, after many decades of research, there is a growing need to explore the metabolic perturbations in various diseases, such as diabetes, cancer, nonalcoholic fatty liver disease (NAFLD), etc. For example, β-cell loss of function is one of the major reasons for developing type 2 diabetes (T2D), and ensembled evidence suggests that impaired β-cell metabolism may be the initial or triggering factor for abnormal β-cell functioning [38, 39]. Although it is known

that altered mitochondrial metabolism, ATP synthesis, glycolysis, some amino acid metabolism pathway, and fatty acid metabolism hampered insulin secretion in T2D [38–44], there is still a void in an in-depth understanding of β-cell metabolism in T2D. The main drawbacks of the current anticancer drugs are that they have many side effects [45] and show different responses in different individuals [46]. Thus there is a need to develop new anticancer drugs to take care of these problems and hence demand an in-depth mechanistic understanding of cancer [47, 48]. Besides, after decades of research, no drug has been FDA-approved for treating NAFLD [49]. Thus a better understanding of the pathophysiology of NAFLD is needed to identify potential drug targets to control the disease progression.

In fact, there are several challenges in studying metabolism. For instance, since metabolic networks are complex and large in nature, it is very difficult to measure the flow of metabolites through each reaction. In contrast to the static-like concentrations of transcripts, proteins, or metabolites, metabolic fluxes are the time-dependent flow of metabolites through a network and, therefore, cannot be quantified directly. Instead, it requires a computer model-based platform to infer from the measurable quantities [50]. Another challenge in experimental studies on human metabolism is that they are costly and time-consuming. The techniques for identifying new therapeutic strategies mostly rely on performing gene knockout [51–55] or phenotypic screening of drugs [51, 56–59] to obtain the desired outcome, like a reduction in the growth rate for cancer cell lines. As doing these without prior screening can cause a waste of time, resources, and money, hence any interdisciplinary approaches can speed up the processes. In this context, mathematical modelling-based approaches can become a successful helping hand. It has also been widely employed to capture disease-associated molecular mechanisms [60–62], identify new drug targets and biomarkers [36, 63–65], and develop new intervention strategies and therapeutic agents [66–69].

1.2 Mathematical modelling

Mathematical modelling, a key part of the systems biology approach, is a process by which a real-world problem is translated into a mathematical language. This kind of formulation is

purely abstract and always based on some assumptions, which means neither all the details of each process will be described, nor all aspects concerning the problem will be considered. For decades, mathematical models have been widely used in biological science to aid in understanding the dynamics of complex biological systems [70]. In general, experiments lead to several hypotheses on individual processes, but it often comes up short in providing a global overview of the whole system [71]. In this context, mathematical modeling can help to understand a more comprehensive knowledge of the dynamics of the system and test the experimentally driven hypotheses. It also provides new hypotheses regarding future development, which can be further validated through experimentation. Formulation of mathematical models and, subsequently, computation have become more and more familiar in biology over the past few decades, even though they have been applied much earlier. In the 13th century, Fibonacci used the famous Fibonacci series in his book "Liber Abaci" (The Book of Calculation, 1202) to describe the growth of the rabbit population [72]. Daniel Bernoulli used mathematics to describe the impact of smallpox on the human population in the 18th century [73]. In 1789, Thomas Malthus proposed the Malthusian growth model (exponential nature of population growth) of the human population in his book "An Essay on the Principle of Population", one of the earliest and most influential books on population biology [74]. Later, Pierre François Verhulst proposed the logistic function for the population growth model in a series of works between 1838 and 1847 [75]. Lotka and Volterra described the population dynamics of predator and prey with their famous equation known as Lotka–Volterra equations, a pair of first-order nonlinear differential equations, in the 1920s [71]. On the other hand, in 1913, Leonor Michaelis and Maud Menten developed mathematical equations known as the Michaelis-Menten equation to describe the rate of enzyme kinetic reactions [76]. Using these equations as a foundation, a series of kinetic models have been developed to understand the dynamics of various metabolic pathways in different organisms.

Mathematical modelling is a subjective and selective process in which specific questions are addressed [71, 77]. Therefore, the model should be constructed according to the problems, with a priority that the structure of the model must accurately reflect the real system (**Fig. 1.3**). Also, need to clarify its level of confidence and limitations. The values of parameters are

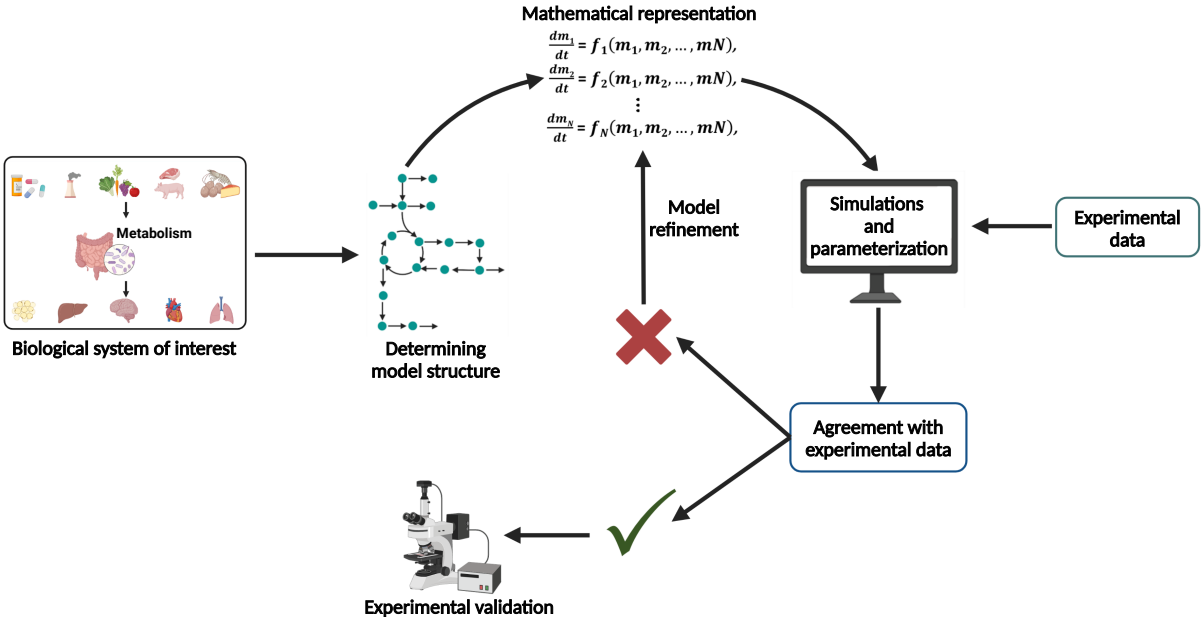

Figure 1.3: **The general steps involved in studying biological systems through mathematical modelling.**

always based on existing knowledge and can also be inferred from the available experimental data. The model is then analyzed, and the result must be validated by existing knowledge or experiments to establish the model. If the models fail to reproduce the known phenomenon of the system, the subsequent modification will be carried out in the model until the desired outcome appears. The model-predicted hypotheses should be further validated through experimentation or extrapolations from comparable systems. The mathematical formulation part can be kept as simple as possible for easy implementation and interpretation of the results. Otherwise, making it very realistic can make the system more complicated to propose new hypotheses. In biological systems, sometimes generalized models are developed to apply to similar objects (e.g., the Michaelis-Menten equation holds for many enzymes). In contrast, others are typically focused on one specific object, like the sequence of a gene, the 3D structure of a protein, etc. In modelling biological systems, we must follow some constraints like non-negativity and boundedness, as the level of biological entities can not be negative or infinite. The attempt at mathematical modelling provides quantitative and qualitative descriptions of the systems and often reveals gaps in current knowledge or understanding. Additionally, it can be utilized to determine the feasibility of the proposed theories.

1.3 Modelling of metabolism

The formulation of a mathematical model on the biological processes can be achieved by employing different approaches depending on the nature of the system and the data availability. Ordinary differential equations (ODE)-based mathematical models are the most extensively used approaches and are applied to capture the time course of biological entities like metabolites [78]. This modelling approach is very useful for capturing the non-linearity of the systems and can explain the interactions between different variables. Besides, the right strategy to capture the diffusion of the variables is to incorporate the partial differential equations (PDE) in the model. This Spatio-temporal modelling provides the spatial information of the system [79]. A major obstacle to these approaches in metabolic modelling is that only a small sub-network can be studied instead of the whole network due to the lack of knowledge on the kinetics of each enzyme in different cells and organisms [80, 81]. In this context, constrained-based modeling provides unique opportunities to capture the steady-state flux distribution through the entire metabolic network [71, 77]. Aside from these, rule-based modelling (or agent-based modelling), delay differential equations, stochastic differential equations, Petri net, and various statistical modelling approaches have been applied in studying biological systems [71]. ODE-based small kinetic models and constrained-based models are the most widely employed approaches to understanding the metabolism and corresponding perturbations in various conditions like genetic manipulation and human diseases.

1.3.1 Kinetic modelling

Kinetic modelling has been extensively used in capturing the dynamics of various metabolites in different cells and organisms. It has a long tradition and finds roots in the early 20th century when Michaels and Menten proposed a mathematical equation to describe the rate of enzyme kinetic reactions [76]. The rate of reactions is given by the formula

$$v = V_{max} \frac{[S]}{K_M + [S]},$$

where V_{max} represents the maximum achieved rate by the enzyme. K_M is known as the Michaelis constant and is numerically equal to the substrate concentration at which the rate is half of the V_{max}. The Michaelis-Menten equation is a generalized model and can be applied to any enzymatic reaction. All the kinetic models are based on the law of mass action: "the rate of the chemical reaction is directly proportional to the product of the activities or concentrations of the reactants", introduced by Guldberg and Waage in the 19th century [82]. Kinetic modelling forms the basis of various metabolic pathways, in which the dynamical equation of each metabolite can be represented by:

$$\frac{dx}{dt} = \text{ rate of production - rate of consumption,}$$

where the production and consumption rate depends on the activity of the corresponding catalyzing enzymes.

The most addressed question through kinetic modelling is to rationally design strategies for improving the ability of cells or organisms to produce the desired product. Till now, numerous biological processes have been studied through kinetic modelling. Among all these, central metabolism receives the most attention as it is the basis of the conserved phenomenon of life and serves as a hub for almost all catabolic and biosynthetic activities [83]. The overall structure of central metabolism is remarkably well conserved in all living organisms, and its regulation plays a crucial role in adapting organisms to environmental changes [84]. Thus, the kinetic models on the central metabolism will also serve as the basis for further integration and extension to peripheral metabolism. Initially, the kinetic models were centered on comprehending glycolytic oscillations in nongrowing yeast cells [85–92]. Later works attempted to understand the control properties and glycolytic responses upon a glucose-perturbed condition [93–96]. Due to the advanced techniques for experimentation and the progressive increase in quality data, more detailed models were formulated for exploring the glycolysis process in yeast [97–100]. The glycolysis and pentose phosphate pathway of *Escherichia Coli* has also been studied by Chassagnole et al. [101], and this is the first ever model that connects the sugar transport system (i.e., phospho-transferase system) with the reactions of the glycolysis and pentose phosphate pathway. This model structure was validated by experimentally observed

concentrations of intracellular metabolites and predicted the potential targets for envisaged re-designing central carbon metabolism. A kinetic model on the central metabolic pathways such as glycolysis, TCA cycle, pentose phosphate pathway, and the anaplerotic pathways for *Escherichia Coli* was formulated for understanding the metabolic perturbations in response to specific gene knockouts [102]. Also, a kinetic model on the central carbon metabolism of E. coli was developed using fluxomics and metabolomics data [103]. Kinetic models on metabolic pathways have often been used to predict the drug targets in the case of pathogens [104–108]. Sensitivity analysis has been a widely used technique to predict drug targets using these kinetic models.

Kinetic modelling has also been used to explore human metabolic pathways and applied in various tissues like the liver, pancreas, brain, etc. [109–114]. The human body is very much complex since different organs and tissues have different functions and metabolism. Also, each of these organs interacts with others. So, to understand human metabolism, whole-body metabolic models are needed. In this context, compartmentalized-based kinetic models are used in which various tissues and their interactions are considered to formulate the model structure. Till now, numerous compartmentalized models have been proposed to study the whole-body metabolism of glucose, triglycerides, cholesterol, etc [115–117]. Kinetic models usually focus on only a small sub-network of the entire metabolism. Whereas, constraint-based modelling is often used to simulate large pathways, and since no enzyme kinetic information is needed, it gets great attention in systems biology.

1.3.2 Constraint-based modelling

Constraint-based modelling is an appropriate mathematical platform for studying and understanding metabolic network flux distribution at steady-state [36, 77, 118]. It bypasses the hurdles in simulating large networks through kinetic modelling and can also serve as a scaffold for capturing the manipulation in metabolic networks. There are approximately four major successive steps in this type of model building and analysis: 1) network reconstruction, 2) formulation of Stoichiometric matrix, 3) identification and implementation of a set of constraints that govern cellular metabolism, and 4) determination of optimal flux distribution through flux

balance analysis. Network construction is the most critical step in constraint-based modelling as it involves an extensive literature survey to make an appropriate list of metabolites, biochemical reactions, and gene–protein reaction relationships. In this context, various resources on metabolic pathways like KEGG [8], MetaCyc [20], BioCyc [19], and EcoCyc [119] can be beneficial. Additionally, genomic and proteomic data also help to get information on relevant metabolic network components. In making the list of metabolic reactions, we must check that each reaction is balanced in mass and charge. Also, it needs proper compartmentalized and directionality information of each reaction for reconstructing the metabolic network. The enzyme reversibility data can be obtained from online resources like KEGG [8] and BRENDA [18].

After the compilation of network reconstruction, the entire reaction list is converted into a stoichiometric matrix (S) with dimension $m \times n$, where m denotes the number of metabolites and n represents the number of reactions present in the network. The numbers in each column correspond to the stoichiometric coefficients of metabolites participating in that reaction. Negative values indicate the consumption of these metabolites, and positive values represent the production. In constraint-based modelling, mainly three types of constraints are applied: 1) the mass–balance constraints and implemented by using the matrix S. This is used to impose the steady-state condition on the metabolites. 2) Thermodynamic constraints, which determine the reversibility of the reactions. 3) Enzyme capacity constraints that fix the maximal flux rate (V_{max}) and can be inferred from the experimental data, like transcriptomics, proteomics, and fluxomics. These constraints establish a geometric solution space of all possible metabolic fluxes [77]. Additionally, the consumption rate of certain metabolites in the cells can be applied to impose the specific nutrient supply in the system. Various optimization-based techniques, like flux balance analysis [120–122], extreme pathway analysis [123], elementary mode analysis [124, 125], etc., are mainly used to characterize the allowable solution space and predict the optimal solution.

Metabolic network reconstruction using biochemical information has been ongoing since the 1930s when the glycolytic pathway was defined [77]. In the late 1980s, the rise of large-scale organism-specific biochemical data collection allowed the systematic generation of organism-

specific metabolic networks [77, 126]. These network reconstructions for various organisms, including *Escherichia Coli* [127–131], *Saccharomyces cerevisiae* [132–134], and *Aspergillus niger* [135–137], were established in a stepwise fashion. The genome-sequencing and corresponding annotation enable researchers to reconstruct the genome-scale metabolic network. The first genome-scale metabolic model (GSMM) was reconstructed for *Haemophilus influenzae* in 1999 [138] and came apparently in shorter time intervals after the publication of its first genome sequencing in 1995 [139]. In the past few decades, GSMMs have been widely used to study the metabolism of bacteria. They are mainly used for metabolic engineering in biochemical synthesis [140–142], drug-target identification [143–145], investigation of novel metabolic functions [146–148], studying host-pathogen interactions [149–154], etc.

Constraint-based metabolic modelling approaches are advancing at an accelerating pace to understand the molecular mechanisms behind various diseases and identify potential therapeutic strategies [155]. Earlier network-level human metabolism studies have focused on the functional characterization of distinct human metabolic pathways and organelles [156–158]. In 2007, two generic human GSMMs were developed based on the evaluation of genomic and bibliomic data: Recon1 [159] and Edinburg Human Metabolic Network [160]. The Recon series has undergone several significant modifications by incorporating additional biological information and rectifying various modelling flaws [161–164]. In 2018, the latest version of the Recon series, Recon3D, was published, and it incorporated the most comprehensive human gene-protein-reaction (GPR) relationships and the structural information of metabolites and enzymes [164]. The clinical significance of the Recon series in investigating human diseases has been demonstrated in numerous studies [64, 165, 166], and most extensively, these have been applied in studying cancer [36, 167]. These generic GSMMs have also been used to model various cells and tissues, including the liver [168, 169], heart [60], kidney [170], brain [171], small intestine [172], macrophages [150], etc., by integrating high-throughput data. Besides, these generic models have been used to enhance the understanding of host-pathogen interactions [149–154].

The human metabolic reaction (HMR) database, another generic human GSMM series, was published first in 2012 [173]. The first version (*iHuman1512*) was developed by col-

lecting information from the previously published generic models of humans [159, 160, 174] and the KEGG database [175]. Compared to the Recon series, the HMR series (HMR1; [173] and HMR2; [62]) contains more extensive and manually curated information on fatty acid metabolism. It, therefore, has been used to obtain comprehensive GSMMs of human adipocyte (*iAdipocytes1809*; [176]), hepatocyte (*iHepatocytes2322*; [62]), and skeletal myocyte (*iMyocyte2419*; [177]). These cell- or tissue-specific GSMMs have been used to study the metabolic characterization of human diseases like obesity, diabetes, and NAFLD. Recently, a unified generic human GSMM (Human1) has been published by integrating and curating the latest Recon (Recon3D) and HMR (HMR2) model lineages [178]. Human1 consists of 13,417 metabolic reactions, 3625 genes, and 4164 unique metabolites, and all the information can be obtained from the web portal Metabolic Atlas.

1.4 Tools and approaches

1.4.1 Analytical tools

Definition 1 (System of differential equation): A system of differential equations of the form

$$\frac{dx}{dt} = \dot{x} = f(x), \tag{1.1}$$

where $X \in \mathbf{R}^n$ and $f = (f_1, f_2, ...f_n)^T$, $f_i = f_i(x_1, x_2, ...x_n)$, is a called a nonlinear system. If the partial derivatives of $f_1, f_2, \ldots, f_n$ are C^1 functions then the initial value problem

$$\frac{dx}{dt} = f(x) \text{ with } x(0) = x_0$$

has a unique solution. The system (1.1) is called autonomous system since the function $f(x)$ does not contain time (t) explicitly. Otherwise, it is said to be non-autonomous system.

Definition 2 (Equilibrium point): A point $\bar{x} \in \mathbf{R}^n$ is called an equilibrium point of the system (1.1) if

$$f(\bar{x}) = 0.$$

An equilibrium point is also called a fixed point, critical point, stationary point, steady state.

Definition 3 (Lyapunov stability): The equilibrium point $\bar{x}$ of (1.1) is said to be Lyapunov stable or simple stable if for any $\varepsilon > 0$ there exists a $\delta(\varepsilon) > 0$ such that for every solution $x(t)$ of (1.1) with initial condition $x(0) = x_0$ if $\|x_0 - \bar{x}\| < \delta$ then $\|x(t) - \bar{x}\| < \varepsilon$ for all $t > 0$, where $\|.\|$ is the Euclidean norm.

Definition 4 (Quasi-asymptotic stability): The equilibrium point $\bar{x}$ of (1.1) is said to be quasi-asymptotic stable iff there exists a number $\delta > 0$ such that if $\|x_0 - \bar{x}\| < \delta$ then $\lim_{t\to\infty} \|x(t) - \bar{x}\| = 0$.

Definition 5 (Asymptotic stability): The equilibrium point $\bar{x}$ of (1.1) is said to be asymptotically stable if it is (a) Lyapunov stable as well as (b) quasi-asymptotically stable.

Let $\bar{x}$ be an asymptotically stable equilibrium point of (1.1) then the set

$$D(\bar{x}) = \{x \in \mathbf{R}^n : \lim_{t\to\infty} \|x(t) - \bar{x}\| = 0\}$$

is called the basin of attraction of $\bar{x}$. If $D(\bar{x}) = \mathbf{R}^n$ then $\bar{x}$ is said to be globally asymptotically stable. Otherwise, it is said to be locally asymptotically stable.

Theorem 1 (Routh-Hurwitz criteria): Let us consider the n-th degree polynomial

$$P(\lambda) = \lambda^n + B_1\lambda^{n-1} + ... + B_{n-1}\lambda + B_n, \tag{1.2}$$

where all the coefficients B_i, $i = 1, 2, ..., n$, are real constants then n Hurwitz matrices are defined as

$$H_k = \begin{pmatrix} B_1 & 1 & 0 & 0 & ... & 0 \\ B_3 & B_2 & B_1 & 1 & ... & 0 \\ B_5 & B_4 & B_3 & B_2 & ... & 0 \\ . & . & . & . & ... & . \\ . & . & . & . & ... & . \\ . & . & . & . & ... & . \\ 0 & 0 & 0 & 0 & ... & B_k \end{pmatrix}, \; k = 1,2,3,...,n,$$

where $B_k = 0$ if $k > n$. All the roots of the polynomial $P(\lambda)$ will have negative real parts iff the determinants of all the Hurwitz matrices are positive. Thus the Routh-Hurwitz criteria for n= 2, 3 and 4 are as follows

- $n = 2: \; B_1 > 0, \; B_2 > 0.$
- $n = 3: \; B_1 > 0, \; B_3 > 0, \; B_1 B_2 - B_3 > 0.$
- $n = 4: \; B_1 > 0, \; B_3 > 0, \; B_4 > 0, \; B_1 B_2 B_3 - B_3^2 - B_1^2 B_4 > 0.$

1.4.2 Sensitivity analysis

Sensitivity analysis is a widely used systems biology tool for identifying the most critical inputs, such as parameters or initial conditions, whose slight variance can affect the model outputs [179]. The sensitivity of each input factor can be computed by varying independently around a nominal value while the others remain constant. This approach is known as local sensitivity analysis as it can only capture the impact of uncertainties of the inputs very close to the nominal values. However, in biological systems, the variations in inputs are often very uncertain, so local sensitivity analysis is insufficient to infer the true nature of these input factors [179]. In this context, global sensitivity techniques are required.

Global sensitivity analysis captures the variation in the model outputs under various combinations of input factors. The combinations of inputs can be generated from several sampling-based methods like random sampling, importance sampling, and Latin hypercube sampling [180, 181]. Finally, the sensitivity index for each input can be measured depending on the

relationship with the model outputs [179]. For linear trends, sensitivity can be measured by applying the Pearson correlation coefficient, Standardized Regression Coefficients, and Partial Correlation Coefficients. For nonlinear monotonic trends, Spearman Rank Correlation Coefficient, Standardized Rank Regression Coefficients, and Partial Rank Correlation Coefficient are applied to measure the sensitivity. For nonlinear non-monotonic relationships, various variance-based methods like the Sobol method and its extended version, Fourier Amplitude Sensitivity Test (FAST), and its extended version (eFAST) are the best options. Among them, PRCC [179] and eFAST [182] are the most commonly used and reliable techniques [183, 184]. PRCC can offer additional informations, such as how changing (increasing or decreasing) the input factors will alter the model output. In contrast, eFAST only provides which parameter uncertainty has the most significant impact on model output [179]. Thus, PRCC can be more informative than eFAST in selecting parameters to target if we intend to attain specific objectives, for example, an increment in the ATP yield or a reduction in glucose consumption, etc.

1.4.3 Context-specific model reconstruction

Genome-scale metabolic models (GSMM) are generally built to contain all the known metabolic reactions and enzymes in a particular organism [185]. These reconstructed networks are generic and always remain a superset of the functioning metabolic reactions at any given time. Determination of active reactions in a cell or organism is often of interest in constraint-based studies as this obtained context-specific sub-network represents the actual metabolism [186]. These can be inferred from the activity of the corresponding enzymes in the particularly interested cells or organisms. In this context, various throughput data, including transcriptomics, and proteomics data, have been used to build context-specific models.

Several methods exist to reconstruct context-specific networks from a generic GSMM (**Table 1.1**), and these methods can be categorized into three classes: “GIMME-like”, “iMAT-like”, and “MBA-like” [187, 188]. The Gene Inactivity Moderated by Metabolism and Expression (GIMME) [186] method belongs to the “GIMME-like’, which minimizes the usage of reactions associated with the lowly expressed genes. The Integrative Metabolic Analysis Tool (iMAT) [189, 190]

and Intergrative Network Inference for Tissues (INIT) [173] methods belong to the "iMAT-like", which finds an optimal trade-off between including reactions corresponding to highly expressed genes and excluding reactions associated with lowly expressed genes. The Model-building algorithm (MBA) [168], metabolic Context-specificity Assessed by Deterministic Reaction Evaluation (mCADRE) [191], and FASTCORE [192] methods belong to the "MBA-like" family, which retains a core reaction set and removes other reactions if not required to support the core set. The E-Flux [193] method uses the gene-protein-reaction (GPR) relationship to map the gene expression value into flux-bound constraints, and it does not fall into any of these three categories. The gene expression data is used here to fix the lower and upper bounds of the fluxes so that reactions associated with the highly expressed genes should be allowed to have higher absolute flux than others.

Table 1.1: **Various methods for the reconstruction of context-specific metabolic network.**

Method	**Description**	**Data input**	**Handling missing data**
GIMME	Defines active and inactive reactions using the gene expression data. Returns a functioning model that meets the objective by minimizing the usage of inactive reactions.	Transcriptomic data are used to define inactive reactions and their respective weights.	Considers as active reactions.
iMAT	Uses expression data to define high, moderate, and low expressed reactions. Finds the optimal trade-off between excluding lowly expressed reactions and including highly expressed reactions.	Any type of data can be used to define the expression status of reactions.	Does not favor exclusion or inclusion.
INIT	Optimizes the exclusion of the lowly expressed reactions and inclusion of highly expressed reactions. Allows secretion (or accumulation) of metabolites.	Any type of data can be used to define the weights of reactions.	Dependents on the user-defined weights.

MBA	Provides a most parsimonious model that includes all the high-confidence reactions and the necessary moderate-confidence reactions.	Any type of data that can provide confidence in reactions.	Removed if not required to support the included reactions.
mCADRE	Core reactions are defined as highly expressed reactions. Other reactions are ranked according to their expression and removed according to their rank if not necessary to support the core reactions.	Transcriptomic data are mainly used to define the core reactions and to rank the others.	Removed if not required to support the core.
FASTCORE	Determines a core reaction set using the data and includes the minimum necessary reactions to support the core.	Any type of data can be used to define the core reactions.	Removed if not required to support the core.
E-Flux	Determines the reaction expression using the GPR relationship from the gene expression data and uses these to fix the bound of each reaction.	Transcriptomic data are mainly used to define the reaction expression.	Does not favor exclusion or inclusion.

1.4.4 Flux balance analysis

Flux balance analysis (FBA) is a widely used constraint-based modeling approach to analyze the flow of metabolites through metabolic pathways [122]. This method mainly relies on the assumption of mass balance and the steady state of metabolites. The mass balance constraints are implemented by the stoichiometric matrix (S) of dimension $m \times n$ (for a metabolic network with m metabolites and n reactions). In this matrix, each row denotes a unique metabolite, and each row represents the individual reactions. The entries in each column correspond to the stoichiometric coefficients of the metabolites participating in a particular reaction. Negative

values indicate consumption, and positive values represent production. The value 0 is given for those metabolites that are not participating. Under the steady-state assumption, a system of linear equations is obtained as

$$S.v = 0,$$

where the flux distribution is represented by the vector v, with length n. Constraints arising from reaction reversibility, enzyme capacity, and experimental measurements are imposed by setting the upper (v_{up}) and lower bounds (v_{low}) of the reactions. In any realistic GSMMs, there are more unknowns than equations, as the corresponding metabolic network contains more reactions than metabolites ($n > m$). It leads to the existence of infinite solutions. Although the imposed constraints define a bounded solution space, it is hard to analyze and interpret the phenotypic state of the network. Therefore to obtain a single point within the solution space, FBA seeks an objective function for optimization. Here, the objective function is any linear combination of fluxes of the form $z = c^T v$, where c denotes the vector of weights and reflects the relative contribution of each reaction. In FBA, the linear programming (LP) solver is used to solve the optimization problem of the form

$$\begin{aligned} max/min\ Z = c^T v, \\ s.t.\ S.v = 0, \\ v_{low} \leq v \leq v_{up}. \end{aligned}$$

The selection of suitable objective functions is purely context-specific. Some of its classic examples include the maximization of growth rate, maximization of ATP production, minimization of substrate utilization, and the maximization of biochemical synthesis. Most of the time, biomass reaction has been used as the objective function based on the assumption that the cell seeks to maximize cellular growth to ensure survival [121, 122]. After solving the above-mentioned LP problem, FBA provides the optimal value of the objective function with the corresponding optimal flux distribution.

1.4.5 Flux variability analysis

LP problems can have multiple optimal solutions, which means various points in the solution space can give the same optimal value. In general, constraint-based models fall under the grasp of such circumstances [194, 195]. In 2003, Mahadevan et al. [196] developed flux variability analysis (FVA) to capture the alternative optimal solutions in constraint-based modelling. FVA provides the ranges of flux values for each reaction, and the calculation is performed using LP and quadratic programming (QP) methods. Typically, FVA solves $2n$ number of LP problems of the form:

$$
\begin{aligned}
max\ v_i \text{ and } min\ v_i,\\
s.t.\ S.v = 0,\\
c^T v = Z_{obj},\\
v_{low} \leq v \leq v_{up},\\
\text{for } i = 1,2,...,n.
\end{aligned}
$$

where Z_{obj} is the optimal value of the objective function obtained from the FBA, and n is the number of reactions. The reactions having the same minimum and maximum non-zero fluxes are essential for accomplishing the objective of interest, as there are no alternative pathways in the network.

1.4.6 Flux sampling

Flux sampling provides the opportunity to compute all possible feasible solutions throughout the entire solution space in a statistically significant manner [197–200]. Flux sampling seeks sufficient and uniform data points from the solution space to keep the analysis accurate and unbiased. Although FVA provides the ranges of flux values, it cannot give the possible flux distributions. Besides, flux sampling does not need any objective function; therefore, it is a very efficient and helpful technique when the specific objective function is unclear. There are several algorithms for performing flux sampling on a constraint-based model. The first pro-

posed algorithm is the rejection sampling technique [201]. This approach becomes inefficient when a huge fraction of the samples have to be rejected. The hit-and-run (HR) algorithm [202] mitigates this problem by performing sampling directly from the solution space. HR picks samples from the solution space by iteratively choosing a random direction from the uniform distribution and an arbitrary step size in a direction so that the next point also lies in the solution space. The artificial centering hit-and-run (ACHR) method [203] computes the random flux distributions by applying the center estimate and random flux vector direction. Coordinate hit-and-run with rounding (CHRR) [204] uses a rounding preprocessing step on the anisotropic flux sets. The uniform random sampling method, known as *gpSampler*, [198] is often used for sampling constraint-based models and is partly based on ACHR. *gpSampler* is implemented in the Constrained Based Reconstruction and Analysis (COBRA) Toolbox [205].

1.4.7 *In silico* network perturbation

There are mainly three approaches in performing *in silico* metabolic network perturbation: 1) Reaction-centric, 2) Gene-centric, and 3) Metabolite-centric. Reaction-centric techniques focus on identifying metabolic reactions from the network that, when perturbed, affect the cell's capacity to carry out essential functions. These are performed mainly by inhibiting or removing the reactions from the network and subsequently capturing the downstream effect on the objective function. Once a crucial reaction has been identified from the analysis, the GPR rules are used to obtain the protein or gene that can be targeted to perturb the reaction. Gene-centric techniques focus on identifying genes that are critical to maintaining cellular function. The first step of these techniques is to identify metabolic reactions that are affected by the removal of this gene by using the GPR rules. Then, the effect of this gene is calculated by inhibiting or removing all of these reactions from the network. Metabolite-centric techniques focus on finding highly connected metabolites in the metabolic network and, when targeted, affect cellular function significantly. The effect is captured by removing those reactions from the network that consume this metabolite. In all these cases, the network perturbations are finally imposed through the associated reactions. The perturb models are generated mainly by changing the bounds of the fluxes; for example, in complete inhibition, the bounds are fixed at

0.

The simulation of the perturbed model can be performed through the FBA [206], in which a particular cellular objective function is optimized. The effect of the network perturbation is defined by calculating the changes in the optimal value compared to the wild-type condition. Several perturbation-specific algorithms, such as minimization of metabolic adjustment (MOMA) [207], regulatory on/off minimization (ROOM) [208], and metabolic transformation algorithm (MTA) [209], etc., have been developed to capture the effect of metabolic network perturbation through GSMM. Instead of looking for an optimal flux state that optimizes the cellular objective function, MOMA provides a unique flux distribution closest to the wild-type flux distribution. The underlying hypothesis is that the metabolic flux state after the network perturbation may undergo a minimal redistribution compared to the wild-type flux state. To obtain such flux distribution, MOMA employs quadratic programming (QP) to minimize the Euclidean norm: $\sqrt{\sum_{i=1}^{n}(V_{wt,i}-V_i)}$, between the given wild-type flux distribution (V_{wt}) and the post-perturbed flux distribution (V). On the other side, ROOM minimizes the number of significant flux changes in the perturbed state compared to the wild-type flux distribution. ROOM employs mixed integer linear programming (MILP) to determine the perturbed flux distribution and allows a few significant flux changes rather than numerous small changes. MTA employs mixed integer quadratic programming (MIQP) to predict the metabolic reactions or genes whose knockout can shift the metabolic flux distribution from one state to another. Before applying this algorithm, it must be required to define the set of reactions whose flux rates have to change to shift the metabolic state. MTA removes each reaction or gene from the network and solves the MIQP problem that minimizes the changes in flux rates through "unchanged" reactions and maximizes the flux rate changes in the "changed" reactions. Finally, a score is given for each reaction or gene according to the success of bringing the metabolic state towards the target state.

1.5 Scope and objectives of the thesis

An abnormal metabolic state is the root cause or consequence of numerous human diseases, including cancer, diabetes, obesity, cardiovascular disorders, and neurological diseases. Therefore, it is an unmet need to explore metabolism in disease conditions to understand the underlying mechanism behind disease development and progression. It also presents a tremendous opportunity to discover new drug targets and design new therapies and diagnostic techniques. Again, human diseases do not derive from the abnormal functioning of a single gene or pathway but reflect the disruption of complex intracellular and intercellular metabolic networks that link tissues and organs. Due to these complexities, it is very challenging for experimental biologists to explore all metabolic pathways.

In this context, mathematical modelling-based approaches could be a good alternative in exploring the entire metabolism and proposing new hypothesises. Although numerous mathematical modelling-based studies have been performed in human diseases, there still exists a lacuna of metabolic perturbations in various conditions, such as diabetes, cancer, NAFLD, cardiovascular disorders, etc. In view of the challenges concerning metabolic perturbation in disease conditions, the objectives of the thesis have been defined as follows:

1. To develop and analyse the large-scale metabolic model for capturing the alteration in metabolic flux states under disease conditions with the help of omics data.

2. To develop simulation methods to explore the role of metabolic genes in controlling disease progression.

3. To build small-scale kinetic models to capture the role of altered metabolites responsible for the disease.

1.6 Thesis layout

The present thesis aims to explore metabolic perturbations in disease to understand the underlying mechanism and develop therapeutic strategies. More precisely, the thesis is devoted to studying the role of metabolites and associated pathways in the progression of the disease and

using it to develop therapeutic strategies. In **Chapter 1**, the introduction of the thesis is discussed. This chapter contains information regarding the significance of studying metabolism in human diseases and how mathematical modelling can help to understand metabolism. It also describes the various mathematical tools and methods used for model development and simulations.

Human metabolism is a highly complex and tightly regulated system consisting of multiple enzymatic reactions and metabolites, and hence very difficult to measure the flow of metabolites through each reaction by experiments. In this context, genome-scale metabolic models (GSMMs) provide a unique opportunity to capture the metabolic flux state in different cell-type and conditions and therefore have been successfully applied for systematically studying human diseases. In **Chapter 2**, we have applied GSMM to capture the metabolic alterations in pancreatic β-cell to understand the key factors responsible for the dysregulated β-cell function in type 2 diabetes (T2D). The metabolic-flux profiles of pancreatic β-cells were predicted by integrating the gene-expression data of ten diabetic patients and ten control subjects into a human genome-scale metabolic model. Analysis of these flux states shows reduction in the mitochondrial fatty acid oxidation and mitochondrial oxidative phosphorylation pathways, that leads to decreased insulin secretion in diabetes. We also observed elevated reactive oxygen species (ROS) generation through peroxisomal fatty acid β-oxidation. In addition, cellular antioxidant defense systems were found to be attenuated in diabetes. Our analysis also uncovered the possible changes in the plasma metabolites in diabetes due to the β-cells failure. These efforts subsequently led to the identification of seven metabolites associated with cardiovascular disease (CVD) pathogenesis, thus establishing its link as a secondary complication of diabetes.

In addition to exploring metabolic alteration, GSMM can be applied to identify critical regulatory points from the metabolic network through *in silico* knockout approaches. **Chapter 3** focuses on identifying the regulatory points in the cancer metabolic networks by performing the gene knockout study on the various cancer-specific GSMMs. We performed single-gene knockout studies on existing GSMMs of the NCI-60 cell-lines obtained from 9 tissue types. The metabolic genes responsible for the growth of cancerous cells were identified and then ranked based on their cellular growth reduction. The possible growth reduction mechanisms, which

matches with the gene knockout results, were described. Gene ranking was used to identify potential drug targets, which reduce the growth rate of cancer cells but not of the normal cells. The gene ranking results were also compared with existing shRNA screening data. The rank-correlation results for most of the cell-lines were not satisfactory for a single-gene knockout, but it played a significant role in deciding the activity of drug against cell proliferation, whereas multiple gene knockout analysis gave better correlation results. We validated our theoretical results experimentally and showed that the drugs mitotane and myxothiazol can inhibit the growth of at least four cell-lines of NCI-60 database.

Combining these two approaches, i.e., identifying metabolic alterations and regulatory points through *in silico* gene knockout, might lead us to potential drug targets that could revert the altered disease metabolic state to a healthy state. The combination of these two approaches was used in **Chapter 4** to identify potential targets for nonalcoholic steatohepatitis (NASH), which is driven by perturbations in gene expressions and thereby tailoring a cascade of events influencing the complex disease dynamics that span through proteins and metabolites. The potential targets were identified using a de novo methodology and could reverse the disease-specific molecular alterations. Our approach resulted in three promising targets for NASH and eight targets for its early-stage NAFL. We also elucidated the possible mechanism of action of these identified targets using GSMM. Inhibition of these identified targets could attenuate hepatic steatosis by promoting higher flux rates for the altered reactions involved in fatty acid activation and mitochondrial beta-oxidation pathways. Although this chapter provides a new perspective on drug discovery, we still need small-scale kinetic models to capture the underlying mechanism associated with metabolic alterations related to a disease condition.

Impaired glucose-stimulated insulin secretion (GSIS) in β-cell is one of the major causes of developing T2D in the presence of insulin resistance (IR). A global picture of metabolic alterations in β-cell under T2D was earlier discussed in **Chapter 2**. However, this study was limited by the inability to explore the dynamics of crucial processes like insulin secretion, which hold the key to T2D. Therefore, to study the cause, effect, and, thereby, the mechanism of T2D, in **Chapter 5**, we have built a six-dimensional kinetic model to study the GSIS process. The model was established by simulating the normal and IR-induced hyperglycemic conditions.

The analysis revealed the possible factors responsible for the impaired GSIS process in IR, whose dysfunction can lead to T2D. Finally, using the parameter recalibration analysis, we uncovered the potential therapeutic strategies for compensating the insulin secretion-reducing alterations that could eventually help prevent the disease progression.

Next, we extended this study by incorporating the insulin synthesis and insulin granule biogenesis processes with the GSIS to decipher the in-depth understanding of glucotoxicity in β-cell dysfunction. In **Chapter 6**, a simplified kinetic model for insulin synthesis and secretion of insulin granules was developed and analyzed. The analysis revealed that the defects in the insulin granule trafficking and exocytosis processes hamper first- and second-phase insulin secretion and might be one of the main reasons for β-cell dysfunction in T2D. The long-term effect of abnormal insulin synthesis could hamper insulin secretion and make the scenario more critical, causing complete insulin loss inside the β-cells. Besides, uncontrolled insulin synthesis could increase basal insulin secretion and drive toward fasting hypoglycemia. The present study also hypothesized the regulation of insulin synthesis through targeting transcription and translation as a potential therapeutic strategy for controlling impaired insulin secretion.

Chapter 7 discusses the conclusions and the future directions of the thesis.

2

Prediction on metabolic alterations from gene expression data using genome-scale metabolic model[1]

2.1 Introduction

Human metabolism is a highly complex and tightly regulated system consisting of multiple enzymatic reactions and metabolites that form a connected and functional network in which the products of one reaction become the substrates of the other reactions [210, 211]. Genome-scale metabolic models (GSMMs) have been successfully applied for systematically studying

[1]The bulk of this chapter has been published in *Computers in Biology and Medicine*, 144 (2022): 105365.

human metabolism to discern underlying mechanisms involved in disease progression's pathophysiology [60–62]. This mathematical framework has also been widely used to identify new drug targets and develop new intervention strategies and therapeutic agents [67, 68]. It is also employed in predicting metabolic biomarkers and capturing metabolites with altered production fluxes [64]. However, to the best of our knowledge, very little work has been carried out to analyze the metabolic pathways related to pancreatic β-cells using GSMM. Previously, Calimlioglu et al. [212] successfully obtained some T2D-related metabolic signatures by incorporating pancreatic β-cell transcriptomics data into GSMM.

β-cell failure (reduction of β-cell mass and function) is central to the pathogenesis of type 2 diabetes (T2D). Multiple metabolic abnormalities including glucotoxicity, lipotoxicity (elevated free fatty acids/triglycerides), glucolipotoxicity, disruptions of lipid metabolism, oxidative and endoplasmic reticulum stress, proinflammatory cellular responses, islet amyloid deposition, disruption of transcriptional control, and β-cell turnover, plasticity, and dedifferentiation have been implicated as drivers of β-cell dysfunction in T2D [43, 213–218]. Taken together, dysregulated β-cell function and loss of mass potentially through multiple mechanisms promote hyperglycemia due to inadequate levels of circulating insulin, ultimately resulting in the development and progression of T2D [219, 220]. Hence, therapeutic strategies targeted at maintaining β-cell function and mass are likely to be most beneficial in the clinical management of T2D.

The underlying mechanism(s) by which β-cell function gets impaired in T2D is yet to be established. Several contributing factors have been proposed so far, such as oxidative stress, endoplasmic reticulum (ER) stress, impaired voltage-gated calcium channels (VGCC), impaired exocytosis, β-cells irregular proliferation, and impaired glucose metabolism [221–223]. Insulin/insulin-like growth factor-1 (IGF-1) signaling pathways also play a vital role in β-cell growth and survival, and any loss of its receptors leads to profound defects in postnatal β-cell development [224, 225]. The insulin signaling cascade is negatively regulated by protein-tyrosine phosphatases, most notably protein-tyrosine phosphatase 1B (PTP1B) and also its inhibitions were proposed as a promising strategy for the treatment of β-cell failure [226–228]. However, the question is, which one is the initial or triggering factor that drives diabetes

progression. Ensembled evidence suggests that impaired β-cell metabolism may be the earliest, as alterations in metabolic genes or metabolism were observed in isolated islets from T2D donors [31, 32], diabetic mouse models [229–231], and high glucose exposed insulin-secreting cell-lines [232, 233]. Chronic hyperglycemia also induces metabolic changes in β-cells which causes reduction of mitochondrial metabolism and ATP synthesis [38, 39]. It is reported that hyperactive glycolysis has been observed in various aged and diabetic β-cells, which results in β-cell dysfunction and loss of cellular identity [40]. Also, the perturbation of isocitrate dehydrogenase 2 (IDH2) catalyzed reductive TCA cycle flux results in impaired GSIS [234], hence may contribute to insulin secretory defects in T2D [220]. It is also reported that metabolic dysregulation, particularly amino acid dysmetabolism, is tightly associated with disease progression, from gestational diabetes mellitus to T2D [41]. L-Glutamine metabolism plays a vital role in insulin secretion either directly or via metabolism or via enhancing malate-aspartate shuttle activity [42]. Plasma levels of both glutamine and arginine were significantly reduced in patients with T2D compared to the control group [235]. Also, the exposure of free fatty acid (FFA) or lipids activates cell stress responses and FFA receptors, which results in cell damage and hampers insulin secretion [39, 43, 44, 220]. The intricacy of these results tempted us to explore the whole metabolic network and identify the key nodes that might have a pathogenic role in the progression of T2D.

The present study aims to address this void by an in-depth application of GSMM to capture the insights of β-cell metabolism in T2D. We integrated the open-source gene expression data [236] of pancreatic β-cells of ten diabetes and ten non-diabetes individuals into a generic GSMM Recon 2.04. The obtained subject-specific models were used to predict the flux states for all the individuals. We then explored these flux states to identify metabolic hot spots in reactions having altered flux rates and relating pathways and metabolites. Co-expression network analysis was also performed to determine the metabolic modules that showed disease-specific changes. We then explored the significantly correlated modules to understand the transcriptional regulation of metabolism in diabetes. Given that diabetes is a significant risk factor for cardiovascular disease (CVD) and that most of the diabetic patients in our study died from cardiovascular complications [236], therefore, we tried to capture the molecular events involved in

cardiovascular complications with relevance to the metabolic impairment of diabetic β-cells. Our analysis revealed the possible changes in the plasma metabolic profile due to the impaired metabolism of β-cell, some of which are associated with cardiovascular complications.

2.2 Material and methods

2.2.1 Transcriptomics data collection for pancreatic β-cells

Gene expression data of pancreatic β-cell profiles were obtained from https://www.ncbi.nlm.nih.gov/geo/ (accession numbers: GSE20966). The data include transcriptomics profiles of the ten control subjects and ten patients with T2D [236]. Out of ten T2D patients, the average duration of diabetes for seven patients was 5.3 years, and no information was available for the rest three. Of the ten patients with diabetes, three were treated with insulin, six were on oral antidiabetic therapy, and no therapeutic information was available for one patient. The rest of the information of the ten control subjects and ten T2D patients is available in Marselli et al. [236]. They also provided the preprocessed transcriptomic data using the DNA-chip Analyzer (dChip) software that uses the invariant set normalization algorithm.

2.2.2 Differentially expressed genes

A two-sample t-test was performed to calculate the p-values for two different phenotype groups using the 'mattest' function in MATLAB. Differentially expressed genes (DEGs) were calculated using the cut-off p-value < 0.05 and fold-change ≥ 1.2.

2.2.3 Weighted gene co-expression network analysis (WGCNA)

Co-expression networks of metabolic genes were constructed using the WGCNA package in R [237], where all the samples were considered for analysis. Pairwise Pearson correlations between gene expression levels were calculated to construct the correlation matrix. A linear transformation was applied to the obtained correlations that retain their sign using the relation. The weighted signed co-expression network was built using a soft power adjacency function called

the soft-threshold power, which ensures that the co-expression network possesses a scale-free topology. In our case, the value was 10. The weighted adjacency matrix was transformed into a topological overlap matrix (TOM), which was further used to perform the hierarchical clustering [238]. Finally, the dynamic tree cut algorithm was applied to identify the modules [239]. The values used here are 30, and 0.25 for the minimum module size and the merge cut height, respectively. The expression value of the module eigengene (ME) was calculatedusing the Singular Value Decomposition. The Pearson correlation coefficient was measured between the ME expression value and the clinical trait to obtain the most relevant modules [237]. The studied subjects' disease state (control-0, diabetic-1) was used as the clinical trait.

Transcriptional factor (TF) enrichment analysis was performed for the DEGs associated with highly correlating modules using Enrichr [240] with the help of two libraries: ChEA, and ENCODE and ChEA Consensus TFs. To obtain the TFs, we used the cut-off value of 0.05 on the p-values obtained from the enrichment analysis.

2.2.4 Reconstruction of subject-specific metabolic models

Recon 2.04 [161], a generic model of human metabolism, was used to build the subject-specific metabolic models together with the E-Flux method [193]. Recon 2.04 includes 1731 enzyme-encoding genes (2140 transcripts), 7440 metabolic reactions, and 2626 unique metabolites distributed over eight cellular compartments (cytosol, mitochondria, endoplasmic reticulum, nucleus, peroxisome, lysosome, golgi apparatus, and extracellular). Besides these, in that model, biomass-producing flux is used as an objective function.

The flux bound constraints were derived from the gene expression data according to the gene–protein–reaction (GPR) rules. These rules are included in the generic models in the form of logical expressions ('*OR*' and '*AND*' operators are used). Below is one example of GPR rules: $r = f(g_1, g_2, g_3) = g_1\ AND\ (g_2\ OR\ g_3)$, where f is the logical expression connecting the reaction r and $g1$, $g2$ and $g3$. That means the catalysing enzyme of r has two subunits: one part is translated from g_1, the remaining part can be translated from either g_2 or g_3. For the case of the E-Flux method, two mathematical operations, 'addition' and 'minimum', were applied for the 'OR' and 'AND' expressions, respectively, to calculate the numerical values for the GPR

rule values. If $a1$, $a2$ and $a3$ be the abundance of the three transcripts $g1$, $g2$ and $g3$ respectively, then according to this method the GPR rule values of r will be: $e = min(a_1,\ a_2 + a_3)$. Next, these GPR rule values of the reactions were normalized by dividing them by the maximum value among all twenty subjects. These normalized values were then used to fix the bounds of the reactions to generate the subject-specific models. These values were used to set both lower and upper bounds for reversible reactions, and only upper bounds were changed for irreversible reactions. Since there are no particular metabolic processes that have to optimize for the pancreatic beta-cells thus, we excluded the objective function from all metabolic models.

2.2.5 Estimation of sample size for solution space

Metabolic models, in general, are under-determined systems, where the number of unknowns is greater than the number of equations, which leads to an infinite number of solutions. In this context, flux balance analysis [122] is normally applied to get the flux rates of each reaction under the steady-state assumption by solving an optimization problem. In our case, the objective function was excluded from the models as there is no such particular metabolic process in beta-cell that has to optimize. Thus, to get the flux values of the reactions, we used the 'gpSampler' function, a uniform sampling technique implemented in the Constrained Based Reconstruction and Analysis (COBRA) Toolbox [205] of MATLAB along with Gurobi^{TM} Solver. In our case, 'gpSampler' helps to get the solutions of the system:

$$\frac{d\overrightarrow{x}}{dt} = S.\overrightarrow{v} = 0 \tag{2.1}$$

where, $\overrightarrow{x}$ and $\overrightarrow{v}$ are vectors of metabolite concentrations and flux values of the reactions and S is the stoichiometric matrix of size $m \times n$, m is the number of metabolites and n is the number of the reactions present in the models. Additionally, each component v_i is bounded by the inequality $v_{i_{min}} \leqslant v_i \leqslant v_{i_{max}}, \forall i \in \{1, 2, \cdots, n\}$ and the bounds are defined earlier.

In this system, the number of unknowns is greater than the number of equations, which leads to an infinite number of solutions. All the computational approaches provide a finite number of solutions from the solution space, so the solutions' mean can be used for further analysis. It was

found that the mean is always dependent on the sample size. Thus it demands the appropriate sample size prediction to obtain the true mean of the solutions. Here, we iteratively varied the sample size and captured the mean values obtained from the sampling. The Euclidean distances between the mean flux values for different sample sizes are depicted in **Fig. 2.1**. Around the sample size of 130k, the Euclidean distances between the consecutive means become negligible. It depicts that the mean is not changing too much after crossing the sample size of 130k. To check the robustness of this predicted sample size (130k), we also calculated the mean flux states of 120k, 130k, and 140k solutions for two independent subject-specific metabolic models (given in **Fig. 2.2**) and found that the Euclidean distances are significantly less for both these models. Thus, this value was used here as the sample size to perform the uniform sampling for all the metabolic models.

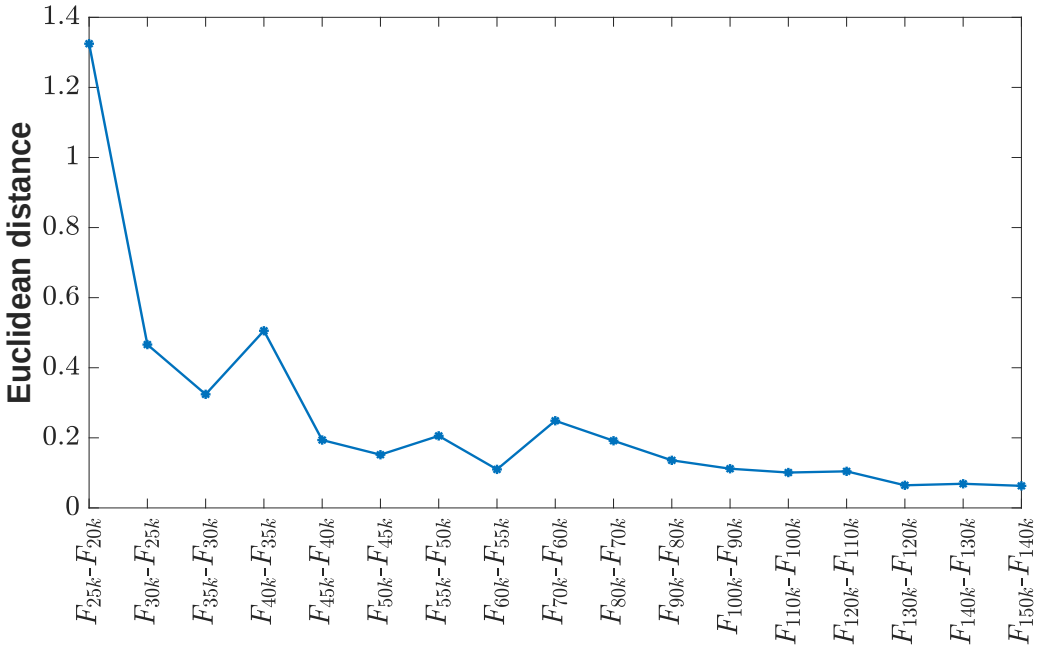

Figure 2.1: **The euclidean distances between the mean flux values for different sample sizes.** Around the sample size 130k, mean distances become very less (less than 0.1). Here, the yellow bar represents the value 0.1.

2.2.6 Identifying significantly altered metabolic reactions

We performed the uniform sampling for each model, and the mean of the 130k solutions was selected for the possible flux state. Here, we obtained the flux rates of each 7440 reactions for

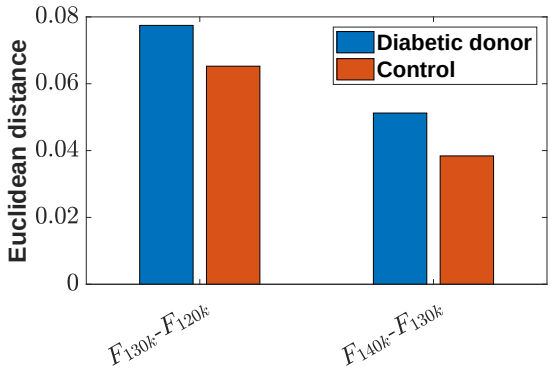

Figure 2.2: **This figure shows the Euclidean distances between the mean flux (MF) values of three consecutive sample sizes 120k, 130k, and 140k.** We performed this exercise for two independent subject-specific metabolic models (one for diabetic and another for control). All of these values are less than 0.1.

every pancreatic β-cell of the ten control subjects and ten patients with T2D. A two-sample t-test was performed to calculate the p-values for two different clinical groups using the 'mattest' function in MATLAB. Significantly altered metabolic reactions were calculated using the cut-off p-value < 0.05 and fold-change ≥ 1.2.

2.2.7 Reporter pathway analysis

To obtain the significantly altered pathways, we performed the reporter pathways analysis [241]. Applying the inverse normal cumulative distribution function (CDF), the p-values ($p_{reaction}$) obtained for each reaction from the t-test were transformed into the Z-scores ($Z_{reaction}$). Pathways were assigned a Z-scores ($Z_{pathway}$) by aggregating the Z-scores of the involved reactions by the relation [241]:

$$Z_{pathway} = \frac{1}{\sqrt{r}} \sum_{reaction=1}^{r} Z_{reaction},\ r = \text{No. of reactions.}$$

Finally, the Z-scores were transformed into p-values by using CDF, and the pathways having p-values < 0.05 were considered as reporter pathways.

2.2.8 Notes on statistical analysis

MATLAB 9.4 (2018a) version was used for all the statistical analysis and the model construction. The 'mattest' function was used to perform the two-sample t-test, in which the *p*-values and *t*-scores were calculated using permutation tests (1000 permutations). The COBRA Toolbox with solver Gurobi^{TM} (version 9.0.1) was used for the uniform sampling of the solutions. WGCNA was performed in R version 4.1.0. The R package 'ggplot2' was used to create the bubble and the circular bar plots. The codes used here can be found in the GitHub repository: https://github.com/AbhijitPaul1993/Beta-cell_GSMM.

2.3 Result

2.3.1 Co-expression of metabolic genes

We investigated the changes in the expression profiles of the enzyme-coding genes in diabetes and found 117 up- and 72 down-regulated genes (p-value$<$0.05 & fold change cut off 1.2). The pathways involved in these genes are summarized in **Table 2.1**. It is apparent from the literature that the significant genes in a disease state always exhibit some inherent expression pattern. Its identification often leads to discovering crucial modules of the disease under investigation. We employed Weighted Gene Co-expression Network Analysis (WGCNA) to capture these modules, which constructs a co-expression network based on the pairwise correlation between genes.

The WGCNA of metabolic genes within all the samples gave four metabolic modules of co-expressed genes, and of these, Module 1 contains the highest number of genes, and module 4 contains the lowest number of genes (see **Table 2.2**). We captured the variations of these modules within the samples, and the correlation between the module Eigen gene (ME) expression value and the disease state were given in **Table 2.2**. We observed that Modules 2, 3, 4 positively correlate with the disease state, and Module 1 negatively correlates. Only Module 2 shows a significant correlation, and also it contains the majority (108 out of 189) of the differentially expressed metabolic genes (DEMGs). Module 2 was found up-regulated in all the

disease samples, while the other modules showed a heterogeneous behavior in different samples (**Fig. 2.3**). The major metabolic pathways associated with each module were also provided in **Table 2.2**.

Table 2.1: **Metabolic pathways containing the differentially expressed genes (DEG).** DEGs were identified using the p-value cut-off < 0.05 and fold change cut-off 1.2.

Pathways	**Up-regulated genes**	**Down-regulated genes**
Alanine and aspartate metabolism	ASS1	
Aminosugar metabolism	RENBP, UAP1L1, GALE, GFPT2	PGM3, GFPT1
Androgen and estrogen synthesis and metabolism		CYP2S1
Arachidonic acid metabolism	CBR3	GPX7, ALOX5, CYP2S1
Arginine and Proline Metabolism	PRODH2, MAOA, ALDH1B1	PRODH
Bile acid synthesis	CH25H, BAAT, ALDH1B1	SLC27A2, ACOT1, ACOT2
Biotin metabolism	BTD	
Butanoate metabolism	ECHDC2	
Cholesterol metabolism	LSS	HMGCR, AACS
Chondroitin sulfate degradation	GUSB, CTSA	
Chondroitin synthesis	NDST3, B3GALT6	HS3ST5, HS6ST2, EXTL1
Citric acid cycle	IDH2	DLD
CoA catabolism	ACP2, VNN1	
Cysteine Metabolism	TST	
D-alanine metabolism	SLC16A7	
Eicosanoid metabolism	CBR3, BAAT, PTGES, DECR2, ALDH1B1	SLC27A2, ACOX1, ACOT2, ACOT1, HADH, ALOX5, CYP2S1
Exchange/demand reaction	SERPINA3, SERPINA1, APOC3	GYG2, TXN

Fatty acid oxidation	FASN, CPT1B, IDH2, CRAT, PPT2, DECR2	SLC27A2, ACOX1, ACOT2, ACOT1, HACL1, HADH, DBI
Fatty acid synthesis	FASN, BAAT, CTSA	ACOT2, ACOT1
Folate metabolism	MTHFD2, MTHFR	MTHFS
Fructose and mannose metabolism	GMPPB	PGM2
Galactose metabolism	GALE, CTSA	
Glutamate metabolism	GAD1, ALDH1B1	
Glutathione metabolism	OPLAH	GPX7, PRDX3
Glycerophospholipid metabolism	CHAT, PLA2G1B, CHKB, DGKB, PLA2G6, PAFAH1B2	DGKD, SGPL1, PAFAH2
Glycine, serine, alanine and threonine metabolism	PSAT1, CHDH	DLD
Glycolysis/gluconeogenesis	PCK1, ALDH1A3, LDHA, ENO3, ALDH1B1	AACS, PGM2, GPD2, DLD, RWDD2A
Glycosphingolipid metabolism		B4GALT6
Glyoxylate and dicarboxylate metabolism	ALDH1A3, LDHA, ALDH1B1	
Heme synthesis		FECH
Heparan sulfate degradation	GUSB	
Histidine metabolism	ALDH1A3, ALDH1B1	
Hyaluronan metabolism	GUSB	
Inositol phosphate metabolism	INPPL1, INPP5J	PIK3CB, PIK3R5
Keratan sulfate degradation	CTSA	
Limonene and pinene degradation	ALDH1B1	

Linoleate metabolism	UGT2B15, UGT2B28	
Lysine metabolism	PLOD2	SPCS2, DLD
Methionine and cysteine metabolism	CBS, LDHA, MAT1A	MAT2B
Miscellaneous	CPA2, CYP21A2, TST, CPA1, GUSB, CA12, UGT2B15, UGT2B28	NLN, DLD
N-glycan degradation	CTSA	
N-glycan synthesis	MAN1B1, MOGS, FUT8	ALG10
NAD metabolism	QPRT	
Nucleotide interconversion	NT5M, ENTPD6, NME4, PDE7A, AK1, PDE4C, ADCY6	DTYMK, NME7, AMPD3, ENTPD3, ADK
Nucleotide sugar metabolism		TGDS
O-glycan synthesis	GALNT7, GALNT5	GALNT14, GCNT1
Oxidative phosphorylation	COX5B	GPD2
Pentose phosphate pathway	G6PD	PGM2, PRPS1
Phenylalanine metabolism	ALDH1A3, TAT, MAOA	
Phosphatidylinositol phosphate metabolism		PIGA, PIK3CB
Propanoate metabolism	LDHA, ACSS3	AACS, DLD
Purine catabolism	NT5M, ACP2	ENTPD3
Purine synthesis		PAICS
Pyrimidine catabolism	DPYSL3, ACP2	UPB1, ENTPD3
Pyrimidine synthesis	NME4	DTYMK
Pyruvate metabolism	ALDH1A3, LDHA, ALDH1B1	ME1
ROS detoxification	SOD3	
Selenoamino acid metabolism	CBS, FMO2, MAT1A	MAT2B

Sphingolipid metabolism	ST6GALNAC6, CTSA, SMPD2, ARSA, GBGT1	SGPL1
Squalene and cholesterol synthesis		HMGCR
Starch and sucrose metabolism	AMY1A, AMY1B, AMY1C, AMY2A, ATHL1	GYG2
Steroid metabolism	CYP21A2, UGT2B28	SRD5A2
Taurine and hypotaurine metabolism	GAD1	
Tetrahydrobiopterin metabolism	TPH2	HADH
Transport, endoplasmic reticular	ABCC1	SLC37A4
Transport, extracellular	SLC24A3, AQP1, AQP8, SLC22A3, SLC26A9, SLC4A1, SLC16A7, PRODH2, SLC52A2, SLC5A2, ATP1B3, ABCC5, SLC2A14, RBP1, SLC17A7, LCO2B1, SLC7A7, ABCC1	SLC6A1, SLC2A2, SLC6A14, TMEM27, SLC27A2, SLC5A1, SLC4A8, SLC1A2, SLC18A2, SLC6A10P, ABCC8, SLC14A2, AQP2, LRP2
Transport, lysosomal	SLC29A3	SLC17A5, ATP6V1A
Transport, mitochondrial	AQP8, SLC16A7, SLC25A13	MMAA, SLC25A14
Transport, peroxisomal	CRAT	
Triacylglycerol synthesis	CEL, PNLIP, PNLIPRP1	
Tryptophan metabolism	IDO2, AOX1, TPH2, MAOA, ALDH1B1	HADH, INMT
Tyrosine metabolism	TYRP1, ALDH1A3, COMTD1, TAT, UGT2B15, UGT2B28, MAOA	SULT4A1
Unassigned	CEL, ALDH1A3, CBS, IDH2, AOX1, CA12, ALDH1B1, ACSS3	ACOX1, PRODH

Urea cycle		ODC1
Valine, leucine, and isoleucine metabolism	PCCA, ALDH1B1	HADH, DLD
Vitamin A metabolism	UGT2B15, UGT2B28	
Vitamin B12 metabolism		MMAA
Vitamin B6 metabolism	AOX1	
Vitamin C metabolism	ALDH1A3, GLRX, ALDH1B1	
Xenobiotics metabolism		CYP2S1
beta-Alanine metabolism	GAD1, ALDH1B1	

Module 2 contains the genes associated with fatty acid oxidation, eicosanoid and glycerophospholipid metabolism, glycolysis and gluconeogenesis, etc., and some extracellular transporters (**Table 2.2**). This module includes the dysregulated genes found in triacylglycerol synthesis (CEL, PNLIP, PNLIPRP1), pentose phosphate and glycolytic pathways (G6PD, PGM2, PRPS1), ROS detoxification (SOD3), sphingolipid metabolism (ST6GALNAC6, SGPL1), starch /glycogen and sucrose metabolism (salivary amylase genes, AMY1A, AMY1B, and AMY1C, pancreatic amylase gene, AMY2A and acid trehalase-like protein 1, ATHL1) and bile acid synthesis (CH25H, BAAT, ACOT1, ACOT2). This module also contains the dysregulated genes associated with amino acids, histidine, arginine, proline, tryptophan, valine, leucine, isoleucine, glycine, serine, alanine, and threonine metabolism; the expressions of ALDH1A3, LDHA, PRODH2, IDO2, AOX1, PCCA, PSAT1, CHDH genes were up-regulated whereas expressions of PRODH, and HADH were down-regulated in β-cell samples from patients with diabetes.

Table 2.2: **The correlation between module eigengene (ME) expression value and disease state.** p-values corresponding to each Pearson correlation coefficient are provided in the parentheses. Metabolic pathways associated with each module and the number of differentially expressed metabolic genes (DEMGs) are also mentioned.

Module (Size)	**Disease state (p-value)**	**DEGs (Up, Down)**	**Pathways (No. of genes)**

Module 1 (287)	-0.34 (0.1)	21 (3, 18)	Transport, extracellular (28); Fatty acid oxidation (24); Oxidative phosphorylation (22); Nucleotide interconversion (20); Unassigned (17); Valine, leucine, and isoleucine metabolism (14)
Module 2 (240)	0.78 ($5e^{-5}$)	108 (75, 33)	Transport, extracellular (37); Fatty acid oxidation (21); Unassigned (19); Miscellaneous (15); Eicosanoid metabolism (15); Glycerophospholipid metabolism (13); Nucleotide interconversion (13); Glycolysis/gluconeogenesis (10)
Module 3 (162)	0.18 (0.4)	10 (10, 0)	Oxidative phosphorylation (18); Nucleotide interconversion (16); Transport, extracellular (16); Eicosanoid metabolism (8); Unassigned (8); Glutathione metabolism (7)
Module 4 (73)	0.21 (0.4)	6 (5, 1)	Oxidative phosphorylation (9); Glycolysis/gluconeogenesis (7); Transport, extracellular (7); N-glycan synthesis (6); Sphingolipid metabolism (5)

By performing the transcriptional factor (TF) enrichment analysis, we found that 11 and 16 TFs, respectively, were associated with the up-and down-regulated genes of Module 2 (p-value$<$0.05). Among these, the protein products of TP63, HNF4A, RELA, STAT3, NR1H3, GATA3, STAG1 (SA1), FOXO3, and ESR1 TFs regulate the expression of elevated genes involved in fatty acid, pyruvate and amino acid metabolism, glycolysis/glucone- ogenesis, and triacylglycerol synthesis. In contrast, the TFs E2F1, SMAD2, SMAD3, FOXH1, NR1H3, ARNT, AHR, CLOCK, FOXM1, TCF3 (E2A), SPI1, and SOX11 regulate the expression of attenuated genes whose protein (enzyme) products participate in fatty acid and sphingolipid metabolism,

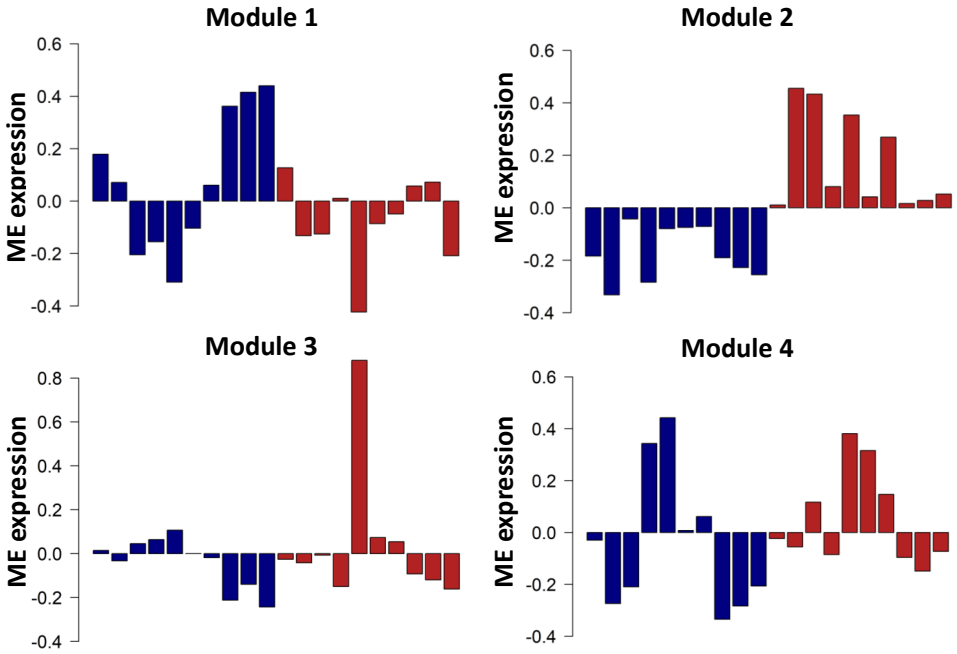

Figure 2.3: **Module eigengene (ME) expression profile of metabolic modules.** The *x*-axis represents samples for different disease profiles (control-blue, diabetes-red), and the *y*-axis represents ME expression values.

glycolysis/gluconeogenesis, oxidative phosphorylation, pentose phosphate pathway, and urea cycle. Functional impairment of HNF4 Adue to mutation can cause maturity-onset diabetes of the young 1 (early-onset type 2 diabetes) [242, 243], but sometimes it can also cause hyperinsulinemic hypoglycemia [243, 244]. Activating mutations in STAT3 can lead to neonatal diabetes accompanied by beta-cell failure, and also its inhibition has been proposed as cell therapy for ameliorating hyperglycemia in diabetes [245]. It is reported that RELA is necessary for maintaining healthy glucose metabolism as its deletion results in loss of insulin secretion [246]. Also, the activation of ESR1 inhibits lipogenesis in beta-cell by suppressing fatty acid synthase expression [247]. GATA3 regulates the genes involved in fatty acid metabolism, amino acid metabolism, glycolysis/gluconeogenesis as well as triacylglycerol synthesis (pancreatic lipase-related protein 1), and its inhibition has been proposed as a therapeutic strategy in obesity-associated insulin resistance and type 2 diabetes [248]. Liver X Receptor α (NR1H3) was found to be a regulator of the dysregulated genes in fatty acid, amino acid, glucose metabolism, and pentose phosphate pathway. It is also reported that liver X Receptors can control insulin secretion and biosynthesis via regulation of glucose and lipid metabolism, but its hyperactivation can lead to lipogenesis with the combination of the LXR/RXR agonists, resulting in reduced

glucose-induced insulin secretion [249]. Here we found that FOXM1, SMAD2, and SMAD3 regulate the expression of genes involved in glycolysis (GPD2) and sphingolipid metabolism (SGPL1). FOXM1 transcriptional program plays a key role in the proliferation of beta-cells, and it is reported that nondiabetic obesity increases the expression of FOXM1, resulting in the increased beta-cell mass, but in diabetic strain, this up-regulation was found to be absent [250]. Activation of SMAD3 reduces insulin production and secretion, whereas inactivation increases glucose-stimulated insulin secretion [251], and SMAD2 disruption leads to impaired glucose tolerance with reduced activity of the K_{ATP} channels [252]. ARNT and E2F1 regulate genes involved in glycolysis (GPD2) and pentose phosphate pathway (PRPS1), and also their expression is decreased in diabetic human islets [253, 254]. Impaired glucose tolerance and abnormal insulin secretion were observed in beta-cell-specific ARNT knockout mice [253] and E2F1 deficient mice, and pancreatic islets [255]. CLOCK and FOXH1 regulate the expression of genes involved in lipid metabolism (ACOT1/ACOX1), sphingolipid metabolism (SGPL1), and pentose phosphate pathway (PRPS1). It has been reported that disruption of CLOCK expression leads to impairment of mitochondrial function, oxidative stress in beta-cell and impaired GSIS, and finally, diabetes [256].

2.3.2 Significant alterations in metabolic flux states

We predicted the metabolic-flux level profile of pancreatic β-cells for ten control and ten T2D subjects by integrating the gene expression data on Recon 2.04. Metabolic tasks are a widely used approach for assessing the technical quality of the reconstructed models [257, 258]. It analyzes a particular set of organ-specific metabolic functions like ATP yields on various carbon sources under aerobic and anaerobic conditions, and production of lipids and vitamins. To evaluate our model, we performed 74 pancreas-specific metabolic tasks as defined in Thiele et al. [257] and found that all the models show 96% of these tasks. The significantly altered pathways obtained from comparing metabolic-flux profiles between the diabetic and control subjects are shown in **Fig. 2.4A**.

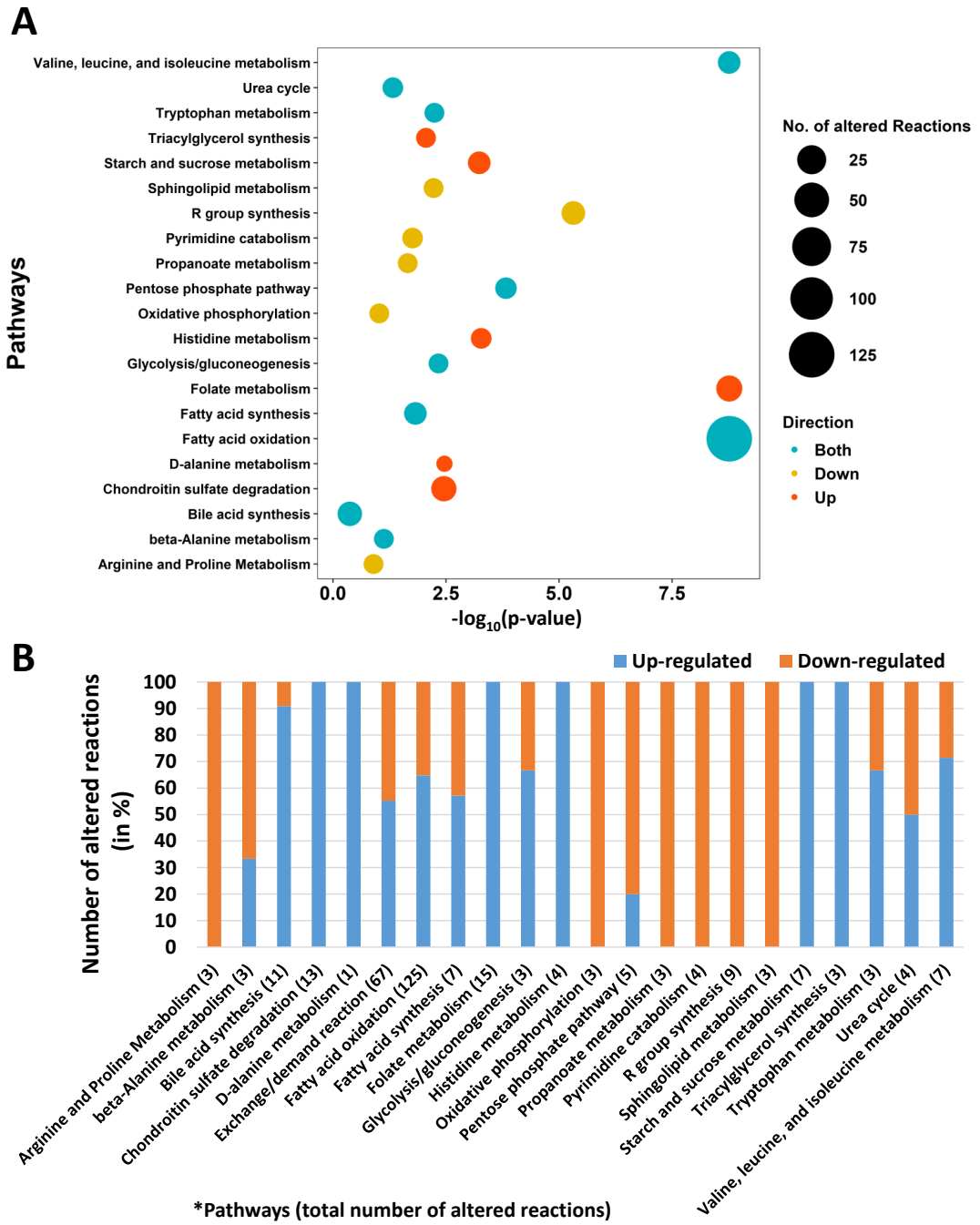

Figure 2.4: **Significantly altered metabolic pathways.** (A) Reporter pathways analysis was performed here to obtain the significantly altered pathways, and the corresponding cut-off p-value < 0.05. (B) Up- and down-regulated reactions were obtained by comparing the flux values in diabetic subjects with respect to the control subjects. The cut-off p-value and fold change are 0.05 and 1.2, respectively. The total number of obtained altered reactions for each pathway is provided in the parentheses.

We noticed that all the altered reactions in arginine and proline metabolism, oxidative phosphorylation, propionate metabolism, pyrimidine catabolism, R group synthesis, and sphingolipid metabolism are down-regulated. Whereas only up-regulated fluxes were observed in

chondroitin sulfate degradation, folate metabolism, histidine metabolism, triacylglycerol synthesis, starch, and sucrose metabolism. Fatty acid oxidation was found as a highly perturbed pathway in diabetic conditions, which exhibited both up-and down-regulated reactions. However, up-regulated reactions (65%) are higher than down-regulated ones (**Fig. 2.4B**). In the diseased state, peroxisomal fatty acid beta-oxidation was found to be up-regulated, whereas mitochondrial and cytosolic fatty acid oxidation was attenuated. The reactions associated with peroxisomal H_2O_2 production had higher flux rates in diabetic conditions, while the mitochondrial NADH and $FADH_2$ producing reactions had significantly lower fluxes (**Fig. 2.5**). We also observed alterations in fatty acid transport within the cellular compartments such as peroxisome, cytoplasm, and extracellular space.

For the triacylglycerol synthesis pathway, we noted increased flux rates for the carboxyl ester lipase (CEL, previously named cholesterol esterase or bile salt-stimulated [or dependent] lipase) catalyzed hydrolysis of triglyceride (**Fig. 2.6**). This enzyme is a lipolytic enzyme capable of hydrolyzing cholesteryl esters, tri-, di-, and monoacylglycerols, phospholipids, lypophospholipids, and ceramide enzymes. No significant changes in the metabolism of CEL-generated triacylglycerol metabolites were observed in this process. However, it did show alterations in their transport rates from the cytoplasm to the extracellular space. Reduced flux rates were also observed in the oxidative phosphorylation pathway for two reactions, coenzyme Q:cytochrome C - oxidoreductase (mitochondrial complex III) and cytochrome C oxidase (mitochondrial complex IV) (see **Fig. 2.7**).

A significant perturbation of amino acid metabolism, which plays a crucial role in insulin secretion either directly or indirectly [42], was observed here (**Figs. 2.6** and **2.7**). High flux rates for two reactions (choline dehydrogenase and betaine-aldehyde dehydrogenase) involved in glycine, serine, alanine, and threonine metabolism were observed, and also the level of choline dehydrogenase (CHDH) was up-regulated. Consequently, elevated glycine betaine production flux from choline was observed and further transported to extracellular space. In addition, histidine metabolism pathway was found up-regulated. In this case, higher flux rates from L-histidine (his_L) to 5-formimino tetrahydrofolic acid (5forthf) were observed. The beta-alanine and alpha-ketoglutaric acid (akg) production flux reduction from glutamic acid

and malonic semialdehyde (msa) was observed in the beta-alanine metabolism pathway. This reduction might be the result of the downregulation of ACOT1 and ACOT2, leading to lower conversion rates of propionic acid to propionyl-CoA (bile acid synthesis pathway). A series of metabolic reactions were altered that participate in bile acid synthesis, propanoate, beta-alanine metabolism, and CoA biosynthesis pathways, leading to reduced fluxes from propionyl-CoA to malonic semialdehyde. Also, the reduced uptake flux of propionic acid was observed here.

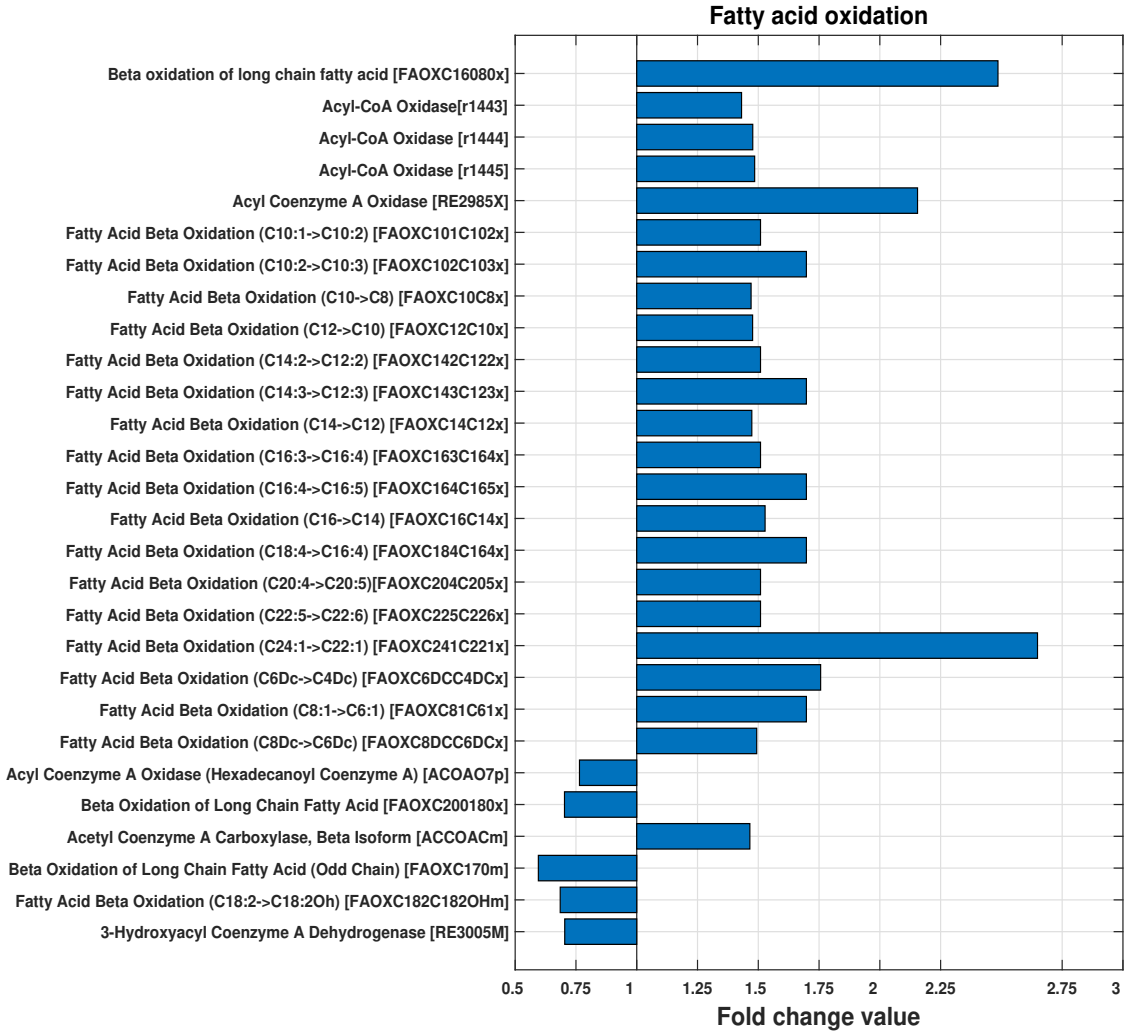

Figure 2.5: **Alteration in fatty acid oxidation pathway related to H_2O_2 and ATP production.** H_2O_2 producing reactions in the peroxisomal compartment are shown at the panel's top row. The last four reactions (in the panel) are associated with mitochondrial ATP, NADH, and $FADH_2$ production. The fold change values for the up-and down-regulated reactions are displayed on the right and left sides of value 1, respectively. These fold-changes were calculated by comparing the median flux values of the diabetic group with respect to the control.

The level of beta-alanine was compensated by the higher conversion rate from aspartic acid (see beta-alanine metabolism in **Figs. 2.6** and **2.7**). In the tryptophan metabolism pathway, a

higher production flux of serotonin from tryptophan was observed due to the higher expression of TPH2. We also found alterations in the arginine, proline, valine, leucine, and isoleucine metabolic pathways.

In the starch and sucrose metabolic pathways, higher flux rates were observed for pancreatic α-amylase, and the corresponding genes were up-regulated in patients with diabetes compared to the control subjects. Pancreatic α-amylase synthesized by pancreatic acinal cells and secreted into the duodenum as a major component of pancreatic fluid catalyzes the initial step of hydrolysis of α-linked polysaccharides (like starch and glycogen) for glucose production in the small intestine. The elevated pancreatic α-amylase may contribute to increased blood glucose levels. Interestingly, its inhibitors have been suggested as potential antidiabetic agents [259]. Reactions of pentose phosphate pathway (PPP), which derives glycolysis in the cytoplasm, were found significantly decreased in diabetic patients, causing reduced yield of ribulose 5-phosphate and NADPH; ribulose 5-phosphate serves as a precursor for nucleotide synthesis by proliferating cells, and NADPH is utilized for lipogenesis and glutathione regeneration by glutathione reductase. Also, a reduced flux rate was observed in the rates of conversion of malate to pyruvate catalyzed by cytosolic malic enzyme 1 (ME1) along with concomitant NADPH production. We also observed an elevated expression of extracellular superoxide dismutase 3 (SOD3), which protects the extracellular space from the toxic effect of ROS intermediates by converting superoxide radicals into hydrogen peroxide and oxygen. However, no significant changes were observed in the expression of SOD1 and SOD2.

Sphingolipids play an important role in glucolipotoxicity-induced apoptosis. It also influences β-cell physiology by regulating proinsulin folding and insulin secretion [260, 261]. In the sphingolipid metabolism, conversion fluxes of cytosolic and ER O- Phosphorylethanolamine (Abbreviation used in Recon 2.04 for O- Phosphorylethanolamine: ethamp) and cytosolic palmitaldehyde (Abbreviation used in Recon 2.04 is: hxdcal) from sphinganine 1-phosphate (Abbreviation used in Recon 2.04 is: sph1p) were found down-regulated. Also, the accumulation of O- Phosphorylethanolamine in ER and the flux rate of sphinganine-1-phosphate pamlmitaldehyde-lyase (glycerophospholipid metabolism), which produces sphinganine 1- phosphate from O-Phosphorylethanolamine and palmitaldehyde, were significantly suppressed.

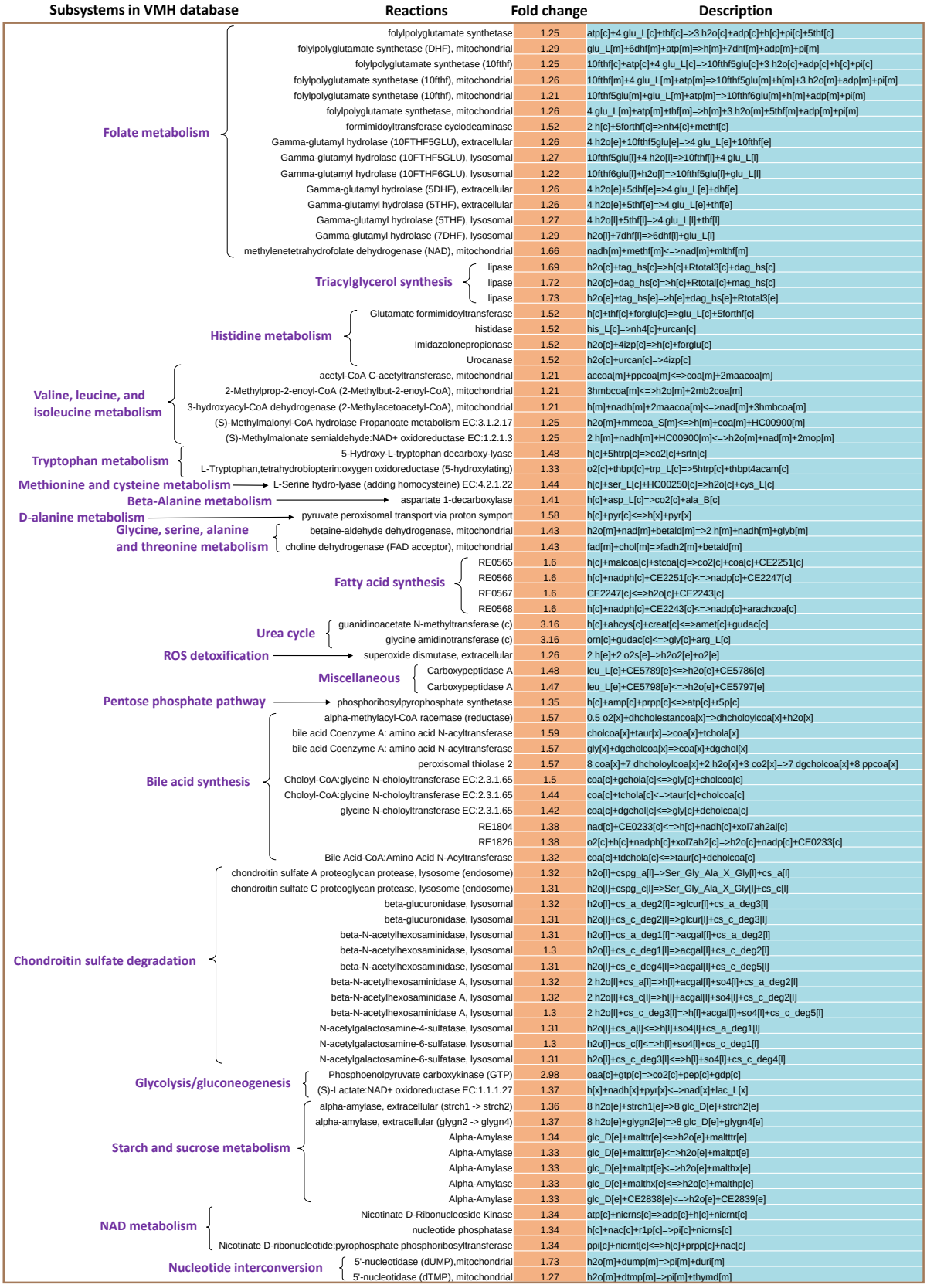

Subsystems in VMH database	Reactions	Fold change	Description
Folate metabolism	folylpolyglutamate synthetase	1.25	atp[c]+4 glu_L[c]+thf[c]=>3 h2o[c]+adp[c]+h[c]+pi[c]+5thf[c]
	folylpolyglutamate synthetase (DHF), mitochondrial	1.29	glu_L[m]+6dhf[m]+atp[m]=>h[m]+7dhf[m]+adp[m]+pi[m]
	folylpolyglutamate synthetase (10fthf)	1.25	10fthf[c]+atp[c]+4 glu_L[c]=>10fthf5glu[c]+3 h2o[c]+adp[c]+h[c]+pi[c]
	folylpolyglutamate synthetase (10fthf), mitochondrial	1.26	10fthf[m]+4 glu_L[m]+atp[m]=>10fthf5glu[m]+h[m]+3 h2o[m]+adp[m]+pi[m]
	folylpolyglutamate synthetase (10fthf), mitochondrial	1.21	10fthf5glu[m]+glu_L[m]+atp[m]=>10fthf6glu[m]+h[m]+adp[m]+pi[m]
	folylpolyglutamate synthetase, mitochondrial	1.26	4 glu_L[m]+atp[m]+thf[m]=>h[m]+3 h2o[m]+5thf[m]+adp[m]+pi[m]
	formimidoyltransferase cyclodeaminase	1.52	2 h[c]+5forthf[c]=>nh4[c]+methf[c]
	Gamma-glutamyl hydrolase (10FTHF5GLU), extracellular	1.26	4 h2o[e]+10fthf5glu[e]=>4 glu_L[e]+10fthf[e]
	Gamma-glutamyl hydrolase (10FTHF5GLU), lysosomal	1.27	10fthf5glu[l]+4 h2o[l]=>10fthf[l]+4 glu_L[l]
	Gamma-glutamyl hydrolase (10FTHF6GLU), lysosomal	1.22	10fthf6glu[l]+h2o[l]=>10fthf5glu[l]+glu_L[l]
	Gamma-glutamyl hydrolase (5DHF), extracellular	1.26	4 h2o[e]+5dhf[e]=>4 glu_L[e]+dhf[e]
	Gamma-glutamyl hydrolase (5THF), extracellular	1.26	4 h2o[e]+5thf[e]=>4 glu_L[e]+thf[e]
	Gamma-glutamyl hydrolase (5THF), lysosomal	1.27	4 h2o[l]+5thf[l]=>4 glu_L[l]+thf[l]
	Gamma-glutamyl hydrolase (7DHF), lysosomal	1.29	h2o[l]+7dhf[l]=>6dhf[l]+glu_L[l]
	methylenetetrahydrofolate dehydrogenase (NAD), mitochondrial	1.66	nadh[m]+methf[m]<=>nad[m]+mlthf[m]
Triacylglycerol synthesis	lipase	1.69	h2o[c]+tag_hs[c]=>h[c]+Rtotal3[c]+dag_hs[c]
	lipase	1.72	h2o[c]+dag_hs[c]=>h[c]+Rtotal[c]+mag_hs[c]
	lipase	1.73	h2o[e]+tag_hs[e]=>h[e]+dag_hs[e]+Rtotal3[e]
Histidine metabolism	Glutamate formimidoyltransferase	1.52	h[c]+thf[c]+forglu[c]=>glu_L[c]+5forthf[c]
	histidase	1.52	his_L[c]=>nh4[c]+urcan[c]
	Imidazolonepropionase	1.52	h2o[c]+4izp[c]=>h[c]+forglu[c]
	Urocanase	1.52	h2o[c]+urcan[c]=>4izp[c]
Valine, leucine, and isoleucine metabolism	acetyl-CoA C-acetyltransferase, mitochondrial	1.21	accoa[m]+ppcoa[m]<=>coa[m]+2maacoa[m]
	2-Methylprop-2-enoyl-CoA (2-Methylbut-2-enoyl-CoA), mitochondrial	1.21	3hmbcoa[m]<=>h2o[m]+2mb2coa[m]
	3-hydroxyacyl-CoA dehydrogenase (2-Methylacetoacetyl-CoA), mitochondrial	1.21	h[m]+nadh[m]+2maacoa[m]<=>nad[m]+3hmbcoa[m]
	(S)-Methylmalonyl-CoA hydrolase Propanoate metabolism EC:3.1.2.17	1.25	h2o[m]+mmcoa_S[m]<=>h[m]+coa[m]+HC00900[m]
	(S)-Methylmalonate semialdehyde:NAD+ oxidoreductase EC:1.2.1.3	1.25	2 h[m]+nadh[m]+HC00900[m]<=>h2o[m]+nad[m]+2mop[m]
Tryptophan metabolism	5-Hydroxy-L-tryptophan decarboxy-lyase	1.48	h[c]+5htrp[c]=>co2[c]+srtn[c]
	L-Tryptophan,tetrahydrobiopterin:oxygen oxidoreductase (5-hydroxylating)	1.33	o2[c]+thbpt[c]+trp_L[c]=>5htrp[c]+thbpt4acam[c]
Methionine and cysteine metabolism →	L-Serine hydro-lyase (adding homocysteine) EC:4.2.1.22	1.44	h[c]+ser_L[c]+HC00250[c]=>h2o[c]+cys_L[c]
Beta-Alanine metabolism →	aspartate 1-decarboxylase	1.41	h[c]+asp_L[c]=>co2[c]+ala_B[c]
D-alanine metabolism →	pyruvate peroxisomal transport via proton symport	1.58	h[c]+pyr[c]<=>h[x]+pyr[x]
Glycine, serine, alanine and threonine metabolism	betaine-aldehyde dehydrogenase, mitochondrial	1.43	h2o[m]+nad[m]+betald[m]=>2 h[m]+nadh[m]+glyb[m]
	choline dehydrogenase (FAD acceptor), mitochondrial	1.43	fad[m]+chol[m]=>fadh2[m]+betald[m]
Fatty acid synthesis	RE0565	1.6	h[c]+malcoa[c]+stcoa[c]=>co2[c]+coa[c]+CE2251[c]
	RE0566	1.6	h[c]+nadph[c]+CE2251[c]<=>nadp[c]+CE2247[c]
	RE0567	1.6	CE2247[c]<=>h2o[c]+CE2243[c]
	RE0568	1.6	h[c]+nadph[c]+CE2243[c]<=>nadp[c]+arachcoa[c]
Urea cycle	guanidinoacetate N-methyltransferase (c)	3.16	h[c]+ahcys[c]+creat[c]<=>amet[c]+gudac[c]
	glycine amidinotransferase (c)	3.16	orn[c]+gudac[c]<=>gly[c]+arg_L[c]
ROS detoxification →	superoxide dismutase, extracellular	1.26	2 h[e]+2 o2s[e]=>h2o2[e]+o2[e]
Miscellaneous	Carboxypeptidase A	1.48	leu_L[e]+CE5789[e]<=>h2o[e]+CE5786[e]
	Carboxypeptidase A	1.47	leu_L[e]+CE5798[e]<=>h2o[e]+CE5797[e]
Pentose phosphate pathway →	phosphoribosylpyrophosphate synthetase	1.35	h[c]+amp[c]+prpp[c]<=>atp[c]+r5p[c]
Bile acid synthesis	alpha-methylacyl-CoA racemase (reductase)	1.57	0.5 o2[x]+dhcholestancoa[x]=>dhcholoylcoa[x]+h2o[x]
	bile acid Coenzyme A: amino acid N-acyltransferase	1.59	cholcoa[x]+taur[x]=>coa[x]+tchola[x]
	bile acid Coenzyme A: amino acid N-acyltransferase	1.57	gly[x]+dgcholcoa[x]=>coa[x]+dgchol[x]
	peroxisomal thiolase 2	1.57	8 coa[x]+7 dhcholoylcoa[x]+2 h2o[x]+3 co2[x]=>7 dgcholcoa[x]+8 ppcoa[x]
	Choloyl-CoA:glycine N-choloyltransferase EC:2.3.1.65	1.5	coa[c]+gchola[c]<=>gly[c]+cholcoa[c]
	Choloyl-CoA:glycine N-choloyltransferase EC:2.3.1.65	1.44	coa[c]+tchola[c]<=>taur[c]+cholcoa[c]
	glycine N-choloyltransferase EC:2.3.1.65	1.42	coa[c]+dgchol[c]<=>gly[c]+dcholcoa[c]
	RE1804	1.38	nad[c]+CE0233[c]<=>h[c]+nadh[c]+xol7ah2al[c]
	RE1826	1.38	o2[c]+h[c]+nadph[c]+xol7ah2[c]=>h2o[c]+nadp[c]+CE0233[c]
	Bile Acid-CoA:Amino Acid N-Acyltransferase	1.32	coa[c]+tdchola[c]<=>taur[c]+dcholcoa[c]
Chondroitin sulfate degradation	chondroitin sulfate A proteoglycan protease, lysosome (endosome)	1.32	h2o[l]+cspg_a[l]=>Ser_Gly_Ala_X_Gly[l]+cs_a[l]
	chondroitin sulfate C proteoglycan protease, lysosome (endosome)	1.31	h2o[l]+cspg_c[l]=>Ser_Gly_Ala_X_Gly[l]+cs_c[l]
	beta-glucuronidase, lysosomal	1.32	h2o[l]+cs_a_deg2[l]=>glcur[l]+cs_a_deg3[l]
	beta-glucuronidase, lysosomal	1.31	h2o[l]+cs_c_deg2[l]=>glcur[l]+cs_c_deg3[l]
	beta-N-acetylhexosaminidase, lysosomal	1.31	h2o[l]+cs_a_deg1[l]=>acgal[l]+cs_a_deg2[l]
	beta-N-acetylhexosaminidase, lysosomal	1.3	h2o[l]+cs_c_deg1[l]=>acgal[l]+cs_c_deg2[l]
	beta-N-acetylhexosaminidase, lysosomal	1.31	h2o[l]+cs_c_deg4[l]=>acgal[l]+cs_c_deg5[l]
	beta-N-acetylhexosaminidase A, lysosomal	1.32	2 h2o[l]+cs_a[l]=>h[l]+acgal[l]+so4[l]+cs_a_deg2[l]
	beta-N-acetylhexosaminidase A, lysosomal	1.32	2 h2o[l]+cs_c[l]=>h[l]+acgal[l]+so4[l]+cs_c_deg2[l]
	beta-N-acetylhexosaminidase A, lysosomal	1.3	2 h2o[l]+cs_c_deg3[l]=>h[l]+acgal[l]+so4[l]+cs_c_deg5[l]
	N-acetylgalactosamine-4-sulfatase, lysosomal	1.31	h2o[l]+cs_a[l]<=>h[l]+so4[l]+cs_a_deg1[l]
	N-acetylgalactosamine-6-sulfatase, lysosomal	1.3	h2o[l]+cs_c[l]<=>h[l]+so4[l]+cs_c_deg1[l]
	N-acetylgalactosamine-6-sulfatase, lysosomal	1.31	h2o[l]+cs_c_deg3[l]<=>h[l]+so4[l]+cs_c_deg4[l]
Glycolysis/gluconeogenesis	Phosphoenolpyruvate carboxykinase (GTP)	2.98	oaa[c]+gtp[c]=>co2[c]+pep[c]+gdp[c]
	(S)-Lactate:NAD+ oxidoreductase EC:1.1.1.27	1.37	h[x]+nadh[x]+pyr[x]<=>nad[x]+lac_L[x]
Starch and sucrose metabolism	alpha-amylase, extracellular (strch1 -> strch2)	1.36	8 h2o[e]+strch1[e]=>8 glc_D[e]+strch2[e]
	alpha-amylase, extracellular (glygn2 -> glygn4)	1.37	8 h2o[e]+glygn2[e]=>8 glc_D[e]+glygn4[e]
	Alpha-Amylase	1.34	glc_D[e]+malttr[e]<=>h2o[e]+malttttr[e]
	Alpha-Amylase	1.33	glc_D[e]+maltttr[e]<=>h2o[e]+maltptr[e]
	Alpha-Amylase	1.33	glc_D[e]+maltpt[e]<=>h2o[e]+malthx[e]
	Alpha-Amylase	1.33	glc_D[e]+malthx[e]<=>h2o[e]+malthp[e]
	Alpha-Amylase	1.33	glc_D[e]+CE2838[e]<=>h2o[e]+CE2839[e]
NAD metabolism	Nicotinate D-Ribonucleoside Kinase	1.34	atp[c]+nicrns[c]=>adp[c]+h[c]+nicrnt[c]
	nucleotide phosphatase	1.34	h[c]+nac[c]+r1p[c]=>pi[c]+nicrns[c]
	Nicotinate D-ribonucleotide:pyrophosphate phosphoribosyltransferase	1.34	ppi[c]+nicrnt[c]<=>h[c]+prpp[c]+nac[c]
Nucleotide interconversion	5'-nucleotidase (dUMP),mitochondrial	1.73	h2o[m]+dump[m]=>pi[m]+duri[m]
	5'-nucleotidase (dTMP), mitochondrial	1.27	h2o[m]+dtmp[m]=>pi[m]+thymd[m]

Figure 2.6: **Description of the high flux valued reactions.** Here, the first column represents the pathways in which these reactions are participating. The second column provides the name of each reaction, the third column shows their fold change value in type 2 diabetes compared to control, and last column depicts the formula of each reaction.

These reactions are associated with the gene Sphingosine-1-Phosphate Lyase 1 (SGPL1) and found down-regulated. In the gluconeogenesis pathway, we noticed a higher flux rate for phosphoenolpyruvate carboxykinase (GTP) and a reduced flux rate for FAD-linked glycerol-3-phosphate dehydrogenase (mGPDH). Reduced activity of mGPDH has already been reported in T2D [262, 263].

Subsystems in VMH database	Reactions	Fold change	Description
Oxidative phosphorylation	cytochrome c oxidase, mitochondrial Complex IV	0.68	o2[m]+4 focytC[m]=>4 h[m]+2 h2o[m]+4 ficytC[m]
	ubiquinol-6 cytochrome c reductase, Complex III	0.65	2 h[m]+2 ficytC[m]+q10h2[m]=>4 h[c]+q10[m]+2 focytC[m]
	sn-Glycerol-3-phosphate:(acceptor) 2-oxidoreductase EC:1.1.5.3	0.77	q10[m]+glyc3p[c]=>dhap[c]+q10h2[m]
Sphingolipid metabolism	Sphingosine-1-phosphate lyase	0.77	h2o[r]+sphs1p[r]=>h[r]+ethamp[r]+hdca[r]
	sphinganine-1-phosphate palmitaldehyde-lyase EC:4.1.2.27	0.8	sphs1p[c]=>ethamp[c]+HC02228[c]
	hexadecanal:NADP+ delta2-oxidoreductase EC:1.3.1.27	0.8	h[c]+nadph[c]+HC02228[c]=>nadp[c]+hxdcal[c]
Glycerophospholipid metabolism →	Sphinganine-1-phosphate pamlmitaldehyde-lyase EC:4.1.2.27	0.8	ethamp[c]+hxdcal[c]=>sph1p[c]
Pentose phosphate pathway	glucose-6-phosphate dehydrogenase, endoplasmic reticulum	0.02	nad[r]+g6p[r]<=>h[r]+nadh[r]+6pgl[r]
	phosphogluconate dehydrogenase, endoplasmic reticulum	0.83	nadp[r]+6pgc[r]=>nadph[r]+co2[r]+ru5p_D[r]
	6-phosphogluconolactonase, endoplasmic reticulum	0.83	h2o[r]+6pgl[r]=>h[r]+6pgc[r]
	2-Deoxy-D-ribose 1-phosphate 1,5-phosphomutase EC:5.4.2.7	0.74	2dr1p[c]<=>2dr5p[c]
Urea cycle	arginase	0.58	h2o[c]+arg_L[c]=>orn[c]+urea[c]
	Ornithine Decarboxylase	0.71	h[c]+orn[c]=>co2[c]+ptrc[c]
Tryptophan metabolism →	kynurenine 3-monooxygenase	0.76	o2[c]+h[c]+nadph[c]+Lkynr[c]=>h2o[c]+nadp[c]+hLkynr[c]
Arginine and Proline Metabolism	Nitric Oxide Synthase (NO forming)	0.79	o2[c]+nadph[c]+nwharg[c]=>h2o[c]+h[c]+nadp[c]+citr_L[c]+no[c]
	proline oxidase (NAD), mitochondrial	0.75	nad[m]+pro_L[m]=>2 h[m]+nadh[m]+1pyr5c[m]
	Proline dehydrogenase (m)	0.75	fad[m]+pro_L[m]=>h[m]+fadh2[m]+1pyr5c[m]
Valine, leucine, and isoleucine metabolism	3-hydroxyisobutyrate dehydrogenase, mitochondrial	0.82	nad[m]+3hmp[m]<=>h[m]+nadh[m]+2mop[m]
	2-Methylpropanoyl-CoA:oxygen 2,3-oxidoreductase EC:1.3.99.2	0.76	ibcoa[m]+q10[m]=>2mp2coa[m]+q10h2[m]
Beta-Alanine metabolism	3-Aminopropanoate:2-oxoglutarate aminotransferase (m)	0.47	glu_L[m]+msa[m]<=>akg[m]+ala_B[m]
	Propenoyl-CoA hydrolase (m)	0.67	h2o[m]+prpncoa[m]=>3hpcoa[m]
Glutamate metabolism	4-Aminobutyraldehyde:NAD+ oxidoreductase EC:1.2.1.3	0.54	h2o[m]+nadp[m]+4abutn[m]<=>2 h[m]+nadph[m]+4abut[m]
	4-Aminobutanal:NAD+ 1-Oxidoreductase	0.54	2 h[m]+nadh[m]+4abut[m]<=>h2o[m]+nad[m]+4abutn[m]
Fatty acid synthesis	palmitoyl-CoA desaturase (n-C16:0CoA -> n-C16:1CoA)	0.76	o2[c]+h[c]+nadh[c]+pmtcoa[c]=>2 h2o[c]+nad[c]+hdcoa[c]
	Palmitoyl Coenzyme A Hydrolase	0.7	h[c]+coa[c]+ocdca[c]<=>h2o[c]+stcoa[c]
	Palmitoyl Coenzyme A Hydrolase	0.77	h[c]+coa[c]+arach[c]<=>h2o[c]+arachcoa[c]
Eicosanoid metabolism	Arachidonate 5-lipoxygenase	0.74	o2[c]+arachd[c]=>5HPET[c]
	Arachidonate 5-lipoxygenase	0.77	5HPET[c]=>h2o[c]+leuktrA4[c]
R group synthesis	R group artificial flux	0.81	arachcoa[c]=>1.25 R2coa_hs[c]
	R group artificial flux	0.82	h[m]+nadph[m]+fadh2[m]+lnlccoa[c]=>nadp[m]+fad[m]+1.125 R2coa_hs[c]
	R group artificial flux	0.78	fadh2[m]+hdd2coa[c]=>fad[m]+R6coa_hs[c]
	R group to palmitate conversion	0.82	Rtotal3coa[c]=>pmtcoa[c]
	R total flux 2 position	0.83	R2coa_hs[c]+R4coa_hs[c]=>2 Rtotal2coa[c]
	R total flux 3 position	0.83	R1coa_hs[c]+R2coa_hs[c]=>2 Rtotal3coa[c]
	R total flux	0.67	R2coa_hs[c]=>Rtotalcoa[c]
	R total flux	0.67	R5coa_hs[c]=>Rtotalcoa[c]
	R total flux	0.78	R6coa_hs[c]=>Rtotalcoa[c]
Unassigned	Propinol adenylate:CoA ligase (AMP-forming)EC:6.2.1.17	0.6	coa[m]+HC01668[m]=>2 h[m]+ppcoa[m]+amp[m]
	Propanoate:CoA ligase (AMP-forming)EC:6.2.1.1 EC:6.2.1.17	0.6	h[m]+atp[m]+ppa[m]=>ppi[m]+HC01668[m]
	steroyl-CoA,hydrogen-donor:oxygen oxidoreductase EC:1.14.19.1	0.82	o2[c]+pmtcoa[c]+2 HC00619[c]=>2 h2o[c]+2 HC00617[c]+HC10852[c]
	Propanoyl-CoA:(acceptor) 2,3-oxidoreductase EC:1.3.3.6 EC:1.3.99.3	0.67	ppcoa[m]+q10[m]=>q10h2[m]+prpncoa[m]
	L-proline:(acceptor) oxidoreductase EC:1.5.99.8	0.79	5 h[m]+q10[m]+1pyr5c[m]<=>q10h2[m]+pro_L[m]
Propanoate metabolism	2-methylcitrate synthase	0.76	h2o[c]+ppcoa[c]+oaa[c]=>h[c]+2mcit[c]+coa[c]
	Propanoyl-CoA:FAD 2,3-oxidoreductase, mitochondrial	0.66	ppcoa[m]+fad[m]=>fadh2[m]+prpncoa[m]
	3-hydroxypropanoate:NAD+ oxidoreductase EC:1.1.1.59	0.67	nad[m]+3hpp[m]=>h[m]+nadh[m]+msa[m]
Purine catabolism →	ITP diphosphohydrolase Purine metabolism EC:3.6.1.5	0.82	h[e]+pi[e]+idp[e]<=>h2o[e]+itp[e]
Pyrimidine catabolism	CDP diphosphohydrolase Pyrimidine metabolism EC:3.6.1.5	0.81	h[e]+pi[e]+cmp[e]<=>h2o[e]+cdp[e]
	CTP diphosphohydrolase Pyrimidine metabolism EC:3.6.1.5	0.82	h[e]+pi[e]+cdp[e]<=>h2o[e]+ctp[e]
	dTDP diphosphohydrolase Pyrimidine metabolism EC:3.6.1.5	0.83	h[e]+pi[e]+dtmp[e]<=>h2o[e]+dtdp[e]
	dTTP nucleotidohydrolase Pyrimidine metabolism EC:3.6.1.39	0.82	h[e]+pi[e]+dtdp[e]<=>h2o[e]+dttp[e]
Glycolysis/gluconeogenesis →	glycerol-3-phosphate dehydrogenase (FAD), mitochondrial	0.77	fad[m]+glyc3p[c]=>fadh2[m]+dhap[c]
Nucleotide interconversion	nucleoside-diphosphatase (GDP), extracellular	0.81	h2o[e]+gdp[e]=>h[e]+pi[e]+gmp[e]
	nucleoside-triphosphatase (GTP)	0.8	h2o[e]+gtp[e]=>h[e]+pi[e]+gdp[e]
Pyruvate metabolism	malic enzyme (NADP)	0.66	nadp[c]+mal_L[c]=>pyr[c]+nadph[c]+co2[c]
	Transport reaction	0.8	dump[m]=>dump[c]
Cholesterol metabolism →	(R)-Mevalonate:NADP+ oxidoreductase (CoA acylating) EC:1.1.1.34	0.59	2 nadp[c]+coa[c]+mev_R[c]<=>2 h[c]+2 nadph[c]+hmgcoa[c]
Bile acid synthesis →	Palmitoyl Coenzyme A Hydrolase	0.78	h[c]+coa[c]+ppa[c]<=>h2o[c]+ppcoa[c]
CoA synthesis →	3-hydroxyisobutyryl-CoA hydrolase	0.67	h2o[m]+3hpcoa[m]=>h[m]+coa[m]+3hpp[m]

Figure 2.7: **Description of the low flux valued reactions.** Here, the first column represents the pathways in which these reactions are participating. The second column provides the name of each reaction, the third column shows their fold change value in type 2 diabetes compared to control, and last column depicts the formula of each reaction.

Our analyses revealed marked alterations in the urea cycle, and one of the associated genes (ornithine decarboxylase (ODC1)) was found downregulated. ODC1 catalyzes the rate-limiting step of polyamine biosynthesis by decarboxylating ornithine (orn) and producing putrescine (ptrc), the precursor for the polyamines. We also observed reduced flux for the upstream reaction, arginase, which converts L-arginine (arg_L) into ornithine and urea. So, these alterations can be considered an effect of reduced plasma level of arginine, which is already reported for T2D patients [235]. A reduced uptake rate for L-arginine was also observed. In addition, up-regulated fluxes were observed for two other reactions in the urea cycle: guanidinoacetate N-methyltransferase and arginine:glycine amidinotransferase that promote the formation of L-arginine and glycine from ornithine by consuming creatine (creat).

2.3.3 Alterations in the secretory profile of the pancreatic β-cell

We obtained 65 perturbed exchange/demand reactions, and of these, 37 reactions had high flux rates, while 28 had low flux rates (names of the associated metabolites provided in **Fig. 2.8**). We observed almost 2-fold increased triglyceride (triacylglycerol) uptake in the diabetes group, resulting in an elevated production rate of diglyceride (diacylglycerol) and monoacylglycerol 2 and FAs. The associated CEL gene was found up-regulated. It is likely that these alterations must be responsible for observed higher secretion of these metabolites into the extracellular space (**Fig. 2.8**). Indeed, a higher abundance of plasma diglyceride and FAs were already reported in patients with diabetess [264, 265]. We also observed higher expression of the CPA2 (carboxypeptidase A2 (pancreatic)) gene, a Zn-dependent digestive enzyme from the pancreas. CPA2 regulates the conversion of kinetensin 1-8 and neuromedin N (1-4) into kinetensin and neuromedin N (NMN), respectively, by consuming L-leucine (see miscellaneous in **Fig. 2.6**). These reactions occur in the extracellular compartment of the cell (information extracted from Recon 2.04), and the plasma level of L-leucine has been reported higher in diabetes subjects [264]. Also, the presence of NMN and its precursor neurotensin (NT) were reported in the extract of a human neuroendocrine pancreatic adenoma [266]. However, the plasma NMN level was undetectable (below 100 pmol/L). We also observed higher secretion rates of betaine due to earlier mentioned alterations in the glycine, serine, alanine, and threonine metabolism.

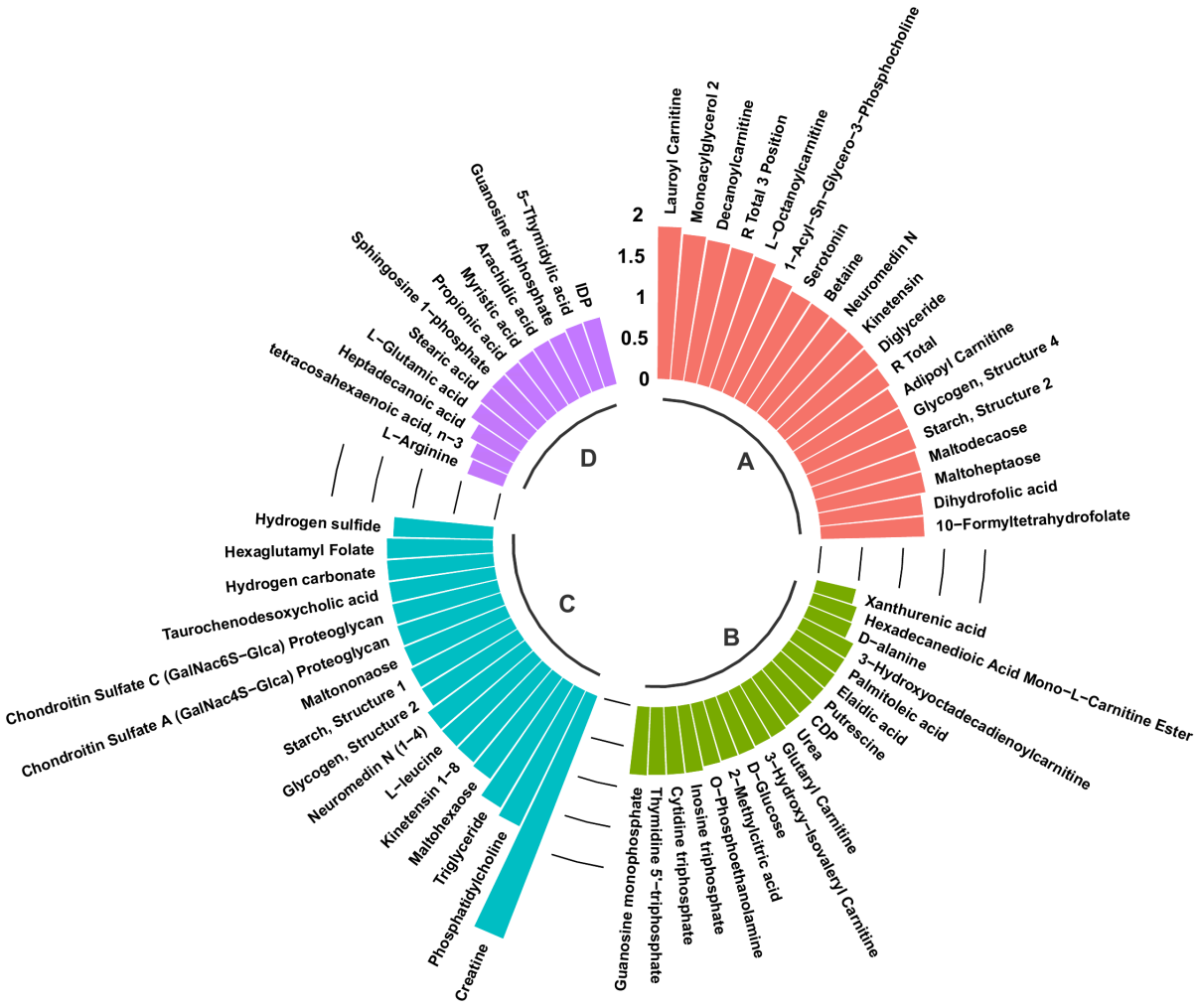

Figure 2.8: **List of metabolites corresponding to altered exchange reactions.** The name of the metabolites corresponding to each exchange reaction was extracted from the Virtual Metabolic Human (VMH) database [267]. The flow of exchange of these metabolites was obtained from the corresponding flux rates. Positive values in the exchange rate denote the secretion of metabolites, and negative values indicate the consumption of metabolites. According to the flow of the exchange and the mode of alterations in diabetes, we grouped the metabolites into four classes: (A) Secreted from β-cells with higher flux rates, (B) Secreted from β-cells with reduced flux rates, (C) Consumed by β-cells with higher flux rates, and (D) Consumed by β-cells with reduced flux rates. The length of the circular bar represents the fold change values of the exchange rates for each metabolite in diabetic patients compared to the control subjects. The five-line segments between the groups A-B, B-C, C-D denote the 0-, 0.5-, 1-, 1.5- and 2-fold change, respectively, from the center to the periphery.

It has been recently reported that plasma betaine level is upregulated in the diabetes group compared to healthy controls [268]. Also, a group of five metabolites (betaine, alpha-linolenic acid, d-mannose, l-glutamine, and methylmalonic acid) was proposed as a combinatorial biomarker to distinguish diabetes mellitus from a healthy control [268]. As a result of the alterations in tryptophan metabolism (described earlier), we observed a higher secretion flux of serotonin.

Earlier studies [269, 270] also reported increased plasma serotonin levels in diabetic patients. Also, reduced uptake of L-glutamic acid and L-arginine was observed here. These may be the effect of low plasma levels of these two amino acids, and it is already reported that their levels are reduced in diabetes [235].

2.4 Discussion

Our study aims to capture the insights of β-cell metabolism responsible for the dysregulated β-cell function in type 2 diabetes. There were 117 up- and 72 down-regulated metabolic genes found to be associated with various metabolic pathways. The co-expression analysis of metabolic genes showed that most dysregulated genes in diabetes follow a similar expression pattern and form a cluster (Module 2). This module could distinguish diabetic samples from the control samples. To unravel the complexities of the metabolic pathways, a constraint-based modeling approach was employed to map the gene expression changes at the level of metabolic flux rates, pathways, and metabolites. The E-flux method, which serves as a scaffold for understanding the changes in the metabolic pathway, was applied in an effort to generate the subject-specific models from the generic human metabolic model. Comparison of the metabolic-flux profiles between the patients with diabetes and control subjects provided mechanistic understanding responsible for blunting of ATP synthesis. This analysis also uncovered potential causes responsible for the activation of oxidative stress-linked pathways.

Mitochondrial metabolism is a major determinant of insulin secretion from pancreatic β-cells [271–273]. Their aerobic metabolism permits the oxidation of glucose and fatty acids for the generation of ATP required for the exocytosis of insulin granules. In addition, β-cell mitochondria play a crucial role in synthesizing other metabolites that can act, both intra- and extra-mitochondrially, as factors that couple glucose sensing to insulin granule exocytosis. Our analysis revealed a significant reduction in the mitochondrial fatty acid oxidation process as evident by reduced fluxes with concomitant decreases in NADH and $FADH_2$ production. Indeed, mitochondrial oxidative phosphorylation is the primary source for ATP generation in which the reducing compounds like NADH and $FADH_2$ are utilized by the electron transport chain to

generate an electrochemical gradient that drives ATP synthesis. Thus, the decreased production of these reducing compounds can lead to reduced fluxes towards oxidative phosphorylation and subsequently affects ATP production. Here, we also found a significant reduction in the fluxes for, coenzyme Q:cytochrome c - oxidoreductase (mitochondrial complex III) and cytochrome c oxidase (mitochondrial complex IV) in the oxidative phosphorylation pathway. These impairments lead to the decline of the ATP level required for the proper closure of the K_{ATP} channels in T2D patients. Thus, reduced insulin secretion was observed in patients with diabetes, and this is potentially one of the major causes of diabetes progression. Similar conclusions were also drawn experimentally where the decreased activity of mitochondrial complex IV was observed for diabetic islets [274, 275], and long-term exposure of high glucose was associated with the reduction in the constituents of mitochondrial complexes I-IV [276]. It is also reported that chronic hyperglycemia causes a change in mitochondrial number, function, and morphology, which leads to impairment in the GSIS process through altered oxidative phosphorylation, reduced mitochondrial Ca^{2+} capacity, and decreased ATP production rate [277].

Oxidative stress induced by chronic hyperglycemia is critically involved in the failure of β-cell function and mass during T2D development. T2D is also accompanied by a chronic elevation of free fatty acids, which contribute to β-cell failure via enhanced lipotoxicity. Fatty acids are oxidized mainly in two compartments, mitochondria, and peroxisome, in which peroxisomal fatty acid oxidation is the major site of H_2O_2 production in β-cells. Peroxisomal fatty acid oxidation shortens long- and very-long-chain fatty acids, resulting in H_2O_2 production, and the shortened fatty acids are subsequently translocated to the mitochondria for their further degradation. Our analysis revealed that the peroxisomal fatty acid oxidation and H_2O_2 production rates are upregulated in patients with diabetes. Consequently, this should lead to increased ROS generation in β-cells leading to excessive oxidative stress. This fatty acid-induced β-cell lipotoxicity is also confirmed experimentally [278]. In addition, analysis of diabetic patient samples showed increased carboxyl ester lipase (CEL) activity, resulting in excess production of diglyceride, monoacylglycerol 2, and fatty acids from the hydrolysis of triglyceride (**Figs. 2.6**). Excess fatty acid accumulation also can induce lipotoxicity, whereas excess diglyceride accumulation has been linked to the β-cell dysfunction in T2D [279, 280].

Thus, the increased CEL activity has the potential to contribute to the β-cell dysfunction in T2D.

In addition to decreased ATP levels, reduction in NADPH production is also likely to negatively impact on providing reducing equivalents to two potent antioxidant systems which scavenge H_2O_2, i.e., the glutathione peroxidase and peroxiredoxin systems [281]. In addition to this, the production flux for putrescine, a precursor for polyamine biosynthesis, is also reduced. Polyamines are polycations that interact with negatively charged molecules such as DNA, RNA and proteins and they play multiple roles in cell growth, survival and proliferation. Moreover, it has been reported that the chronic depletion of cellular polyamine levels leads to oxidative stress-mediated cellular apoptosis [282]. Thus, continuing depletion of NADPH and polyamine levels in diabetic β-cells could negatively impact the efficacy of antioxidant defense systems and secondarily exaggerate the extent of oxidative damage to macromolecules and activation of stress-related signaling pathways.

Analysis of the secretory profile of pancreatic β-cell in the diabetic state leads to increased secretion rates of 19 metabolites. Among these, diacylglycerol, monoacylglycerol 2, fatty acids, betaine, serotonin, kinetensin, and neuromedin N (NMN) are the seven metabolites that were associated with cardiovascular complications. Diacylglycerol, monoacylglycerol 2, and fatty acids all can contribute to the increased circulating levels of FFA in diabetes. Under normoglycemia, FFAs are used as essential fuel, but their high levels under pathological conditions may eventually lead to lipotoxicity and excessive fat accumulation in the heart [283]. It has also been reported that elevated plasma betaine concentration is a marker of cardiovascular risk in diabetes [284]. Serotonin acts as a neurotransmitter and as a peripheral hormone in the human body. Higher plasma serotonin level has been proposed as a marker for decompensation in patients with chronic heart failure [285]. The elevated serotonin concentrations have already been described in various cardiovascular diseases [286–289]. Kinetensin is known to increase blood pressure via activation of angiotensin-II type 1 receptors, and also it shows a variable effect on heart rate [290]. The NMN does not show any direct role in cardiovascular complexity. However, its precursor, pro-neurotensin/ neuromedin N (pro-NT/NMN) [291], shows association with metabolic diseases, diabetes, cardiovascular disease, breast cancer, ischemic stroke [292].

Thus, our findings suggest that impaired metabolism of pancreatic β-cells not only leads to dysregulated insulin secretion but also may contribute to the pathogenesis of cardiovascular disease and associated complications. Although, investigators mainly directed their efforts on β-cell metabolism in order to examine the cause and effect of diabetes. Our current studies, however, raised the possibility that alteration in the β-cell metabolism affects the plasma insulin levels and impaired plasma metabolic profiles in diabetes, which may further exaggerate diabetes-related cardiovascular complications. On the one hand, we have shown the application of GSMM in capturing metabolic alterations, while on the other hand, it can also be applied to identify critical regulatory points through knockout approaches. In the next chapter, we have explored GSMM in finding regulatory points for different cancer metabolic networks through *in silico* gene knockout study.

3

In-silico gene knockout studies using genome-scale metabolic model[1]

3.1 Introduction

Gene knockout study in cancer cell-lines is used to see the effect of an existing cancer drug or to develop new cancer drug [51–55]. Another approach is the phenotypic screening of drugs in cancer cell-lines to find its effect on the cell growth [51, 56–59]. Both of these processes are very costly and time consuming [293–295]. Therefore, a computational method, like metabolic networks, could be a good alternative to find drugs having better selective ability in killing cancerous cells [296–298]. One tool which is particularly suitable to deal with problems like per-

[1]The bulk of this chapter has been published in *Scientific reports*, 11.1 (2021): 1-13.

sonalized medicine and finding a larger therapeutic window is genome-scale metabolic models (GSMMs) [69]. Through flux balance analysis (FBA) on these GSMMs, one can evaluate the metabolic capabilities of the cell, e.g., the capability of synthesizing biomass building blocks. GSMMs have successfully been used in cancer drug development [63, 65, 66, 173, 299]. For example, Folger et al. [63] made a generic metabolic model of cancer and predicted some growth-supporting genes for cancer, which were validated with experimental shRNA data. GSMMs were also used to predict the putative effects of drugs of DrugBank database [69], but the results were not compared with the experimental data.

Chronic progressive diseases such as cancer do not derive from abnormal functioning of a single gene or a single pathway but reflect the disorder of complex intracellular and intercellular networks that link tissues and organs [300]. Various tissues and organs like breast, central nervous system (CNS), colon, lung, ovary, prostate, renal are affected by cancer. Millions of people are suffering from cancer and the number is increasing [301–303]. Available drugs that are used for treating cancer, unfortunately, have many side effects [45]. Therefore, there is an increasing demand for new therapies with better therapeutic windows, implying that the drug will target a particular cell type (such as tumour cells) with no or minimum negative effects on healthy cells. The search for such suitable therapeutic windows is an important and challenging problem in the case of cancer. Another problem with the existing cancer drugs is that a particular drug shows different responses when applied to different individuals. This is because the effects of a drug on a patient depend not only on the interaction with its targets but also on the activities of many other enzymes which form a complex network of metabolic reactions in which the products of a reaction become the substrates of other reactions [69]. This leads to the emerging field of personalized medicine and personalized drug-choice [46]. Thus there is a need for developing new anti-cancer drugs taking care of the above problems and demands for an in-depth mechanistic understanding of cancer [47, 48].

The present study is an attempt to explore gene knockout strategies that apply GSMMs in finding possible targets and mechanisms related to cancer disease. For the analysis, we considered the GSMMs of the NCI-60 cell-lines built by Yizhak et al. [299] using Personalized Reconstruction of Metabolic models (PRIME) approach. They established their cell-specific

model based on molecular and phenotypic data. It is shown that the models can find drug targets that inhibit the proliferation of specific cell-lines. Their models can also infer on the prognosis of breast and lung cancer. In this study, we applied their model for a more comprehensive study on the single and multiple gene knockout effects on the growth rate of the cancer cell-line and compared the results with the online experimental database. We also attempted to capture the underlying mechanisms associated with the observed growth reduction rate due to gene knockout. We further analysed our top-ranked genes to get potential targets which were then validated experimentally. It is also observed that multiple knockout tests give a better correlation with experimental observation than single-gene knockout results.

3.2 Materials and methods

3.2.1 Predicting cancer cell growth by gene knockout

We used minimization of metabolic adjustment (MOMA) technique [207] for observing gene knockout effect on the growth rates of 60 cancer cell-line models. To mimic the knockout condition of a gene, we changed the lower and upper bounds of flux values of the reactions associated with the gene to zero. In the case of simultaneous knockout of multiple genes, the bounds of all reactions of these participating genes were set to zero. To measure the growth rate, we used two models as input for MOMA: one representing the knockout condition and the other one representing the wild-type condition of a particular cell-line. The fractional cell growth (FCG) was then calculated by taking the ratio of growth rates in knockout condition to wild-type condition. COBRA toolbox was used from the MATLAB package [304] for MOMA. Though there exists several genes associated with the same reaction with non-trivial '*AND*' and '*OR*' combinations, in order to keep our analysis simple, we followed the literatures [63, 299, 305, 306] and assumed zero flux for the reaction associated with the knockout gene.

3.2.2 Gene symbol to Gene ID conversion

In GSMMs, the identity of genes is given in gene ID format and therefore the gene symbols need to be converted into gene IDs. For this purpose, we used the Uniprot database, which

provides the mapping between gene IDs and gene symbols of the metabolic genes. Using this method, one can find out the metabolic genes from any given gene set having gene ID information. One can also extract genes from any given gene set, which are present in the cancer cell-line metabolic models, by taking intersection with the 1905 gene IDs present in the cancer models.

3.2.3 Gene knockout effect on the production flux rate of metabolite

Flux balance analysis (FBA) was applied to get the flux values of each of the metabolic reactions present in the metabolic networks under the wild-type and gene knockout condition. Then, the production flux rate of a metabolite was obtained by summing up the flux values of the reactions in which it is produced. Finally, the ratio between the production flux rates under the two different conditions was calculated.

3.2.4 Biomass reduction score (BRS)

Total 43 metabolites are used as the substrate in the biomass reaction, and we termed them as biomass metabolites (see **Table 3.1**). These biomass metabolites are then arranged in the decreasing order of their coefficient values in the biomass reaction and scored them accordingly. For example, the biomass metabolite having the highest coefficient was scored 43 and the biomass metabolite with the lowest coefficient was scored 1. To capture the individual gene knockout effect on the biomass reaction, we first listed out the biomass metabolites whose production flux rates are reduced by more than two folds. We then calculated the sum of the scores of these biomass metabolites and termed them as biomass reduction score (BRS).

Table 3.1: **The list of metabolites that are used as substrate in the Biomass reaction.** We listed them accordingly to their coefficients given in the biomass reaction. Negative sign represents the consumption of this metabolites in biomass reaction.

Metabolites Names	**Metabolites Symbol**	**Coefficient in Biomass reaction**	**Rank**	**Score**
ATP	atp[c]	-43.153	1	43

H_2O	h2o[c]	-43.153	2	42
L-Aspartate	asp-L[c]	-2.452366	3	41
glycogen, structure 1 (glycogenin-11[1,4-Glc])	glygn1[c]	-0.939899	4	40
L-Glutamine	gln-L[c]	-0.676289	5	39
L-Glutamate	glu-L[c]	-0.594216	6	38
Glycine	gly[c]	-0.492442	7	37
L-Alanine	ala-L[c]	-0.420217	8	36
L-Serine	ser-L[c]	-0.131318	9	35
L-Histidine	his-L[c]	-0.10177	10	34
triacylglycerol (homo sapiens)	tag_hs[c]	-0.097285	11	33
L-Threonine	thr-L[c]	-0.072226	12	32
phosphatidylethanolamine (homo sapiens)	pe_hs[c]	-0.07098	13	31
L-Proline	pro-L[c]	-0.063691	14	30
Phosphatidylcholine (homo sapiens)	pchol_hs[c]	-0.060784	15	29
phosphatidic acid (homo sapiens)	pa_hs[c]	-0.058105	16	28
L-Asparagine	asn-L[c]	-0.042678	17	27
L-Valine	val-L[c]	-0.042678	18	26
L-Leucine	leu-L[c]	-0.039396	19	25
GMP	gmp[c]	-0.037088	20	24
L-Lysine	lys-L[c]	-0.032829	21	23
CMP	cmp[c]	-0.032723	22	22
Cholesterol	chsterol[c]	-0.029279	23	21
cholesterol ester	xolest_hs[c]	-0.023261	24	20

phosphatidylserine (homo sapiens)	ps_hs[c]	-0.020854	25	19
L-Tyrosine	tyr-L[c]	-0.019696	26	18
AMP	amp[c]	-0.019636	27	17
UMP	ump[c]	-0.019636	28	16
monoacylglycerol 2 (homo sapiens)	mag_hs[c]	-0.013664	29	15
L-Isoleucine	ile-L[c]	-0.013133	30	14
L-Phenylalanine	phe-L[c]	-0.013133	31	13
diacylglycerol (homo sapiens)	dag_hs[c]	-0.01114	32	12
phosphatidylinositol (homo sapiens)	pail_hs[c]	-0.010963	33	11
sphingomyelin (homo sapiens)	sphmyln_hs[c]	-0.008545	34	10
dAMP	damp[c]	-0.00805	35	09
dTMP	dtmp[c]	-0.00805	36	08
L-Methionine	met-L[c]	-0.006567	37	07
dCMP	dcmp[c]	-0.005367	38	06
dGMP	dgmp[c]	-0.005367	39	05
lysophosphatidylcholine (homo sapiens)	lpchol_hs[c]	-0.004474	40	04
L-Cysteine	cys-L[c]	-0.004269	41	03
L-Arginine	arg-L[c]	-0.003282	42	02
L-Tryptophan	trp-L[c]	-0.003282	43	01

3.2.5 MTT Assay

Different cancerous cell-lines were maintained at 37°C in a humidified incubator with 5% CO_2 supply. A549 (Human lung carcinoma), HCT116 (Human colorectal carcinoma), K562 (Human chronic myelogenous leukaemia) cells were grown in Dulbecco's Modified Eagle Medium (DMEM) (Hyclone, West South logan, USA) and HL60 (Human promyeloblast) was grown in RPMI 1640 (Gibco) supplemented with 10% fetal bovine serum (FBS). The SOAT1 inhibitor mitotane and CYTB inhibitor myxothiazol were purchased from Sigma Aldrich (St. Louis, USA). They were dissolved in dimethyl sulfoxide (DMSO) (Sigma-Aldrich, MO, United States) and stored in -20°C as a stock concentration of 10 mM and 50 mM respectively. The effect of mitotane and myxothiazol on the proliferation and viability of all cell-lines was monitored using 3-(4,5-dimethylthiazol-2-yl)-2,5-diphenyltetrazolium bromide (MTT) assay. MTT powder was purchased from Merck, USA and was dissolved in PBS (5mg/ml) prior to the assay. MTT assay is based on the principle of reduction of 3-(4,5-dimethylthiazol-2-yl)-2,5-diphenyltetrazolium bromide to purple coloured formazan by the mitochondria of metabolically active cells. Cells were seeded at a density of 2×10^4 cells per well in 96 well plate for 24 hours followed by addition of the drug at different concentrations. The MTT assay was performed after 48 hours of incubation with the drug. Each experiment was performed three times with five replicates. Mean, standard deviation and standard error were determined using Graphpad prism.

3.2.6 Extraction of experimental gene knockdown information from database

We used DEMETER database [307] to obtain the experimental gene knockdown effect on cell growth. It contains a knockdown effect on the viability of cells from 501 cancer cell-lines using the shRNA library. The data is given in the form of log fold change in cell number due to gene knockdown. A gene with a negative log fold change value implies that there is a reduction in the cell growth upon knockdown of this gene [307]. The database contains the knockdown results of 17098 genes on 501 cell-lines, out of which 30 cell-lines are present in NCI-60 cell-lines panel. In our cancer models, we got only 1444 genes from those 17098 genes. So, we obtained the gene knockdown effect of 1444 metabolic genes on 30 cancer cell-lines.

3.2.7 Permutation test

Permutation test was applied to get the p-value corresponding to each Spearman rank-correlation. In the first step, Spearman rank-correlation was calculated between the predicted data and the experimental data. Next, the predicted data were randomly permuted by using the '*randperm*' function in MATLAB. The function '*randperm*' gives a randomly permuted vector of the integers from 1 to n without repeating elements. In our case, n represents the number of data points. The elements of the randomly generated vector is used as index of the original data to generate the permuted data. Spearman rank-correlations were calculated between the permuted data and the experimental data. This process was repeated for 1000 times and the p-value was obtained by using the formula $(r+1)/1001$, where r is the number of cases for which random permuted set gave better rank-correlation than the non-permuted case.

To verify the usefulness of the permutation test we obtained the distribution of the rank-correlations for the 1000 randomly permuted set (see **Fig. 3.1** for three cell-lines). It was observed that they follow normal distribution.

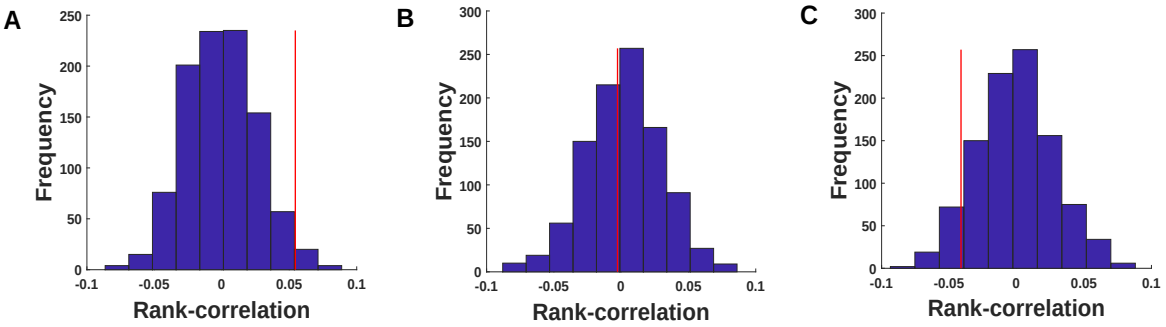

Figure 3.1: **Distribution of Rank-correlation for the 1000 randomly permuted set.** The red line represents the rank-correlation for the non-permuted case. We presented here three cases, where the rank-correlation for the non-permuted cases are: (A) Positive, (B) Almost zero and (C) Negative. "Anderson-Darling test" was applied to check the normality. This give a test decision for the null hypothesis that the vector is coming from a population with a normal distribution. In our case we got zero value which indicates that the test fails to reject the null hypothesis at 5% significance level.

3.2.8 Finding drugs with inhibitory type nature from DrugBank database

In DrugBank database [308], 6490 drugs (out of 8283) have information about its targets and the corresponding mechanism of action. These targets are given in the form of gene names.

There are 1684 drugs which have gene ID information of at least one metabolic target (see method “Gene symbol to Gene ID conversion"). We then searched for the drugs that can decrease the activity of at least one metabolic target. For this purpose, we selected the following three mechanisms of actions: (i) inhibition, (ii) antagonist, (iii) inverse agonist. We found 410 drugs out of 1684 which decreased the activity of at least one metabolic gene. Out of these 410 drugs, only 380 drugs have at least one inhibitory type target on cancer cell-lines GSMMs.

3.2.9 Link between DrugBank database and NCI-60 growth inhibition database

DrugBank database has DrugBank ID, whereas NCI-60 growth inhibition database [309] has NSC ID. So, we first converted their IDs into a single ID for further analysis. In the DrugBank database, the conversion of drug ID to PubChem CID or CAS ID is provided and the conversion of CAS ID to NSC ID is given in the chemical data section of the NCI-60 growth inhibition database. We therefore used CAS ID information of the drugs to link these two datasets. There are 373 drugs, out of previously described 380 drugs, which have CAS ID information and out of them only 200 drugs have NSC IDs. However, all NSC IDs do not have information regarding GI50 value. So, we finally obtained 64 drugs with NSC IDs that have a GI50 score in negative log value.

3.2.10 Finding active drugs using GI50 score

GI50 score is an important measure of drug activity. It quantifies the dosage of the drug required to inhibit the cell growth by 50%. In the NCI-60 growth inhibition database, the range of log value of GI50 score of the drugs is given between -10 to -1. Drugs with log GI50 score less than -5 was considered to be active against cancer [310, 311].

3.3 Results

3.3.1 Single gene knockout ranking based on their influence on cancer cell proliferation using the genome-scale metabolic models

We used the study of Yizhak et al. [299] to obtain the GSMMs of cancer from different tissue types. The networks were made using the molecular (gene expression) and phenotypic data (proliferation rate) of cancer cell-lines by applying PRIME method. These data were used to constrain the bounds on the flux values of the corresponding reactions in metabolic networks. The data for NCI-60 collection were taken from the study by Lee et al. [312], in which RPMI-1640 was used to grow the cell-lines experimentally. We used 60 cancer metabolic networks across 9 tissue types of NCI-60 panel to find cancer drug targets which inhibit cell growth across all cell-lines. We aimed to rank metabolic genes according to their growth inhibitory effect in cancer cell-lines.

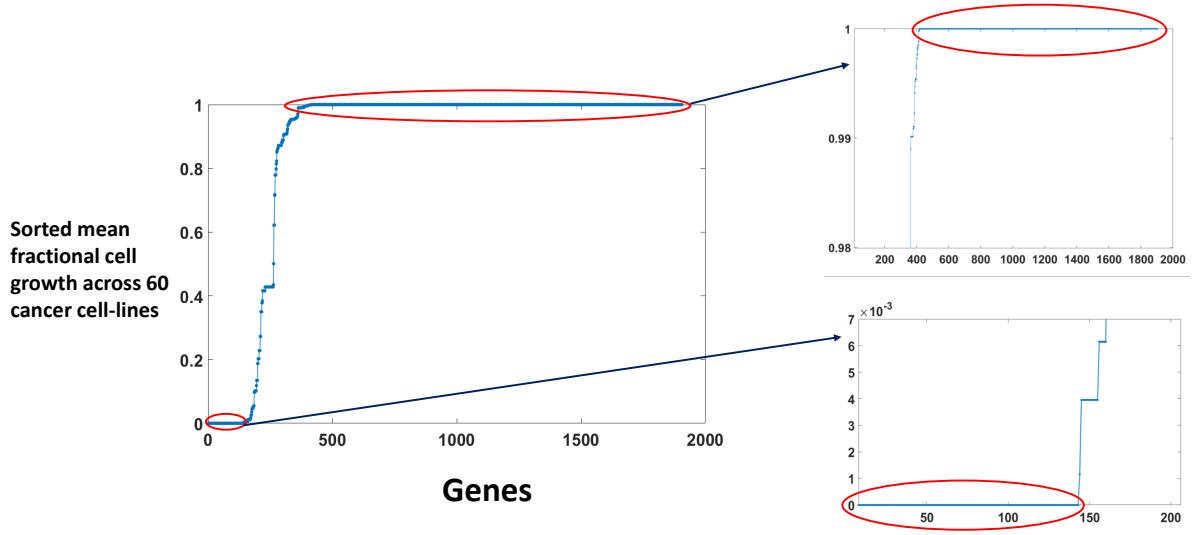

Figure 3.2: **Gene knockout simulation result.** Mean value of the fractional cell growth (FCG) across 60 cancer metabolic models for each individual of 1905 metabolic genes. The right lower panel represents the 143 genes which give very low growth rate after knocking out across all 60 cancer models (mean value$< 10^{-6}$ & s.d.$< 1.2874 \times 10^{-6}$) and the upper panel represents the 1488 genes which show no change in the growth rate after knocking out across all 60 cancer models (mean value> 0.99995 & s.d.$< 3.2838 \times 10^{-6}$).

Cancer cell-lines metabolic models used in our work contains 1905 genes. We simulated the models via MOMA [207, 304] and predicted the growth rate of cancer cell-lines after knocking

out each gene one by one. Taking the average of fractional cell growth (FCG) of 60 cell-lines, we obtained the mean FCG of each 1905 genes (**Fig. 3.2**). Using a cut off value of 10^{-6} (lower circled portion in **Fig. 3.2**) on the sorted mean FCG, we obtained 143 genes that are responsible for very low growth rate in our knockout cancer models. On the other hand, we got 1488 genes, using a cut off value of 0.99995 (the upper circled portion in the **Fig. 3.2**), which show a negligible effect on the growth rate. Interestingly, looking at the reactions corresponding to the 143 genes, we found that all of them, except one gene, is associated with the coupled reactions (**Fig. 3.3**).

3.3.2 Mechanistic insight into the genes giving a low growth rate after knockout

We looked for the underlying mechanisms associated with the observed growth reduction rate due to gene knockout. We applied parsimonious enzyme usage FBA (pFBA) [313] using COBRA Toolbox [314]. pFBA classifies each gene into six categories depending on the optimal growth solutions: essential genes, pFBA optima, enzymatically less efficient (ELE), metabolically less efficient (MLE), zero flux genes and blocked genes. There are 71 essential genes, 470-530 pFBA optima, 230-280 ELE, 545-577 MLE, 82 zero flux genes and 427 blocked genes across 60 cancer cell-lines models. We looked for the classification of the 143 growth reducing genes and found that these genes contain all the 71 essential genes and the rests are pFBA optima (**Fig. 3.4A**). On the other hand, all zero flux and blocked genes, with almost all ELE and MLE genes belong to the 1488 non-effecting genes set (**Fig. 3.4B**). Though there are some genes from the 1488 set, which are present in pFBA optima class, but no essential genes are there in the 1488 gene set.

The production fluxes of the metabolites involved in the biomass reaction is changed due to gene knockout. The biomass reaction in the GSMMs uses 43 metabolites as substrate, termed as biomass metabolites. We measured the fold changes in the production flux of these biomass metabolites under individual gene knockout condition with respect to wild-type condition. The biomass metabolites whose production flux are reduced by more than 2 folds are shown in **Fig. 3.5A**. The upper panel of this figure shows the number of biomass metabolites associated

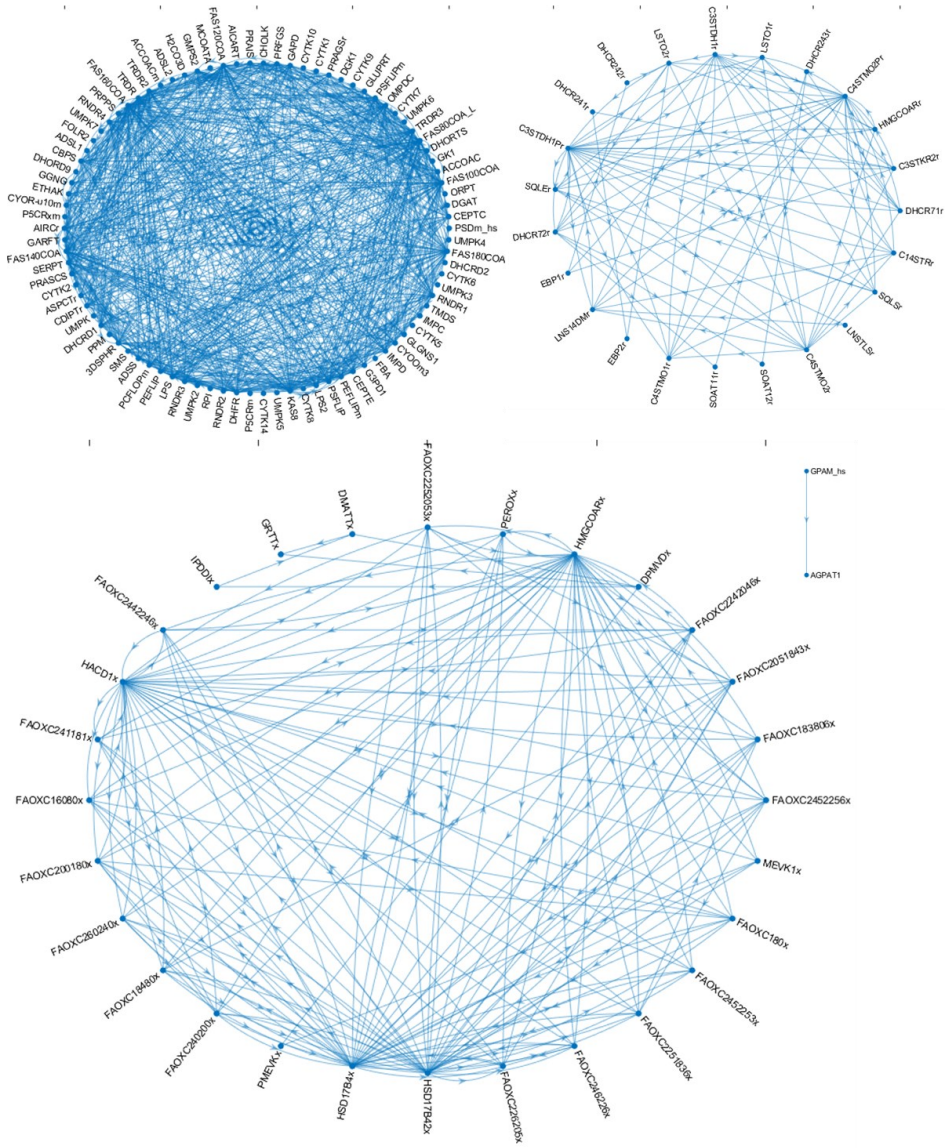

Figure 3.3: **Flux coupled reactions corresponding to the 143 growth-reducing genes.** In total, 176 reactions are associated to the 143 gene set.Among these 176 reactions, 143 reactions formed group of coupled reactions which is presented here. There are only one genes out of 143, whose any associated reactions are not present in these coupled reaction set.

with 143 genes responsible for growth reduction, and the lower panel shows the number of biomass metabolites associated with 1488 genes, which do not affect the growth rate. One can observe that the number of biomass metabolites associated with the 143 genes is much higher than that of 1488 genes. To confirm the association of 143 genes with the biomass reaction,

we introduced a biomass reduction score (BRS) for each gene (see “Materials and methods" for details). A gene with higher BRS has more knockout effect on the biomass reaction. It was observed that BRS of 143 genes are much higher than 1488 genes (**Fig. 3.5B**), confirming that they are more effective in reducing the flux of biomass reaction.

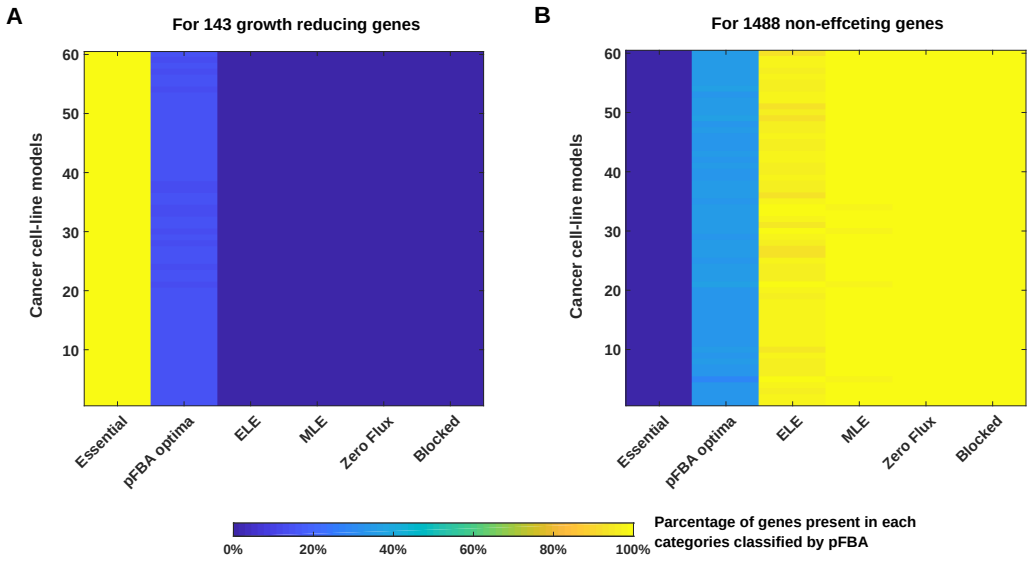

Figure 3.4: **Coverage of pFBA classes by the 143 growth reducing and 1488 non-effecting genes set.** For each of the 60 models, pFBA was applied to classify the genes into six categories and then the parentage of involvement for each class into the (A) 143 growth reducing genes set and (B) 1488 non-effecting genes set was calculated.

Finally, we looked for the biomass metabolites that are associated specifically with the 143 growth reducing genes. We observed that the production flux of 37 biomass metabolites are reduced by knocking out different genes from 143 genes set (**Fig. 3.6A**), while different genes from 1488 genes set reduced production flux of 27 biomass metabolites (**Fig. 3.6B**). Calculating the set difference, we obtained 16 biomass metabolites that are specifically associated with different genes from the 143 gene set. It is observed that 12 out of 16 biomass metabolites showed association with most of the 143 genes (see **Fig. 3.6C**). Next, we looked for these 16 metabolites whether they are flux coupled or not. If they are flux coupled, then one can expect that the corresponding genes become essential for the production of both for the metabolites. We observed that only 4 metabolites out of 16 are flux coupled (**Fig. 3.6D**). L-Aspartate (asp-L[c]) is produced from L-Glutamate (glu-L[c]) by the enzyme kinetic reactions Aspartate Transaminase (ASPTA) but there is another transport reaction L-aspartate transport via Na, H symport and K antiport (ASPt6) in which influx of cytosolic L-Aspartate happens from the extracellular

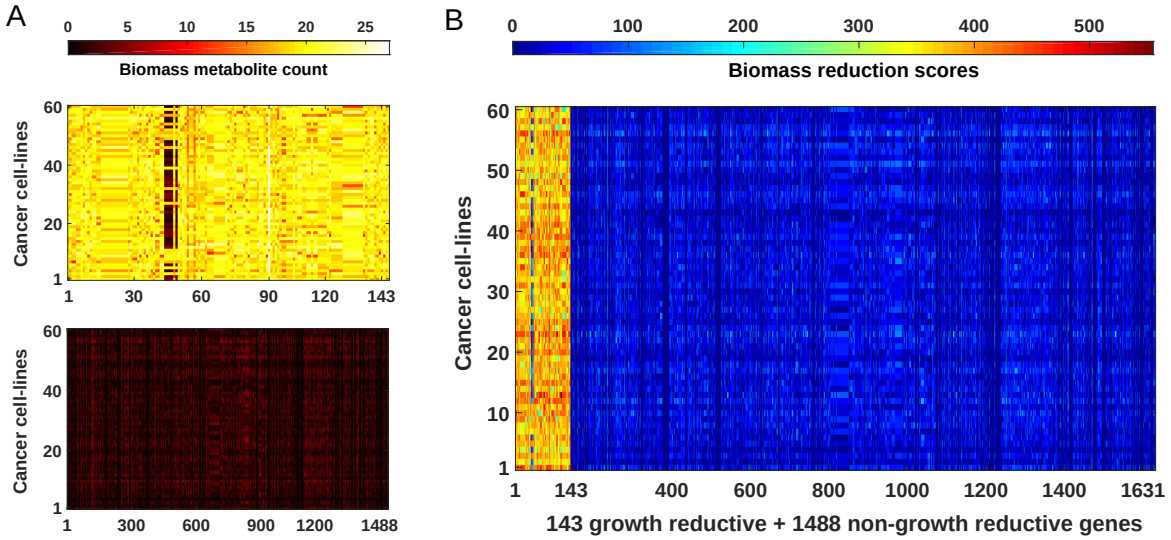

Figure 3.5: **Effect of metabolic genes on biomass function.** (A) The upper and lower panels indicate the number of biomass metabolites whose production flux at least 2 folds decreased by each of the 143 growth reducing genes and 1488 non-growth reducing genes, respectively. (B) Biomass reduction scores (BRS) of genes following synergic effect. BRS is high for first 143 growth reducing genes and it is low for 1488 non-growth reducing genes.

space. For the three cell-lines (SNB-75, HOP-9 and SK-OV-3), flux values of another transport reaction aspartate-glutamate mitochondrial shuttle (ASPGLUm) was observed, which transfer L-Aspartate from mitochondria to cytosol, and as a consequence, cytosolic L-Glutamate enters into the mitochondria. There is another reaction sterol O-acyltransferase (SOAT11) which uses cholesterol (chsterol[c]) to produce cholesterol ester (xolest_hs[c]).

3.3.3 Finding potential cancer drug targets from the top-ranked genes

Our top-ranked genes can be a potential drug target if their knockout does not significantly affect the growth of non-cancerous cells. So, we need to see the effect of our growth reducing genes on normal cell model. The 60 cell-line panel covers nine different tissues. So, we considered nine models [161] built on different cell-type from these nine tissues representing their normal condition. The cell-specific models [161] were built from a global reconstruction (Recon 2), which contains 7,440 reactions and 2,194 transcripts, using protein expression data from the Human Protein Atlas [315]. These models consist of 2,426 $\pm$ 467 reactions ($\pm$ s.d.) and 1,262 $\pm$ 204 transcripts. They applied a published algorithm [189, 205] to predict the flux activity states of the genes by applying an optimization method. The method maximizes the

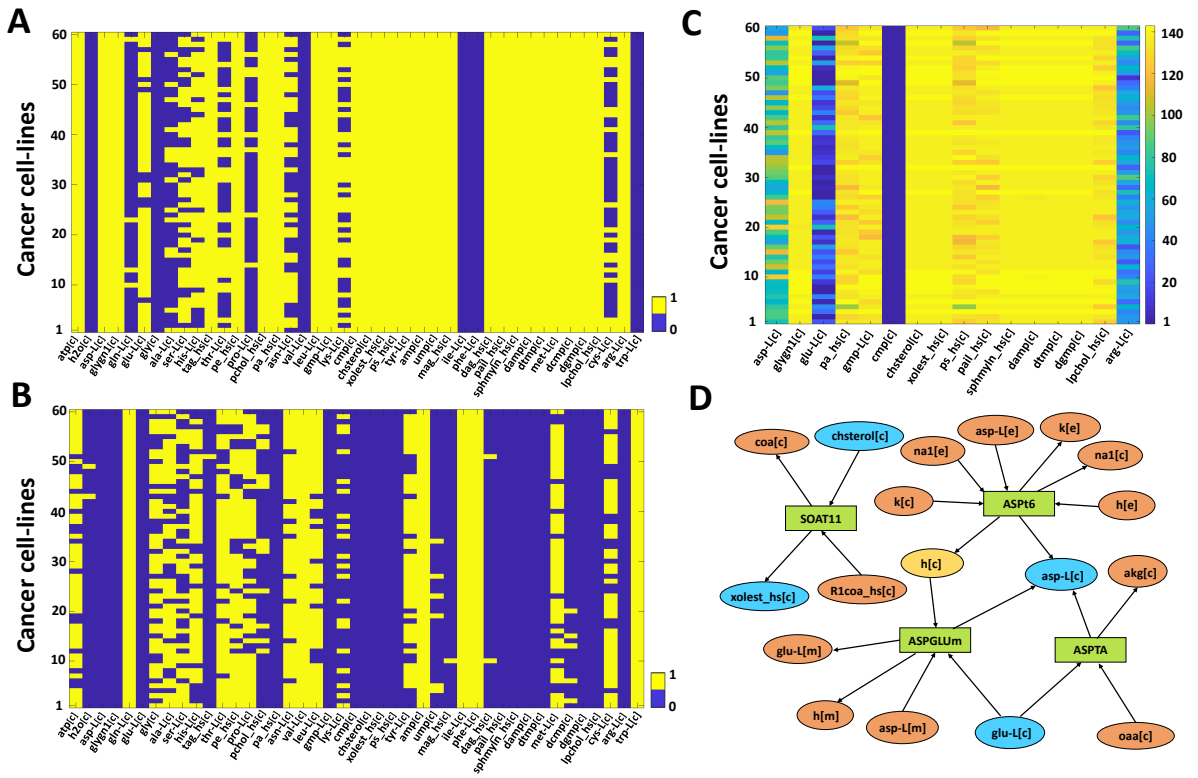

Figure 3.6: **Biomass metabolites affected by the 143 growth reducing genes and 1488 non-effecting genes.** Reduction in production fluxes for each individual biomass metabolites were captured in the gene knockout condition. (A) Represent the production flux are 2 fold decreased or not for any 143 genes and (B) represents the case for 1488 genes. We gave value 1 if the production flux of a metabolite is decreased in at least one gene knockout condition across each cell-lines, otherwise, the value remains zero. For 16 metabolites, all values are zero across the 60 cancer cell-lines in (B) but there are non-zero values in (A). (C) The number of genes among the set of 143 growth reducing genes whose knockout shows at least 2 fold reduction in the production fluxes for each of the 16 metabolites. (D) A bipartite network that represents the connection between L-Aspartate, L-Glutamate, cholesterol and cholesterol ester. Rectangular and ellipse-shaped boxes indicate the reaction and metabolite respectively and the arrow shows the flow of the flux.

consistency between gene expression and the corresponding enzyme activity. A comparison of the result of normal cells with that of the cancer cell-lines will help us to find targets that can reduce the growth of cancer cells but has minimal effect on the normal cells. Our gene knockout simulation result gave us 143 genes whose knockout can reduce the growth rate in cancer cell-line metabolic models. Some of these genes have multiple isoforms. After removing those isoforms, the gene list reduced to 121 unique genes and all of them could be potential drug targets. However, to be a potential drug target, a gene should show a minimal activity in normal cells. So, we looked for the activity of these 121 genes on normal cell models and

found from the literature [161] that only 13 genes (**Table 3.2**) out of 121 are inactive across all the 9 normal cell models. Thus we have 13 genes that reduce the growth in 60 cancer cell-lines models but have no effect on the flux state of the normal cell models. Therefore, these 13 genes can be considered as potential drug targets against cancer for these 9 tissues with minimal side effects. Interestingly, each of these 13 genes has very high BRS (>353) (see **Table 3.2**). Most of the genes (UQCR11, CYC1, UQCRQ, UQCR10, MT-CYB, UQCRB, UQCRC1, UQCRC2, UQCRFS1 and UQCRH) given in **Table 3.2** have same BRS because they are associated with the same reactions "Ubiquinol-6 Cytochrome C Reductase, Complex III" with '*AND*' combinations. This reaction is catalysed by cytochrome bc1 complex (EC 1.10.2.2), which is the third complex in the electron transport chain in mitochondria and the subunit proteins are encoded by these ten genes. It plays a critical role in ATP generation process by catalysing electron transfer from ubiquinol to cytochrome c, coupled to proton transport from the matrix space to the intermembrane space of mitochondria [316, 317].

Table 3.2: **Gene ID, gene symbol and the corresponding average value of the biomass metabolic score (BRS) across 60 cancer cell-line models of the cancer specific drug targets.**

No.	Gene ID	Gene symbol	Avg. of BRS
1	10975	UQCR11	379
2	1537	CYC1	379
3	27089	UQCRQ	379
4	29796	UQCR10	379
5	31	ACACA	385
6	32	ACACB	370
7	4519	MT-CYB	379
8	6646	SOAT1	383
9	7381	UQCRB	379
10	7384	UQCRC1	379
11	7385	UQCRC2	379
12	7386	UQCRFS1	379
13	7388	UQCRH	379

3.3.4 Experimental validation of the identified potential drug targets

To validate our simulation results for identifying potential drug targets, we searched for the inhibitors of these 13 genes and used two commercially available inhibitors, i.e., mitotane (SOAT1 inhibitor) [318] and myxothiazol (CYTB inhibitor) [319] for in-vitro studies. Mitotane

is reported to show anticancer activity in some cell-lines such as NCI-H295, Hela, HepG2, IMR-32 and HEK293 [318]. So we considered four cell-lines (HCT116, K562, HL60 and A549) from NCI-60 cell-line panel, which are different from the cell-lines reported in [318]. The effect of these two inhibitors on the cell viability was studied by adding the inhibitor at different concentrations and measuring the growth rate of cell-lines. Fold change in the growth rate (i.e., cell viability) was calculated for each cell-line at different drug concentrations for both the drugs and was plotted in **Fig. 3.7**. An EC50 value (concentration of drug at 50% fold change cell viability) was calculated for each cell-line from the resultant curve. The EC50 value of mitotane was 37.83 μM (for HCT116), 60.85 μM (for K562), 38.51 μM (for HL60) and 57.99 μM (for A549) and for myxothiazol, it was 18.28 μM (for HCT116), 84.92 μM (for K562), 8.21 μM (for HL60) and 9.25 μM (for A549). Thus, mitotane and myxothiazol both are effective in inhibiting the growth of these four cell-lines.

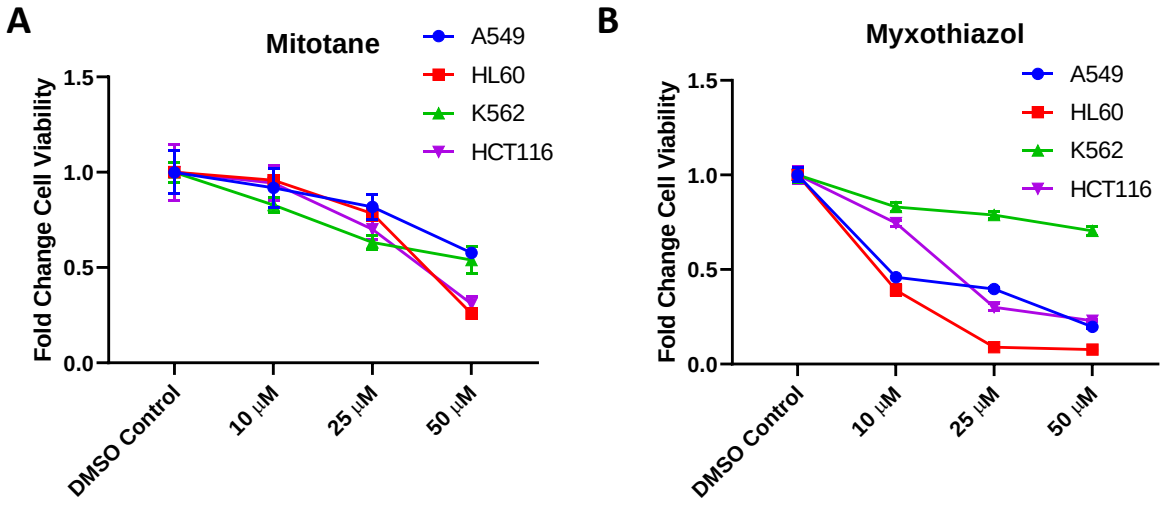

Figure 3.7: **Effect of mitotane and myxothiazol in cell viability.** Experimentally measured fold change in cell viability of four different cell-lines (A549, HL60, K562, HCT116) at different concentrations of mitotane and myxothiazol.

3.3.5 Testing the predictive ability of GSMM for single-gene knockout

We extracted the information from DEMETER database [307] on the knockdown effect of 1444 genes in 30 cell-lines. We calculated the Spearman rank-correlation between the predicted FCG from our GSMM and the experimental data from DEMETER database for each of the 30 cell-lines. The corresponding p-value of the rank-correlation for each cell-line was obtained by

permutation test. It was observed that most of the obtained positive rank-correlation were not significant (**Fig. 3.8**). There were only 5 cell-lines, which are showing significant positive rank-correlation but their correlation value was less than 0.15. Thus, the obtained gene ranking from single-gene knockout results does not show much correlation with the experimentally observed result. So, we looked for the effect of multiple genes knockout on the growth rate.

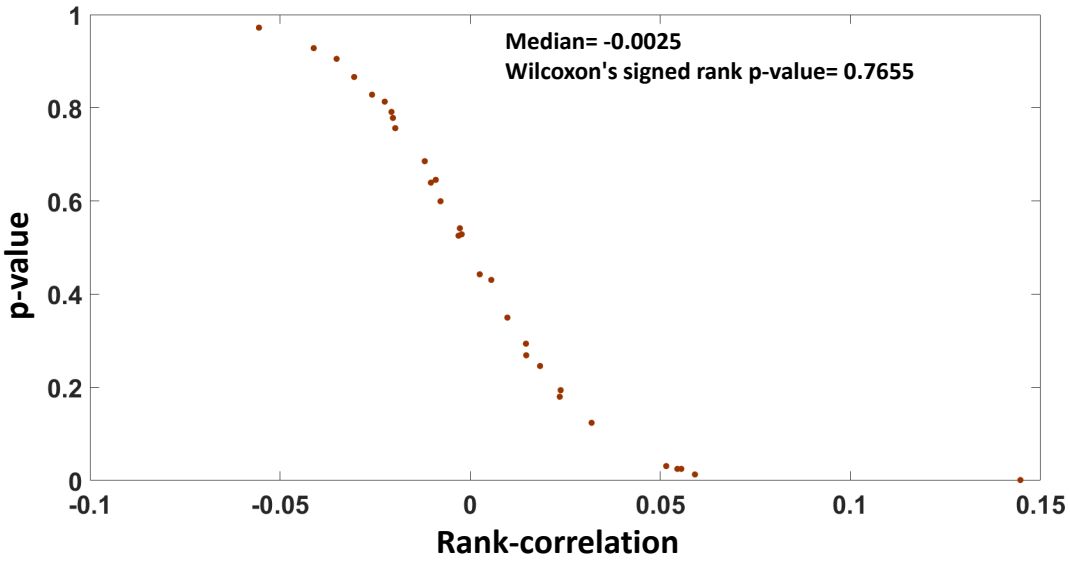

Figure 3.8: **Comparison of gene knockout simulation results with DEMETER database.** Distribution of measured Spearman rank-correlation between predicted FCG of genes using GSMM and experimental data from DEMETER for the 30 cell-lines. The *p*-values were measured using permutation test.

3.3.6 Identification of multiple targets using DrugBank database information

We took the drugs available in the DrugBank database [308] based on the gene target information. DrugBank database contains the biochemical and pharmacological information about the drugs. We only selected 380 drugs which are inhibitory and the corresponding target genes are present in the cancer cell-lines metabolic models. These 380 drugs have 202 metabolic targets in the models. To observe the effect of a particular drug on the growth rate, we knocked out all the genes that were inhibited by that drug and simulated the models via MOMA. This exercise was repeated for all the 380 drugs across all the 60 cancer cell-line models. We used a cut off

value of 0.5 on FCG (representing at least 50% reduction on the growth rate) to call a drug active and obtained 76 drugs. 10 out of these 76 drugs have already been approved in cancer treatment and another 18 drugs are in different phases of the clinical trial.

We considered NCI-60 growth inhibition database [309] to get the GI50 values of the drugs and compared the predicted anti-proliferative activity with the experimentally measured potency of the drugs. There are 64 drugs with GI50 value in the NCI-60 growth inhibition database. Out of these 64 drugs, 23 drugs have mean log GI50 value less than -5 across 60 cell-lines and therefore considered to be active against cancer for most of the cell-lines. Comparing these 23 drugs with our list of 76 drugs, we obtained 17 drugs common in both sets.

Finally, a cell-wise comparison between predicted FCG of drugs using GSMM and their log GI50 values was performed and the Spearman rank-correlations was obtained. It is observed that around 50% cell-lines were showing significant rank-correlation and their correlations were also higher than single knockout result, see **Fig. 3.9** (median Spearman rank-correlation= 0.2137, Wilcoxon's signed-rank p-value= 1.6296×10^{-11}).

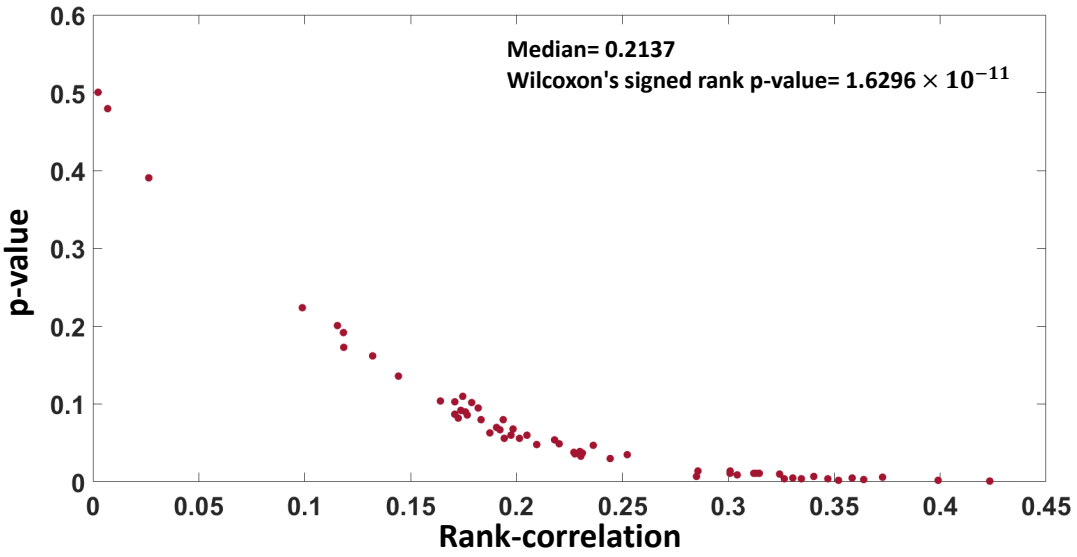

Figure 3.9: **Validation of predicted cell-line specific responses of drugs.** Distribution of measured Spearman rank-correlation between predicted FCG of drugs using GSMM and their log GI50 values for the 60 cell-lines. The p-values were measured using permutation test.

3.3.7 Linking the significance of single-gene knockout ranking on the activity of drug

We used our gene knockout results of 202 target genes corresponding to those 380 drugs to test the significance of gene ranking. It was observed that 37 genes were present at the top position and 146 genes at the bottom in our gene ranking list. The drugs corresponding to these 37 genes significantly reduced (mean FCG $< 10^{-6}$) the growth rate of cancer models (**Fig. 3.10**). On the contrary, those drugs whose targets belong to the set of 146 genes, placed at the bottom in our gene ranking list, showed no effect in the cancer models.

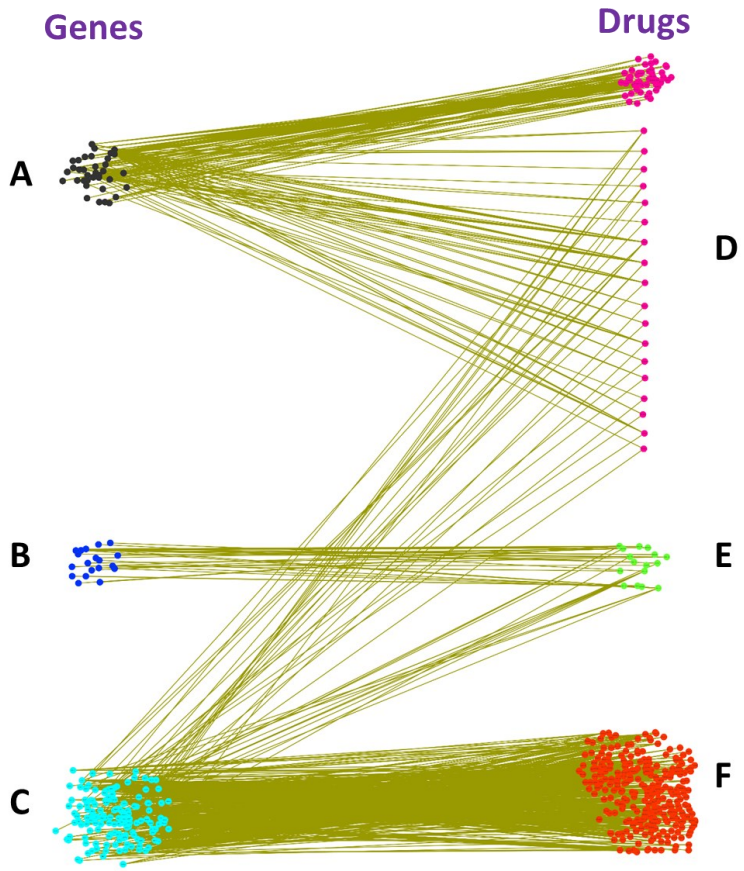

Figure 3.10: **Robustness of gene ranking.** (A-C) Gene ranking of total 202 targets of at least one of the 380 drugs. (A) Top 37 genes lie on the lower circled portion (mean FCG$< 10^{-6}$) in **Fig. 3.2**. (B) 19 Genes lie in between the lower and upper circled portion (mean FCG lies between 10^{-6} to 0.99995) in **Fig. 3.2**. (C) Bottom 146 genes lie on the upper circled portion (mean FCG$>$ 0.99995) in **Fig. 3.2**. (D) 73 drugs (mean FCG$< 10^{-6}$) significantly reduce the growth rate of cancer models. (E) 16 drugs which gives mean FCG between 10^{-6} to 0.99995 in cancer models. (F) 291 drugs that show no effect (mean FCG$>$ 0.99995) in the cancer models.

3.4 Discussion

Recently, GSMM gained a lot of attention in drug discovery. It has been used to study drugs related to cancer. Ghaffari et al. [320] explored strategy for identifying anti-growth factors for the inhibition of cell growth using GSMM on 11 cell-lines and identified potential antimetabolites that could inhibit the growth or kill any of the cell-lines. They also checked the in-silico toxicity by employing GSMMs for 83 human healthy cell-types. The same methodology had been applied by Agren et al. [66] in a different study to find potential drugs for hepatocellular carcinoma (HCC) by reconstructing and analysing personalized GSMMs for six HCC patients. Raškevičius et al. [69] used GSMMs to predict the putative effects against cancer of those compounds which are structurally similar to human metabolite and also gave a concept of finding therapeutic windows through GSMMs. Turanil et al. [68] introduced a drug repositioning based method via GSMMs to predict therapeutic agents for cancer treatment. They reconstructed prostate cancer-specific GSMM by combining personalized GSMMs ($n > 450$) and proteomics data. They used drug-perturbed gene expression data of three cell-lines (PC3, HL60, and MCF7) from the ConnectivityMap2 (CMap2) [321] to reveal drug off-targets by predicting novel gene-drug interactions and evaluated in-silico cell viability. The present study aimed to develop a knockout strategies for identifying potential drug targets and the associated mechanisms using GSMM and gene expression data. This will help us to get novel drug targets as well as targets that might be used for drug repurposing. We used existing GSMMs of NCI-60 cell-lines [299] to predict the anti-proliferative activity of single metabolic genes as targets against cancer and ranked them accordingly. We got 143 genes whose knockout reduced the cell growth across all the metabolic models of the NCI-60 panel. We also obtained a list of 1488 genes whose knockout does not show any effect on the growth rate of any cancer model. We searched for the underlying mechanism for such reduction in the growth rate of cancer cells by 143 genes and found that the biomass reduction score (BRS) of those genes were much higher than those of 1488 genes. The synergic effect in biomass reaction is much more for 143 gene list than 1488 gene list. It is observed that there are 12 biomass metabolites which are influenced by almost all the 143 genes but not by any of the 1488 genes for all the 60 cell-lines. Glycogen is the top-ranked among those 12 biomass metabolites. It is already reported that

glycogen pathway is up-regulated in various cancers [322, 323] and funneled into glycolysis to promote cell growth, invasion and metastasis [324]. Likewise, glycogen is used by cancer cells to survive under nutrient starvation condition [325]. Considering its importance, inhibition of glycogen metabolism has become a new potential strategy for cancer treatment [322, 326–328].

We looked for potential targets from these 143 genes which showed a significant reduction in the growth rate following knockout. To be a potential target, these genes need to show the minimal knockout effect on the normal cells. We obtained 13 such targets from 143 genes whose knockout reduced the proliferation rate of cancer cells but were inactive across all the 9 normal cell models. One of the main features of the identified targets was that they were showing their effect in all the NCI-60 cell-lines. To experimentally validate the effect of these targets on multiple cell-lines, we chose SOAT1 and CYTB and showed that it's inhibition reduces the growth rate in multiple cell-lines. Inhibition of SOAT1 is known to reduce growth rate in 5 cell-lines [318] and additionally we have showed its effect on 4 more cell-lines. These cell-lines are taken from different tissues like blood peripheral, colon, adrenocortical gland, cervix, liver, kidney and brain. We have used mitotane to inhibit SOAT1, which is already known for the treatment of adrenocortical carcinoma and Cushing's syndrome [329–331]. However, the inhibitor of CYTB, myxotyiazol, is not known as an anticancer drug, but we have seen its growth inhibiting effect on four cancer cell-lines. This could be a potential novel repurposed drug and need further evaluation. Moreover, literature survey showed that inhibition of SOAT1 and CYTB do not have any significant influence on the growth of the normal cells [332–334]. Literature also supports the validity of our other identified targets (given in **Table 3.2**). For example, atovaquone, a potent and selective mitochondrial inhibitor [335, 336], has been shown to reduce proliferation in cervical cancer cell-lines [337], Du145 prostate cancer cells [338] and MCF7-derived Cancer Stem-like CSCs [334]. Another identified target is UQCRB, whose inhibitor terpestacin blocks vascular endothelial growth factor (VEGF)-induced angiogenesis in endothelial cells and is proposed to be applied as a drug for human cancer [339, 340]. Cytochrome c-1 (CYC1) is found to play an important role in breast cancer patients. Knocking down of CYC1 inhibits proliferation in human breast cancer cell-lines [341]. In another study, it was observed that silencing CYC1 by shRNA transfection also inhibits proliferation in hu-

man osteosarcoma (OS) cells [342]. Another identified gene target UQCRFS1 appears to be involved in the progression of gastric cancers and in the development of more aggressive phenotype of breast cancer [343, 344]. Lentivirus-mediated knockdown of UQCRC2 suppresses cell growth and colony formation in RKO. HCT116 cells result in cell cycle arrest and induce cell apoptosis in vitro in colorectal cancer (CRC) [345]. The knockdown of ACACA expression inhibits cell proliferation in prostate [346] and breast [347] cancer cell-lines.

We used Spearman rank-correlation method to compare our single-gene knockout ranking obtained from the GSMM with the experimental data. Most of the observed rank-correlations were very low and/or not significant. This was in agreement with other studies where single-gene knockout does not show the desired result [348–350]. On the other hand, when applied multiple gene knockout strategies, we obtained a higher and significant rank-correlations with the experimental results. It leads to the conclusion that multiple genes knockout show a better result than single-gene knockout, confirming the similar observations by other studies [349–353]. This might be because genes or proteins interact in a complex network, where alternative pathways always exist to carry the function [349, 354]. Though the single knockout results did not give the desired correlations, the gene ranking obtained using this strategy seemed to be significant. It was noticed that a drug could only be active if it has at least one target belonging to the top rank. In case, none of the targets is from the top rank then that drug is observed to be ineffective.

The developed strategy to use gene knockout in GSMMs to identify drug targets has general applicability with any novel set of gene expression data associated with a tumour. The tumour-specific GSMM can be built from the gene expression data to go for the single or multiple gene knockout strategies. We proposed to use drug information for multiple gene knockout strategies that can also serve as drug repurposing technique. This method could be used to identify novel drug targets as well as targets that might be used by existing drugs on novel kinds of tumour. It is, therefore, possible to identify genes that are more relevant to specific cancer. The developed methodology could also be used to screen for common therapy. This strategy was used in the present study where we obtained 143 genes whose knockout were showing significant growth reduction across all cell-lines (see **Fig. 3.11**)

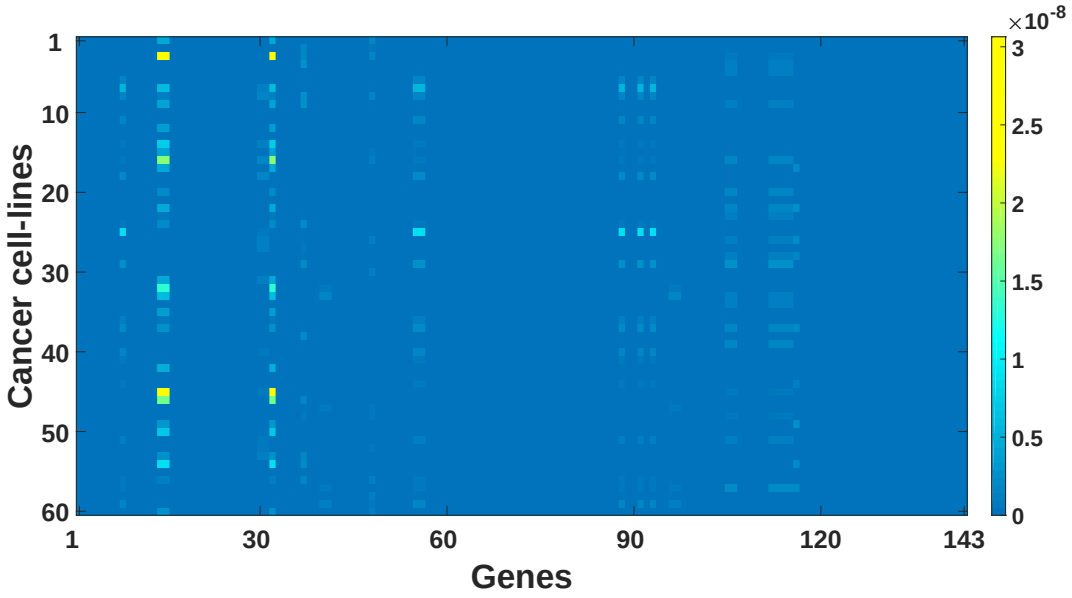

Figure 3.11: **Gene knockout simulation result for 143 genes across 60 cancer cell-line models.** Here the colour bar represents the fractional cell growth (FCG), the ratio of growth rates in knockout condition to wild-type condition. Here, we observed very low FCG value across all the 60 cancer models.

In the previous two chapters, we have shown the application of GSMM in finding metabolic alterations and regulatory points through *in silico* gene knockout studies. Combining these two applications of GSMM could lead us to the identification of potential drug targets that might revert the altered metabolic state from disease to healthy condition. In the next chapter, we have applied GSMM to identify potential targets for nonalcoholic steatohepatitis (NASH).

4

Importance of genome-scale metabolic model in identifying drug-targets[1]

4.1 Introduction

Nonalcoholic steatohepatitis (NASH), characterized by steatosis, lobular inflammation, and hepatocellular ballooning, is the second stage of the nonalcoholic fatty liver disease (NAFLD) continuum. It is a slowly progressive disease that often remains clinically discerned, resulting in late detection, curbing the therapeutic options, and contributing to poor outcomes. Hence, there is a need to reveal the underlying molecular mechanisms of the disease that might lead to the development of effective treatment strategies. Probing context-specific networks, such

[1]The bulk of this chapter has been communicated for possible publication in peer reviewed journal.

as protein-protein interaction (PPI) and/or metabolic networks, is the only way to make proper sense of the anomalies in the cellular systems that occur with a disease's progression. Metabolic networks can investigate alterations in the metabolism that befalls across the entire histological spectrum of disease, probing the changes that develop during the progression of benign to severe stages [154]. Genome-scale metabolic models (GSMMs) capture the altered metabolic pathways through a bottom-up systems-level understanding of the metabolic network. Over the past decade, GSMM has widely been employed to capture the disease-associated molecular mechanisms [61, 64], which are further used to identify potential drug targets [36] and biomarkers [64]. Some therapeutic strategies are proposed in NAFLD by identifying altered metabolic pathways using GSMM [62, 67]. Besides the metabolic alterations, pathways like inflammation, fibrosis, apoptosis, etc., also contribute to the disease progression. Thus, protein and metabolic level rewiring is required to control the disease progression. Hence, to better understand the feasibility of the targets, their role in the disease system should be adequately investigated, which brings the collaborative effort of the context-specific molecular networks into the scenario. Probing these context-specific networks is probably the only way to make sense of the cellular anomalies during disease progression.

The present study aims to identify the potential drug targets for NASH. We integrated the open-source gene expression data of the liver biopsy sample [355] into a functional GSMM for hepatocytes [62] to capture the metabolic alterations in the disease condition. Understanding molecular alterations were then used to identify candidate targets that might cause disease transversality towards a healthy state. Finally, the knockdown profiles of these identified candidate genes were investigated through GSMM to obtain the potential drug targets. Here, we also explored their mechanism of action in attenuating NASH.

4.2 Material and methods

4.2.1 Transcriptomics data collection

Gene expression data of liver biopsy samples were obtained from the Gene Expression Omnibus (https://www.ncbi.nlm.nih.gov/geo/); the accession number is GSE126848 [355]. The

data include RNA-Seq profiles of the 15 NAFL, 16 NASH, and 26 control individuals. The control group comprises 14 healthy normal-weight subjects and 12 overweight subjects. Genes having missing values in at least one sample were excluded from the analysis. The data was normalized by using Transcripts Per Million (TPM) normalization method and the outliers were replaced by using the 'filloutliers' function in MATLAB.

4.2.2 Differentially expressed genes

To compare the expression values between the two groups, a two-sample t-test was performed using the 'mattest' function in MATLAB. The 'mafdr' function in MATLAB was applied to the p-values to implement the Benjamini and Hochberg false discovery rate (FDR). Genes with a fold change of 1.2 and FDR adjusted p-value < 0.05 were selected as differentially expressed genes (DEGs) [356].

4.2.3 Reconstruction of context-specific metabolic models

We used a functional GSMM for hepatocytes, *iHepatocytes2322* [62], generated based on the hepatocyte-specific proteomics data and included 2322 genes, 7930 reactions, and 2895 unique metabolites across eight different cellular compartments. The pre-processed transcriptomic data corresponding to the metabolic genes was mapped into the *iHepatocytes2322* using the E-Flux method [193].

A fasting condition was imposed on all the models as the liver biopsy samples were taken at a fasting state. During fasting, the liver uptakes gluconeogenic substrates (like lactate, glycerol, etc.), non-esterified fatty acids and amino acids, and produces glucose, very-low-density lipoprotein (VLDL), ketone bodies, and plasma proteins [67]. Thus, the input variables of our models are: 1) lactate, 2) glycerol, 3) fatty acids, 4) amino acids, and the output variables are: 1) glucose, 2) VLDL, and 3) ketone bodies. We also allowed the uptake of oxygen, phosphate, minerals, and protein secretion (mainly albumin), urea, H_2O, and CO_2.

4.2.4 Flux-based analysis

Flux variability analysis (FVA) [196] was applied to evaluate the flux ranges (minimum and maximum) for each reaction flux that satisfies the model constraints. Here, we performed FVA in the CobraToolbox 3.0 [314] on the reconstructed GSMMs by minimizing the sum of flux rates based on the assumption that fasting condition cells will try to reduce the pathway usage for economic purposes [67]. To perform FVA, 'fluxVariability' function was applied (using the gurobi solver v9.0) with only considering the solutions that give at least 90% [357] of the optimal solution.

Perturbed reactions are predicted based on the flux ranges between the two clinical groups. We first listed out the reactions that have significant changes in the flux ranges (i.e., either lower or upper range). In this step, a two-sample t-test was performed on the lower and upper flux ranges separately and applied the cutoff value on Benjamini and Hochberg FDR adjusted p-value ≤ 0.05. The reactions having flux values in both coordinates (i.e., lower and upper flux ranges are negative and positive, respectively) were excluded from the analysis. The flux ranges A=[$minA$, $maxA$] and B=[$minB$, $maxB$] for each altered reaction were then compared to get the direction of the alterations (i.e., up or down), where A and B represent the super flux ranges for these two clinical groups [64]. Here, we considered:

$B > A$ if $\big((min_A < min_B)$ & $(max_A \leq max_B)\big)$ or $\big((min_A \leq min_B)$ & $(max_A < max_B)\big)$,

and

$B < A$ if $\big((min_B < min_A)$ & $(max_B \leq max_A)\big)$ or $\big((min_B \leq min_A)$ & $(max_B < max_A)\big)$

for the case where A and B both belong to the positive coordinate. Conversly,

$B < A$ if $\big((min_A < min_B)$ & $(max_A \leq max_B)\big)$ or $\big((min_A \leq min_B)$ & $(max_A < max_B)\big)$,

and

$B > A$ if $\big((min_B < min_A)$ & $(max_B \leq max_A)\big)$ or $\big((min_B \leq min_A)$ & $(max_B < max_A)\big)$

for the case where A and B both belong to the negative coordinate. The fold change value for the ranges was calculated from the relation:

$fold = 1 + \frac{|b|-|a|}{max(|a|,|b|)}$, where ($a$, b) can take ($maxA$, $maxB$) or ($minA$, $minB$).

4.2.5 *In silico* gene knockdown exercise using GSMM

We performed an *in silico* single gene knockdown approach to obtain the gene set responsible for the network perturbations towards the healthy state. To get the disease-specific GSMM, we integrated the average gene expression values into the *iHepatocytes2322* by applying the E-Flux method [193]. On the other hand, the knockdown model was built by considering the 90% reduction in the expression value of a particular gene, and the corresponding flux state (V^{res}) was obtained by using minimization of metabolic adjustment (MOMA) [207]. This process requires the state (V^{ref}) of disease-specific GSMM. The 'gpSampler' function available in the CobraToolbox 3.0 [314] was used for flux sampling and the mean value of the flux distributions was considered. Finally, we assigned scores for each gene knockdown similar to the method proposed in the metabolic transformation algorithm (MTA) [209], following the rule

Transformation Score (TS) = $\frac{\sum_{i \in R_{success}} |V_i^{ref} - V_i^{res}| - \sum_{i \in R_{unsucces}} |(V_i^{ref} - V_i^{res}|}{\sum_{i \in R_s} |V_i^{ref} - V_i^{res}|}$.

The altered relations are classified into two groups $R_{success}$ and $R_{unsuccess}$ based on the changes in flux rates in the required direction and R_s represents the set of unaltered reactions.

4.2.6 Method to predict metabolic network level perturbation using the gene knockdown profile

Here, we used four inputs: (i) a generic GSMM (*iHepatocytes2322*), (ii) up-and downregulated genes under each gene knockdown case, (iii) disease-specific gene expression data (average gene expression values under the specific disease stage), and (iv) flux state (V^{ref}) of disease-specific GSMM. The knockdown-specific gene expression data were generated from the disease-specific gene expression data by considering a 2-fold up/down in the expression values of the up/downregulated genes. Next, the obtained expression data was integrated into the *iHepatocytes2322* by applying the E-Flux method [193], and the corresponding flux state (V^{res}) was predicted by using MOMA [207]. This process requires the flux state (V^{ref}) of disease-specific GSMM. Finally, a score was assigned for each gene knockdown similar to the method mentioned in the earlier section. We also extracted the metabolic reactions whose fluxes shifted from the diseased state toward the target state.

4.3 Results

4.3.1 Changes in metabolic flux in NAFLD

We investigated a dataset GSE126848 [355], which includes RNA-Seq liver biopsy data of the 15 NAFL, 16 NASH, and 26 control individuals. To delve into the changes in the expression profiles, the differentially expressed genes (DEGs) were identified. We found 5672 and 5468 DEGs (FDR adjusted p-value$<$0.05 & fold change cut off 1.2) in the NASH and NAFL categories, respectively (**Table 4.1**). Also a significant number of metabolic genes (included in *iHepatocytes232215*) were found differentially expressed in this two stages of NAFLD (**Table 4.1**). Thus, understanding metabolic pathway level alterations are very crucial for gaining more insights into the disease mechanism.

Table 4.1: **Number of differentially expressed genes (DEGs).** The second row represents the total up- and downregulated genes obtained in NASH and NAFL categories, while the third row denotes the number of DEGs involved in *Hepatocytes232215*.

	NASH vs Control		**NAFL vs Control**	
	Upregulated	**Downregulated**	**Upregulated**	**Downregulated**
DEGs	2810	2862	1480	3988
DEGs involved in *iHepatocytes2322*	412	464	245	590

Metabolic flux level profiles were predicted for each individual by integrating the gene expression data on *iHepatocytes232215* [62] followed by flux variability analysis (FVA) [196]. 2,859 and 1,721 reactions were altered for the NAFL and NASH categories, respectively, in which 998 were common in both categories. It is known that NAFLD is strongly correlated with carbohydrates, lipids, bile acids, amino acids, and lipid metabolism dysfunctioning [358]. So, the altered reactions were linked with these processes (**Fig. 4.1A**). It was observed that 26% of the associated reactions of carbohydrate metabolism were altered in NAFL. Additionally, transport reactions, exchange reactions, and vitamin metabolism also showed alteration. The numbers of up- and downregulated reactions for the same metabolism process were different

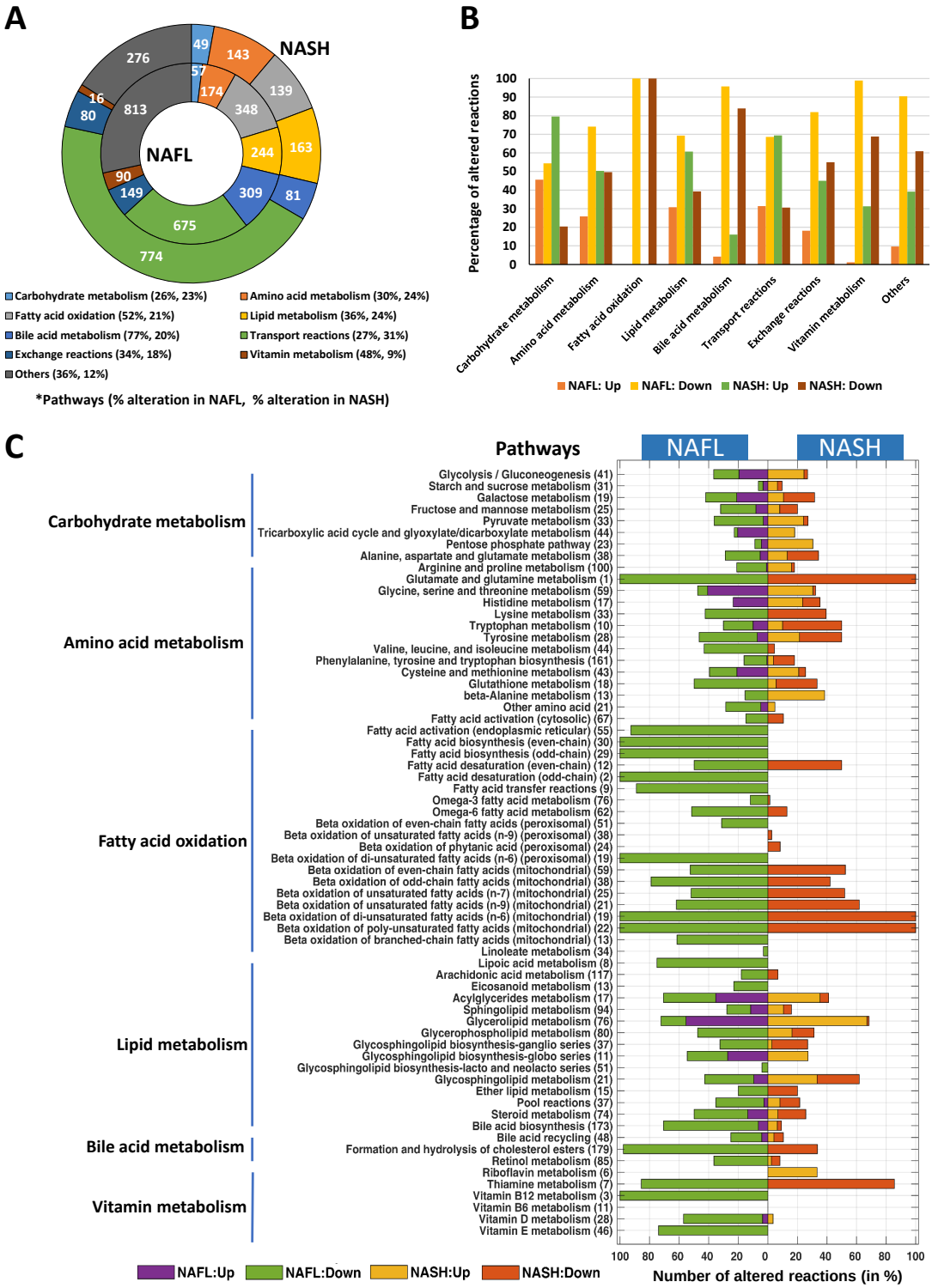

Figure 4.1: **Metabolic flux level alterations.** A) Represents the doughnut plot of the major metabolic processes associated with the altered reactions, and the corresponding numbers are mentioned inside. The inner and outer circles respectively represent the NAFL and NASH categories. Also, the level of alterations of each process is provided inside the parenthesis of the color legend. B) The bar plot represents the percentage of up–and downregulated reactions in each metabolic process. C) Significantly altered metabolic pathways obtained for NASH and NAFL in comparison to the control group. The bar length represents the percentage of altered reactions for each pathway. The number inside the Y-label denotes the number of total reactions in the corresponding pathway.

for NAFL and NASH (**Fig. 4.1B**). Interestingly, the fatty acid oxidation process were found downregulated for both groups and it primarily reflects the alterations in the fatty acid activation, desaturation, and beta-oxidation pathways (**Fig. 4.1C**). We also found that the reactions in the NASH group were showing higher degree of alterations compared to its counterpart. The glycolysis or gluconeogenesis, tricarboxylic acid cycle, glyoxylate or dicarboxylate metabolism, and pyruvate metabolism were the most upregulated pathways in the carbohydrate metabolism for the NASH group. These promote higher production fluxes of acetate, pyruvate, acetyl-CoA, and glycerate. Similar results were found for the NAFL group, except some reactions were downregulated in glycolysis or gluconeogenesis and pyruvate metabolism pathways. In case of lipid metabolism, most reactions in the glycerolipid metabolism were upregulated, and the reactions in the arachidonic acid metabolism and glycosphingolipid biosynthesis-ganglio series were downregulated. Up- and downregulations were both observed for other pathways in the lipid metabolism process. On the other hand, marked alterations (mostly downregulation) were observed for bile acid biosynthesis, recycling, and formation and hydrolysis of the cholesterol esters pathways. We observed decreased production fluxes of cholate, glycocholate, taurocholate, glycochenodeoxycholate, and taurochenodeoxycholate from cholesterol. Significant alterations in amino acid metabolism were also noticed. The reactions involved in arginine and proline, glycine, serine and threonine, cysteine and methionine, and beta-Alanine, were upregulated. The reactions involved in the glutathione metabolism, lysine metabolism, phenylalanine, tyrosine, and tryptophan biosynthesis pathways were downregulated for the NASH group. For the NAFL group, these pathways were downregulated except for glycine, serine, threonine metabolism, cysteine, and methionine metabolism pathways. Here, we observed reduced fluxes of glutathione peroxidase in cytoplasmic, mitochondrial, and extracellular compartments for both groups, suggesting defects in antioxidant defence mechanisms. Glutathione peroxidase plays a vital role in cellular defence against oxidative stress by converting H_2O_2 to H_2O [359]. Besides that, we also found reduced fluxes for glutathione oxidoreductase in cytoplasmic and mitochondrial compartments, which regenerates glutathione through the reduction of glutathione disulfide by utilising NADPH and NADH as a cofactor.

4.3.2 Genes causing metabolic transformation

These observed disease-associated molecular alterations were further used to determine potential recovery options. At the metabolic stage, we systematically carried out a 90% gene knockdown and calculated the transformation score (TS) [209], reflecting the extent to which it may transform the disease state towards a healthy state (**Fig. 4.2A**). Genes with positive TS (hereafter referred to as metabolic candidate genes, MCG) were selected for further evaluation. From this *in silico* knockdown analysis, we obtained 91 and 112 MCG for the NAFL and NASH groups, respectively. Also, a significant overlap (58 genes) was observed between the MCGs of both groups. These obtained MCG for both groups were enriched in retinol metabolism, one carbon pool by folate, tyrosine metabolism, drug metabolism, pyruvate metabolism, glycolysis/gluconeogenesis, and alanine, aspartate, and glutamate metabolism.

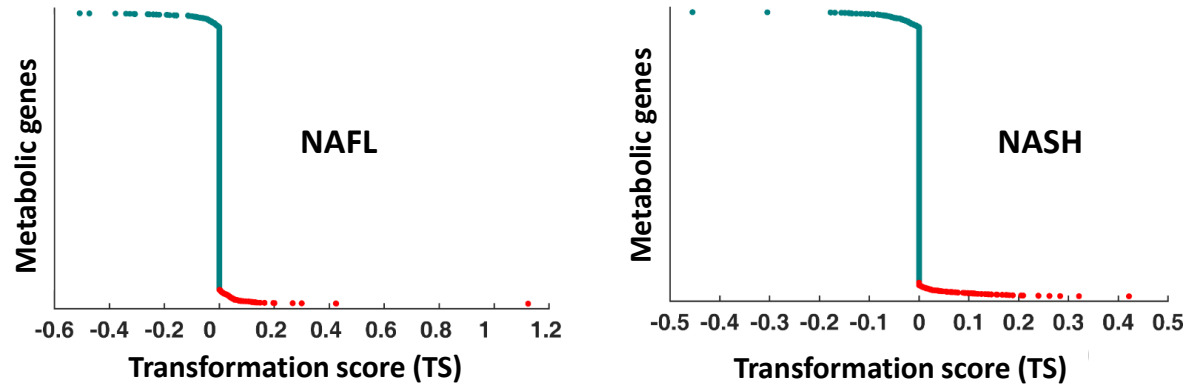

Figure 4.2: **Transformation score (TS) analysis.** TS of the metabolic genes, obtained by performing 90% gene knockdown exercise. Here, the red dots represent the genes with TS>0.

4.3.3 Identifying targets in NAFLD using GSMM

Besides the metabolic alterations, pathways like inflammation, fibrosis, apoptosis, etc., also contribute to the disease progression. Thus, protein level rewiring is also required to control the disease progression. Therefore, we need a set of genes that can influence the metabolic network and DEGs. So, here we used the indispensable candidate proteins (ICp) [360] obtained from the investigation of the directional PPI networks containing the DEGs, candidate proteins (Cp), and the MCGs.

We next aimed to filter the predicted candidate targets obtained from the network analysis by investigating their knockdown effect on the disease-specific GSMMs. Analysis of GSMM provides the unique opportunity to explore the knockdown effect on the metabolic networks systematically and can help in quantifying their impact on the transformation from the disease state to the healthy state. For this purpose, knockdown profiles of each ICp in the HEPG2 cell line were used to capture the transition of metabolic flux from the disease state to the healthy state. We calculated the TS for each ICp (**Fig. 4.3A**) and then considered the proteins with positive TS scores as potential targets. The identified proteins are crucial in the physiology of NASH as these proteins affect the controllability of the network containing DEGs, Cps and MCGs, capable of inducing reverse gene expression to the DEGs and initiating the metabolic flux level transition from the disease to a healthy state. We obtained three potential targets for NASH, namely, BAG6, CYCS, and CASP3.

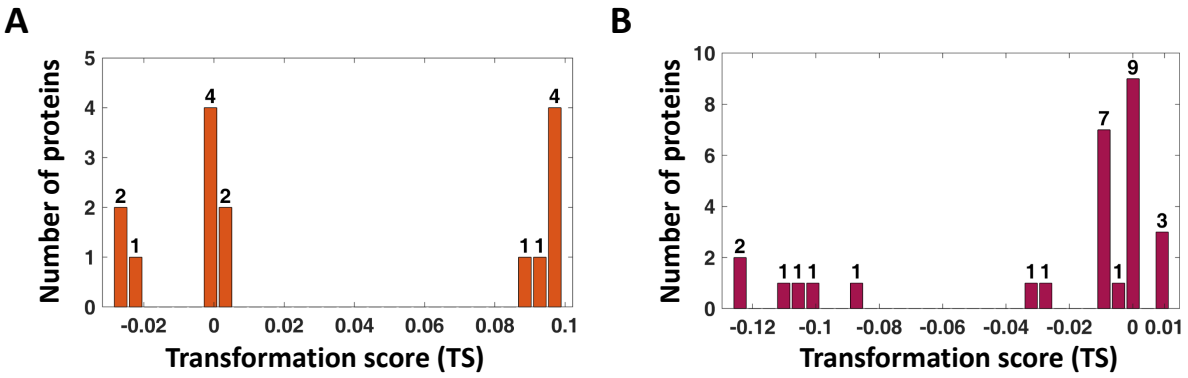

Figure 4.3: **The potential targets in NAFL and NASH.** A) The histogram of transformation scores (TS) per protein in ICp . The TS is plotted in the X-axis, while the bar length denotes the number of proteins. A gene is considered as a potential target if it has a positive TS.

In the NAFL category, eight proteins (ACVR1, BMP4, CASP3, FGFR3, GABPB1, PLAU, PPP1CC and VDAC1) were identified as potential targets. A literature review of these eight prospective targets reveals an intriguing fact that most of these proteins have already been implicated in NAFLD. Bone morphogenetic protein 4 (BMP4) belongs to the TGF-β superfamily and acts as pro-fibrogenic factor potentiating HSC transdifferentiation [361]. Besides the contribution to hepatic fibrosis, BMP signaling plays a role in developing NAFLD, and the treatment with BMP inhibitors was observed to reduce hepatic triglyceride content in diabetic db/db mice [362]. The canonical BMP signaling occurs through another target ACVR1

which echoes its importance [362]. Being a member of the fibroblast growth factor receptor family, FGFR3 is reported to contribute to fibrogenesis [363]. PLAU (also known as UPR) has been shown to stimulate the synthesis of triglycerides in Huh7 hepatoma cells [364]. Finally, a VDAC-based peptide R-Tf-D-LP4 was reported to halt the progression of steatosis and NASH progression in a high-fat diet (HFD-32) mouse model [365].

4.3.4 Effects of the identified targets in reversing the disease metabolic flux state

Often, targeting a gene results in changes in the expression levels of specific genes since these gene products share several similar pathways, processes, and functions. Thus, an investigation of these affected genes and their associated pathways and ontological properties facilitates deciphering the mechanistic understanding of the targeted gene. The knockdown profiles of these potential targets were further used to evaluate their effect on NASH-specific traits: lipid accumulation (steatosis), inflammation, apoptosis, and fibrosis (**Fig. 4.4A**). The knockdown of CYCS and PLAU affected most metabolic genes in the NASH and NAFL categories, respectively (**Fig. 4.4B-C**). The knockdown of CYCS and CAPS3 could improve inflammation, fibrosis, and apoptotic pathways, whereas the knockdown of BAG6 ameliorates the latter two and the knockdown effects of the targets for the NAFL category have a heterogeneous impact [360].

To elucidate the beneficial effects of the identified potential targets on hepatic steatosis, the knockdown profile of each target in the disease-specific GSMM was integrated. The percentages of upregulated reactions transferred towards the control were higher than the downregulated ones for all these targets (**Fig. 4.4D**). In the NAFL category, knockdown of the PPP1CC and VDAC1 shows a higher impact on the metabolic level alterations than the other genes, particularly in the lipid, bile acid metabolism, and transport reactions (**Fig. 4.5A**). The other six targets have almost similar effects in all the altered metabolic processes. All three NASH targets have a similar impact. However, their influences are minor compared to the NAFL category. They are, nevertheless, more potent than others in the fatty acid oxidation process. The reactions involved in the fatty acid activation and mitochondrial beta-oxidation were already

downregulated in the NAFL and NASH groups. The knockdowns of potential targets of NASH

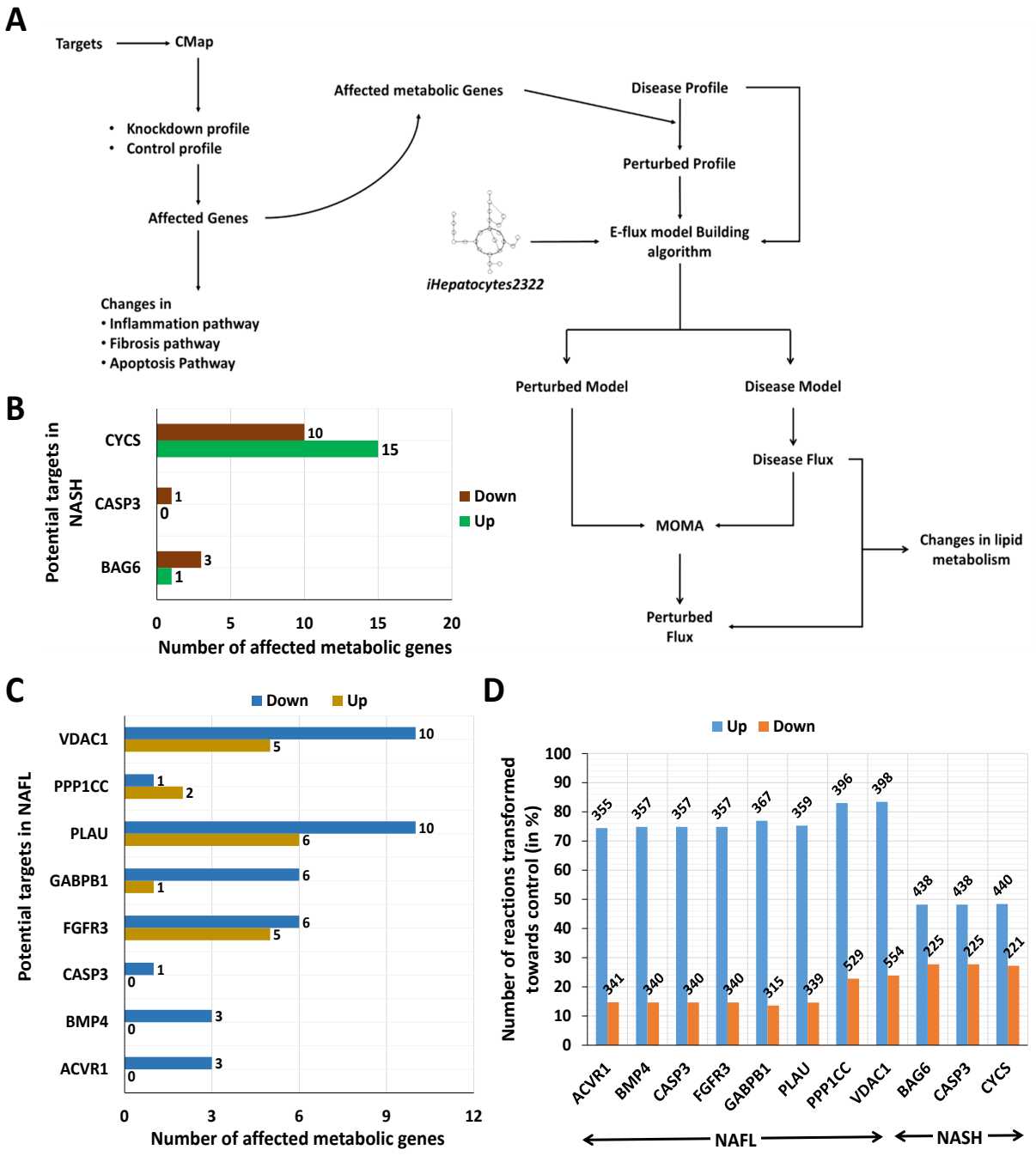

Figure 4.4: **Mechanistic understanding of the potential targets.** A) The schematic diagram for exploring the potential targets on the disease-specific traits. The process starts with extracting the gene knockdown profiles from the CMap database and ends with identifying changes in the disease-specific traits such as lipid accumulation (steatosis), inflammation, apoptosis, and fibrosis. B-C) Bar plot representing the numbers of affected metabolic genes following the knockdown of each potential target in the NAFL and NASH groups. D) The figure illustrates the number of reactions transferred towards normal following the knockdown of each target in their respective category, and the value is provided at the top of each bar. The number of up-and downregulated reactions in the NAFL category are 477 and 2382. In the NASH category, these numbers are 909 and 812, respectively.

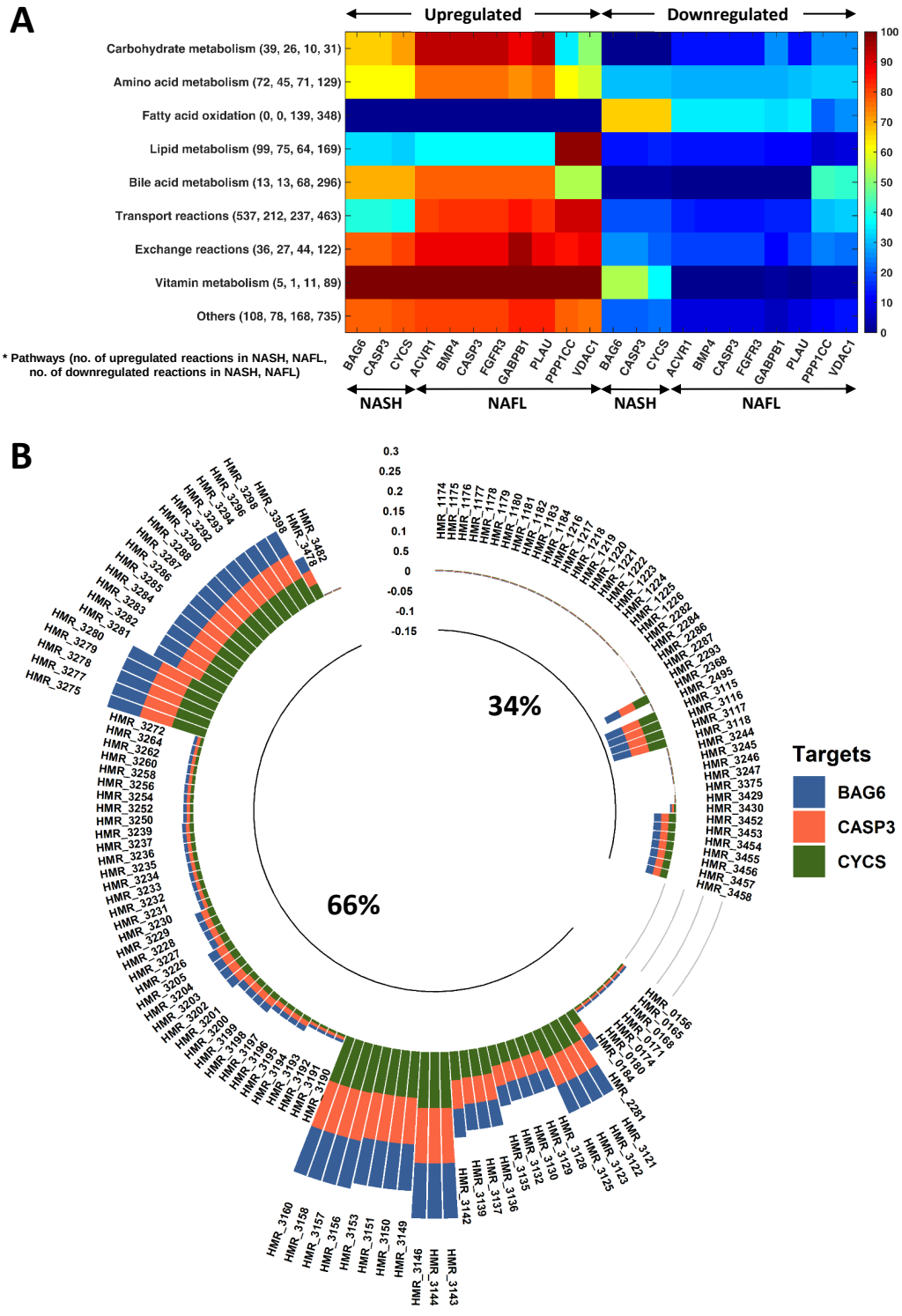

Figure 4.5: **Knockdown effect of the potential targets in the metabolic level alterations.** A) This figure depicts the effect of each target on the metabolic processes altered in the NAFLD spectrum. The numbers of altered reactions transferred towards control are shown here in percentages, while the number of total altered reactions is provided inside each process's parenthesis. B) Knockdown effect of the potential targets of NASH in the downregulated reactions of fatty acid oxidation. Here, the bar plot represents the observed flux rate differences between the knockdown and NASH conditions. A reaction is placed in two categories depending on its decreased or increased flux rate.

were found to increase the flux rates of 66% altered reactions in the fatty acid oxidation pathways, including fatty acid activation and mitochondrial beta-oxidation (**Fig. 4.5B** and **Fig. 4.6**). The knockdown of the potential targets for NAFL could do the same for mitochondrial beta-oxidation, whereas all but PPP1CC were able to do so for some of the reactions in the cytosolic fatty acid activation (**Fig. 4.7**). Additionally, our proposed targets can revert some altered carbohydrate, amino acid metabolism, glycerolipid, and sphingolipid metabolism reactions. It was also found that the knockdown profiles of these proposed targets (both NASH and NAFL categ-

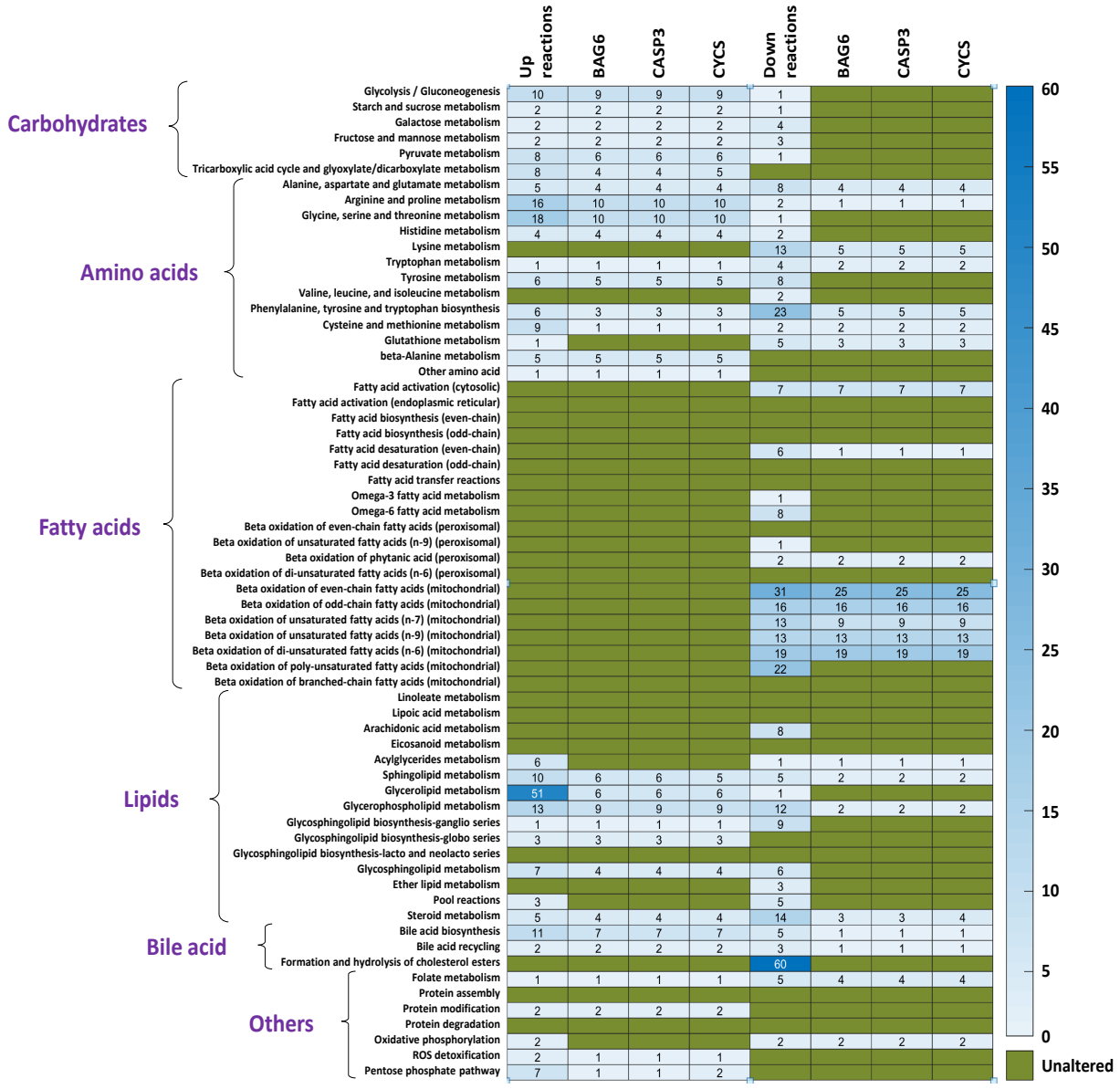

Figure 4.6: **Beneficial effects of the proposed potential targets against NASH on reverting the disease-specific metabolic alterations.** The column represents the number of reverted reactions for each pathway.

ories) are associated with the increased flux of mitochondrial glutathione peroxidase, except for PPP1CC and VDAC1, which increase the flux rate of extracellular glutathione peroxidase. It was also found that the knockdown profiles of these proposed targets (both NASH and NAFL categories) are associated with the increased flux of mitochondrial glutathione peroxidase, except for PPP1CC and VDAC1, which increase the flux rate of extracellular glutathione peroxidase. The flux rate of mitochondrial glutathione oxidoreductase was found to be upregulated after the knocking down of all three recovery options for the NASH category, but in the cytoplasm, only the NADH-associated flux rate was increased. On the other hand, a heterogeneous effect was observed for the recovery proteins for the NAFL group. Hence, our proposed targets have the potential to revert the metabolic alterations and could attenuate hepatic steatosis by promoting higher flux rates for the altered reactions involved in fatty acid activation and mitochondrial beta-oxidation pathways.

4.4 Discussion

NASH is a multifactorial progressive disease that initiates from a benign NAFL and may move to severe cirrhosis and liver failure [366]. Currently, it is the main reason for global liver transplants, and unabated, the numbers are going to rise only. NASH is driven by various inflammatory pathways, multiple fibrosis pathways, and metabolic alterations such as lipid metabolism, pathways associated with lipotoxicity, and oxidative defence [366]. However, despite being studied for decades, the molecular mechanism governing NASH is yet to be deciphered, thus making the disease very hard to control. Thus, demanding potential drug targets for NASH has become a top priority. Therefore, we have endeavored to study NASH to identify a set of potential targets with high confidence.

Here, we have proposed an *in silico* pipeline involving GSMM in combination with results from protein-protein interaction (PPI) networks to identify drug targets. The pipeline first identifies the most significant elements of the genomic and metabolic level perturbations, which can initiate the disease reversibility. A list of indispensable candidate proteins (ICp) was obtained from the directional PPI network analysis containing the DEGs, candidate proteins (Cp), and

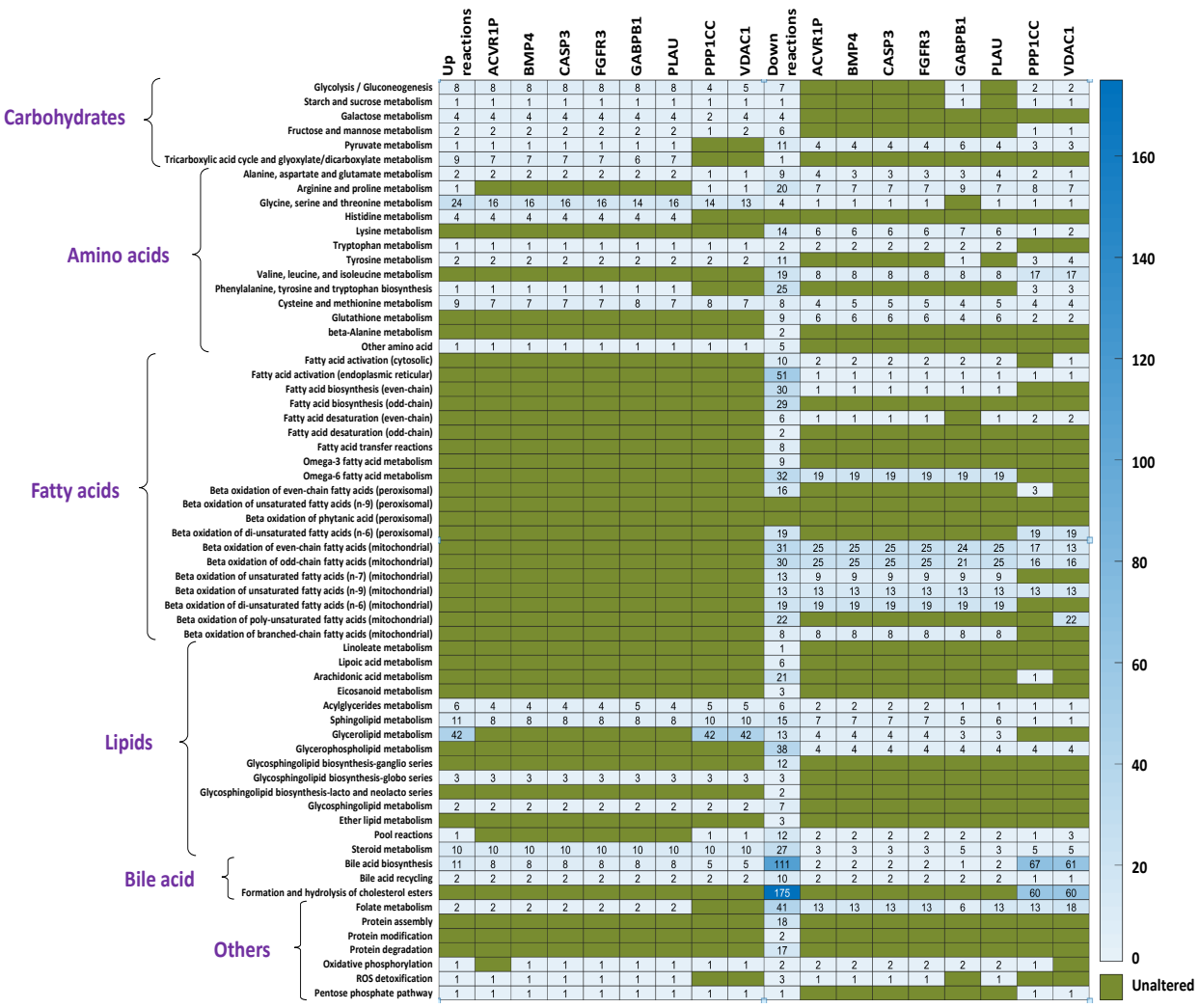

Figure 4.7: **Beneficial effects of the proposed potential targets against NAFL on reverting the disease-specific metabolic alterations.** The column represents the number of reverted reactions for each pathway.

the MCGs [360]. We have checked the knockdown effects of each ICp on the disease-specific GSMMs by performing a metabolic network level transformation since they can influence the network controllability and generate reverse gene expression profiles. Finally, ICps with positive transformation scores were deemed potential targets because they can affect the network controllability, induce reverse gene expression to the DEG, and revert the disease metabolic flux state towards healthy.

GSMM is at the heart of this collaborative investigation. It starts from understanding the molecular alterations to deciding the potential drug targets from indispensable candidate protein (ICp). It is known that abnormal metabolism is the primary cause or consequence of human diseases. Therefore, exploring the metabolic alterations in multifactorial diseases like NASH is

necessary. In addition to capturing metabolic alterations, GSMM provides a unique opportunity to identify genes that can regulate or revert the alterations from the disease state. Here, we performed the *in silico* knockdown analysis using GSMM to identify the metabolic genes that can transform the disease-metabolic state towards control. However, a PPI network analysis can give important nodes that have the potential to influence the network, still unable to provide the information that it is driving the disease or can control the disease progression. In this context, GSMM can be used to quantify their impact on the transformation from the disease state to the healthy state. Here, we have incorporated the knockdown profile of each ICp to capture their effect on the metabolic network, as most of the proteins are non-enzymatic. After identifying the potential targets based on the transformation score, we asked how these targets could reverse the metabolic alterations. Therefore, after integrating the knockdown profiles, we looked for fluxes of each of the altered reactions. This approach helps us identify the metabolic reactions whose flux rates can actually reverse by targeting these identified potential targets. From there, we also identified the impact of these targets on hepatic steatosis.

We obtained three proteins (CASP3, CYCS, and BAG6) that can cause reversibility in NASH at both the metabolic level and as well as protein level. Using *in silico* gene knockdown, we have shown that these proteins are associated with steatosis, inflammation, apoptosis, and fibrosis. Caspase 3, Apoptosis-Related Cysteine Peptidase (CASP3), is a member of the caspase family and plays a central role in apoptosis execution [367]. The genetically modified mice with loss of CASP3 activity were reported as resistant to diet-induced NASH development [368]. Cytochrome C (CYCS) is a small soluble heme protein found abundantly in the inner mitochondrial membrane, and its exodus to cytosol triggers apoptosis, whereas its translocation into the extracellular space induces inflammation [369]. BCL2 Associated Athanogene 6 (BAG6) is an ATP-independent molecular chaperone involved in cellular quality control processes. It prevents misfolded protein aggregation by promoting their degradation through the cellular proteasome machinery [370]. It is involved in insulin-like growth factor receptor signaling pathway [371] and DNA damage-induced apoptosis [372]. It is also a ligand of the natural killer/ NK cells receptor NCR3 [373]. However, no report exists regarding the involvement of BAG6 in NASH. Moreover, the studied liver biopsy data indicated that BAG6

was not differentially expressed in NASH. Thus it's not involved in NASH development, rather, its inhibition can reduce the disease progression. Thus, BAG6 can potentially become a suitable drug target in NASH and need further evaluation through experimental studies.

Our strategy of leveraging and interconnecting the context-specific molecular networks identified three potential targets for NASH and eight for NAFL. These targets exert their effects at the gene and metabolic levels and reverse disease-associated molecular signatures. We have shown that knocking them down affects steatohepatitis, inflammation, and fibrosis development. Our proposed methodology lays out a pragmatic framework for identifying potential therapeutic targets with their possible mechanism of action. Though it will significantly speed up the drug discovery process by providing a better experimental design to biologists for further exploration, we need small-scale kinetic models to capture the underlying mechanism associated with metabolic alterations related to a disease condition.

5

Small-scale kinetic model and therapeutic strategies[1]

5.1 Introduction

In **Chapter 2**, we have applied genome-scale metabolic model (GSMM) to identify metabolic alterations in pancreatic β-cell responsible for the dysregulated β-cell function in type 2 diabetes (T2D). One of the major causes of developing T2D in the presence of insulin resistance (IR) is the impaired glucose-stimulated insulin secretion (GSIS) in β-cell. Though GSMM provides a global picture of metabolic alterations, we need a focused small-scale kinetic modelling approach to better capture the GSIS process and unravel the cause, effect, and mechanism of

[1]The bulk of this chapter has been published in *Applied Mathematical Modelling*, 108 (2022): 408-426.

T2D.

T2D usually manifests years after prediabetes or impaired glucose tolerance. This happens due to loss in β-cell function to compensate for the insulin resistance through augmented insulin secretion [374–376]. During prediabetes, blood glucose levels rise over time, causing harmful effects on various organs, including pancreatic β-cells, a condition known as glucotoxicity [377, 378]. It creates an unnatural environment in β-cells that leads to alteration in function and, most notably, the loss of acute GSIS. Impaired GSIS is the fundamental flaw in T2D progression since the β-cell loss of mass varies greatly between different studies and comes into the picture in later stages [377, 379, 380]. The β-cell is highly susceptible to caloric overload, as GSIS is attenuated following glucose infusion in healthy persons and after the culture of human islets under glucotoxicity [381, 382]. It is reported that loss of specialised gene expression [377, 383] or loss in ATP production through defective mitochondrial metabolism [31, 374, 383, 384] can lead to complete disruption of the acute phase of GSIS. Although many experimental [385, 386] and theoretical [377, 387–390] studies have been conducted to understand the GSIS process in β-cell, the exact mechanisms responsible for this loss of GSIS during prediabetes have not been fully elucidated [387]. Moreover, theoretical studies mainly focused on the glucose-insulin dynamics by constructing a minimal model that contains a minimal number of parameters. They estimate the glucose effectiveness and insulin sensitivity from intravenous glucose tolerance test (IVGTT) or oral glucose test (OGTT) data (detailed review can be found in [387–390]).

Some work has been done on the impaired GSIS process during IR-induced hyperglycemia; however, the mechanisms underlying this phenomenon are still poorly understood [387]. As a result, a detailed understanding of this system through different parameter variations would provide the possible solutions to stop or delay the progression of T2D. This is the primary motivation behind the present study, where we explored the GSIS through mathematical modelling to investigate the possible factors responsible for the reduced insulin secretion in IR-induced hyperglycemic state.

The current study aims to capture key factors responsible for the progression of diabetes in the IR condition. To get a better understanding of the system, we need to consider more players

other than glucose and insulin. In β-cell, glucokinase (GK) plays a vital role in the insulin secretion process and acts as a glucose sensor [391, 392]. Besides, the oxidative phosphorylation process is an essential step in GSIS, as ATP production from glucose metabolism solely depends on this process. So, we have also incorporated these two factors in our study. Calcium is another key factor that could influence the GSIS process. The role of calcium and ATP in the GSIS process was already known for a long time. However, the underlying interactions were incorporated in the model considerably later (like the work by Giugliano et al. [393]). In the pancreatic β-cells, plasma glucose enters the cell via GLUT-2 transporters and subsequently generates energy in the form of ATP through mitochondrial oxidative phosphorylation followed by glucose metabolism. The elevated cytoplasmic ATP concentration resulted in the rising of cytoplasmic calcium (Ca^{2+}) concentration through the closure of the K_{ATP} channels [394, 395]. The cytoplasmic Ca^{2+} triggers the exocytosis of insulin-containing granules from the β-cell, which results in a rise in insulin concentration in the blood plasma [396, 397]. In the glucose-Ca^{2+}-insulin interactions, several models were proposed to understand the glucose metabolism, membrane potential, calcium levels, and insulin secretion, as reviewed in [387, 398–400]. McKenna et al. [401] proposed a mathematical model (Dual Oscillator Model (DOM)) on glucose-calcium interactions to simulate their observations obtained from ex vivo experimental studies, in which loss in slow calcium oscillations was found at an elevated glucose concentration. A sinusoidal glucose stimulus with a sufficiently large amplitude and period can recover this loss in oscillations. Recently, Das et al. [402] proposed a minimal mathematical model to understand the GSIS mechanism through glucose metabolism and ATP-dependent calcium influx. The work mainly focused on elucidating the role of ATP-dependent calcium input rate on insulin secretion. It is reported that chronic hyperglycemia results in ATP depletion by activating uncoupling protein 2 (UCP2) [403–405] or by up-regulating the voltage-dependent anion channel (VDAC) [374], and is also proposed as one of the major causes for obesity-induced T2D progression. Overactivity of the K_{ATP} channel can cause a diabetic state due to under secretion of insulin, and its polymorphism (E23K) is proposed as one of the T2D risk factors [406]. Also, a loss in intracellular calcium content through diminished voltage-gated calcium channels (VGCC) function and/or density can be considered a threat for T2D devel-

opment [407–410], but sometimes hyperactivation of the VGCC channel also leads to β-cell death [410–412].

In the present study, we proposed and analysed the GSIS process through a six-dimensional model incorporating calcium and ATP. The proposed mathematical model was established by generating the normal condition provided in [115]. This model also captured the hyperglycemic state induced by IR and loss of β-cell mass and mimicked the diabetic condition. Here, we identified crucial factors in the GSIS process whose dysfunction can lead to T2D development or hypoglycemia. The acquired understanding of the crucial factors was then used to explore different potential strategies that would prevent the progression of IR towards T2D.

5.2 Formulation of the mathematical model

The pancreatic β-cell is considered where plasma glucose enters the cell via glucose transporters (GLUT-2) present on the cell membrane. After entering the cell, the glucokinase phosphorylates it, which then enters into the energy metabolism pathway. In the process of metabolism, energy is generated in the form of ATP; as a result, cytoplasmic ATP concentration increases. Mainly two types of ion channels are essential for insulin secretion:- K_{ATP} channels and the voltage-gated Ca^{2+} channels [394, 395]. At low plasma glucose, the K_{ATP} channels are spontaneously active, allowing potassium ions (K^+) to flow out of the cell that holds the membrane potential near the hyperpolarized resting potential (near -60 mV) [413]. In the presence of higher plasma glucose, the elevated cytoplasmic ATP concentration leads to the closure of the K_{ATP} channels. This, in turn, results in the depolarization of the plasma membrane and the potential shifts from negative to positive. When the plasma membrane potential crosses -40 mV, the VGCC open and allow the influx of extracellular Ca^{2+} into the β-cells [413]. Also, from the endoplasmic reticulum (ER), calcium comes into the cytoplasm via RyR2 channels. The cytoplasmic Ca2+ goes back outside the cell through Na^+/Ca^{2+} exchangers and PMCA channel, present in the plasma membrane and into ER via SERCA pump. The rise in cytoplasmic Ca^{2+} concentration triggers the exocytosis of insulin-containing granules, resulting in a surge in insulin concentration in blood plasma [396, 397]. The production

of ATP is solely dependent on the oxidative phosphorylation process, which occurs in the mitochondrial compartment. A term is included in the model that represents the total pool of intermediated metabolites available for oxidative phosphorylation as per previous work [413]. The ATP synthesis rate is determined by the consumption rate of these intermediate metabolites. The proposed mathematical model on the glucose-induced insulin secretion process is schematically presented in **Fig. 5.1**.

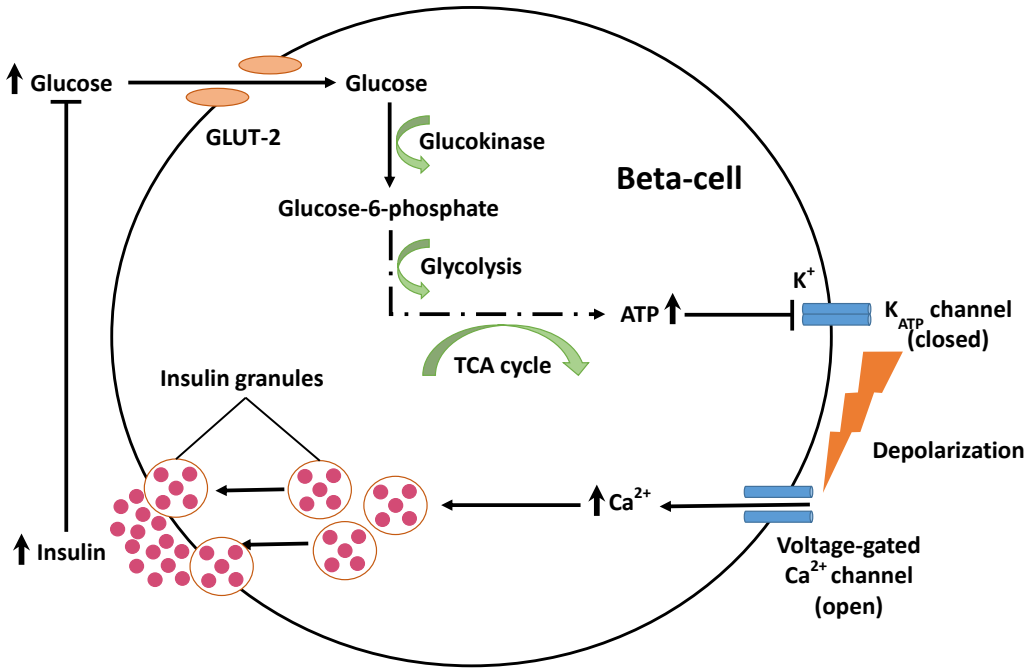

Figure 5.1: **Schematic diagram of the proposed mathematical model**(5.12) **on GSIS process.**

While formulating the mathematical model, we considered six variables G, I, $[Re]_i$, $[ATP]_i$, $[Ca^{2+}]_i$ and $[Ca^{2+}]_{ER}$ as the concentrations of plasma glucose, plasma insulin, the total pool of intermediated metabolites, cytoplasmic ATP, cytoplasmic Ca^{2+} and ER Ca^{2+} respectively. A rise in plasma glucose (G) occurs due to glucose input in the blood plasma from food and hepatic glucose production. The fall of G is due to two effluxes; one is insulin-independent utilization by cells like β-cells, brain, erythrocytes, etc., and another is insulin-dependent utilization by cells like muscle cells, hepatic cells, etc. Here we have considered a time-dependent function for the dietary glucose input in the form of [117]:

$$V = v_{11} t e^{-t/k_{11}} \tag{5.1}$$

The other three terms were taken from the study by Andrea De Gaetano et al. [414], in which a minimal model on the intravenous glucose tolerance test (IVGTT) was proposed. The rate equation of the concentration of plasma glucose (G) is expressed as:

$$\frac{dG}{dt} = v_{11} t e^{-t/k_{11}} + v_{12} - v_{13} G - v_{14} G I \tag{5.2}$$

where, $k_{11} ln2$ denotes the approximate value of the half-life of the glucose absorption, $v_{11} k_{11}^2$ is the total amount of uptaken glucose, v_{12} is the hepatic glucose production, v_{13} is the insulin-independent glucose utilization rate constant and v_{14} is the insulin-dependent glucose utilization rate constant. The production rate of intermediated metabolites depends on the glycolysis flux, and we assume that this flux is determined by the glucose phosphorylation rate [415]. The flux of the phosphorylation reaction depends on the activity of glucokinase and the level of the glucokinase's two substrates, glucose and ATP. The ATP-dependent activity is best fitted to Michaelis-Menton equation [416]. Glucokinase shows a sigmoidal fashion for glucose with a Hill coefficient, h=1.7 [417]. Therefore, in the present model, we use the rate expression for glucokinase from [418] as follows:

$$V_{Glu} = v_{21} \frac{G^h}{G^h + k_{21}^h} \frac{[ATP]_i}{[ATP]_i + k_{22}} \tag{5.3}$$

where, V_{Glu} is the reaction rate of glucokinase with v_{21} is the maximum rate of glucose consumption, k_{21} is the half-maximal glucose concentration, h is the Hill coefficient, and k_{22} is the Michaelis-Menton constant for ATP. So, in our study, the $[Re]_i$ production rate was assumed to be proportional to the phosphorylation rate of glucose to glucose-6-phosphate with conversion efficiency ε. The ATP synthesis rate from the intermediated metabolites through the oxidative phosphorylation process may be expressed as Hill equation [413, 418]:

$$V_{OP} = v_{22} [Re]_i \frac{[MgADP_f]_i^2}{[MgADP_f]_i^2 + k_{23}^2} \tag{5.4}$$

with

$$[MgADP_f]_i = 0.055[ADP]_i \tag{5.5}$$

$$A_0 = [ATP]_i + [ADP]_i \tag{5.6}$$

where, v_{22} is the maximum ATP production rate, $[MgADP_f]_i$ is concentration of cytosolic free MgADP, k_{23} is the half-maximal cytosolic free MgADP concentration and $[ADP]_i$ is concentration of cytosolic ADP. A_0 is the general concentration of intracellular nucleotides which was assumed to be constant. According to the previous studies [413, 419], we assumed the values of A_0 equals 4000 μM. Thus, the rate equation of the concentration of intermediated metabolites expressed as:

$$\frac{d[Re]_i}{dt} = \varepsilon \left(v_{21} \frac{G^h}{G^h + k_{21}^h} \frac{[ATP]_i}{[ATP]_i + k_{22}} \right) - v_{22}[Re]_i \frac{[MgADP_f]_i^2}{[MgADP_f]_i^2 + k_{23}^2} \tag{5.7}$$

31 ATP molecules are produced from one glucose molecule [420], so we considered the value of ε equal to 31. Here, we also considered the linear degradation of ATP with rate constant v_{31} for uses in various activities into the cell. Therefore, the rate equation of the concentration of cytoplasmic ATP is expressed as:

$$\frac{d[ATP]_i}{dt} = v_{22}[Re]_i \frac{[MgADP_f]_i^2}{[MgADP_f]_i^2 + k_{23}^2} - v_{31}[ATP]_i \tag{5.8}$$

A rise in the concentration of cytoplasmic Ca^{2+} ions has two sources:- the influx of Ca^{2+} ions from extracellular space via VGCC and from the ER via RyR2 channels. As the influx of Ca^{2+} ions through voltage-gated Ca^{2+} channels is a downstream effect of a rise in cytoplasmic ATP concentration, we considered the rate is linearly dependent on cytoplasmic ATP concentration with rate constant v_{41} for simplicity of the model. The influx of Ca^{2+} ions via RyR2 channels is dependent on the concentration of ER calcium. Here, we used a previously mentioned mechanism [421] for calcium-induced calcium release, $v_{42}\left([Ca^{2+}]_{ER} - [Ca^{2+}]_i\right)$, where v_{42} is the activity of the RyR2 channels. On the other hand, cytoplasmic Ca^{2+} ions concentration declines for two effluxes, sequestration of intracellular Ca^{2+} into the calcium store ER via

SERCA pump and efflux of Ca^{2+} ions outside of the cell through the cell membrane. Following [422], the equation for SERCA was taken as $\frac{v_{43}[Ca^{2+}]_i^2}{k_{41}^2+[Ca^{2+}]_i^2}$, where v_{43} is the maximum rate and k_{41} is the corresponding half-maximal cytoplasmic Ca^{2+} concentration. Here, we considered linear term $v_{44}[Ca^{2+}]_i$ for removal of cytoplasmic Ca^{2+} ions into extracellular space with rate constant v_{44}. The dynamics of the concentration of cytoplasmic Ca^{2+} and ER Ca^{2+} ions in our model are expressed as:

$$\frac{d[Ca^{2+}]_i}{dt} = v_{41}[ATP]_i + v_{42}\left([Ca^{2+}]_{ER} - [Ca^{2+}]_i\right) - \frac{v_{43}[Ca^{2+}]_i^2}{k_{41}^2 + [Ca^{2+}]_i^2} - v_{44}[Ca^{2+}]_i \tag{5.9}$$

$$\frac{d[Ca^{2+}]_{ER}}{dt} = -v_{42}\left([Ca^{2+}]_{ER} - [Ca^{2+}]_i\right) + \frac{v_{43}[Ca^{2+}]_i^2}{k_{41}^2 + [Ca^{2+}]_i^2} \tag{5.10}$$

The rise of insulin in blood plasma is due to the exocytosis of insulin-containing granules, triggered by intracellular Ca^{2+} ions. Bokvist et al. [423] proposed a mathematical expression for Ca^{2+} dependent insulin secretion rate and got the value of the co-operativity coefficient of 2 by applying least-squares fit with experimentally observed data. Thus, we employ Hill function $\frac{v_{61}[Ca^{2+}]_i^2}{k_{61}^2+[Ca^{2+}]_i^2}$, with co-operativity coefficient of 2 for the releasing rate of insulin from single β-cell, where v_{61} is maximum rate of insulin release and k_{61} is the corresponding half-saturation intracellular Ca^{2+} concentration. We considered a linear degradation of blood insulin concentration (I) with degradation rate constant v_{65}. So, the dynamical equation of I is expressed as:

$$\frac{dI}{dt} = \frac{v_{61}v_{62}v_{63}[Ca^{2+}]_i^2}{v_{64}(k_{61}^2 + [Ca^{2+}]_i^2)} - v_{65}I \tag{5.11}$$

where, v_{62} is the total number of β-cells, v_{63} is the effective volume of each β-cell and v_{64} is the effective volume of the plasma insulin space [424]. Thus, the minimal model of glucose-induced insulin release process in β-cell is proposed by the following system of a nonlinear ordinary differential equation (ODE):

$$
\begin{aligned}
&\frac{dG}{dt} = v_{11} t e^{-t/k_{11}} + v_{12} - v_{13} G - v_{14} G I \\
&\frac{d[Re]_i}{dt} = \varepsilon \left(v_{21} \frac{G^h}{G^h + k_{21}^h} \frac{[ATP]_i}{[ATP]_i + k_{22}} \right) - v_{22} [Re]_i \frac{[MgADP_f]_i^2}{[MgADP_f]_i^2 + k_{23}^2} \\
&\frac{d[ATP]_i}{dt} = v_{22} [Re]_i \frac{[MgADP_f]_i^2}{[MgADP_f]_i^2 + k_{23}^2} - v_{31} [ATP]_i \\
&\frac{d[Ca^{2+}]_i}{dt} = v_{41} [ATP]_i + v_{42} \left([Ca^{2+}]_{ER} - [Ca^{2+}]_i \right) - \frac{v_{43} [Ca^{2+}]_i^2}{k_{41}^2 + [Ca^{2+}]_i^2} - v_{44} [Ca^{2+}]_i \\
&\frac{d[Ca^{2+}]_{ER}}{dt} = -v_{42} \left([Ca^{2+}]_{ER} - [Ca^{2+}]_i \right) + \frac{v_{43} [Ca^{2+}]_i^2}{k_{41}^2 + [Ca^{2+}]_i^2} \\
&\frac{dI}{dt} = \frac{v_{61} v_{62} v_{63} [Ca^{2+}]_i^2}{v_{64} (k_{61}^2 + [Ca^{2+}]_i^2)} - v_{65} I
\end{aligned}
\tag{5.12}
$$

with the initial conditions $G(0) > 0$, $[Re]_i(0) > 0$, $[ATP]_i(0) > 0$, $[Ca^{2+}]_i(0) > 0$, $[Ca^{2+}]_{ER}(0) > 0$, $I(0) > 0$ and

$$
\begin{aligned}
[MgADP_f]_i &= 0.055 [ADP]_i \\
A_0 &= [ATP]_i + [ADP]_i = 4000 \mu M
\end{aligned}
$$

5.3 Preliminary results

5.3.1 Positive invariance of the solutions

The system of equations (5.12) can be written as:

$$
\dot{X} = F(X) \tag{5.13}
$$

together with initial conditions $X(0) = X_0 \in \mathbf{R}_+{}^6$.

Where, $X = \text{col}\left(G, [Re]_i, [ATP]_i, [Ca^{2+}]_i, [Ca^{2+}]_{ER}, I \right) \in \mathbf{R}^6$ and

$$F(X) = \begin{bmatrix} F_1(X) \\ F_2(X) \\ F_3(X) \\ F_4(X) \\ F_5(X) \\ F_6(X) \end{bmatrix} = \begin{bmatrix} v_{11}te^{-t/k_{11}} + v_{12} - v_{13}G - v_{14}GI \\ \varepsilon\left(v_{21}\frac{G^h}{G^h+k_{21}^h}\frac{[ATP]_i}{[ATP]_i+k_{22}}\right) - v_{22}[Re]_i\frac{[MgADP_f]_i^2}{[MgADP_f]_i^2+k_{23}^2} \\ v_{22}[Re]_i\frac{[MgADP_f]_i^2}{[MgADP_f]_i^2+k_{23}^2} - v_{31}[ATP]_i \\ v_{41}[ATP]_i + v_{42}\left([Ca^{2+}]_{ER} - [Ca^{2+}]_i\right) - \frac{v_{43}[Ca^{2+}]_i^2}{k_{41}^2+[Ca^{2+}]_i^2} - v_{44}[Ca^{2+}]_i \\ -v_{42}\left([Ca^{2+}]_{ER} - [Ca^{2+}]_i\right) + \frac{v_{43}[Ca^{2+}]_i^2}{k_{41}^2+[Ca^{2+}]_i^2} \\ \frac{v_{61}v_{62}v_{63}[Ca^{2+}]_i^2}{v_{64}(k_{61}^2+[Ca^{2+}]_i^2)} - v_{65}I \end{bmatrix} \tag{5.14}$$

It is easy to check in equations (5.14) that whenever choosing $X_0 \in {\mathbf{R}_+}^6$ with $X_i = 0$, then $F_i(X_0)|_{X_i=0} = 0 \geq 0, (i = 1,2,3,4,5,6)$. Due to the lemma of Nagumo [425], any solution of equation (5.13) with $X_0 \in {\mathbf{R}_+}^6$, say $X(t) = X(t;X_0)$, is such that $X(t) \in {\mathbf{R}_+}^6$ for all $t > 0$.

5.3.2 Boundedness of the solutions

From the first equation of (5.12), we get

$$\begin{aligned} \frac{dG}{dt} &= v_{11}te^{-t/k_{11}} + v_{12} - v_{13}G - v_{14}GI \\ &= \frac{v_{11}t}{e^{t/k_{11}}} + v_{12} - v_{13}G - v_{14}GI \\ &= \frac{v_{11}t}{\left[1 + \frac{t}{k_{11}} + \frac{1}{2!}\frac{t^2}{k_{11}^2} + \frac{1}{3!}\frac{t^3}{k_{11}^3} + \cdots\right]} + v_{12} - v_{13}G - v_{14}GI \\ &\leq \frac{v_{11}t}{\frac{t}{k_{11}}} + v_{12} - v_{13}G - v_{14}GI \\ &\leq v_{11}k_{11} + v_{12} - v_{13}G \end{aligned} \tag{5.15}$$

Thus we obtain,

$$\frac{dG}{dt} + v_{13}G \leq v_{11}k_{11} + v_{12} \tag{5.16}$$

Using the variation of constants formula, inequality (5.16) is transformed into

$$0 \leq G(t) \leq \frac{v_{11}k_{11} + v_{12}}{v_{13}}(1 - e^{-v_{13}t}) + G(0)e^{-v_{13}t} \tag{5.17}$$

From which we get,

$$G(t) \leq M_1, \forall t \geq 0 \tag{5.18}$$

where, $M_1 = \frac{v_{11}k_{11}+v_{12}}{v_{13}} + G(0)$.

From the system equation of (5.12), we can easily find that

$$\frac{d[ATP]_i}{dt}\Big|_{[ATP]_i=A_0} \leq 0 \tag{5.19}$$

This implies that the value of $[ATP]_i$ always remains within the range $(0, A_0]$.

By merging fourth and fifth equations of (5.12), we get

$$\begin{aligned} \frac{d[Ca^{2+}]_i}{dt} + \frac{d[Ca^{2+}]_{ER}}{dt} &= v_{41}[ATP]_i - v_{44}[Ca^{2+}]_i \\ &\leq v_{41}A_0 - v_{44}[Ca^{2+}]_i \end{aligned} \tag{5.20}$$

Let us assume, for a instance $t_1 \geq 0$ first time the value $[Ca^{2+}]_i(t_1) \geq \frac{v_{41}A_0}{v_{44}}$. Then from equation (5.20) we have

$$\frac{d[Ca^{2+}]_i}{dt} + \frac{d[Ca^{2+}]_{ER}}{dt} \leq 0. \tag{5.21}$$

Here, we also mentioned that in the time interval $[0, t_1)$, the value of $[Ca^{2+}]_{ER}(t)$ cannot crosses the threshold value $\frac{v_{41}A_0}{v_{44}} + \frac{v_{43}}{v_{42}}$. It is easily can derive from the fifth equations of (5.12) that $\frac{d[Ca^{2+}]_{ER}}{dt} \leq 0$, when $[Ca^{2+}]_{ER}(t) \geq \frac{v_{41}A_0}{v_{44}} + \frac{v_{43}}{v_{42}}\ \forall t < t_1$. Thus, we got, $[Ca^{2+}]_{ER}(t_1) \leq \frac{v_{41}A_0}{v_{44}} + \frac{v_{43}}{v_{42}}$.

When, equation (5.21) holds, then three possibilities may arise:

(I) $\frac{d[Ca^{2+}]_i}{dt} \leq 0$ and $\frac{d[Ca^{2+}]_{ER}}{dt} \leq 0$,

(II) $\frac{d[Ca^{2+}]_i}{dt} \leq 0$ and $\frac{d[Ca^{2+}]_{ER}}{dt} > 0$ and

(III) $\frac{d[Ca^{2+}]_i}{dt} > 0$ and $\frac{d[Ca^{2+}]_{ER}}{dt} \leq 0$

For case (I) and (II), the value of $[Ca^{2+}]_i$ always remains in the interval $(0, \frac{v_{41}A_0}{v_{44}}]$ and then bounded there for all $t \geq 0$, i.e., $[Ca^{2+}]_i(t) \leq \frac{v_{41}A_0}{v_{44}}\ \forall t \geq 0$. Similarly for case (I) and (III), the value of $[Ca^{2+}]_{ER}$ always remains in the interval $(0, [Ca^{2+}]_{ER}(t_1)]$ and then $[Ca^{2+}]_{ER}(t) \leq [Ca^{2+}]_{ER}(t_1)\ \forall t \geq t_1$. Thus we obtained that $[Ca^{2+}]_{ER}$ is for all $t \geq 0$, i.e., $[Ca^{2+}]_{ER}(t) \leq \frac{v_{41}A_0}{v_{44}} + \frac{v_{43}}{v_{42}}\ \forall t \geq 0$.

For case (II), it is easily can derive from the fifth equations of (5.12) that $\frac{d[Ca^{2+}]_{ER}}{dt} \leq 0$, when $[Ca^{2+}]_{ER}(t) \geq \frac{v_{41}A_0}{v_{44}} + \frac{v_{43}}{v_{42}}$, as $[Ca^{2+}]_i(t) \leq \frac{v_{41}A_0}{v_{44}}\ \forall t \geq 0$. Thus the value of $[Ca^{2+}]_{ER}$ always remains in the interval $(0, \frac{v_{41}A_0}{v_{44}} + \frac{v_{43}}{v_{42}}]$ and then bounded there for all $t \geq 0$, i.e., $[Ca^{2+}]_{ER}(t) \leq \frac{v_{41}A_0}{v_{44}} + \frac{v_{43}}{v_{42}}\ \forall t \geq 0$.

In case (III), we obtain from equation (5.21) that $\frac{d[Ca^{2+}]_i}{dt} < -\frac{d[Ca^{2+}]_{ER}}{dt}$ and also we have $[Ca^{2+}]_{ER}(t) \leq \frac{v_{41}A_0}{v_{44}} + \frac{v_{43}}{v_{42}}\ \forall t \geq 0$. Using the fifth equations of (5.12), we have

$$\begin{aligned}
\frac{d[Ca^{2+}]_i}{dt} &< -\frac{d[Ca^{2+}]_{ER}}{dt} \\
&< v_{42}\left([Ca^{2+}]_{ER} - [Ca^{2+}]_i\right) - \frac{v_{43}[Ca^{2+}]_i^2}{k_{41}^2 + [Ca^{2+}]_i^2} \\
&< v_{42}\left([Ca^{2+}]_{ER} - [Ca^{2+}]_i\right)
\end{aligned} \tag{5.22}$$

Thus, when $[Ca^{2+}]_i \geq [Ca^{2+}]_{ER}$, the value of $\frac{d[Ca^{2+}]_i}{dt} \leq 0$. Thus the value of $[Ca^{2+}]_i$ always remains in the interval $(0, \max([Ca^{2+}]_{ER})]$ and then bounded there for all $t \geq 0$, i.e., $[Ca^{2+}]_i(t) \leq \frac{v_{41}A_0}{v_{44}} + \frac{v_{43}}{v_{42}}\ \forall t \geq 0$.

Let us consider the case, where the value $[Ca^{2+}]_i(t) < \frac{v_{41}A_0}{v_{44}}\ \forall t \geq 0$. From the fifth equation of (5.12), we get

$$\begin{aligned}
\frac{d[Ca^{2+}]_{ER}}{dt} &= -v_{42}\left([Ca^{2+}]_{ER} - [Ca^{2+}]_i\right) + \frac{v_{43}[Ca^{2+}]_i^2}{k_{41}^2 + [Ca^{2+}]_i^2} \\
&= -v_{42}[Ca^{2+}]_{ER} + v_{42}[Ca^{2+}]_i + \frac{v_{43}[Ca^{2+}]_i^2}{k_{41}^2 + [Ca^{2+}]_i^2} \\
&\leq -v_{42}[Ca^{2+}]_{ER} + \frac{v_{41}v_{42}A_0}{v_{44}} + v_{43}
\end{aligned} \tag{5.23}$$

Thus we obtain,

$$\frac{d[Ca^{2+}]_{ER}}{dt} + v_{42}[Ca^{2+}]_{ER} \leq \frac{v_{41}v_{42}A_0}{v_{44}} + v_{43} \tag{5.24}$$

Using the variation of constants formula, inequality (5.24) is transformed into

$$0 \leq [Ca^{2+}]_{ER}(t) \leq \frac{\frac{v_{41}v_{42}A_0}{v_{44}} + v_{43}}{v_{42}}(1 - e^{-v_{42}t}) + [Ca^{2+}]_{ER}(0)e^{-v_{42}t} \tag{5.25}$$

From which we get,

$$[Ca^{2+}]_{ER}(t) \leq M_2, \forall t \geq 0 \tag{5.26}$$

where, $M_2 = \frac{v_{41}v_{42}A_0}{v_{42}v_{44}} + \frac{v_{43}}{v_{42}} + [Ca^{2+}]_{ER}(0)$.

From the sixth equation of (5.12), we get

$$\begin{aligned} \frac{dI}{dt} &= \frac{v_{61}v_{62}v_{63}[Ca^{2+}]_i^2}{v_{64}(k_{61}^2 + [Ca^{2+}]_i^2)} - v_{65}I \\ &\leq \frac{v_{61}v_{62}v_{63}}{v_{64}} - v_{65}I \end{aligned} \tag{5.27}$$

Thus we obtain,

$$\frac{dI}{dt} + v_{65}I \leq \frac{v_{61}v_{62}v_{63}}{v_{64}} \tag{5.28}$$

Using the variation of constants formula, inequality (5.28) is transformed into

$$0 \leq I(t) \leq \frac{v_{61}v_{62}v_{63}}{v_{64}v_{65}}(1 - e^{-v_{65}t}) + I(0)e^{-v_{65}t} \tag{5.29}$$

From which we get,

$$I(t) \leq M_3, \forall t \geq 0 \tag{5.30}$$

where, $M_3 = \frac{v_{61}v_{62}v_{63}}{v_{64}v_{65}} + I(0)$.

From the second equation of (5.12), we get

$$\begin{aligned}\frac{d[Re]_i}{dt} &= \varepsilon\left(v_{21}\frac{G^h}{G^h+k_{21}^h}\frac{[ATP]_i}{[ATP]_i+k_{22}}\right) - v_{22}[Re]_i\frac{[MgADP_f]_i^2}{[MgADP_f]_i^2+k_{23}^2} \\ &\leq \varepsilon v_{21} - v_{22}[Re]_i\frac{[MgADP_f]_i^2}{[MgADP_f]_i^2+k_{23}^2}\end{aligned} \tag{5.31}$$

Thus, $\frac{d[Re]_i}{dt} \leq 0$ if in any time t_2

$$v_{22}[Re]_i(t_2)\frac{[MgADP_f]_i^2(t_2)}{[MgADP_f]_i^2(t_2)+k_{23}^2} \geq \varepsilon v_{21} \tag{5.32}$$

$$\begin{aligned}[Re]_i(t_2) &\geq \frac{\varepsilon v_{21}}{v_{22}}\left[\frac{[MgADP_f]_i^2(t_2)+k_{23}^2}{[MgADP_f]_i^2(t_2)}\right] \\ &\geq \frac{\varepsilon v_{21}}{v_{22}}\left[1+\frac{k_{23}^2}{[MgADP_f]_i^2(t_2)}\right]\end{aligned} \tag{5.33}$$

Thus, whenever the value of $[Re]_i$ crosses the threshold value given in (5.33), the value of $\frac{d[Re]_i}{dt}$ becomes ≤ 0, and so, the value of $[Re]_i$ remains in a bounded region. This property always holds except the case when for a given time t_3 the value of $[MgADP_f]_i = 0\ \forall t \geq t_3$ and this happens if $[ATP]_i = A_0\ \forall t \geq t_3$. That means $[ATP]_i$ reaches a fixed point with value A_0.

5.4 Numerical simulation

5.4.1 Model validation

The model (5.12) with the parameter set (provided in **Table 5.1**) is validated with the clinical data [115] for 204 normal subjects, receiving a mixed meal containing 1 $\pm$0.02 g/kg of glucose (see **Fig. 5.2**). The model simulated results lie within the normal range, which validates our model. Next, we investigate whether our proposed model (5.12) is capable of captur-

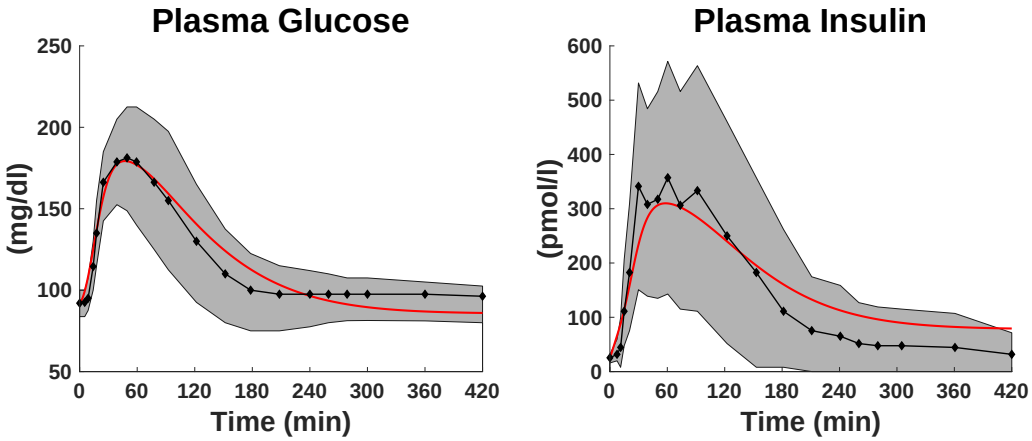

Figure 5.2: **Postprandial plasma glucose and insulin concentrations observed in normal subjects through model simulation.** The black-colored line represents the average plasma glucose and insulin levels of 204 normal subjects (age 56±2 years, body weight 78±1 kg) [115], and the grey area represents the mean±SD range. Our model simulated results using the parameter set reported in **Table 5.1** are shown in a red-colored line.

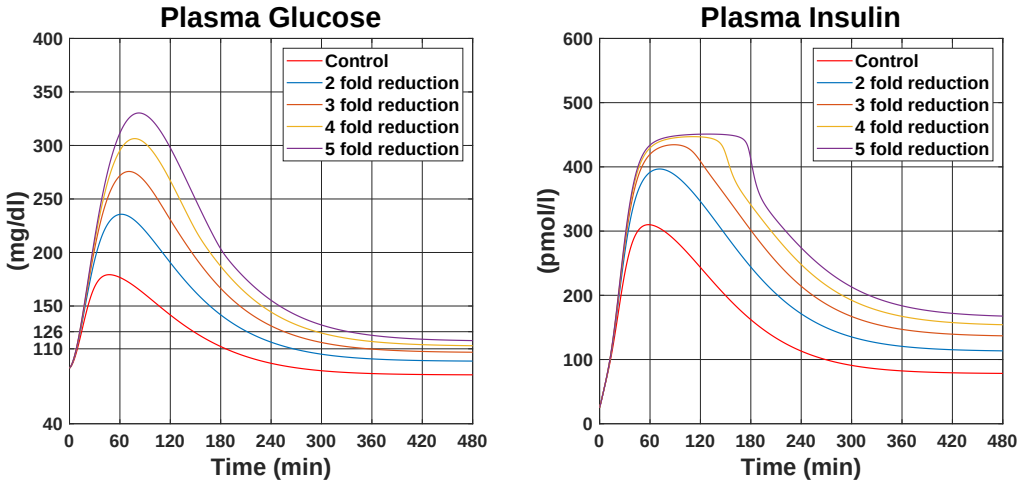

Figure 5.3: **Effect of reduction in insulin-dependent glucose utilization rate (v_{14}) on plasma glucose and insulin level.**

ing the effect of the insulin resistance (IR) scenario or not. IR is connoted as a clinical state in which a normal or increased insulin level produces an attenuated biologic response like insulin-mediated glucose uptake, metabolism, or storage [426, 427]. To mimic this condition, we reduced the value of insulin-dependent glucose utilization rate (v_{14}) in our system, and subsequently, plasma glucose level was captured (**Fig. 5.3**). It was found that 2-h plasma glucose level goes beyond the normal range (given in grey shaded area in **Fig. 5.2**) by the 2- or 3-fold reduction of v_{14}, but fasting plasma glucose remains in the normal range, which established the impaired glucose tolerance (IGT) condition. Fasting plasma glucose was found to cross

the normal range after the 4-fold reduction of v_{14}, and it remains within the range of 110-126 mg/dl for 4 & 5-fold reduction, which established the impaired fasting glucose (IFG) condition [428]. Additionally, we observed that these alterations lead to higher plasma insulin levels due to increased plasma glucose levels.

Table 5.1: **Parameter values with the corresponding reference:** Values of the parameters were collected mostly from the available literature. For some unknown parameters, we estimated their values so as to keep the value of the plasma glucose and insulin levels within the normal range provided in the study by Dalla Man et al. [115].

Parameters	**Definition**	**Value with unit**	**Reference**
v_{11}	see equation (5.2) for explanation	25.37 $\mu M min^{-1}$	Estimated
k_{11}	see equation (5.2) for explanation	45 min	[117]
v_{12}	Constant glucose input from liver	107 $\mu M min^{-1}$	[414]
v_{13}	Rate constant of insulin-independent glucose utilization/excretion	0.012 min^{-1}	[414]
v_{14}	Rate constant of insulin-dependent glucose utilization	135 $\mu M^{-1} min^{-1}$	[414]
ε	ATP conversion constant in the β-cell	31	[420]
v_{21}	Maximum rate of glucose consumption	80 $\mu M min^{-1}$	Estimated
h	Hill coefficient	1.7	[417]
k_{21}	Half-activation glucose level	7000 μM	[413, 418]
k_{22}	Michaelis-Menten constant for ATP	500 μM	[413, 418]
v_{22}	Maximum ATP production rate	12 min^{-1}	[413]
k_{23}	Half-activation cytosolic free MgADP concentration	20 μM	[413, 418]
v_{31}	ATP degradation rate constant	0.45 min^{-1}	Estimated
v_{41}	ATP dependent calcium input rate constant	0.007 min^{-1}	Estimated
v_{42}	Activity of RyR2 channel	0.2 min^{-1}	Estimated
v_{43}	Maxium rate for SERCA pump	20 $\mu M min^{-1}$	Estimated

k_{41}	Half maximal calcium concentration	0.5 μM	[419]
v_{44}	Removal rate constant for plasma membrane pump activity	28 min^{-1}	Estimated
v_{61}	Calcium-dependent maximum insulin release rate constant	1.08 $\mu M min^{-1}$	Estimated
k_{61}	Half-maximal calcium concentration	1.4 μM	[423]
v_{62}	Total number of β-cells	8.16×10^8	[429]
v_{63}	Effective volume of a β-cell	$1.5 \times 10^{-12} l$	[424]
v_{64}	Effective volume of the plasma insulin space	3 l	[424]
v_{65}	Insulin degradation rate constant	0.323 min^{-1}	[430]

5.4.2 Effects of loss in β-cell mass in the glucose-insulin dynamics

The total insulin released from the pancreas is determined by the product of the morphological mass of β-cells and the insulin secreted by each cells. Thus, the glucose homeostasis in our body requires an adequate number of insulin-secreting β-cells that respond appropriately to plasma glucose levels. T2D is a complex metabolic disorder in which inadequate β-cell mass is observed with the IR, mainly in the late, inulin-requiring phase of β-cell [431], and the reported deficits of β-cell mass in autopsy studies are ~ 0˜65% [432]. The chronically increased glucose levels may negatively affect the β-cell mass by promoting apoptosis without no significant change in β-cell proliferation [431].

To investigate the loss of β-cell mass in glucose-insulin dynamics, we reduced the value of the β-cell number (v_{62}) in our model and subsequently captured the changes in plasma glucose and insulin levels through the simulation. Stepwise fold reduction in β-cell number results in elevated plasma levels of peak postprandial glucose, 2-h glucose, and 8-h glucose compared to the normoglycemic situation (**Fig. 5.4A**). In these conditions, we also observed significant reductions in the postprandial plasma insulin levels (**Fig. 5.4B**). In the 2-fold loss

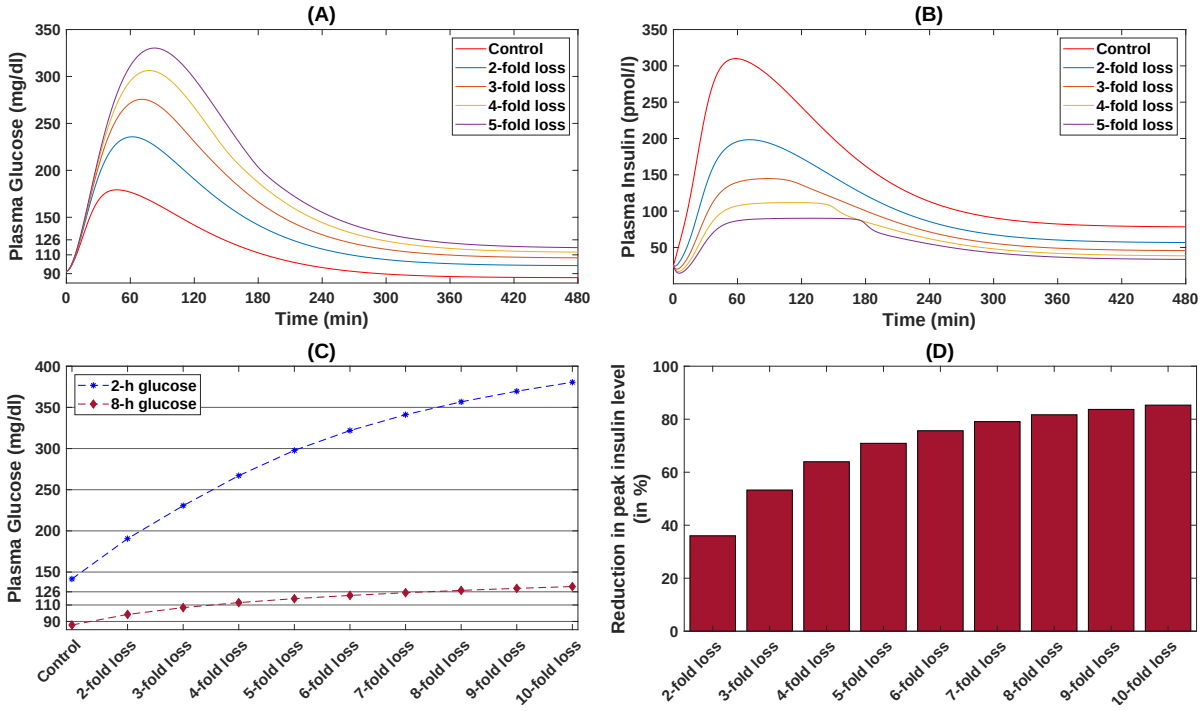

Figure 5.4: **Impact of β-cell mass loss on plasma glucose and insulin levels.** To capture the loss of β-cell mass, we stepwise only reduced the value of the β-cell number (v_{62}) up to 10-fold on our model simulation. The variations in (A) plasma glucose and (B) insulin levels up to the 5-fold reduction of β-cell number are shown here. (C) represents the effect of loss of β-cell mass on 2-h and 8-h plasma glucose levels, in which it was observed that both these levels are elevated compared to the control condition. In (D), we showed the reduction (in percentage) in peak postprandial plasma insulin level during the loss of β-cell number from the control condition.

of β-cell number, the 2-h plasma glucose crosses the normal range, and the 8-h glucose level reaches beyond the normal range in the 4-fold loss (**Fig. 5.4C**). We also noticed a 36% and 64% reduction in peak postprandial plasma insulin level in the 2- and 4-fold loss of β-cell number, respectively (**Fig. 5.4D**). Additionally, we observed that the 8-h plasma glucose level remains above the 126 mg/dl value in the 8-fold loss of β-cell number, which causes an 80% reduction in peak postprandial plasma insulin level. It reflects that the critical loss in β-cell number has enough potential to cause diabetes development. Type 1 diabetes (T1D), characterized by the attenuated insulin secretion due to the destruction of β-cells [433], comes into the grasp of such circumstances in which nearly 100% losses were observed for patients with long-standing T1D [434–436].

5.4.3 Glucose-insulin dynamics in type 2 diabetes

The model structure of the normal subject shows a reasonably good fit to experimental data (**Fig. 5.2**). T2D patients might also be described using the same model with different parameter values. T2D is mainly characterized by the coexistence of IR and reduced β-cell function/mass. A very recent study [429] shows around 37% reduction in β-cell number in T2D participants compared with those without diabetes ($5.1 \times 10^8 \pm 2.35 \times 10^8$ vs. $8.16 \times 10^8 \pm 4.27 \times 10^8$, $p < 0.01$). Thus, here we reduced the value of the total number of β-cells (v_{62}) to 5.1×10^8. Similarly, to impose the IR and loss of β-cell function, we reduced the values of the rate constants of the insulin-dependent glucose utilization (v_{14}) and the calcium-dependent maximum insulin release (v_{61}). It is also reported that before the meal consumption, the plasma glucose concentrations were much higher in diabetic subjects compared to non-diabetic subjects (9.1 ± 0.7 vs. 5.2 ± 0.1 mmol/l) [437]. Thus, we also changed the initial condition of plasma glucose concentration for the simulation.

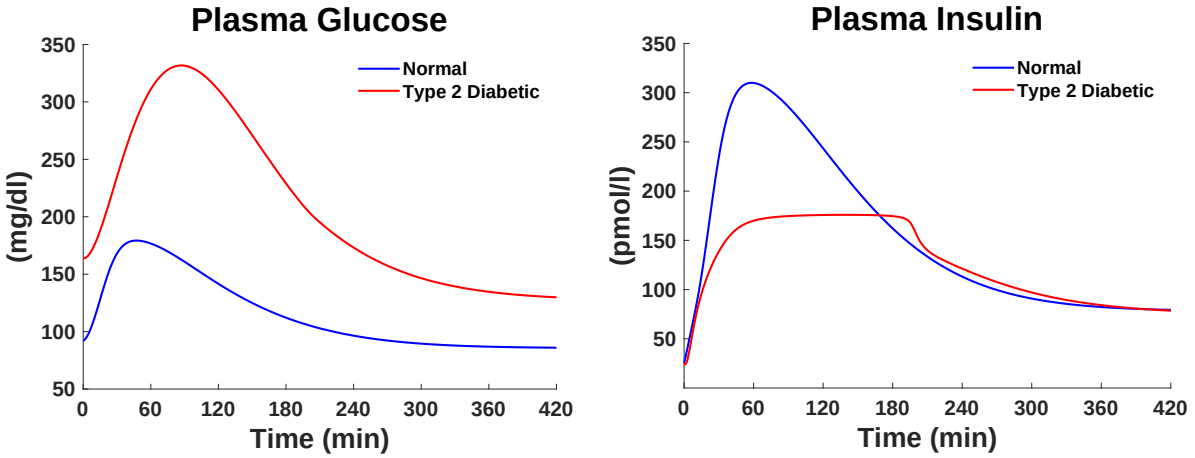

Figure 5.5: **Postprandial plasma glucose and insulin concentrations observed in diabetic (red-colored line) and normal (blue-colored line) conditions through model simulation.** The parameter set for diabetic conditions are $v_{11} = 19.82\ \mu M min^{-1}, v_{14} = 42.2\ \mu M^{-1} min^{-1}, v_{61} = 0.673\ \mu M min^{-1}, v_{62} = 5.1 \times 10^8$, and the remaining parameters are as in **Table 5.1**. Additionally, we changed the initial condition of plasma glucose concentration, $G(0)$ = 9.1 mmol/l = 164 mg/dl according to the study [437].

The model simulated glucose-insulin curves for the diabetic condition are shown in **Fig. 5.5** and compared with the simulated results for the normal condition provided in **Fig. 5.2**. It was found that both 2- and 8-h plasma glucose levels in the diabetic condition (310 and 128 mg/ dl, respectively) are much higher than in the normal condition (141 and 85 mg/ dl, respectively).

We also observed a marked reduction in plasma insulin level in the diabetic situation during the first 3-h time interval of the simulation, i.e., after the meal consumption. However, fasting insulin concentrations (8-h insulin level) did not differ between diabetic and normal conditions. The peak postprandial plasma insulin concentrations were found to be reduced by 43.25% in debates compared to the normal (176 vs. 310 pmol/l). The same amount of alteration (43.24%) was also observed in an experimental study performed by Basu et al. [437].

5.4.4 Factors responsible for the development of diabetes during the IR-induced hyperglycemia

IR is one of the primary factors that lead to T2D development, where prolonged plasma glucose level leads to loss of β-cell function/mass, and subsequently, plasma insulin level falls. Thus, here we aimed to identify crucial parameters that have a significant effect on β-cell function. That will help bring forward the possible triggers responsible for the loss of plasma insulin level during the development of T2D from the IR situation.

5.4.4.1 Parameters having association with different glycemic conditions

At the very beginning, we performed global sensitivity analysis (GSA) to obtain the sensitive parameters of our model (5.12) by performing Latin Hypercube Sampling (LHS), and Partial Ranked Correlation Coefficient (PRCC) analysis [438]. In total, 16 sensitive parameters (v_{11}, k_{11}, v_{12}, v_{13}, v_{14}, ε, v_{21}, k_{21}, k_{22}, v_{31}, v_{41}, v_{44}, v_{61}, k_{61}, v_{62} and v_{65}) were obtained for the plasma glucose and insulin level (see **Figs. 5.6** and **5.7**). To uncover the effect of these sensitive parameters on blood glucose level, we varied each parameter individually by 10-fold up and down from their default values (given in **Table 5.1** for which glucose remains in the normal range). We partitioned the parameter ranges into five compartments based on the glycemic conditions: hypoglycemia, normoglycemic, IGT, IFG, and diabetes mellitus (**Table 5.2**). Among these sensitive parameters, changes in the values of four parameters (v_{12}, v_{21}, k_{21} and v_{31}) can cause both hypoglycemia and diabetes. These parameters represent hepatic glucose production rate, glucose consumption rate by the β-cells, glucose sensitivity of glucokinase, and ATP utilization rate by the cell. Alteration in the values (beyond the threshold value provided in **Table 5.2**)

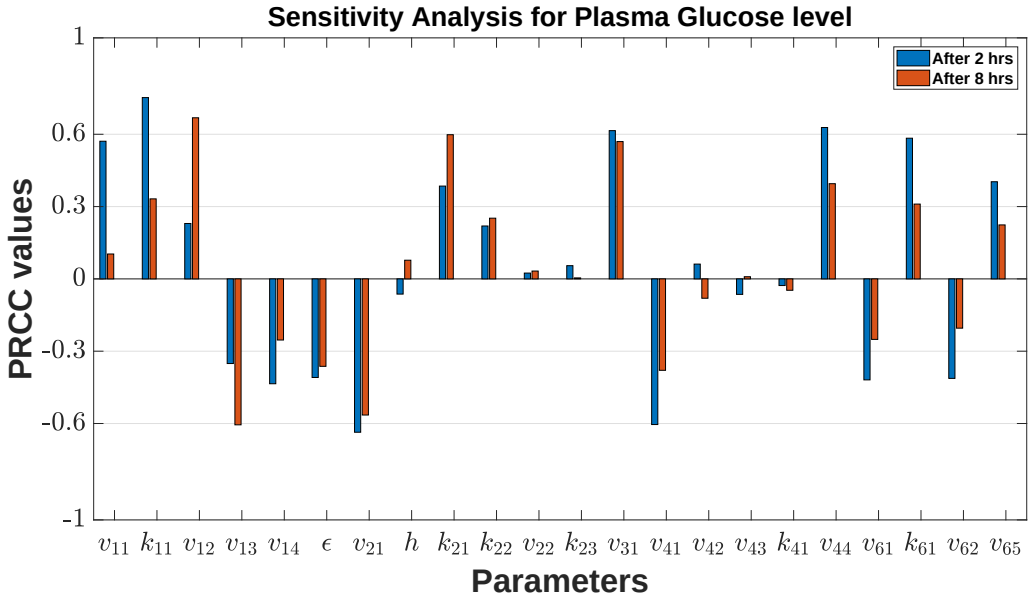

Figure 5.6: **Sensitive parameters for plasma glucose level.** Global sensitivity analysis was performed by using Latin Hypercube Sampling (LHS) and Partial Ranked Correlation Coefficient (PRCC) technique [438]. The bar represents the sensitivity of each parameter on the two and eight hours plasma glucose level after meal consumption. Sensitive parameters were selected based on the threshold value $\pm$ 0.3 on PRCC value [402, 439]. Total 15 sensitive parameters were found. Among them 14 parameters ($v_{11}, k_{11}, v_{13}, v_{14}, \varepsilon, v_{21}, k_{21}, v_{31}, v_{41}, v_{44}, v_{61}, k_{61}$, v_{62} and v_{65}) are sensitive for two hours plasma glucose level and 10 parameters ($k_{11}, v_{12}, v_{13}, \varepsilon, v_{21}, k_{21}, v_{31}, v_{41}, v_{44}$ and k_{61}) are sensitive for eight hours plasma glucose level.

of the remaining sensitive parameters, except v_{11} and v_{13}, can also make the system diabetic. These parameters represent the following biological processes: glucose absorption from dietary food, insulin-dependent glucose utilization, the sensitivity of glucokinase for ATP, ATP production through glucose metabolism, ATP dependent calcium entry, efflux of calcium ions outside of the cell through the cell membrane, calcium-dependent exocytosis of insulin granules, total number of β-cells and degradation of insulin. Changes in the values of v_{11} and v_{13} can only make system IGT and hypoglycemia, respectively. Thus, we obtained 14 parameters responsible for the diabetic condition and five parameters for hypoglycemia. This analysis also helps to capture the parameter ranges for the maintenance of glucose homeostasis. IR is one of the primary factors that lead to T2D development, where prolonged plasma glucose level leads to loss of β-cell function/mass, and subsequently, plasma insulin level falls. Thus, here we aimed to identify crucial parameters that have a significant effect on β-cell function. That will help bring forward the possible triggers responsible for the loss of plasma insulin level during

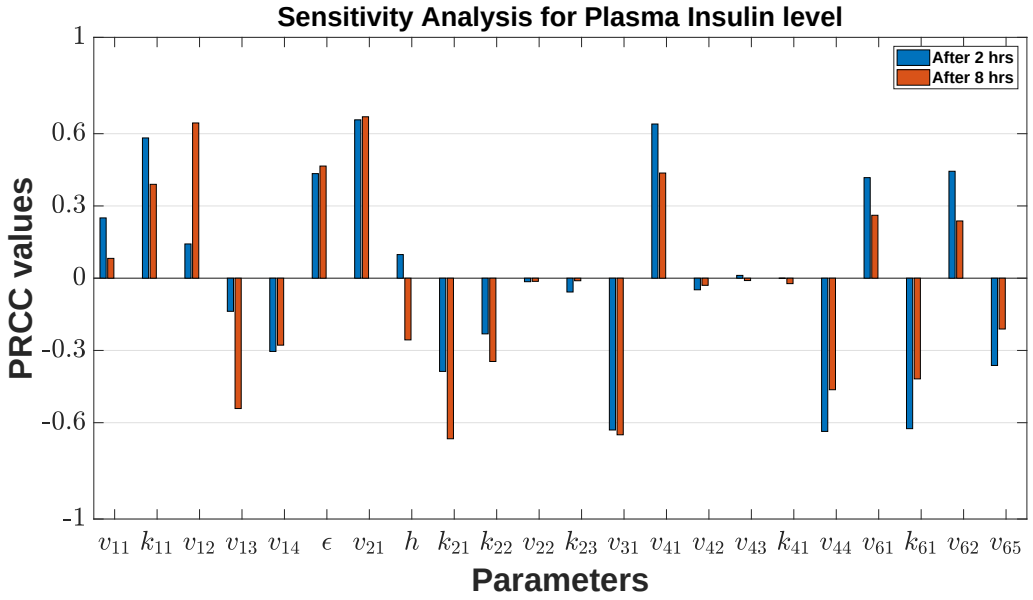

Figure 5.7: **Sensitive parameters for plasma insulin level.**Global sensitivity analysis was performed by using Latin Hypercube Sampling (LHS) and Partial Ranked Correlation Coefficient (PRCC) technique [438]. The bar represents the sensitivity of each parameter on the two and eight hours plasma insulin level after meal consumption. Sensitive parameters were selected based on the threshold value $\pm$ 0.3 on PRCC value [402, 439]. Total 14 sensitive parameters were found. Among them 11 parameters ($k_{11}, \varepsilon, v_{21}, k_{21}, v_{31}, v_{41}, v_{44}, v_{61}, k_{61}$, v_{62} and v_{65}) are sensitive for two hours plasma insulin level and 11 parameters ($k_{11}, v_{12}, v_{13}, \varepsilon, v_{21}, k_{21}, k_{22}, v_{31}, v_{41}, v_{44}$ and k_{61}) are sensitive for eight hours plasma insulin level.

the development of T2D from the IR situation.

5.4.4.2 Possible causes for the reduced plasma insulin level in the presence of IR

Now, we focused on identifying the crucial parameters that significantly affect β-cell function. So, we varied each parameter associated with the diabetic condition together with the insulin-dependent glucose utilization rate (v_{14}) around their default values and captured the glucose level for the 8 hours time frame. The whole parameter space is mainly divided into four different regions (green, cyan, red, and blue) according to the different outcomes (see **Fig. 5.8I**), like cyan-colored regions representing where the 2-h or 8-h glucose levels or both cross the normal range described in **Table 5.2**. Variation in the plasma glucose and insulin concentrations dynamics was also captured for each parameter pair selected from the different colored regions. We observed that the plasma glucose levels are much higher for the parameter pairs selected from the red-colored regions than the green-colored regions, and also 8-h glucose levels reach

Table 5.2: **Robustness of the sensitive parameters with respect to various glycemic conditions.** Different glycemic conditions are defined as follows: hypoglycemia: plasma glucose level reaches below the level 40 mg/dl [440]; impaired glucose tolerance (IGT): two hours plasma glucose level crosses the upper limit of the grey shaded area given in **Fig. 5.2**; impaired fasting glucose (IFG): eight hours plasma glucose level ≥ 110 and < 126 mg/dl [428]; diabetes mellitus: eight hours plasma glucose level $\geq$126 mg/dl and two hours plasma glucose level $>$ 200 mg/dl [428].

Parameters	Hypoglycaemia	Normal	IGT	IFG	Diabetes
v_{11}	-	$v_{11} < 40.1$	$v_{11} \geq 40.1$	-	-
k_{11}	-	$k_{11} < 55$	$k_{11} \geq 55$	$96 \leq k_{11} < 109$	$k_{11} \geq 109$
v_{12}	$v_{12} \leq 25.1$	$25.1 < v_{12} < 193.1$	$v_{12} \geq 241.4$	$193.1 \leq v_{12} < 263.1$	$v_{12} \geq 263.1$
v_{13}	$v_{13} \geq 0.0483$	$v_{13} < 0.0483$	-	-	-
v_{14}	-	$v_{14} > 90.2$	$v_{14} \leq 90.2$	$18 < v_{14} \leq 38$	$v_{14} \leq 18$
ε	-	$\varepsilon > 25$	$\varepsilon \leq 25$	$14 < \varepsilon \leq 18$	$\varepsilon \leq 14$
v_{21}	$v_{21} \geq 191$	$64 < v_{21} < 191$	$v_{21} \leq 64$	$36 < v_{21} \leq 49$	$36 \leq v_{21}$
k_{21}	$k_{21} \leq 1830$	$1830 < k_{21} < 9500$	$k_{21} \geq 9500$	$11000 \leq k_{21} < 14300$	$k_{21} \geq 14300$
k_{22}	-	$k_{22} < 1200$	$k_{22} \geq 1200$	$1450 \leq k_{22} < 2000$	$k_{22} \geq 2000$
v_{31}	$v_{31} \leq 0.19$	$0.19 < v_{31} < 0.557$	$v_{31} \geq 0.557$	$0.735 \leq v_{31} < 0.975$	$v_{31} \geq 0.975$
v_{41}	-	$v_{41} > 0.0054$	$v_{41} \leq 0.0054$	$0.0024 < v_{41} \leq 0.00359$	$v_{41} \leq 0.0024$
v_{44}	-	$v_{44} < 36$	$v_{44} \geq 36$	$55 \leq v_{44} < 81.5$	$v_{44} \geq 81.5$
v_{61}	-	$v_{61} > 0.72$	$v_{61} \leq 0.72$	$0.14 < v_{61} \leq 0.3$	$v_{61} \leq 0.14$
k_{61}	-	$k_{61} < 1.8$	$k_{61} \geq 1.8$	$2.73 \leq k_{61} < 4.1$	$k_{61} \geq 4.1$
v_{62}	-	$v_{62} > 5.4 \times 10^8$	$v_{62} \leq 5.4 \times 10^8$	$1.1 \times 10^8 < v_{62} \leq 2.3 \times 10^8$	$v_{62} \leq 1.1 \times 10^8$
v_{65}	-	$v_{65} < 0.481$	$v_{65} \geq 0.481$	$1.127 \leq v_{65} < 2.376$	$v_{65} \geq 2.376$

beyond the limit of 126 mg/dl. For example, we showed the obtained different glucose-insulin dynamics for only two parameters pairs (v_{21}, v_{14}) and (v_{31}, v_{14}) in **Fig. 5.8II**. We also found that the plasma insulin levels remain high throughout the simulation for the hypoglycemic conditions, i.e., for the parameter pairs given in the blue-colored regions. Here, we mainly focused on parameters that show a red-colored region in the 2D parameter space since it shows more than a 43% reduction in peak postprandial plasma insulin level than the default parameter set. A total of eleven such parameters were obtained that affect the peak postprandial plasma insulin levels (**Fig. 5.8I c-m**). We also observed that different parameters have different synergic effects on the outcomes. Like, parameters whose reduction is responsible for the reduced plasma insulin level are associated with the alterations in ATP production through glucose metabolism, glucose consumption rate by the β-cells, ATP-dependent calcium entry into the cells, calcium-dependent exocytosis of insulin granules, and reduced β-cell number. There are six parameters whose up-regulation can cause a significant reduction in postprandial plasma insulin level, and they are associated with the alterations in the activity of GK, ATP utilization rate, efflux of calcium ions outside of the cells, and the degradation of plasma insulin.

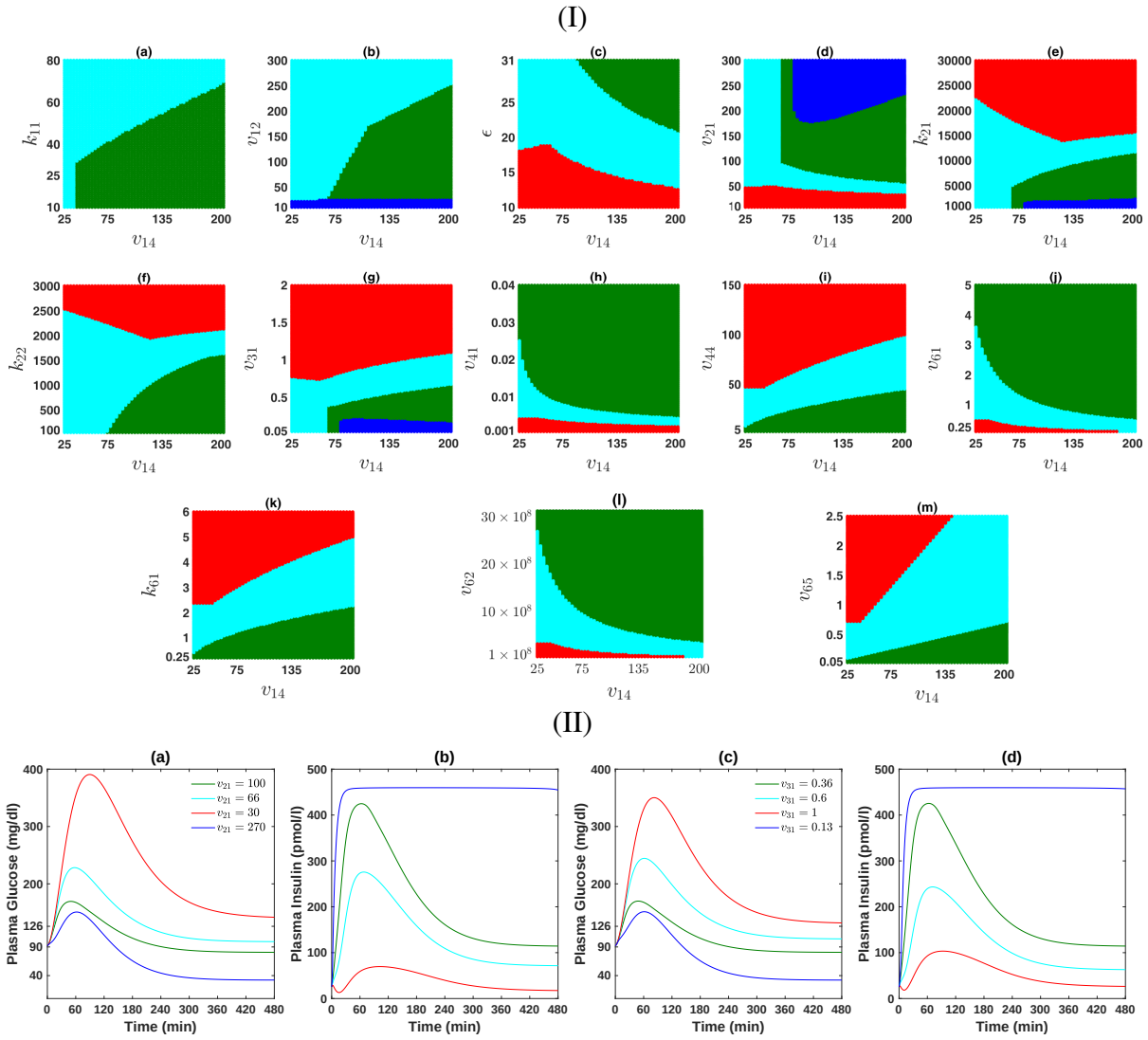

Figure 5.8: **The combined effect of each sensitive parameter with the rate constant of insulin-dependent glucose utilization (v_{14}) on the plasma glucose and insulin level.** (I) The whole 2D parameter space is divided into different regions to represent different glycemic conditions, like red, cyan, green, and blue colors representing diabetic (hyperglycemia+reduced insulin level), prediabetic (hyperglycemia), healthy and hypoglycemic state, respectively. Values of the fixed parameters are given in **Table 5.1**. We used the study by Basu et al. [437] to get the degree of alterations in the peak postprandial plasma insulin concentrations in diabetes compared to healthy individuals. (II) The glucose-insulin dynamics for each parameter pair selected from the different colored regions. Here, we only showed the dynamics for two parameters pairs: (a)-(b) (v_{21}, v_{14}) and (c)-(d) (v_{31}, v_{14}). For the model simulation, we set the value of v_{14}=105, and the values of other parameters were selected randomly from the different colored regions.

GK plays a vital role in the GSIS process by phosphorylating glucose into glucose-6-phosphate, and it also serves as a glucose sensor in β-cells [391, 392]. It is known that MODY-2 specific mutations of GK either reduce its activity or increase the half-maximal glucose concentration or change in both [441]. Here, we observed that elevation in the half-maximal concen-

tration of glucose and ATP for GK (k_{21} and k_{22}) reduces the postprandial plasma insulin level. This loss of activity in GK affects insulin secretion by reducing glucose consumption, which further diminishes the glycolytic flux. Decreased value of ATP conversion coefficient from glucose (ε) also came here as another factor for impaired insulin secretion, which can be considered a consequence of improper glucose metabolism or any defects in ATP synthesis from NADH or $FADH_2$. These all contribute to the impaired GSIS by hampering glucose-evoked rise in intracellular ATP levels. Besides that, up-regulation of ATP utilization can also diminish cytosolic ATP content, resulting in reduced insulin secretion. It is reported that chronic hyperglycemia results in diminished ATP generation by activating uncoupling protein 2 (UCP2), which is one of the major causes of obesity-induced type 2 diabetes development [403–405].

Undoubtedly ATP is the primary metabolic factor for GSIS, but our analysis revealed that the only loss in rising cytosolic Ca^{2+} concentration could hamper insulin secretion. Here, we found that the down-regulation of ATP-dependent calcium input rate constant (v_{41}) and the up-regulation of calcium extrusion rate (v_{44}) significantly reduces peak postprandial plasma insulin level by reducing the intracellular calcium content. Decreased value of v_{41} can be caused due to either overactivity of K_{ATP} channels or loss in function and/or density of VGCC. This is reported that activating mutations in Kir6.2 and sulfonylurea receptor 1 (SUR1) subunits of the K_{ATP} channel are the major cause of neonatal diabetes, and also a polymorphism in the K_{ATP} channel (E23K) is a type 2 diabetes risk factor [406]. Besides that, diminished VGCC function and/or density causes a loss in intracellular Ca^{2+} content, and so these changes can be considered a threat for type 2 diabetes development. This association is already found in some patients [407–410], but sometimes hyperactivation of the VGCC channel also leads to β-cell death [410–412]. We also obtained a crucial parameter, v_{61} (calcium-dependent maximum insulin release rate), responsible for the diminished plasma insulin level and reduction in its value leads towards either the improper calcium-induced exocytosis of insulin-containing granules or loss of insulin content. Studies also support our observation that glucotoxicity-induced loss of β-cell function is caused due to loss of insulin mRNA expression, content, and secretion [442, 443].

5.4.5 Parameter recalibration: providing possible therapeutic strategies

We are now in a position to explore the effects of each parameter in controlling the normal plasma glucose and insulin levels under each condition obtained from the previous analyses. This understanding helps to provide possible therapeutic strategies under these circumstances. Our previous analysis established that IR causes hyperglycemia without reducing the plasma insulin level. So, here we captured the tuning effect of each of the parameters not directly associated with the GSIS process in maintaining glucose homeostasis under the hyperglycemic conditions related to the reduced value in v_{14} (see **Fig. 5.9**). These parameters are mainly associated with the dietary input of glucose (v_{11} and k_{11}), hepatic glucose production (v_{12}) and insulin-independent glucose utilization (v_{13}). It was found that a gradual change in the value of all four except v_{12} can able to control the 2-h plasma glucose. Besides, 8-h plasma glucose levels can be maintained only by tuning v_{12} and v_{13}, but there is a risk of hypoglycemia.

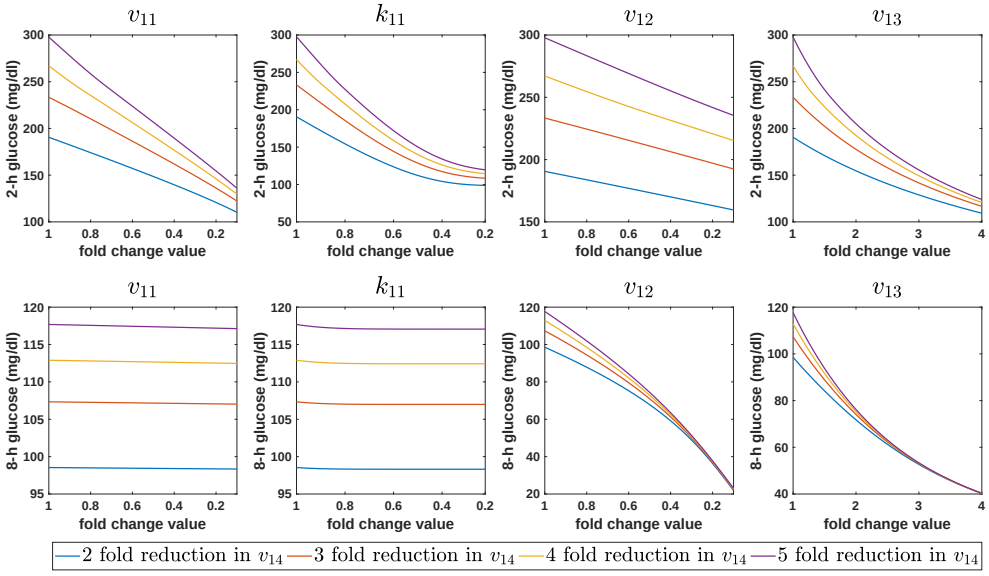

Figure 5.9: **Parametric recalibration with the help of each of the four parameters:** v_{11}**,** k_{11}**,** v_{12} **and** v_{13}**.** This figure represents the required changes for each of these parameters to revert back the plasma glucose level from the different glycemic conditions generated from the reduction in the value of v_{14}.

One of the main aims of this study was to identify potential parameters that will help increase the plasma insulin levels in T2D patients. For this, we considered each of the cases that resulted in reduced plasma insulin levels in the presence of IR and tried to identify the potential restoration possibilities through parameter variation. The parameter regulation was made here

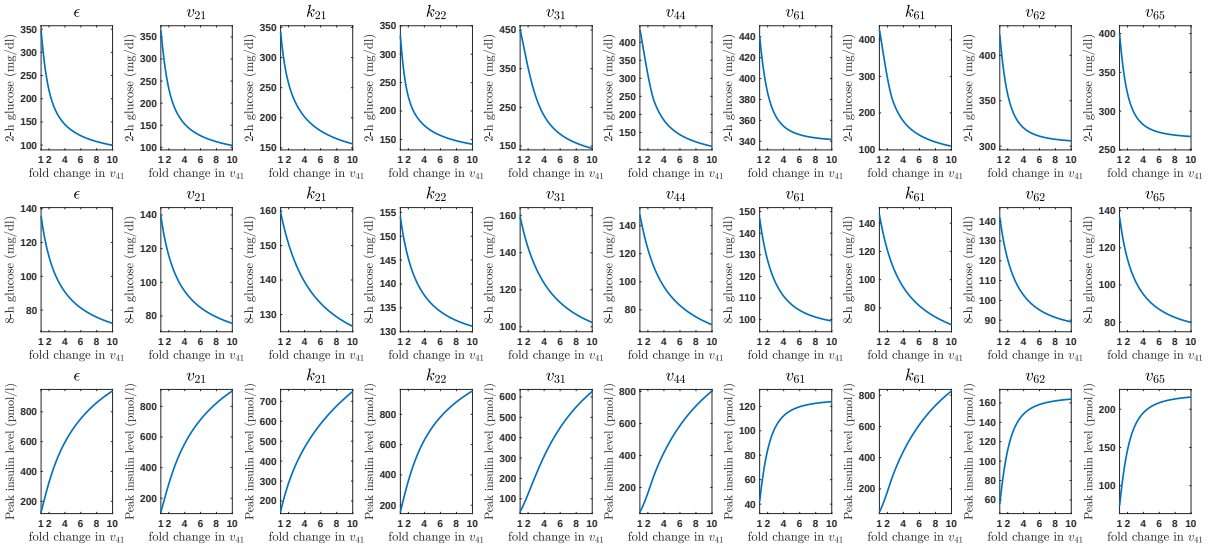

Figure 5.10: **Parametric recalibration with the help of v_{41} while restoring the system from diabetic to normal state.** This exercise was done with the setup that v_{14} was fixed at 75, and other parameters like ε, v_{21}, k_{21}, k_{22}, v_{31}, v_{44}, v_{61}, k_{61}, v_{62}, and v_{65} were chosen randomly from the red-coloured region of **Fig. 5.8I**. The first, second and third row represents the changes in 2-h glucose level, 8-h glucose level and peak insulin level, respectively, while each column corresponds to the parameters written on the top for which the restoration is happening.

by manually tuning individual parameters around their default value. The disease condition was imposed in this analysis by considering any random point from the red shaded region given in **Fig. 5.8I**, since this region represents the hyperglycemic state associated with the reduced insulin levels and sensitivity. Here, we obtained three potential parameters (v_{41}, v_{44}, and v_{61}) to restore the diabetic state to normal (see **Figs. 5.10**, **5.11** and **5.12**). In this process, we changed the values of v_{41}, v_{44} and v_{61} from their default values separately and estimated the 2-h glucose level, 8-h glucose level, and peak insulin level. For example, in the first column of these figures, we have $\varepsilon = 15$ (random value) and $v_{14} = 75$, i.e., the system is in a diabetic state. Now, if we increase v_{41} or v_{61} or decrease v_{44} up to 10-fold, the elevated plasma glucose level starts to fall in its normal range in both 2-h and 8-h cases, and also the corresponding peak insulin level increases. We observed that the plasma glucose and insulin levels could be restored through these parameters except for some cases. For example, recalibration of v_{41} and v_{44} could not significantly increase the plasma insulin level for the circumstances associated with v_{61}, v_{62} and v_{65}. However, these can control the 8-h plasma glucose level. Otherside, up-regulation of v_{61} completely fails to restore the system for the circumstances associated with k_{21}, k_{22} and v_{31},

and only the 8-h plasma glucose level can be controlled for the case of v_{44}.

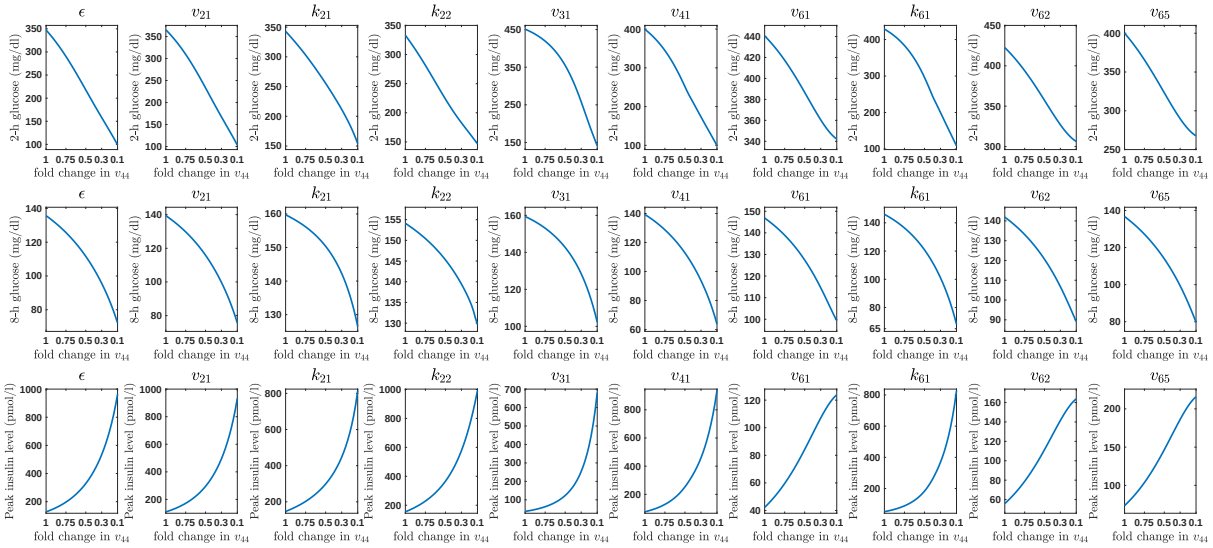

Figure 5.11: **Parametric recalibration with the help of v_{44} while restoring the system from diabetic to normal state.** This exercise was done with the setup that v_{14} was fixed at 75, and other parameters like ε, v_{21}, k_{21}, k_{22}, v_{31}, v_{44}, v_{61}, k_{61}, v_{62}, and v_{65} were chosen randomly from the red-coloured region of **Fig. 5.8I**. The first, second and third row represents the changes in 2-h glucose level, 8-h glucose level and peak insulin level, respectively, while each column corresponds to the parameters written on the top for which the restoration is happening.

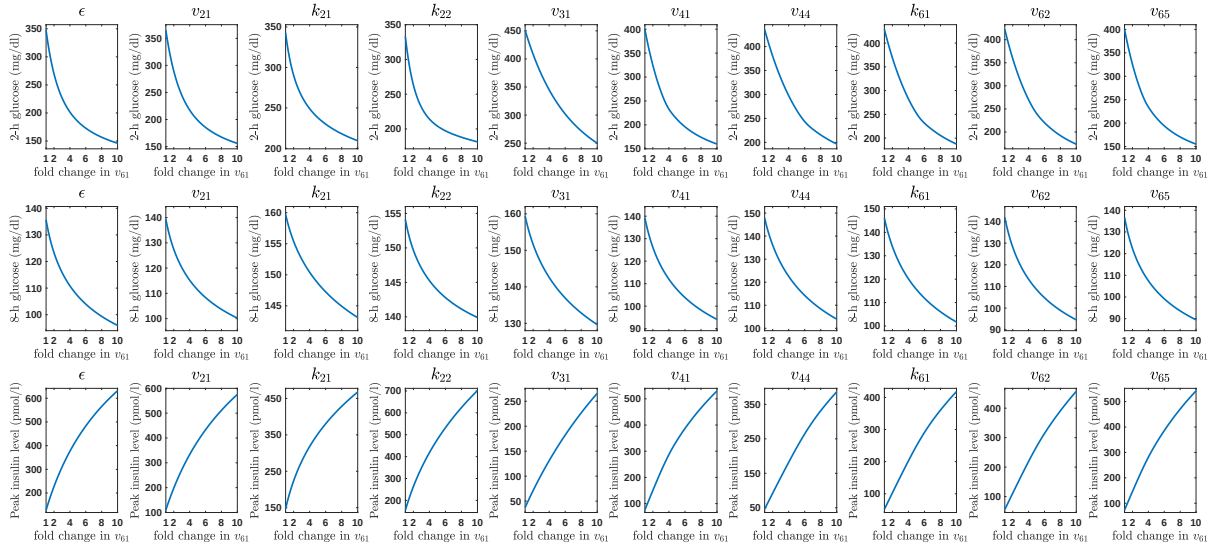

Figure 5.12: **Parametric recalibration with the help of v_{61} while restoring the system from diabetic to normal state.** This exercise was done with the setup that v_{14} was fixed at 75, and other parameters like ε, v_{21}, k_{21}, k_{22}, v_{31}, v_{44}, v_{61}, k_{61}, v_{62}, and v_{65} were chosen randomly from the red-coloured region of **Fig. 5.8I**. The first, second and third row represents the changes in 2-h glucose level, 8-h glucose level and peak insulin level, respectively, while each column corresponds to the parameters written on the top for which the restoration is happening.

Also, we did not find any sufficient changes in the plasma insulin levels in these cases. **Table 5.3** summarises all of these strategies obtained here through the parameter recalibration techniques, which could be used to maintain glucose homeostasis during improper insulin secretion.

Table 5.3: **Proposed hypothesis for maintaining glucose homeostasis through increasing the insulin secretion from β-cells in case of improper insulin secretion.**

	Possible restoration strategies		
Reasons behind reduced plasma insulin level	Increase in ATP-dependent Ca^{2+} entry	Down-regulation in Ca^{2+} extrusion	Increase in Ca^{2+}-induced exocytosis of insulin-containing granules
Reduced ATP production through glucose metabolism	✓	✓	✓
Decreased glucose consumption in β-cell	✓	✓	✓
Reduced activity of glucokinase	✓	✓	No
Up-regulation in ATP utilization rate	✓	✓	No
Down-regulated ATP-dependent Ca^{2+} input rate	Not considered	✓	✓
Increased Ca^{2+} extrusion	✓	Not considered	partially
Improper Ca^{2+}-induced exocytosis of insulin-containing granules	partially	partially	Not considered
Reduced β-cell number	partially	partially	✓
Higher insulin degradation rate	partially	partially	✓

5.5 Discussion

Insulin, released from the pancreatic β-cells, plays a significant role in maintaining glucose homeostasis by stimulating glucose absorption from the blood into the liver, fat, and skeletal muscle cells [444]. However, in insulin resistance (IR) conditions, the system does not respond well to insulin, and as a result, glucose absorption from the blood to different cells decreases. IR is one of the primary causes of type 2 diabetes (T2D) development. However, according to current research, IR alone cannot cause T2D in people with normal glucose tolerance because IR-induced hyperglycemia is mainly compensated by increased insulin production from pancreatic β-cells in people with normal islet function [431, 445]. So, abnormalities in glucose-stimulated

insulin secretion from pancreatic β-cells are also required to cause diabetes [446–448]. This motivates us to investigate the possible factors responsible for the reduced insulin secretion in IR-induced hyperglycemic state. We proposed a six-dimensional minimal model to identify crucial factors in the glucose-stimulated insulin secretion (GSIS) process whose dysfunction can lead to T2D or hypoglycemia. We established our model by generating the normal [115]. We further used this model to capture the glucose-insulin dynamics in diabetes and observed a good fit with the disease state. For instance, a 43.25% reduction was observed in the peak postprandial plasma insulin concentrations similar to the experimental study performed by Basu et al. [437]. Also, the 2- and 8-h plasma glucose levels were markedly elevated in diabetic conditions (310 and 128 mg/ dl, respectively) compared to the normal (141 and 85 mg/ dl, respectively). We also captured the effect of loss in β-cell number in glucose-insulin dynamics and found drastic changes in plasma glucose and insulin concentrations, establishing the role in disease development [429, 431, 432]. We then analyzed the model and captured different factors responsible for the progression of the disease. The underlying causes of decreased insulin secretion will aid in the prevention of IR-induced diabetes. So, we finally used the information to identify different potential strategies that would prevent the progression of IR towards T2D.

We seek the parameters that reduced the peak postprandial plasma insulin concentrations. This type of investigation highlights the specific biological processes whose impairment leads towards the more critical condition in the presence of IR-induced hyperglycemia. We obtained eleven parameters responsible for the reduced peak postprandial plasma insulin levels, and also, the associated processes were elaborated here. So, any alterations in these parameters due to IR-induced persistent hyperglycemia can result in loss of β-cell function. These alterations mainly reflect the improper glucose-evoked rise in intracellular calcium content in β-cell, which is caused either by hindering the calcium entry or raising the cell's calcium export rate. Aside from the downregulation of voltage-gated calcium channels (VGCC), more factors interrupt the glucose-evoked entry of calcium, such as the reduced activity of GK, the decline in ATP production from glucose metabolism, increased ATP utilization rate, and most importantly, overactivity of the K_{ATP} channels. In addition to these factors, improper calcium-induced exocytosis of insulin-containing granules, loss of insulin content, and loss in β-cell

mass could contribute to disease development. It is reported that ATP depletion is observed in chronic hyperglycemia due to activation of uncoupling protein 2 (UCP2) and the upregulation of voltage-dependent anion channel (VDAC) and also proposed as one of the major contributors towards the obesity-induced T2D progression [374, 403–405]. Besides, the polymorphism of the K_{ATP} channel (E23K) is proposed as one of the T2D risk factors [406]. Studies also support our observation on hyperglycemia-induced β-cell failure due to loss of insulin content and β-cell mass leads to T2D development [377, 442, 443].

Identifying some crucial factors that cause disease progression brings us to the key question of how to control these alterations to prevent the progression. Our model demonstrated that IR-induced hyperglycemic conditions are not fully controlled by reducing hepatic glucose production. Although this lowers plasma glucose levels, the postprandial glucose levels remain out of the normal range, and also there is a risk of hypoglycemia. Metformin is a widely recommended antidiabetic drug whose primary function is to reduce hepatic glucose production and improve insulin sensitivity. So, patients treated with metformin may experience higher postprandial glucose levels, which should not be ignored as this can further cause β-cell dysfunction. Thus, additional interventions are required to control the postprandial glucose levels for the patients on metformin monotherapy. It will be beneficial for preventing the disease progression for the prediabetic patients as well as those with no loss of β-cell mass. Here, we observed that reducing dietary glucose input and increasing insulin-independent glucose utilization could reduce postprandial glucose levels in the IR-induced hyperglycemic state. Hence, strategies that reduce carbohydrates absorption from the small intestine (i.e., diet control or alpha-glucosidase inhibitors) or increase glucose excretion through urine (i.e., SGLT2 inhibitors) could be more beneficial for the patients treated with metformin.

The initial treatment of T2D includes a self-management education program that emphasizes lifestyle changes such as diet, physical activity, and weight loss [449]. Even though diet and physical activity are fruitful, most people require oral antidiabetic drugs to control their blood glucose levels. Our analysis revealed three possible strategies to control the progression of diabetes: (1) increase in ATP-dependent Ca^{2+} entry, (2) down-regulation in Ca^{2+} extrusion and (3) increase in Ca^{2+}-induced exocytosis of insulin-containing granules, by im-

proving β-cell function (**Table 5.3**). In support of our first strategy, there is an antidiabetic drugs sulphonylureas and glinides that target the ATP-dependent calcium influx mechanism by blocking the K_{ATP} channels, resulting in calcium entry through VGCC channels. Our second strategy hypothesizes that down-regulation in Ca^{2+} extrusion might prevent diabetes progression. People have recently focused on inhibiting calcium extrusion from preventing and treating diabetes due to the risk of hypoglycemia in sulfonylurea therapy [450, 451]. More importantly, there is no absolute requirement for high plasma glucose for working sulfonylureas, so insulinotropic drugs with improved glucose sensitivity are demanded [451]. In β-cell, two channels are mainly responsible for calcium extrusion: the Na/Ca exchange (NCX) and the plasma membrane Ca^{2+} ATPase (PMCA) [452]. Thus, prevention of calcium extrusion through inhibiting these channels could be a promising strategy for controlling diabetes. The recent works also agree with our statement, in which inhibition of any of these channels increases glucose-induced insulin release, β-cell proliferation, and mass [452–455].

All this literature support add confidence to our proposed strategies. However, we didn't get a single strategy to control all these considered alterations. The first two listed strategies failed to meet the desired outcome for the circumstances associated with the reduced Ca^{2+}-induced exocytosis of insulin-containing granules, reduced β-cell number and higher insulin degradation rate. It seems evident that their tuning relies on the glucose-evoked rise in calcium content in the cells, so they can only control the remaining alterations. So, sulfonylureas will no longer be helpful for the patients who have reached the stage of illness associated with alterations in these factors. The last one entirely fails to restore the system for the circumstances associated with reduced glucokinase activity and up-regulation in ATP utilization rate and only controlled the 8-h plasma glucose level for the case of increased calcium extrusion. However, with these limitations, the main goal of treating patients is to slow the progression and occurrence of secondary failure [377, 456, 457]. Secondary failure is mainly defined as a deterioration of glucose control in T2D patients and caused due to progressive loss of β-cell function and insulin sensitivity [458]. This demands combination therapy, which has already been under process in some cases. Recently, GLP-1 receptor agonists have been approved in the United States for treating T2D patients, which have therapeutic effects such as enhancing glucose-induced insulin

secretion, increasing insulin synthesis, and β-cell proliferation [459, 460].

In this study, we also captured the possible reason for hypoglycemia. It is a well-known fact that unregulated insulin secretion from β-cells is the primary cause of hypoglycemia. Excess plasma insulin can also contribute to hypoglycemia development by suppressing hepatic glucose production that is reported for insulinoma patients [461]. The deletion of the C/EBPβ gene in the liver can also cause hypoglycemia by reducing hepatic glucose production [462]. Our model analysis revealed that elevated β-cells glucose consumption rate, glucose sensitivity of GK and insulin-independent glucose utilization/excretion rate, and the reduction in hepatic glucose production and ATP utilization rate in β-cells could cause hypoglycemic.

Our model identifies all of the crucial factors in the GSIS process whose impairment can either lead to hyperglycemia or hypoglycemia. Our analysis uncovers the potential strategies for preventing the progression of T2D during these alterations. In this study, we have also identified the probable limitations of the current antidiabetic drugs contributing to secondary failure and this demands more in-depth study on combination therapy. In the next chapter, we have proposed a model by incorporating the insulin synthesis and insulin granule biogenesis processes with the GSIS to decipher the in-depth understanding of the negative effect of glucotoxicity in β-cell function.

6

Small-scale kinetic model and mechanistic understanding of disease pathophysiology[1]

6.1 Introduction

Insulin is an endocrine peptide hormone essential for maintaining glucose homeostasis in our body and is produced generally from the β-cells of the pancreatic islets. It controls the blood glucose levels by promoting cellular uptake of glucose into the liver, fat, and skeletal muscle and regulating the metabolism of carbohydrates, lipids, and protein [444]. The high blood insulin concentration also strongly inhibits glucose production and secretion by the liver [444]. Glucose is the primary stimulus for insulin release from pancreatic β-cells,

[1]The bulk of this chapter has been communicated for possible publication in peer reviewed journal.

though other macronutrients (fatty acids and amino acids), hormones, and neural input may augment this response [213, 463]. In various pathophysiological conditions like diabetes, cancer, etc., this glucose-insulin dose-response relationship is dysregulated and ultimately affects the body's homeostasis. At the initial stage of type 2 diabetes (T2D), insulin resistance-induced hyperglycemia impairs β-cell function and eventually leads to reduced insulin secretion (GSIS) [380]. Although this is the major cause of developing T2D, the intrinsic mechanism underlying the β-cell failure remains largely unclear [464]. Conversely, insulinoma cells, a rare type of neuroendocrine pancreatic tumour cell, secrete insulin autonomously [465]. The insulinoma cells can not suppress insulin secretion under low glucose conditions, leading to fasting hypoglycemia [465, 466].

Insulin secretion from β-cells is mainly biphasic and requires accelerated cellular uptake of glucose, and its metabolism [467–469]. The first phase, known as the triggering pathway [470], lasts 4-8 minutes. It involves a series of cellular events, such as uptake of glucose through glucose transporters 2 (GLUT2), cytoplasmic and mitochondrial metabolism of glucose, increases in cytoplasmic ATP/ADP concentration, closure of ATP-sensitive potassium channels (K_{ATP}), cell membrane depolarization, Ca^{2+} influx through voltage-gated Ca^{2+} channels and exocytosis of the 'primed' insulin granules [471, 472]. The second phase of insulin secretion, known as the amplifying pathway [470], can be sustained for up to several hours, depending on blood glucose levels. This phase also depends on glucose metabolism and intracellular rise of Ca^{2+} content and also involves signals important for recruiting, priming, and docking insulin granules [469]. Glucose is also a main physiological regulator of insulin production and influences the production by multiple mechanisms, including the proinsulin gene transcription, mRNA stability, and the translational process [469, 472]. In the short term ($<$4 h), the insulin production increases due to augmented translation of pre-existing mRNA; however, the prolonged stimulus ($>$12 h) also increases the mRNA expression of the proinsulin gene either through transcription and/ or stabilizing the mRNA [473–475]. Thus, any impairment of these processes can directly influence the insulin level and leads to dysregulation in glucose homeostasis. However, there is still a lack of knowledge on the mechanisms regulating glucose-stimulated insulin synthesis and secretion under physiological and pathophysiological conditions [464].

In the previous chapter, we investigated the GSIS process to understand the possible factors affecting insulin secretion in insulin resistance-induced hyperglycemic state [476]. We observed that insulin secretion could be hampered due to the loss in the glucose-evoked rise in cytosolic Ca^{2+} content. The probable mechanisms include the reduced activity of glucokinase (GK), decreased ATP synthesis from glucose metabolism, increased ATP usage rate, overactivity of the K_{ATP} channels, and increased efflux of Ca^{2+}. Even though we found that a diminished calcium-induced exocytosis rate of insulin-containing granules may contribute to T2D development, the whole mechanisms still need to be fully explored. For instance, the rate of insulin production and dynamics of formation and trafficking to the cell membrane of insulin granules were not studied. There are also models on insulin granule dynamics that studied the defects in amplifying pathways, including translocation from the reserve pool to the immediately releasable pool, suggesting possible other reasons behind the defective insulin secretion [387, 477–479]. However, none has explored the defects in insulin synthesis processes, although these could also cause depletion in insulin granules. It is well-known that chronic hyperglycemia affects the insulin gene expression by reducing promoter activity and levels of two important transcription factors, PDX1 and MAFA, and leads to diminished β-cell insulin content [431].

In the present study, we proposed a simplified model for insulin synthesis and secretion of insulin granules. We incorporated the insulin mRNA as a variable in the model to investigate the consequences of defects in the transcription and translation processes of the insulin gene. One of the aims of the study was to identify parameters that could hamper insulin secretion. Another aim of this study is to capture the important factors responsible for the continuous secretion of insulin by β-cells under low glucose conditions, a condition observed in insulinoma patients. The model was further analyzed to compare insulin synthesis and exocytosis processes in restoring impaired insulin secretion. Finally, the study ends by proposing possible restoration strategies against different β-cells masses.

6.2 Formulation of the mathematical model

To capture the insulin synthesis, we here introduced two variables the insulin gene mRNA and the proinsulin pool. Besides, the insulin granules trafficking and exocytosis processes were explored through the dynamics of three intracellular pools of insulin granules: the reserve pool, the pool of docked granules, and the pool of immediately releasable granules. Glucose is the major physiological regulator of the entire system. It regulates insulin gene transcription, mRNA stability, mRNA translation, and the secretion of insulin granules. A schematic diagram of insulin biosynthesis and the formation and secretion of insulin granules processes is presented in **Fig. 6.1** and a minimal model representing schematic diagram is discussed below.

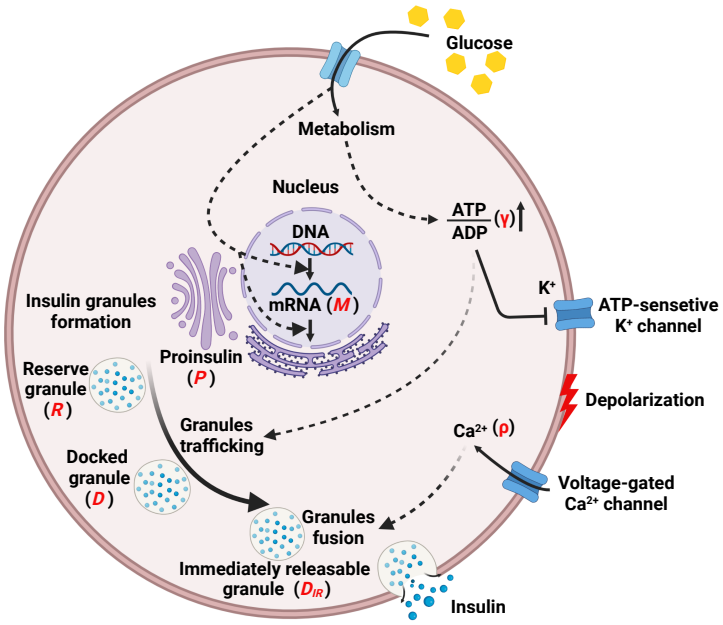

Figure 6.1: **Schematic diagram of the proposed mathematical model on glucose-stimulated insulin synthesis and secretion process.** The entire process was studied here by constructing the dynamical equations for seven key players. These are as follows: 1) insulin gene mRNA, 2) the proinsulin pool, 3) ATP-to-ADP ratio, 4) cytosolic Ca^{2+} concentration, and three intracellular pools of insulin granules: 5) the reserve pool, 6) the pool of docked granules, and 7) the pool of immediately releasable granules. The effect of glucose stimulus was imposed by considering the increased transcription and translation rate and a regulatory function on the dynamics of the ATP-to-ADP ratio.

Let $M(t)$ denote the insulin mRNA level at time t. The transcription rate of the insulin gene is controlled by complex interactions between the transcription factors (PDX1, MAFA, BETA2, and ATF2) and the specific elements within the insulin promoter site [213, 480, 481]. Glucose enhances the transcription rate through several complementary mechanisms, including

the recruitment of transcription factors to regulatory sites, histone modifications, and initiation of transcription [482]. It also increases the stability of insulin mRNA [474]. For simplicity, we considered the transcription rate a constant and a linear term for mRNA degradation. So, the dynamical equation of M is expressed as:

$$\frac{dM}{dt} = \alpha_1 - \delta_1 M,$$

where α_1 and δ_1 denote constant transcription rate and a constant degradation rate constant respectively. It is reported that long-term exposure to glucose stimulus could approximately increase a 2-fold level of insulin mRNA. So, to capture this phenomenon, we considered the increased values for α_1 and δ_1 for the high glucose model simulation (see **Appx. 6.4**). The insulin mRNA product encodes preproinsulin (the insulin precursor), which is translated into the rough endoplasmic reticulum (rER) compartment. The synthesis of proinsulin is also a very complex process. It depends on the series of steps, starting from the translational of mRNA, translocation of the products into the rER lumen, the rapid folding, formation of the disulfide bond, and finally, the transportation into the Golgi apparatus [483]. The biosynthesis rate of the pool of proinsulin aggregates ($P(t)$) from the insulin mRNA is expressed as vM, where v is the rate constant. Similar to the transcription rate, the proinsulin pool formation rate also increases in glucose stimulus. Therefore, a higher value of v was considered for the high glucose model simulation compared to the low glucose case [473]. The governing equation for P is expressed as:

$$\frac{dP}{dt} = vM - \delta_2 P - kP\rho D_{IR},$$

where δ_2 is a degradation rate constant. The last term denotes the formation rate of insulin granules in the trans-Golgi apparatus, a function of pool of proinsulin aggregates ($P(t)$) and the available free granules membrane materials. At the exocytosis of insulin granules, the granule membrane materials become part of the plasma membrane and are successively removed and returned to the trans-Golgi apparatus for recycling. We denoted the rate of granule membrane fusion with the cell membrane by ρD_{IR}, where ρ represents the rate coefficient that accounts for the factors that promote the exocytosis of insulin granules. D_{IR} represents the immediately

releasable pool. The dynamical equation for the reserve pool (R) is expressed as:

$$\frac{dR}{dt} = kP\rho D_{IR} - \gamma R,$$

where γR was considered as the conversion rate of reserve pool into the pool of docked granules (D) [478]. The dynamics of the pool of docked granules and pool of immediately releasable pool were taken from [478], and are expressed as:

$$\begin{aligned} \frac{dD}{dt} &= \gamma R - k_1^+ (C_T - D_{IR}) D + k_1^- D_{IR}, \\ \frac{dD_{IR}}{dt} &= k_1^+ (C_T - D_{IR}) D - k_1^- D_{IR} - \rho D_{IR}, \end{aligned}$$

where C_T denotes the constant pool of total Ca^{2+} channels. k_1^+ and k_1^-, respectively, are the rate constants of association and dissociation for the binding between docked granule and Ca^{2+} channel. Glucose-stimulated insulin secretion from β-cells is biphasic. The first phase lasts for 4-8 minutes and involves a series of cellular events; uptake of glucose through glucose transporters 2 (GLUT2); metabolism of glucose; increases in cytoplasmic ATP/ADP concentration; closure of K_{ATP} channels; cell membrane depolarization; Ca^{2+} influx through voltage-gated Ca^{2+} channels and exocytosis of the 'primed' insulin granules [471, 472]. The second phase of insulin secretion can be sustained for up to several hours, depending on blood glucose levels. This phase also depends on glucose metabolism and intracellular rise of Ca^{2+} content but also involves signals important for recruiting, priming, and docking the insulin granules [469]. All these are incorporated by taking a simplified dynamics of γ (factor representing ATP-to-ADP ratio), and ρ (factor representing cytosolic Ca^{2+} concentration) [478]. The governing equations of γ is as follows:

$$\frac{d\gamma}{dt} = \eta \left(-\gamma + \gamma_b + \alpha_2(G) \right),$$

where η is the rate constant and γ_b denotes the basal value of γ at low glucose. The function $\alpha_2(G)$ indicates the response of glucose stimulus and is expressed as:

$$\alpha_2(G) = \begin{cases} 0, & G \leq G^* \\ \frac{\hat{h}(G-G^*)}{\hat{G}-G^*}, & G^* < G \leq \hat{G} \\ \hat{h}, & G > \hat{G} \end{cases}$$

where $\hat{h}$ is the maximal value of α_2 and is achieved at $G = \hat{G}$. The rate equation of ρ depends on γ with increase in the ATP-to-ADP ratio. This leads to the closure of K_{ATP} channels and results in Ca^{2+} influx through voltage-gated Ca^{2+} channels. Thus the dynamical equation for ρ is expressed as:

$$\frac{d\rho}{dt} = \zeta \left\{ -\rho + \rho_b + k_\rho (\gamma - \gamma_b) \right\},$$

where ζ is the rate constant and the last term defines the action of γ on ρ. Thus, the simplified model of insulin synthesis and the biogenesis and secretion of insulin granules is proposed by the following system of ordinary differential equation (ODE):

$$\begin{aligned} \frac{dM}{dt} &= \alpha_1 - \delta_1 M, \\ \frac{dP}{dt} &= vM - \delta_2 P - kP\rho D_{IR}, \\ \frac{dR}{dt} &= kP\rho D_{IR} - \gamma R, \\ \frac{d\gamma}{dt} &= \eta \left(-\gamma + \gamma_b + \alpha_2 \right), \\ \frac{dD}{dt} &= \gamma R - k_1^+ (C_T - D_{IR}) D + k_1^- D_{IR}, \\ \frac{dD_{IR}}{dt} &= k_1^+ (C_T - D_{IR}) D - k_1^- D_{IR} - \rho D_{IR}, \\ \frac{d\rho}{dt} &= \zeta \left\{ -\rho + \rho_b + k_\rho (\gamma - \gamma_b) \right\}, \end{aligned} \tag{6.1}$$

with the initial conditions $M(0) > 0$, $P(0) > 0$, $R(0) > 0$, $\gamma(0) > 0$, $D(0) > 0$, $D_{IR}(0) > 0$, $\rho(0) > 0$. Insulin secretion rate is denoted by

$$[ISR](t) = I_0 \rho D_{IR}(t) f N, \tag{6.2}$$

where I_0 is the amount of insulin content in a granule, N is the total number of β-cells in the

pancreas and $f(G)$ represents the fraction of total β-cell population responds to the glucose stimulus and defined by the following relation as proposed in [478]:

$$f(G) = \begin{cases} f_b, & G < G^* \\ f_b + (1 - f_b)\frac{G-G^*}{K_f+G-G^*}, & G \geq \hat{G} \end{cases}$$

where f_b is the fraction of responding β-cells at glucose concentration below the threshold G^* and K_f is the constant related to the effectiveness of β-cells requirement.

6.3 Analytical results

6.3.1 Positive invariance

By setting

$$X = (M, P, R, \gamma, D, D_{IR}, \rho)^T \in \mathbf{R}^7_+$$

and $F(X) = [F_1(X), F_2(X), F_3(X), F_4(X), F_5(X), F_6(X), F_7(X)]^T$, Eq.(6.1) can be written as the system

$$\dot{X} = F(X), \tag{6.3}$$

together with initial conditions $X(0) = X_0 \in \mathbf{R}^7_+$. It is easy to check that whenever choosing $X(0) \in \mathbf{R}^7_+$ with $X_i = 0$, for $i = 1, .., 7$, then $F_i(X)|_{X_i=0} \geq 0$. Due to the lemma of Nagumo [425], any solution of equation (6.3) with $X_0 \in \mathbf{R}^7_+$, say $X(t) = X(t; X_0)$, is such that $X(t) \in \mathbf{R}^7_+$ for all $t > 0$.

6.3.2 Boundedness

All solutions of the system (6.1) with positive initial conditions are uniformly bounded within a region Γ,

where $\Gamma = \{(M, P, R, \gamma, D, D_{IR}, \rho) \in \mathbf{R}^7_+ : \ 0 < M(t) \leq M_1, \ 0 < P(t) \leq P_1, \ 0 < R(t) \leq R_1, \ l_1 \leq \gamma(t) \leq H_1, \ 0 < D(t) \leq D_1, \ 0 < D_{IR} < C_T, \ 0 < \rho(t) \leq H_2 \ \forall \ t \geq 0\}$, with $M_1 = \frac{\alpha_1}{\delta_1} + M(0)$, $P_1 = \frac{\nu M_1}{\delta_2} + P(0)$, $l_1 = \gamma_b + \alpha_2$, $H_1 = \gamma_b + \alpha_2 + \gamma(0)$, $H_2 = \left\{\rho_b + k_\rho \left(H_1 - \gamma_b\right)\right\} +$

$\rho(0),\ R_1 = \frac{kP_1C_TH_2}{l_1} + R(0),\ D_1 = \frac{H_1R_1+k_1^-C_T}{k_1^+\varepsilon} + D(0).$

Proof: From the first equation of (6.1), we get

$$\frac{dM}{dt} + \delta_1 M = \alpha_1$$

From the theory of differential inequalities [484], we then obtained

$$0 \leq M(t) \leq \frac{\alpha_1}{\delta_1}(1 - e^{-\delta_1 t}) + M(0)e^{-\delta_1 t}$$

From which we get,

$$M(t) \leq M_1, \forall t \geq 0 \tag{6.4}$$

where, $M_1 = \frac{\alpha_1}{\delta_1} + M(0)$.

From the second equation of (6.1), we get

$$\begin{aligned}\frac{dP}{dt} &= vM - \delta_2 P - kP\rho D_{IR} \\ &\leq vM - \delta_2 P \\ &\leq vM_1 - \delta_2 P\end{aligned}$$

Thus we obtain,

$$\frac{dP}{dt} + \delta_2 P \leq vM_1$$

From the theory of differential inequalities [484], we get

$$0 \leq P(t) \leq \frac{vM_1}{\delta_2}(1 - e^{-\delta_2 t}) + P(0)e^{-\delta_2 t}$$

From which we get,

$$P(t) \leq P_1, \forall t \geq 0 \tag{6.5}$$

where, $P_1 = \frac{\nu M_1}{\delta_2} + P(0)$.

From the fourth equation of (6.1), we get

$$\frac{d\gamma}{dt} + \eta\gamma = \eta\left(\gamma_b + \alpha_2\right)$$

By solving this we obtained

$$\gamma(t) = (\gamma_b + \alpha_2)(1 - e^{-\eta t}) + \gamma(0)e^{-\eta t}$$

From which we get,

$$l_1 \leq \gamma(t) \leq H_1, \forall t \geq 0 \tag{6.6}$$

where, $l_1 = \gamma_b + \alpha_2$ and $H_1 = \gamma_b + \alpha_2 + \gamma(0)$.

From the seventh equation of (6.1), we get

$$\begin{aligned}\frac{d\rho}{dt} + \zeta\rho &= \zeta\left\{\rho_b + k_\rho\left(\gamma - \gamma_b\right)\right\} \\ &\leq \zeta\left\{\rho_b + k_\rho\left(H_1 - \gamma_b\right)\right\}\end{aligned}$$

From the theory of differential inequalities [484], we obtained

$$0 \leq \rho(t) \leq \left\{\rho_b + k_\rho\left(H_1 - \gamma_b\right)\right\}\left(1 - e^{-\zeta t}\right) + \rho(0)e^{-\zeta t}$$

From which we get,

$$\rho(t) \leq H_2, \forall t \geq 0 \tag{6.7}$$

where, $H_2 = \left\{\rho_b + k_\rho \left(H_1 - \gamma_b\right)\right\} + \rho(0)$.

From the sixth equation of (6.1), we have

$$\frac{dD_{IR}}{dt} = k_1^+ \left(C_T - D_{IR}\right) D - k_1^- D_{IR} - \rho D_{IR} \tag{6.8}$$

Let us assume, for any instance $t_1 \geq 0$ the value $D_{IR}(t_1) = C_T$. Then from Eq. (6.8) we have

$$\frac{dD_{IR}}{dt}|_{t=t_1} = -(k_1^- + \rho)C_T < 0$$

Thus, the value of D_{IR} cannot crosses the threshold value C_T. Hence, $D_{IR}(t_1) < C_T$. Let us assume, $[D_{IR}]_{max} = C_T - \varepsilon$, where $\varepsilon > 0$. From the third equation of (6.1), we get

$$\begin{aligned}\frac{dR}{dt} &= kP\rho D_{IR} - \gamma R \\ &\leq kP\rho D_{IR} - l_1 R\end{aligned}$$

Thus,

$$\frac{dR}{dt} + l_1 R \leq kP_1 C_T H_2$$

From the theory of differential inequalities [484], we obtained

$$0 \leq R(t) \leq \frac{kP_1 C_T H_2}{l_1}(1 - e^{-l_1 t}) + R(0)e^{-l_1 t}$$

From which we get,

$$R(t) \leq R_1, \forall t \geq 0 \tag{6.9}$$

where, $R_1 = \frac{kP_1C_TH_2}{l_1} + R(0)$.

From the fifth equation of (6.1), we get

$$\begin{aligned}\frac{dD}{dt} &= \gamma R - k_1^+ (C_T - D_{IR}) D + k_1^- D_{IR} \\ &\leq H_1 R_1 - k_1^+ \varepsilon D + k_1^- C_T\end{aligned}$$

Thus we obtain,

$$\frac{dD}{dt} + k_1^+ \varepsilon D \leq H_1 R_1 + k_1^- C_T$$

From the theory of differential inequalities [484], we obtained

$$0 \leq D(t) \leq \frac{H_1 R_1 + k_1^- C_T}{k_1^+ \varepsilon}(1 - e^{-k_1^+ \varepsilon t}) + R(0) e^{-k_1^+ \varepsilon t}$$

Thus,

$$D(t) \leq D_1, \forall t \geq 0 \tag{6.10}$$

where, $D_1 = \frac{H_1 R_1 + k_1^- C_T}{k_1^+ \varepsilon} + D(0)$.
Hence, this ensures the existence of a bounded region $\Gamma \in \mathbf{R}_+{}^7$ such that for any initial values $(M(0), P(0), R(0), \gamma(0), D(0), D_{IR}(0), \rho(0))^T$, solutions of the system (6.1) will always remain within the region Γ. This completes the proof.

6.3.3 Equilibrium points

The system (6.1) has

I. one non-interior equilibrium point, $E_{B0} \equiv (M_0^*, P_0^*, 0, \gamma_0^*, 0, 0, \rho_0^*)$, where $M_0^* = \frac{\alpha_1}{\delta_1}, P_0^* = \frac{v\alpha_1}{\delta_1\delta_2}, \gamma_0^* = \gamma_b + \alpha_2, \rho_0^* = \rho_b + k_\rho \alpha_2$ which exists for all parameter values, and

II. one interior equilibrium point, namely $E^* \equiv (M^*, P^*, R^*, \gamma^*, D^*, D_{IR}^*, \rho^*)$ is given by $M^* =$

$\frac{\alpha_1}{\delta_1}$, $P^* = \frac{1}{k}$, $R^* = \frac{kv\alpha_1 - \delta_1\delta_2}{k\delta_1(\gamma_b+\alpha_2)}$, $\gamma^* = \gamma_b + \alpha_2$, $D^* = \frac{(kv\alpha_1-\delta_1\delta_2)(\rho_b+k_\rho\alpha_2+k_1^-)}{k_1^+[C_T k\delta_1(\rho_b+k_\rho\alpha_2)-(kv\alpha_1-\delta_1\delta_2)]}$, $D_{IR}^* = \frac{kv\alpha_1-\delta_1\delta_2}{k\delta_1(\rho_b+k_\rho\alpha_2)}$ and $\rho^* = \rho_b + k_\rho\alpha_2$. E^* exists if (i) $(kv\alpha_1 - \delta_1\delta_2) > 0$ and (ii) $C_T k\delta_1(\rho_b + k_\rho\alpha_2) > (kv\alpha_1 - \delta_1\delta_2)$.

6.3.4 Stability analysis

To study the local stability properties of the equilibrium points we computed the Jacobian matrix (J) of system (6.1) around an arbitrary point $(M, P, R, \gamma, D, D_{IR}, \rho)$ and has the form

$$J = \begin{bmatrix} -\delta_1 & 0 & 0 & 0 & 0 & 0 & 0 \\ v & -(\delta_2 + k\rho D_{IR}) & 0 & 0 & 0 & -kP\rho & -kPD_{IR} \\ 0 & k\rho D_{IR} & -\gamma & -R & 0 & kP\rho & kPD_{IR} \\ 0 & 0 & 0 & -\eta & 0 & 0 & 0 \\ 0 & 0 & \gamma & R & -k_1^+(C_T - D_{IR}) & k_1^+D + k_1^- & 0 \\ 0 & 0 & 0 & 0 & k_1^+(C_T - D_{IR}) & -(k_1^+D + k_1^- + \rho) & -D_{IR} \\ 0 & 0 & 0 & \zeta k_\rho & 0 & 0 & -\zeta \end{bmatrix} \tag{6.11}$$

At the non-interior equilibrium point E_{B0}, the Jacobian becomes

$$J_{B_0} = \begin{bmatrix} -\delta_1 & 0 & 0 & 0 & 0 & 0 & 0 \\ v & -\delta_2 & 0 & 0 & 0 & -kP_0^*\rho_0^* & 0 \\ 0 & 0 & -\gamma_0^* & 0 & 0 & kP_0^*\rho_0^* & 0 \\ 0 & 0 & 0 & -\eta & 0 & 0 & 0 \\ 0 & 0 & \gamma_0^* & 0 & -k_1^+C_T & k_1^- & 0 \\ 0 & 0 & 0 & 0 & k_1^+C_T & -(k_1^- + \rho_0^*) & 0 \\ 0 & 0 & 0 & \zeta k_\rho & 0 & 0 & -\zeta \end{bmatrix}$$

The eigenvalues of J_{B_0} are λ_{0i}'s, $i = 1$ to 7, where $\lambda_{01} = -\delta_1 < 0$, $\lambda_{02} = -\delta_2 < 0$, $\lambda_{04} = -\eta < 0$, $\lambda_{07} = -\zeta < 0$ and $\lambda_{03,05,06}$ are given by the root of the equation

$$\lambda^3 + A_1\lambda^2 + A_2\lambda + A_3 = 0, \tag{6.12}$$

where,

$A_1 = (k_1^+ C_T + k_1^- + \rho_0^* + \gamma_0^*) > 0, A_2 = k_1^+ C_T \rho_0^* + \gamma_0^* (k_1^+ C_T + k_1^- + \rho_0^*) > 0$ and $A_3 = k_1^+ C_T \rho_0^* \gamma_0^* (1 - kP_0^*)$.

According to Routh-Hurwitz criterion, E_{B0} will be locally asymptotically stable if

(i) $A_n > 0, (n = 1,2,3)$,

(ii) $A_1 A_2 - A_3 = (k_1^+ C_T + k_1^- + \rho_0^*) \left\{ k_1^+ C_T \rho_0^* + \gamma_0^* (k_1^+ C_T + k_1^- + \rho_0^*) + \gamma_0^{*2} \right\} + k k_1^+ C_T \rho_0^* \gamma_0^* P_0^* > 0$.

Therefore E_{B0} will be locally asymptotically stable if $A_3 > 0$, and $kv\alpha_1 < \delta_1 \delta_2$.

At the interior equilibrium point E^*, the Jacobian becomes

$$J^* = \begin{bmatrix} -\delta_1 & 0 & 0 & 0 & 0 & 0 & 0 \\ v & -(\delta_2 + k\rho^* D_{IR}^*) & 0 & 0 & 0 & -kP^*\rho^* & -kP^* D_{IR}^* \\ 0 & k\rho^* D_{IR}^* & -\gamma^* & -R^* & 0 & kP^*\rho^* & kP^* D_{IR}^* \\ 0 & 0 & 0 & -\eta & 0 & 0 & 0 \\ 0 & 0 & \gamma^* & R^* & -k_1^+ (C_T - D_{IR}^*) & k_1^+ D^* + k_1^- & 0 \\ 0 & 0 & 0 & 0 & k_1^+ (C_T - D_{IR}^*) & -(k_1^+ D^* + k_1^- + \rho^*) & -D_{IR}^* \\ 0 & 0 & 0 & \zeta k_\rho & 0 & 0 & -\zeta \end{bmatrix}$$

The eigenvalues of J^* are λ_i's, $i = 1$ to 7, where $\lambda_1 = -\delta_1 < 0$, $\lambda_4 = -\eta < 0$, $\lambda_7 = -\zeta < 0$ and $\lambda_{2,3,5,6}$ are given by the root of the equation

$$\lambda^4 + A_1 \lambda^3 + A_2 \lambda^2 + A_3 \lambda + A_4 = 0$$

where,

$$\begin{aligned} A_1 &= (B + C + \gamma^*) > 0, \\ A_2 &= \{A + B\gamma^* + (B + \gamma^*) C\} > 0, \\ A_3 &= \{\gamma^* A - kP^* \gamma^* A + (A + \gamma^* C) B\}, \\ A_4 &= (\gamma^* AB - \delta_2 kP^* \gamma^* A). \end{aligned}$$

The values of A, B and C are given by

$A = \rho^* k_1^+ (C_T - D_{IR}^*) > 0$

$B = (\delta_2 + k\rho^* D_{IR}^*) > 0$

$C = (k_1^+ D^* + k_1^- + \rho^*) + k_1^+ (C_T - D_{IR}^*)\rho^* = (k_1^+ D + k_1^- + \rho^*) + A\rho^* > 0.$

Thus, according to Routh-Hurwitz criterion, E^* will be locally asymptotically stable if

$$a.\ \gamma^* A + (A + \gamma^* C)B > kP^* \gamma^* A,$$

$$b.\ B > \delta_2 kP^*,$$

$$c.\ (B + C + \gamma^*)\{A + B\gamma^* + (B + \gamma^*)C\} > \{\gamma^* A - kP^* \gamma^* A + (A + \gamma^* C)B\},$$

$$d.\ (B + C + \gamma^*)\{A + B\gamma^* + (B + \gamma^*)C\}\{\gamma^* A - kP^* \gamma^* A + (A + \gamma^* C)B\} >$$
$$\{\gamma^* A - kP^* \gamma^* A + (A + \gamma^* C)B\}^2 + (B + C + \gamma^*)^2(\gamma^* AB - \delta_2 kP^* \gamma^* A).$$

If all of these conditions satisfies then E^* will be globally asymptotically stable, since according to the existence criterion of E^*, E_{B0} will be unstable.

6.4 Description on parameter estimation from literature

Numerical value of δ_1: The half-life ($t_{1/2}$) of insulin mRNA depends on glucose concentration, and the value is 29 h and 77 h, respectively, at low and high glucose levels [474]. We calculated the degradation rate of insulin mRNA using the following equation:

$$\delta_1 = \frac{ln(2)}{t_{1/2}} \tag{6.13}$$

The obtained values for δ_1 were 3.98×10^{-4} min^{-1} and 1.5×10^{-4} min^{-1}, respectively, at low and high glucose concentrations.

Numerical value of α_1: The mRNA expression value of insulin genes is 126753 in tpm counts [485], so we used this value as the steady state value of M (M^*). We assumed that the system would always stay in a steady state at low glucose concentration, and the high glucose would act as a stimulus in the system. Thus, the value of α_1 at the low glucose setting was

calculated from equation: $M^* = \frac{\alpha_1}{\delta_1}$, and the obtained value was 50.4934 tpm min^{-1}.

It was reported that prolonged glucose stimulation (24 h) resulted in ∼2-fold increase in insulin mRNA level (M) [473]. By solving the first equation of the system (6.1). we obtained

$$M(t) = \frac{\alpha_1}{\delta_1}(1 - e^{-\delta_1 t}) + M(0)e^{-\delta_1 t} \tag{6.14}$$

Now, we have information that $M(t_1) = 2 \times M(0)$ at $t = t_1$=24 h. Putting these values in Eq. (6.14), we get

$$\begin{aligned} 2M(0) &= \frac{\alpha_1}{\delta_1}(1 - e^{-\delta_1 t_1}) + M(0)e^{-\delta_1 t_1} \\ \implies M(0)(2 - e^{-\delta_1 t_1}) &= \frac{\alpha_1}{\delta_1}(1 - e^{-\delta_1 t_1}) \\ \implies \alpha_1 &= \frac{M(0)\delta_1(2 - e^{-\delta_1 t_1})}{(1 - e^{-\delta_1 t_1})} \end{aligned} \tag{6.15}$$

Finally, we put $M(0)$=126753, t_1=24 h and $\delta_1 = 1.5 \times 10^{-4}$ in Eq. (6.15) and obtained α_1 = 116.89 for the high glucose model simulation.

6.5 Numerical results

We begin the analysis assuming that the system remains in the steady state (i.e., in interior equilibrium point, E^*) at low glucose concentration, and the high glucose concentration would act as a stimulus. To capture the effect of glucose stimulus on the system, two threshold values of glucose, G^*= 4.58 mmol/l and $\hat{G}$= 10 mmol/l, were used. Based on this values, we obtained α_2=0 for low glucose setting ($G \leq$ 4.58 mmol/l) and α_2=$\hat{h}$= 3.93×10^{-3} min^{-1} for high glucose setting ($G \geq$ 10 mmol/l). The rest of the parameters were collected or derived from the information given in available literature (detailed descriptions are provided in **Table 6.1** and **Section 6.4**). The values of v and k were estimated such that for low glucose, the system (6.1) provides the stable interior equilibrium point (E^*), where M^*=126753, P^*=10, R^*=10,000, D^*=950, D^*_{IR}=50, γ^*=γ_b and ρ^*=ρ_b [478, 485]. It is well-known that high glucose levels in β-cells increase the translation rate of the insulin gene [474]. So, we also increased the value of v for the high glucose model simulation. v was estimated by reproducing the time

series data given in [478]. The obtained parameter set (given in **Table 6.1**) for the high glucose model stimulation also satisfies the existence and stability criterion for the interior equilibrium of the system (6.1). The aim of the present study was to identify crucial parameters that significantly affect insulin secretion from β-cells under high or low-glucose conditions. This would help to understand the pathophysiology of T2D as well as insulinoma.

Table 6.1: **Description of the parameters:** Values of the parameters were mostly collected from the available literature. For some unknown parameters, we estimated their values by using the available information literature, and detailed descriptions were provided in **Appx. 6.4**.

Parameters	**Definition**	**Value with unit**	**Ref.**
α_1	Transcription rate constant	50.4934 tpm min^{-1} (low glucose), 116.89 tpm min^{-1} (high glucose)	Section 6.4
δ_1	mRNA degradation rate constant	3.98×10^{-4} min^{-1} (low glucose), 1.5×10^{-4} min^{-1} (high glucose)	Section 6.4
v	Biosynthesis rate constant of proinsulin aggregates from insulin mRNA	3.16×10^{-5} tpm^{-1} min^{-1} (low glucose), 7.89×10^{-5} tpm^{-1} min^{-1} (high glucose)	Estimated
δ_2	Degradation rate constant of proinsulin pool	0.3 min^{-1}	[478]
k	Rate constant of formation of insulin granules	0.1	Estimated
η	Rate constant for γ	4 min^{-1}	[478]
γ_b	Basal value of γ at low glucose	10^{-4} min^{-1}	[478]
$\hat{h}$	Maximal value of glucose-stimulated γ input rate	3.93×10^{-3} min^{-1}	[478]
${k_1}^+$	Association rate constant for the binding between granule and Ca^{2+} channels	1.447×10^{-5} min^{-1}	[478]

C_T	Constant pool of total Ca^{2+} channels	500	[486]
$k_1{}^-$	Dissociation rate constant for the binding between granule and Ca^{2+} channels	0.10375 min^{-1}	[478]
ζ	Rate constant for ρ	4 min^{-1}	[478]
ρ_b	Basal value of ρ at low glucose	0.02 min^{-1}	[478]
k_ρ	Sensitivity of ρ on the activatory action of γ	350	[478]
I_0	Amount of insulin content in a granule	1.6 amol	[487]
f_b	Fraction of responding β-cells at glucose concentration below the threshold G^*	0.05	[478]
K_f	Constant related to the effectiveness of β-cells requirement	3.43 mmol/l	[478]
N	Total number of β-cells	2.76×10^6	[488]

6.5.1 Factors responsible for reduction in glucose-stimulated insulin secretion

Global sensitivity analysis (GSA) was performed to get an initial picture of the crucial parameters responsible for reducing insulin secretion under a high glucose medium. The simulations were performed for the time interval 0-120 min. The initial value for the simulation was taken from literature [478, 485] representing the basal of the variables. We sought to identify parameters that hampered insulin secretion in T2D patients and focused only on the insulin secretion

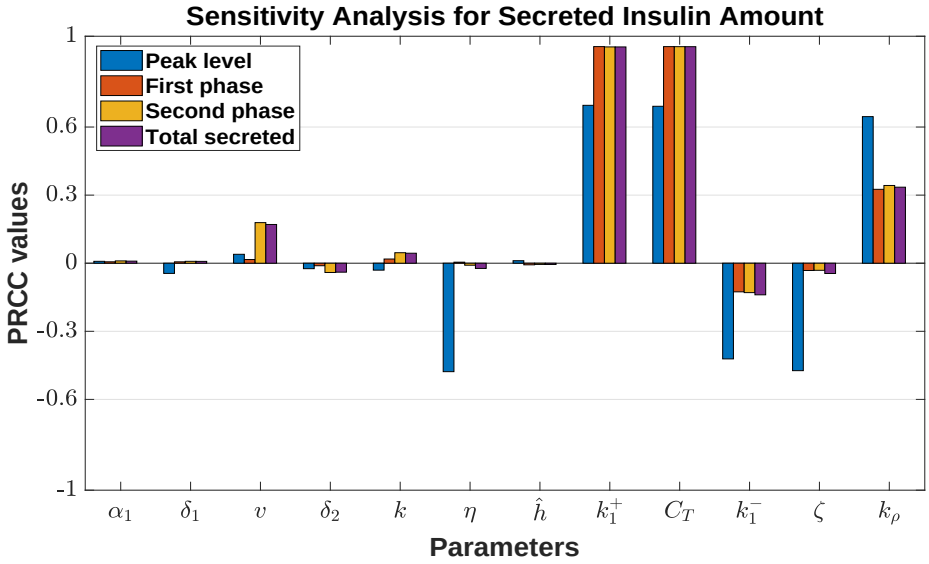

Figure 6.2: **Global sensitivity analysis for glucose-stimulated insulin secretion rate.** This was performed by using Latin Hypercube Sampling (LHS) and Partial Ranked Correlation Coefficient (PRCC) technique [438] under high glucose situation. The length of each bar represents the sensitivity of each parameter on the output (given in figure legend). Sensitive parameters were selected based on the threshold value $\pm$ 0.3 on PRCC value [439, 476].

rate. The highest value in the insulin secretion rate within this time interval was considered as the peak level. The first phase of insulin secretion was denoted by the amount of insulin secreted within 0-8 min. The second phase of insulin secretion was represented by the amount of insulin secreted within 9-120 min. The total secreted amount was calculated by taking the sum of the first and second phases of insulin secretion. The sensitivity of the parameter was captured for these four outputs (**Fig. 6.2**). Six system parameters (η, ${k_1}^+$, C_T, ${k_1}^-$, ζ and k_ρ) were obtained sensitive to insulin secretion and were associated with insulin granules trafficking and the exocytosis processes. Among them, η, ${k_1}^-$ and ζ were only sensitive to peak insulin secretion rate, and the other three were sensitive for all four outputs. To uncover the effect of these parameters on the loss of insulin secretion in glucose stimulus, we varied them 5-fold up-and-down from their default values (provided in **Table 6.1**). Down-regulation of ${k_1}^+$, C_T and k_ρ, and up-regulation of ${k_1}^-$ from their baseline values resulted in reduced first-and second-phase insulin secretion (**Fig. 6.3**). Altered values of ${k_1}^+$, ${k_1}^-$ and C_T reflect the defects in the formation of immediately releasable granules from the docked granules due to loss in the level of Ca^{2+} channels or any impairment in binding with insulin granules. Impairment in the value of k_ρ represents the defects in the activatory action of ATP on intracellular Ca^{2+} contents,

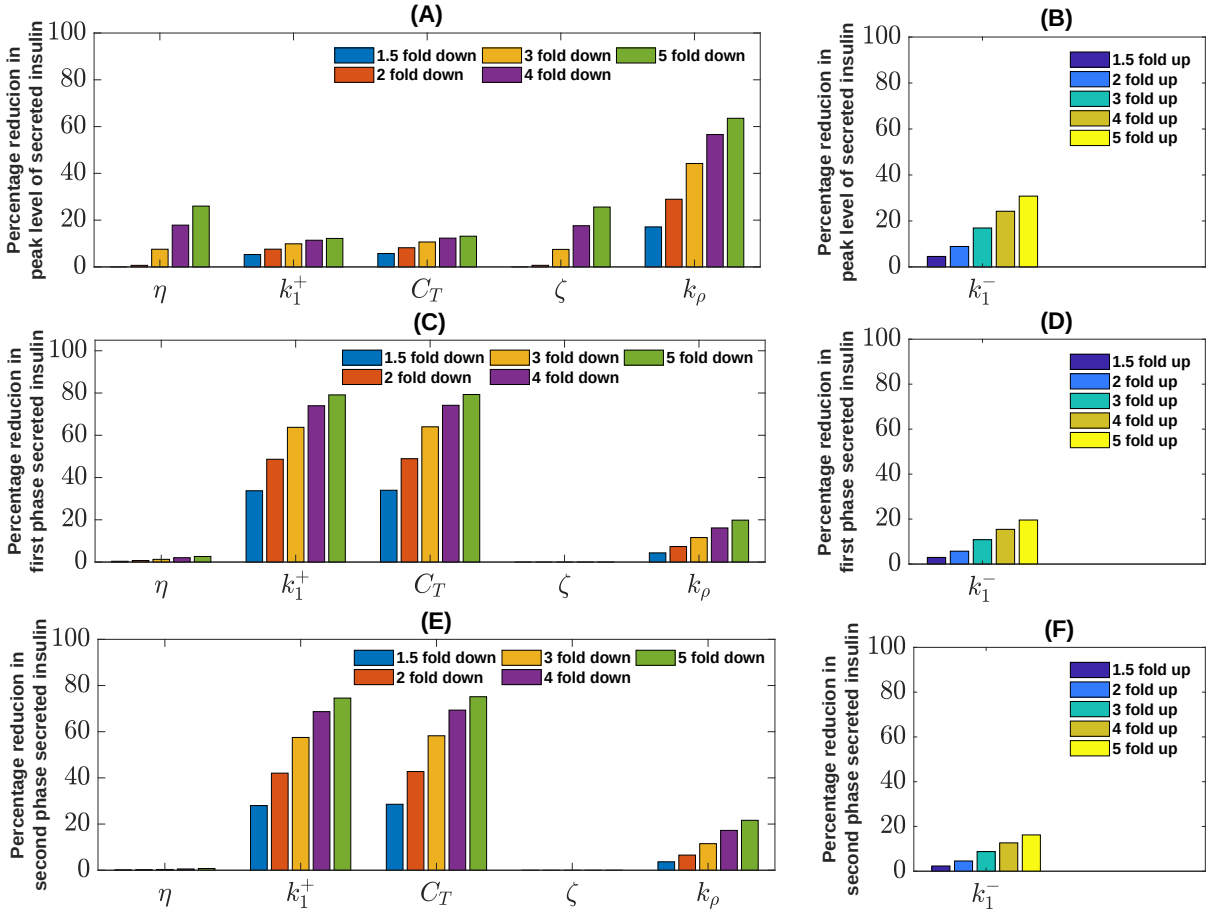

Figure 6.3: **Effect of sensitive parameters on glucose-stimulated insulin secretion rate.** We classified the findings into two categories: one is where down-regulation of the parameters reduces insulin secretion (first column), and another one is where up-regulation reduces insulin secretion (second column). Each of these parameters was varied up to 5-fold, and subsequently, the reductions in the values of peak insulin secretion rate (first row) and amount of secreted insulin in the first (second row) and second (third row) phases were observed.

which can be caused due to overactivity of the K_{ATP} channels. Additionally, we observed that reducing the value of η and ζ could only diminish the value of the peak insulin secretion rate. Any impairment of their values represents the defects in the proper rise in the ATP-to-ADP ratio and cytosolic Ca^{2+} concentration in response to the glucose stimulus, respectively.

From the analytical analysis, we observed that parameters related to the insulin synthesis process have a vital role in the existence of an axial equilibrium point (E_{B0}). Still, their effects were not observed here in the simulations within 0-120 min intervals. The most likely explanation is that their variations had no discernible impact on the level of proinsulin aggregates during these periods. We also observed that changes to the transcription and mRNA stability-associated parameters could not affect the insulin mRNA expression level within this

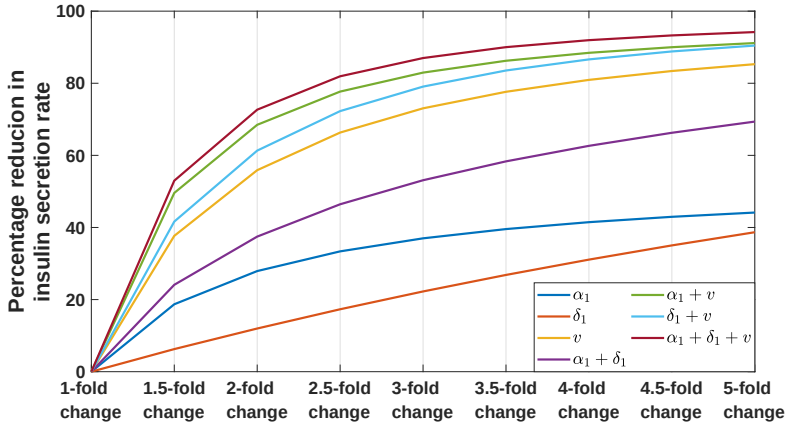

Figure 6.4: **Effect of transcription, mRNA stability and translation-associated parameters on glucose-stimulated insulin secretion rate.** To mimic the reduction in transcription and translation rate, here we decreased the value of α_1 and v, respectively, whereas the reduced mRNA stability rate was imposed by increasing the value of δ_1. All the simulations were performed for the time interval of 0-24 hrs and the effect of parameter variations was captured at the final time point.

short period. People with insulin resistance experience high glucose for longer than normal individuals after taking the food. So, an important question is whether they have any impact in the long term. It is reported that chronic hyperglycemia decreases insulin mRNA expression by reducing promoter activity and downregulating the expression of two important transcription factors of insulin [431]. So, exploring the effect of transcription, mRNA stability, and translation-associated parameters on the insulin secretion rate could help us understand the impact of reduced insulin synthesis on the pathophysiology of T2D. We varied the three parameters (α_1, δ_1, and v) individually and synergistically in the system for the time interval 0-24 hrs and captured the insulin secretion rate. It was found that reduction in α_1 and v, and increment in δ_1 causes a marked reduction in the insulin secretion rate at the final time point (**Fig. 6.4**). Among them, the impact of the reduction in v is much more than the others. This represents the reduced biosynthesis rate of proinsulin aggregates from inulin mRNA and might be caused due to defects in the translation and post-translational modification processes. Reduction in α_1 and increment in δ_1 causes reduced insulin secretion by reducing insulin mRNA level and represents the defects in the transcription and mRNA stability, respectively.

In our study, the insulin secretion rate is a function of the pool of immediately releasable pool (D_{IR}), so it is also interesting to understand the parameters responsible for the existence of the stable axial equilibrium point (E_{B0}, D_{IR}=0) in high glucose situations. It would capture

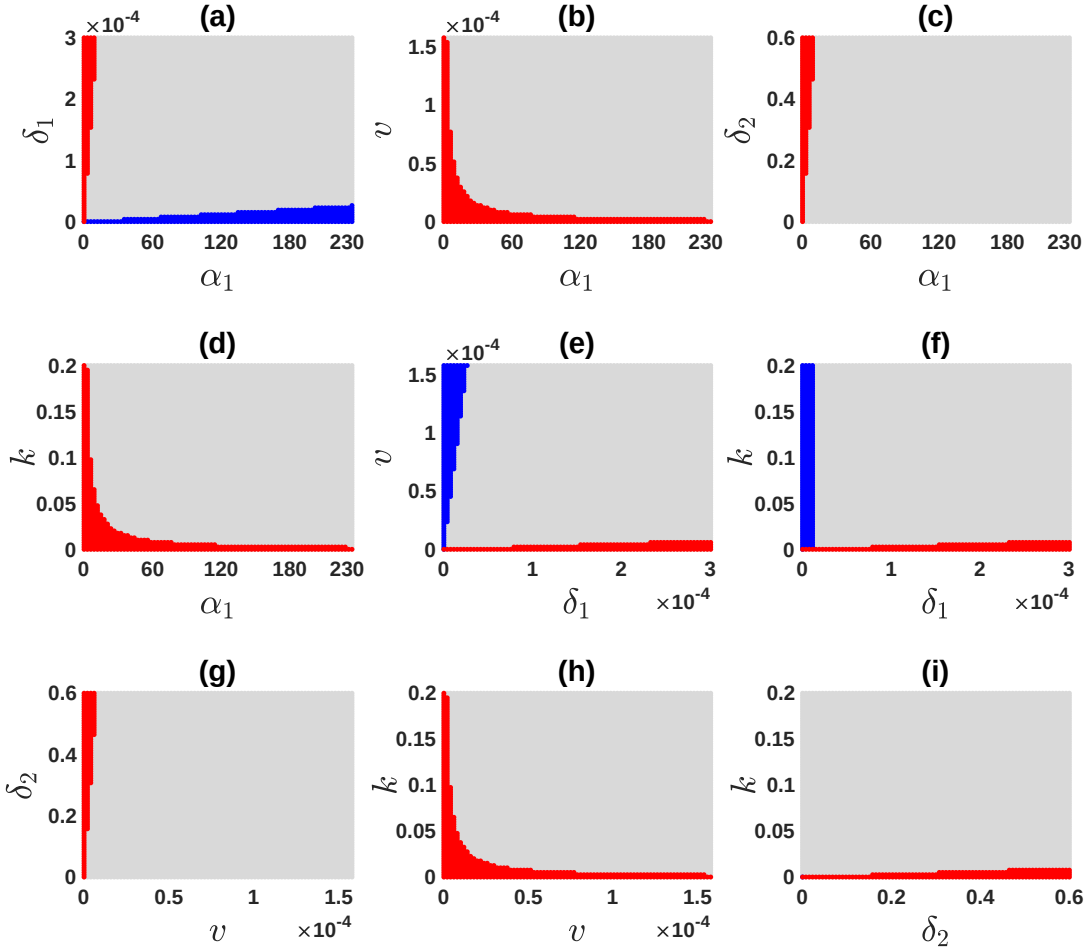

Figure 6.5: **Two-dimensional parameter space representing the nature of the equilibrium point for the system (6.1).** In the grey-colored region, the system has one stable interior equilibrium point (E^*) and one unstable axial equilibrium point (E_{B0}). In the blue-colored region, condition (ii) for the existence of E^* is not satisfied. In the red-colored region, condition (i) for the existence of E^* is not satisfied and the axial equilibrium point (E_{B0}) becomes stable.

the molecular mechanisms behind the loss of insulin secretion from β-cells under high glucose concentrations. To capture the significance of the parameters, we varied them between the range from 0 to 10-fold up. It was observed that E_{B0} would be stable if either of the three parameters α_1, v, and k become zero. These three are associated with insulin's transcription and translation processes and the formation of insulin granules. The two-dimensional parameter variation captures the possible ranges for the stability of E_{B0} (**Fig. 6.5**). We obtained two additional parameters (δ_1 and δ_2) whose imbalance with the above three parameters made the axial equilibrium point stable. However, the 2D parameter analysis shows the dominance of the former three over the later two in maintaining the stable axial point. Our analysis also highlighted that decreased values of the former three parameters and the elevated values of

the latter two could be the possible causes for the loss of insulin secretion from β-cell. It's noteworthy to note that all of these primarily reflect the defects in insulin synthesis and the formation of insulin granules.

Hence, the reduced insulin synthesis rate and defects in granule exocytosis processes cause reduced insulin secretion from β-cells. The latter has an immediate effect and can hamper first- and second-phase insulin secretion. Whereas the former lowers the insulin secretions after a long period and can cause a complete loss of insulin. We were now focused on identifying parameters that can cause elevated insulin secretion from β-cell under the low glucose condition to understand the mechanisms behind hyperinsulinemia.

6.5.2 Uncontrolled insulin secretion under low glucose

The insulinoma cell, a rare neuroendocrine pancreatic tumour cell, secretes insulin at low blood glucose [465]. So, all insulinoma patients experience hyperinsulinemic hypoglycemia [489]. Understanding the pathophysiology of insulinoma requires identifying the factors responsible for the elevated insulin secretion from β-cell under the low glucose condition. We assumed the system would always stay at the basal level (i.e., in a steady state) in low glucose concentration. The simulations focus on identifying parameters affecting the basal insulin secretion rate at low glucose settings. To get the basal insulin secretion rate, we calculated the interior equilibrium (E^*) point for each parameter set, and then equation (6.2) was used. GSA provided five system parameters (α_1, δ_1, v, δ_2 and k) sensitive to the basal insulin secretion rate (**Fig. 6.6**). Hence, we concentrated on these parameters for further exploration. Each of these parameters was varied 5-fold up-and down from their default values (provided in **Table 6.1**), and subsequently, the increment in the steady-state insulin secretion rate was observed. Up-regulation of α_1, v and k, and down-regulation of δ_1 and δ_2 resulted in elevated steady-state insulin secretion rate (**Fig. 6.7**). Interestingly, none of them are associated with the insulin granules trafficking and exocytosis processes but rather reflect the uncontrolled insulin synthesis inside the β-cell.

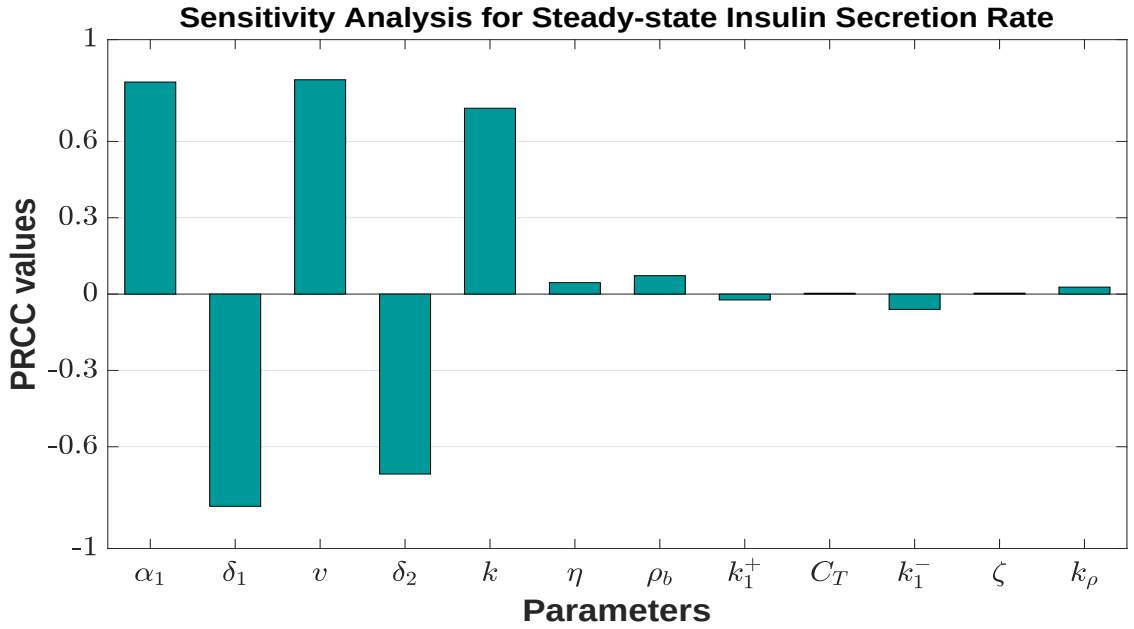

Figure 6.6: **Global sensitivity analysis for the insulin secretion rate at the steady state of the system.** This was performed by using Latin Hypercube Sampling (LHS) and Partial Ranked Correlation Coefficient (PRCC) technique [438] under low glucose situation. The length of each bar represents the sensitivity of each parameter to the value of insulin secretion rate at the interior equilibrium point (E^*). Sensitive parameters were selected based on the threshold value $\pm$ 0.3 on PRCC value [439, 476].

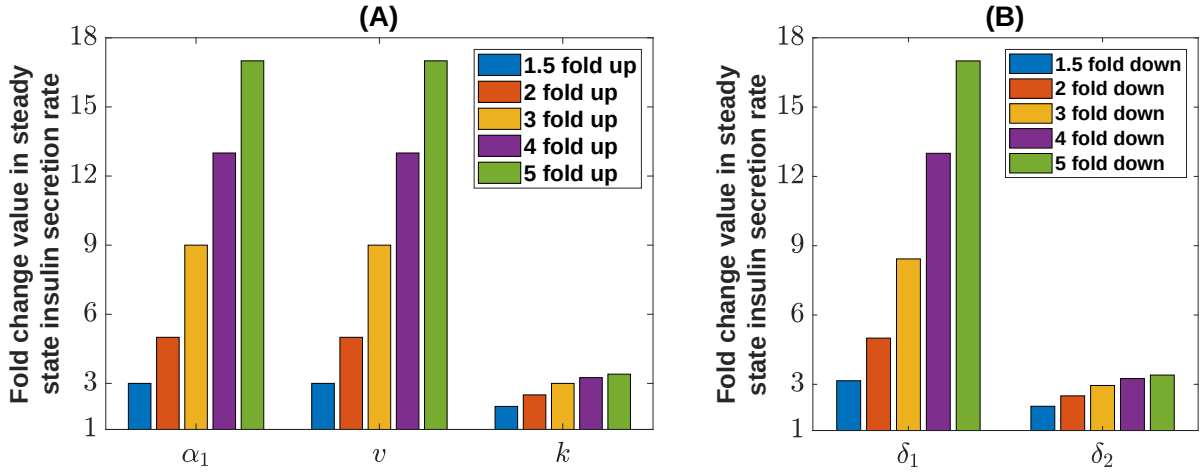

Figure 6.7: **Effect of sensitive parameters on insulin secretion rate at the low glucose concentration.** We classified the findings into two categories: one is where up-regulation of the parameters increases insulin secretion (first column), and another one is where down-regulation increases insulin secretion (second column). Each of these parameters was varied up to 5-fold, and subsequently, the increment in the insulin secretion rate was observed. Each of these parameters was varied up to 5-fold, and subsequently, the increment in the steady state insulin secretion rate was observed because we assumed that the system would stay in a steady state at low glucose concentration.

6.5.3 Insulin synthesis and exocytosis processes in managing the insulin secretion dynamics

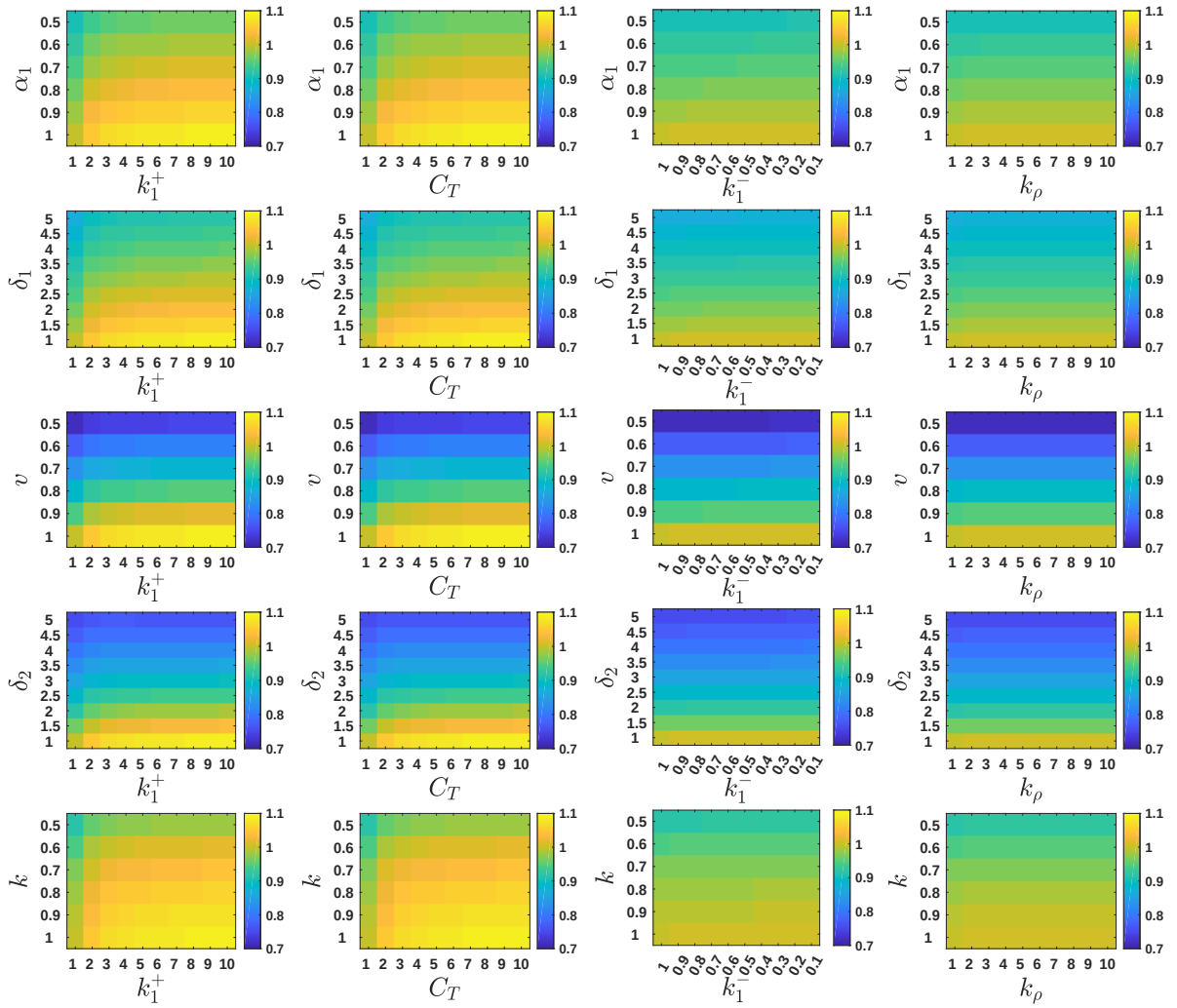

Figure 6.8: Tuning effect of the parameters related to the insulin granule trafficking and exocytosis processes in compensating insulin secretion due to decreased insulin synthesis inside the β-cell. Here the y-axis denotes the fold changes for those parameters for which the restoration was performed. In contrast, the x-axis represents the fold changes for the parameters by which the tuning was made. The color bar represents the fold change value in the total secreted insulin level compared to the default parameters for the high glucose model simulation. In all of these cases, simulations were performed for the time interval 0-24 hrs.

It is observed that the reduced insulin synthesis rate and defects in granule exocytosis processes cause reduced insulin secretion from β-cells. The latter has an immediate effect and the former act after a long period. However, it was observed that only the small perturbations in the parameters related to insulin synthesis processes were compensated by the parameters associated with insulin granule trafficking and exocytosis (**Fig. 6.8**). For example, up to 0.7-fold

changes in transcription rate (α_1), 3-fold changes in mRNA degradation rate (δ_1), and 0.6-fold changes in insulin granules formation rate (k) was fully compensated, but it requires almost 10-fold changes in tuning parameters. In contrast, the parameters related to insulin synthesis showed better restoration capability in case of reduced insulin secretion due to defective insulin granule trafficking and exocytosis (**Fig. 6.9**). Up-regulation of transcription (α_1) and translation (v) rates were found as the most effective strategies for restoring insulin secretion during impaired insulin granule trafficking and exocytosis.

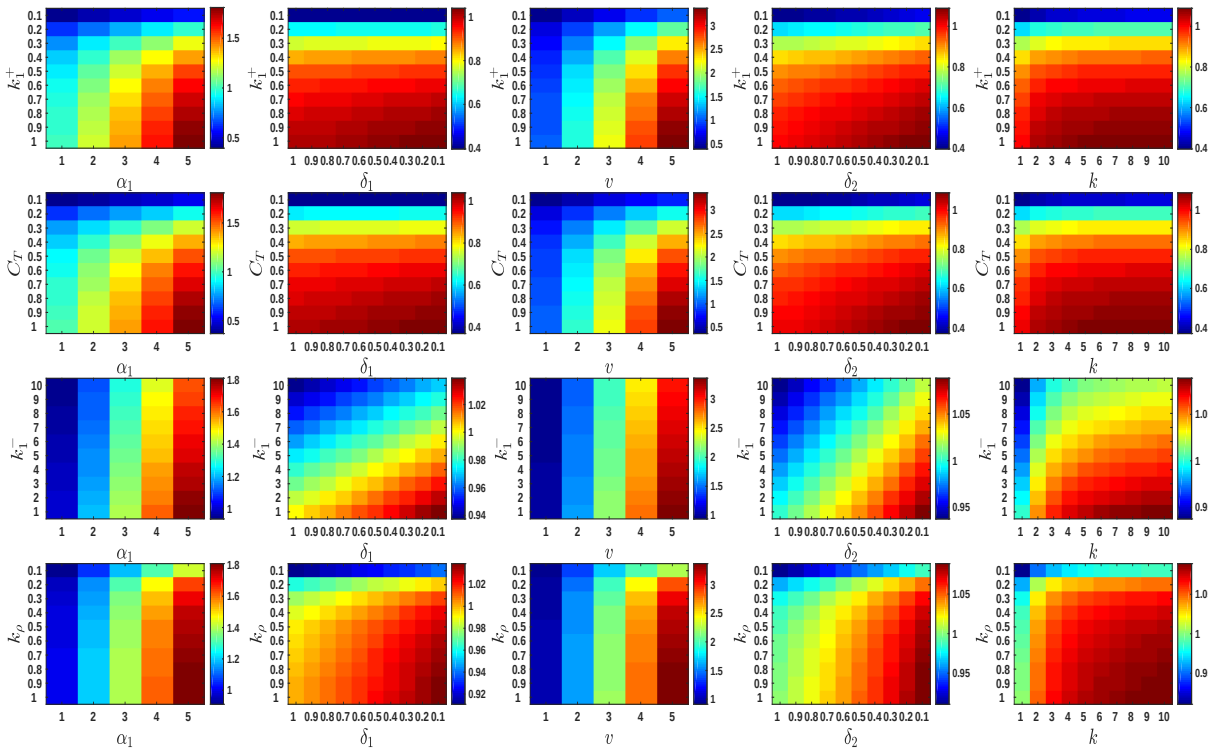

Figure 6.9: This figure depicts the tuning effect of the parameters related to insulin synthesis for reverting reduced insulin secretion due to defective insulin granule trafficking and exocytosis. Here the y-axis denotes the fold changes for those parameters for which the restoration was performed. In contrast, the x-axis represents the fold changes for the parameters by which the tuning was made. The color bar represents the fold change value in the total secreted insulin level compared to the default parameters for the high glucose model simulation. In all of these cases, simulations were performed for the time interval 0-24 hrs.

We already established that increased insulin synthesis could cause uncontrolled insulin secretion from pancreatic β-cells during the normoglycemic state. However, single parameter variation related to the insulin granules trafficking and exocytosis processes showed no effect in restoring increased basal insulin secretion from β-cells (**Fig. 6.10**).

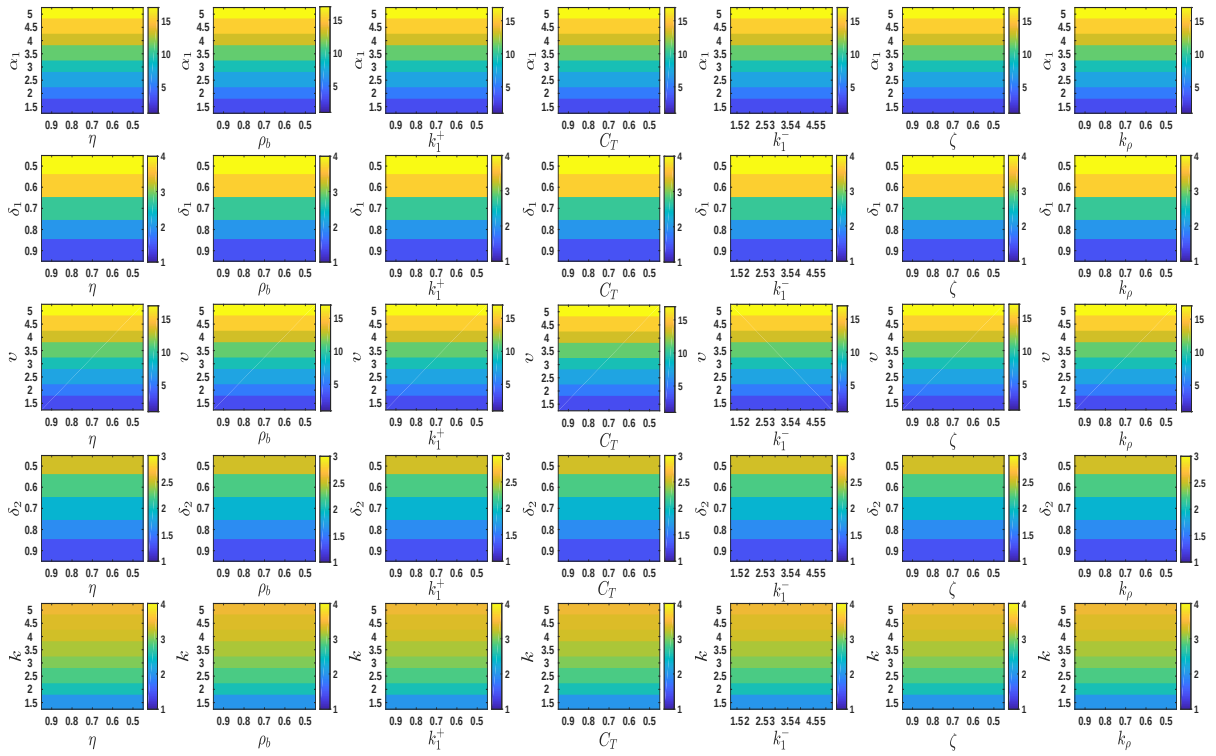

Figure 6.10: This figure depicts the tuning effect of the parameters related to insulin granule trafficking and exocytosis processes for reverting uncontrolled insulin secretion due to upregulated insulin synthesis inside the β-cell. Here the y-axis denotes the fold changes for those parameters for which the restoration was performed. In contrast, the x-axis represents the fold changes for the parameters by which the tuning was made. The color bar represents the fold change value in the steady-state insulin secretion rate compared to the default parameters for the low glucose model simulation.

6.5.4 Restoration strategies for compensating the β-cells mass

The amount of insulin released from the pancreas is mainly determined by the product of the β-cells functional mass and the insulin secreted by each cell. So, the body requires an appropriate number of insulin-secreting β-cells to maintain homeostasis. T2D is a complex metabolic disorder in which chronically increased glucose levels causes the loss of β-cell mass by promoting cell death [377, 429, 431, 432]. Hence, we focused on identifying possible restoration strategies for compensating the β-cells mass by tuning different systems parameters. Our analysis revealed that regulation of the transcription (α_1) and translation (v) have a significant impact on restoring insulin secretion (**Fig. 6.11**). Besides, δ_1, δ_2, k, ${k_1}^+$ and C_T had very minor effect.

When β-cell mass increases due to a tumor inside the pancreatic islet (like in insulinoma patients), insulin secretion also increases [490]. In this context, reducing the basal insulin

secretion rate would be beneficial to control fasting hypoglycemia. We tuned each system parameter to control the basal insulin secretion rate for different β-cell numbers. Only three parameters (α_1, v and k) were obtained as possible restoration candidates (**Fig. 6.12**). These mainly reflect the reduction of the insulin synthesis through the tuning of transcription (α_1) and translation (v) and the downregulation of insulin granules formation rate (k).

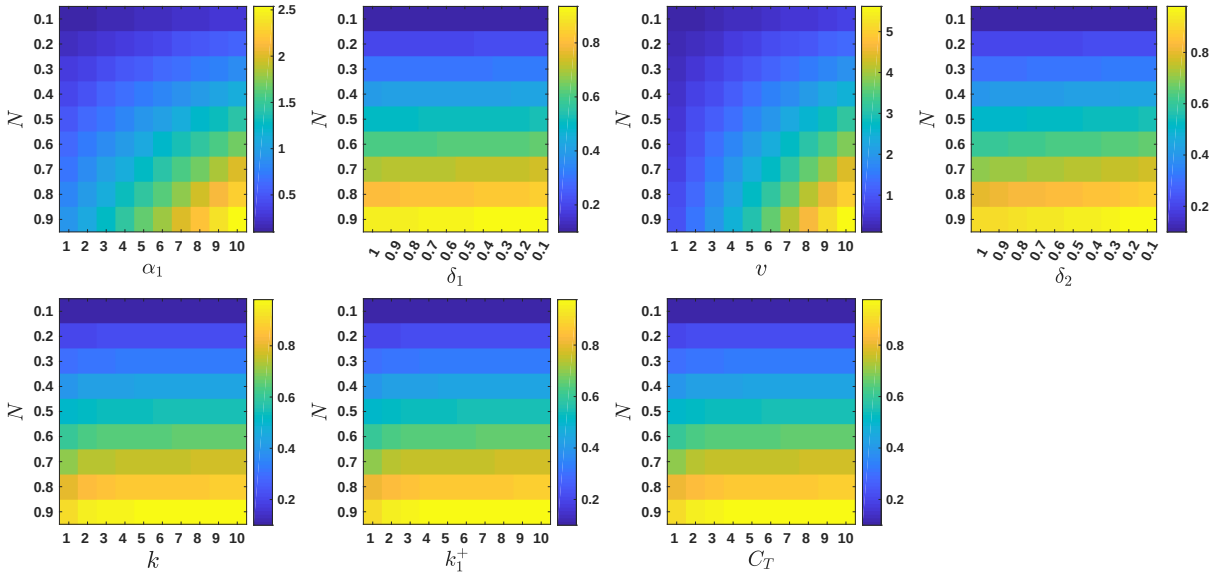

Figure 6.11: This figure depicts the tuning effect of the parameters related to insulin synthesis and secretion processes for reverting reduced insulin secretion due to loss of β-cell mass. Here the y-axis denotes the fold changes for the parameter representing the β-cell mass. In contrast, the x-axis represents the fold changes for the parameters by which the tuning was made. The color bar represents the fold change value in the total secreted insulin level compared to the default parameters for the high glucose model simulation. In all of these cases, simulations were performed for the time interval 0-24 hrs.

6.6 Discussion

Insulin is an endocrine peptide hormone secreted from pancreatic β-cells that plays an essential role in maintaining glucose homeostasis in our body. Its secretion from β-cells in response to the glucose stimulus is mainly biphasic [467–469]. Glucose also regulates insulin synthesis by controlling various processes, including the proinsulin gene transcription, mRNA stability, and the translational process [469, 472]. The glucose-insulin relationship gets affected under various pathophysiological conditions like diabetes, cancer, etc [380, 465, 491]. Numerous studies have been performed to comprehend this complex dynamical process. However, the

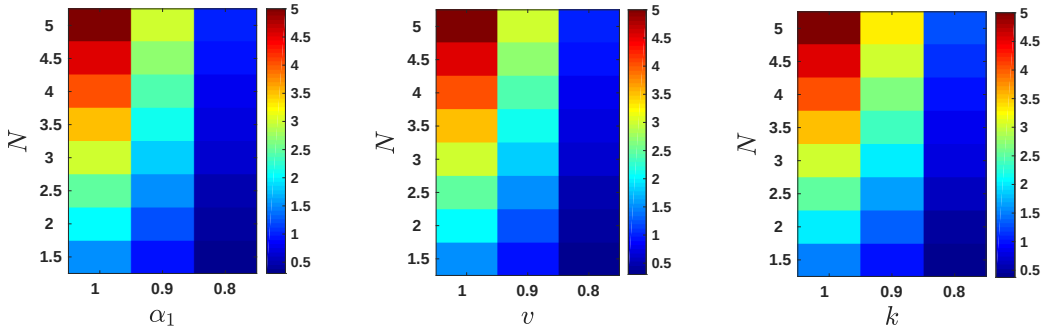

Figure 6.12: This figure depicts the tuning effect of the parameters related to insulin synthesis for controlling insulin secretion due to increased β-cell mass. Here the y-axis denotes the fold changes for the parameter representing the β-cell mass. In contrast, the x-axis represents the fold changes for the parameters by which the tuning was made. The color bar represents the fold change value in the steady-state insulin secretion rate compared to the default parameters for the low glucose model simulation.

mechanisms regulating glucose-stimulated insulin synthesis and secretion under physiological and pathophysiological conditions are not clear [464]. This motivates us to investigate the potential causes that change insulin secretion with different glucose conditions. The current study proposed and analyzed a minimal model involving insulin synthesis, biogenesis, and secretion. It identifies crucial factors whose abnormalities could lead to either Type 2 diabetes (T2D) or hyperinsulinemic hypoglycemia. Here, we included the insulin mRNA level as a variable in the model to investigate the consequences of defects in the transcription and translation processes of the insulin gene. We first studied the model analytically and identified the existence and stability conditions for the interior (E^*) and axial (E_{B0}, absence of insulin granules) equilibrium points. We found that the stability of E_{B0} depends on five parameters satisfying the inequality $kv\alpha_1 < \delta_1\delta_2$. The parameter set acquired for the numerical simulations satisfies the stability conditions for the interior steady state as well as the normal physiology of the system. We varied these parameters to obtain different conditions correlating with various pathophysiological conditions.

β-cell dysfunctioning plays a crucial role in the initial stages of T2D development and persists as the disease progresses [492]. We seek parameters that could hamper the insulin secretion rate. The parameter variation analysis identified four parameters responsible for reducing first and second-phase insulin secretion rates and two parameters responsible for the diminished value in the peak insulin secretion rate. These highlights the two major areas of in-

sulin granules trafficking and secretory processes. They are 1) defects in forming immediately releasable granules from the docked granules and 2) defects in the glucose-evoked rise in intracellular Ca^{2+} content. Our analysis suggests that immediately releasable granule formation could be hampered due to a decreased level in Ca^{2+} channels or any impairment in its binding with insulin granules. On the other hand, overactivity of the K_{ATP} channels and improper rise in the ATP-to-ADP ratio in response to the glucose stimulus could also hamper the glucose-evoked rise in intracellular Ca^{2+}. It has been observed in the literature that polymorphism of the K_{ATP} channel (E23K) could also be a risk factor for T2D [406]. It is also reported that activating mutations in Kir6.2 and sulfonylurea receptor 1 (SUR1) subunits of the K_{ATP} channel are the major causes of neonatal diabetes [406]. The above shorter time frame simulation did not capture the effect of decreased insulin synthesis rate on insulin secretion. However, the impact was observed in a longer time frame simulation, which showed that reduced insulin synthesis rates could hamper insulin secretion.

We observed that the pancreatic β-cells could become empty in insulin granules (i.e., E_{B0} becomes stable) due to combined reductions of any two processes: transcription, translation, and insulin granules formulation rates. Besides, an increased degradation rate of insulin mRNA or proinsulin pool, along with reductions in any of the above mentions three processes, could cause the same. However, the former three are more dominant over the latter two in causing loss of insulin content inside the β-cells. Literature suggests that metabolic stress due to the chronic oversupply of nutrients could lead to reduced expression or activity of critical β-cell transcription factors, including FOXO1, PDX1, NKX6.1, and MAFA [493–496]. Subsequently, some crucial end-differentiated genes, including insulin itself, were lost [497], causing depletion in insulin synthesis. So, defects in the insulin synthesis and the insulin granules formation processes might contribute to the complete loss of insulin inside the β-cells during T2D development.

The present study also focuses on identifying parameters that elevate insulin secretion from the pancreas during the normoglycemic state. The investigation highlights the specific biological processes whose impairment might cause hyperinsulinemic hypoglycemia. The insulin secretion rate is a function of several factors, including the number of granules that undergo

exocytosis, insulin content in each granule, β-cell mass, and the fraction of cells responding to the glucose stimulus. So, it is evident that an increase in their value might lead to excess insulin secretion from the pancreas. Apart from these factors, we obtained five additional system parameters that might cause abnormalities in the β-cells ability to adequately suppress insulin release in the presence of low circulating glucose. Thus, we might conclude that the up-regulation of insulin granule formation due to elevated transcription rate, increased mRNA stability, elevated translation rate, or reduced degradation rate of the proinsulin pool could cause hyperinsulinemic hypoglycemia. Although the insulin secretion rate depends on the number of granules undergoing exocytosis, we didn't find any impact of the parameters associated with the insulin granules trafficking and exocytosis processes on causing increased basal insulin secretion rate. Instead, our results suggest that the uncontrolled insulin synthesis inside the β-cell or the increased β-cell mass could be the major reasons for fasting hypoglycemia in insulinoma patients.

Our analyses revealed that alterations in the insulin synthesis and granule formation processes are difficult to manage by tuning parameters related to granule trafficking and exocytosis. Although these parameters could restore impaired insulin secretion due to a slight reduction in insulin synthesis, it requires almost 10-fold perturbation. Even beyond a certain level, increasing the rate of granule exocytosis cannot compensate for the decreased insulin synthesis. It also seems reasonable, as any defects in the insulin synthesis process, either by transcription or translation, ultimately affect the flux from the proinsulin pool to the immediately releasable granules pool. Subsequently, the exocytosis rate might get hampered due to the loss of insulin granules inside the β-cell. Hence, only the regulation of granules trafficking and exocytosis processes might fail to compensate for the impaired insulin synthesis. On the other hand, the accelerating insulin synthesis might restore the decreased insulin secretion driven by defective insulin granule trafficking and exocytosis processes. It can also potentially restore insulin secretion from the pancreas in the case of significant loss in β-cell mass. Thus, rather than only targeting the insulin secretion process, we need to target insulin synthesis and secretion both in managing T2D. Recently, several GLP-1 receptor agonists have been approved in the United States for the treatment of T2D, which have beneficial effects on both insulin synthesis

and insulin secretion [459, 460]. These increase insulin synthesis by targeting the transcription of insulin. However, we found that transcriptional regulation also has good restoration capabilities; hence, it might give new directions toward T2D management. In the case of insulinoma patients, our analysis suggests that targeting insulin synthesis by reducing transcription or translation could become a potential therapeutic strategy for controlling hyperinsulinemic hypoglycemia. This will reduce the insulin secretion from β-cells and also have the potential to compensate for the increased β-cell proliferation, as observed in insulinoma tumours.

In conclusion, the present study proposed a minimal model for insulin synthesis and secretion of insulin granules to understand the pathophysiology of T2D and hyperinsulinemic hypoglycemia. Defects in the insulin granule trafficking and exocytosis processes were observed to be one of the main reasons for β-cell dysfunction in T2D. The long-term effect of abnormal insulin synthesis could hamper insulin secretion and make the scenario more critical, causing complete insulin loss inside the β-cells. Perturbations in the insulin granules trafficking and exocytosis processes do not change the uncontrolled insulin secretion in a normoglycemic state. Instead, upregulated insulin synthesis or the increased β-cell proliferation were two major reasons for fasting hypoglycemia in insulinoma patients. This study also hypothesized that targeting insulin synthesis through the regulation of transcription and translation might become a potential therapeutic strategy and hence needs further exploration.

7

Conclusions and future directions

7.1 Conclusions

An abnormal metabolic state is the primary cause or consequence of various human diseases, like cancer, diabetes, obesity, neurological diseases, cardiovascular disorders, etc. Therefore, exploring metabolic alterations in disease conditions is necessary to comprehend the underlying mechanism behind disease development and progression. In parallel, it also offers a tremendous opportunity to identify potential drug targets and design new therapeutic strategies. Due to the complexity and high dimensionality of human metabolism, mathematical modelling has been extensively used to study the metabolic alterations in human diseases. However, there still exists a lacuna of metabolic perturbations in several conditions, such as diabetes, cancer, NAFLD, cardiovascular disorders, etc.

The present thesis aims to study the role of metabolites and associated pathways in disease progression using mathematical models and use it to develop therapeutic strategies. Here, we have used two types of mathematical models: genome-scale metabolic model (GSMM) and ordinary differential equation-based small-scale kinetic model. We predicted the metabolic-flux state of pancreatic β-cells for ten control and ten type 2 diabetes (T2D) subjects by integrating the gene expression data on a generic human GSMM. Analysis of the predicted flux state revealed that impaired β-cell metabolism affects ATP production, activates stress-activated signalling pathways, and potentiates diabetes and associated cardiovascular complications. It provides a global view of the metabolic alterations in β-cell during diabetes, which has clinical implications. We captured twenty-seven relevant transcription factors associated with these metabolic changes in diabetes and identified seven secreted metabolites from β-cell associated with cardiovascular disease (CVD) pathogenesis. In addition to exploring metabolic alteration, GSMM can be applied to identify critical regulatory points from the metabolic network through *in silico* knockout approaches. We performed single-gene knockout studies on existing GSMMs of the NCI-60 cell-lines obtained from nine tissue types. The metabolic genes responsible for the growth of cancerous cells were identified, and their possible growth reduction mechanisms were explored. We obtained 13 metabolic genes whose knockout reduced the proliferation rate of all cancer models but were inactive across all nine normal cell models. The growth inhibitory effect of two of these genes (SOAT1 and CYTB) was experimentally validated in four cancer cell-lines of the NCI-60 database. Although the comparison of gene ranking results with existing shRNA screening data was not satisfactory for most of the cell-lines, it played a significant role in deciding the activity of the drug against cell proliferation, whereas multiple gene knockout analysis gave better correlation results. Again, the combination of these two applications of GSMM, i.e., identifying metabolic alterations and regulatory points through *in silico* gene knockout, could give us the potential drug targets that might revert the altered metabolic state from disease to a healthy condition. The combination of these two approaches was used to identify potential targets for nonalcoholic steatohepatitis (NASH). We elucidated the possible mechanism of action of these identified targets using GSMM. Our strategy of interconnecting the metabolic modelling and protein-protein interaction network

analysis identified three potential targets for NASH. These targets exert their effects at the gene and metabolic levels and might reverse disease-associated molecular signatures. Inhibition of these identified targets could attenuate hepatic steatosis by promoting higher flux rates for the altered reactions involved in fatty acid activation and mitochondrial beta-oxidation pathways. Although these proposed methodologies using GSMM provide a new perspective on addressing human diseases, it still requires small-scale kinetic models to capture the underlying mechanism associated with the metabolic alterations in disease conditions. Impaired glucose-stimulated insulin secretion (GSIS) in β-cell is one of the major causes of developing T2D in the presence of insulin resistance (IR). A global picture of metabolic alterations in β-cell under T2D was captured by integrating gene expression data on human GSMM. It was observed that metabolic alterations in β-cell could lead to a decline in ATP synthesis, resulting in decreased insulin secretion. By proposing and analyzing a six-dimensional kinetic model on the GSIS process, we identified the crucial factors whose impairment can either lead to hyperglycemia or hypoglycemia. Our analysis uncovers the potential strategies for preventing the progression of T2D during these alterations. The probable limitations of the current anti-diabetic drugs contributing to secondary failure were discussed. Finally, we have proposed another seven-dimensional small-kinetic model for insulin synthesis and secretion of insulin granules to decipher the in-depth understanding of the pathophysiology of T2D and hyperinsulinemic hypoglycemia. The model analysis revealed that the defects in the insulin granule trafficking and exocytosis processes hamper first- and second-phase insulin secretion and might be one of the main reasons for β-cell dysfunction in T2D. The long-term effect of abnormal insulin synthesis could hamper insulin secretion and make the scenario more critical, causing complete insulin loss inside the β-cells. Perturbations in the insulin granules trafficking and exocytosis processes do not change the uncontrolled insulin secretion in a normoglycemic state. Instead, upregulated insulin synthesis or the increased β-cell proliferation were two major reasons for fasting hypoglycemia in insulinoma patients. Our study also suggests that targeting insulin synthesis through the regulation of transcription and translation might become a potential therapeutic strategy for controlling impaired insulin secretion.

Overall, the work presented in this thesis explores the application of GSMMs and small-

scale kinetic models in studying the role of metabolites and associated pathways in disease progression. By applying GSMM, we captured the alterations in the metabolic-flux state in human diseases and identified potential drug targets that could reverse the altered state towards a healthy state. Using the small-scale kinetic models, we studied the underlying mechanism behind impaired insulin secretion from β-cell and explored the potential strategies for preventing the aberrant insulin secretion.

7.2 Future directions

The work presented in the thesis can be extended from various aspects of mathematical modelling. We have explored the metabolic-flux state in pancreatic β-cell by integrating the transcriptomics data into the generic human GSMM. It is a well-known fact that the flux state of the cell depends on the proteome and metabolome profiles [189, 498]. Therefore, more details data, such as proteomics and metabolomics, can be used to develop a β-cell-specific GSMM. The primary function of β-cell is to adequately secrete insulin in response to elevated blood glucose during the postprandial state. Therefore, it is essential to establish a proper cellular objective function for the β-cell that can represent insulin secretion for obtaining a more accurate flux state. Here, we have observed a cross-link between the diabetic-associated metabolic alterations in β-cell and cardiovascular disease. So to better understand the pathogenesis of cardiovascular complications in type 2 diabetic (T2D) patients, we need to analyse a multi-tissue metabolic model.

In our gene knockout study using GSMM, we identified 13 potential targets against cancer, however the overall correlation with the experimental data is still unsatisfactory. Therefore the gene knockout strategies can be revisited to decipher the proper reason for obtaining the negative results. In this context, new *in silico* gene knockout algorithms can be developed to mitigate the problems.

The targets identified in the present thesis through GSMM can further be evaluated through experiments in collaboration with biologists. Similar attempts have also been made in **Chapter 3** to validate our hypothesis. We observed that the inhibition of SOAT1 and CYTB reduces the

growth rate of 4 cancer cell lines. These establish that the identified genes have the potential to become successful drug targets and hence need further evaluation.

The identified potential targets against NASH using combined strategy of GSMM, exhibits the reversibility of metabolic alterations in only hepatocytes. However, lipid homeostasis in our body can be hampered due to metabolic alterations in other tissues like adipose tissue and skeletal muscle. So, it is necessary to investigate whole-body lipid metabolism through a mathematical model and identify the potential factors that can cause lipid accumulation in the liver. These would enhance our understanding of the molecular mechanisms behind NAFLD development. It will also help to propose therapeutic strategies for controlling NAFLD progression. The whole-body model can be used to investigate the effect of insulin resistance (IR) on dyslipidemia, which would enhance our experience of the molecular mechanisms behind the various complications related to obesity or T2D, like NAFLD, cardiovascular diseases, etc. Therefore, the whole-body model can also establish the link between T2D and NAFLD.

The present thesis also proposed a small-scale kinetic model for insulin synthesis and the biogenesis and secretion of insulin granules processes. This model can also be used to construct a more realistic whole-body multi-level model for glucose homeostasis for better capturing the physiological events that occur after a meal. This proposed model can also be modified by considering the β-cell mass as a variable in this system to capture a clear picture of the various stages of T2D.

References

[1] L Nealson David, L Nealson David, and M Cox Michael. *Lehinger, Principles of Biochemistry*. WH Freeman, 2008.

[2] Ayesha Judge and Michael S. Dodd. Metabolism. *Essays in Biochemistry*, 64(4):607–647, 08 2020.

[3] Chao Lu and Craig B Thompson. Metabolic regulation of epigenetics. *Cell metabolism*, 16(1):9–17, 2012.

[4] Kathryn E Wellen and Craig B Thompson. A two-way street: reciprocal regulation of metabolism and signalling. *Nature reviews Molecular cell biology*, 13(4):270–276, 2012.

[5] Stanley Dagley, Donald E Nicholson, et al. *An introduction to metabolic pathways.* Blackwell Scientific Publications, Ltd., Oxford, 1970.

[6] Richard A Harvey and Denise R Ferrier. *Biochemistry*. Lippincott Williams & Wilkins, 2011.

[7] D Voet, J Voet, and C Pratt. Fundamentals of biochemistry: Life at molecular level (4th edit), 2012.

[8] Minoru Kanehisa and Susumu Goto. Kegg: kyoto encyclopedia of genes and genomes. *Nucleic acids research*, 28(1):27–30, 2000.

[9] Abu Shadi Al-Roubi. Ibn al-nafis as a philosopher. In *Symposium on Ibn al-Nafis*, 1982.

[10] Garabed Eknoyan. Santorio sanctorius (1561–1636)–founding father of metabolic balance studies. *American journal of nephrology*, 19(2):226–233, 1999.

[11] Henry Smith Williams. *A History of science v. 3*, volume 3. Harper, 1904.

[12] Keith L Manchester. Louis pasteur (1822–1895)—chance and the prepared mind. *Trends in biotechnology*, 13(12):511–515, 1995.

[13] E Kinne-Saffran and RKH Kinne. Vitalism and synthesis of urea. *American journal of nephrology*, 19(2):290–294, 1999.

[14] Hans Kornberg. Krebs and his trinity of cycles. *Nature Reviews Molecular Cell Biology*, 1(3):225–228, 2000.

[15] Chapter 1 definition and classification of lipids. volume 3 of *Laboratory Techniques in Biochemistry and Molecular Biology*, pages 279–329. Elsevier, 1972.

[16] Martin Kohlmeier. *Nutrient metabolism: structures, functions, and genes*. Academic Press, 2015.

[17] Jianhua Xiong. A 'nobel'look at metabolism. *Trends in Endocrinology & Metabolism*, 29(12):809–813, 2018.

[18] Sandra Placzek, Ida Schomburg, Antje Chang, Lisa Jeske, Marcus Ulbrich, Jana Tillack, and Dietmar Schomburg. Brenda in 2017: new perspectives and new tools in brenda. *Nucleic acids research*, page gkw952, 2016.

[19] Peter D Karp, Richard Billington, Ron Caspi, Carol A Fulcher, Mario Latendresse, Anamika Kothari, Ingrid M Keseler, Markus Krummenacker, Peter E Midford, Quang Ong, et al. The biocyc collection of microbial genomes and metabolic pathways. *Briefings in bioinformatics*, 20(4):1085–1093, 2019.

[20] Ron Caspi, Tomer Altman, Richard Billington, Kate Dreher, Hartmut Foerster, Carol A Fulcher, Timothy A Holland, Ingrid M Keseler, Anamika Kothari, Aya Kubo, et al. The metacyc database of metabolic pathways and enzymes and the biocyc collection of pathway/genome databases. *Nucleic acids research*, 42(D1):D459–D471, 2014.

[21] Bijay Jassal, Lisa Matthews, Guilherme Viteri, Chuqiao Gong, Pascual Lorente, Antonio Fabregat, Konstantinos Sidiropoulos, Justin Cook, Marc Gillespie, Robin Haw, et al. The reactome pathway knowledgebase. *Nucleic acids research*, 48(D1):D498–D503, 2020.

[22] Ralph J DeBerardinis and Craig B Thompson. Cellular metabolism and disease: what do metabolic outliers teach us? *Cell*, 148(6):1132–1144, 2012.

[23] Elaine Holmes, Ian D Wilson, and Jeremy K Nicholson. Metabolic phenotyping in health and disease. *Cell*, 134(5):714–717, 2008.

[24] M Koffas, C Roberge, K Lee, and G Stephanopoulos. Metabolic engineering. *Annual Review of Biomedical Engineering*, 1(1):535–557, 1999.

[25] Yu Matsuoka and Kazuyuki Shimizu. Importance of understanding the main metabolic regulation in response to the specific pathway mutation for metabolic engineering of escherichia coli. *Computational and Structural Biotechnology Journal*, 3(4):e201210018, 2012.

[26] Jay D Keasling. Manufacturing molecules through metabolic engineering. *Science*, 330(6009):1355–1358, 2010.

[27] Ram Kulkarni. Metabolic engineering. *Resonance*, 21(3):233–237, 2016.

[28] Kai Mi, Yanan Jiang, Jiaxin Chen, Dongxu Lv, Zhipeng Qian, Hui Sun, and Desi Shang. Construction and analysis of human diseases and metabolites network. *Frontiers in Bioengineering and Biotechnology*, 8:398, 2020.

[29] Douglas Hanahan and Robert A Weinberg. Hallmarks of cancer: the next generation. *cell*, 144(5):646–674, 2011.

[30] Patrick S Ward and Craig B Thompson. Metabolic reprogramming: a cancer hallmark even warburg did not anticipate. *Cancer cell*, 21(3):297–308, 2012.

[31] M Anello, R Lupi, D Spampinato, S Piro, M Masini, Ugo Boggi, Stefano Del Prato, AM Rabuazzo, F Purrello, and Piero Marchetti. Functional and morphological alterations of mitochondria in pancreatic beta cells from type 2 diabetic patients. *Diabetologia*, 48(2):282–289, 2005.

[32] Åsa Segerstolpe, Athanasia Palasantza, Pernilla Eliasson, Eva-Marie Andersson, Anne-Christine Andréasson, Xiaoyan Sun, Simone Picelli, Alan Sabirsh, Maryam Clausen, Magnus K Bjursell, et al. Single-cell transcriptome profiling of human pancreatic islets in health and type 2 diabetes. *Cell Metabolism*, 24(4):593–607, 2016.

[33] Cher-Rin Chong, Kieran Clarke, and Eylem Levelt. Metabolic remodelling in diabetic cardiomyopathy. *Cardiovascular Research*, 113(4):422–430, 2017.

[34] Joel T Haas, Sven Francque, and Bart Staels. Pathophysiology and mechanisms of non-alcoholic fatty liver disease. *Annual review of physiology*, 78:181–205, 2016.

[35] Karl Herholz, Cathleen Haense, Alex Gerhard, Matthew Jones, José Anton-Rodriguez, Shailendra Segobin, Julie S Snowden, Jennifer C Thompson, and Christopher Kobylecki. Metabolic regional and network changes in alzheimer's disease subtypes. *Journal of Cerebral Blood Flow & Metabolism*, 38(10):1796–1806, 2018.

[36] Livnat Jerby and Eytan Ruppin. Predicting drug targets and biomarkers of cancer via genome-scale metabolic modeling. *Clinical Cancer Research*, 18(20):5572–5584, 2012.

[37] Jason W Locasale and Lewis C Cantley. Metabolic flux and the regulation of mammalian cell growth. *Cell metabolism*, 14(4):443–451, 2011.

[38] Elizabeth Haythorne, Maria Rohm, Martijn van de Bunt, Melissa F Brereton, Andrei I Tarasov, Thomas S Blacker, Gregor Sachse, Mariana Silva dos Santos, Raul Terron Exposito, Simon Davis, et al. Diabetes causes marked inhibition of mitochondrial metabolism in pancreatic β-cells. *Nature Communications*, 10(1):1–17, 2019.

[39] Guy Las, Marcus F Oliveira, and Orian S Shirihai. Emerging roles of β-cell mitochondria in type-2-diabetes. *Molecular Aspects of Medicine*, 71:100843, 2020.

[40] Naoya Murao, Norihide Yokoi, Harumi Takahashi, Tomohide Hayami, Yasuhiro Minami, and Susumu Seino. Increased glycolysis affects β-cell function and identity in aging and diabetes. *Molecular metabolism*, 55:101414, 2022.

[41] Mi Lai, Ying Liu, Gabriele V Ronnett, Anne Wu, Brian J Cox, Feihan F Dai, Hannes L Röst, Erica P Gunderson, and Michael B Wheeler. Amino acid and lipid metabolism in post-gestational diabetes and progression to type 2 diabetes: A metabolic profiling study. *PLoS Medicine*, 17(5):e1003112, 2020.

[42] P Newsholme, K Bender, A Kiely, and L Brennan. Amino acid metabolism, insulin secretion and diabetes. *Biochemical Society Transactions*, 35(5):1180–1186, 2007.

[43] Maria Lytrivi, Anne-Laure Castell, Vincent Poitout, and Miriam Cnop. Recent insights into mechanisms of β-cell lipo-and glucolipotoxicity in type 2 diabetes. *Journal of molecular biology*, 432(5):1514–1534, 2020.

[44] Yoon S Oh, Gong D Bae, Dong J Baek, Eun-Young Park, and Hee-Sook Jun. Fatty acid-induced lipotoxicity in pancreatic beta-cells during development of type 2 diabetes. *Frontiers in Endocrinology*, 9:384, 2018.

[45] Hai Ying Fu, Mikio Mukai, Nobuhisa Awata, Yasushi Sakata, Masatsugu Hori, and Tetsuo Minamino. Protein quality control dysfunction in cardiovascular complications induced by anti-cancer drugs. *Cardiovascular drugs and therapy*, 31(1):109–117, 2017.

[46] Michelle Whirl-Carrillo, Ellen M McDonagh, JM Hebert, Li Gong, K Sangkuhl, CF Thorn, Russ B Altman, and Teri E Klein. Pharmacogenomics knowledge for personalized medicine. *Clinical Pharmacology & Therapeutics*, 92(4):414–417, 2012.

[47] Henrica MJ Werner, Gordon B Mills, and Prahlad T Ram. Cancer systems biology: a peek into the future of patient care? *Nature reviews Clinical oncology*, 11(3):167–176, 2014.

[48] Keren Yizhak, Barbara Chaneton, Eyal Gottlieb, and Eytan Ruppin. Modeling cancer metabolism on a genome scale. *Molecular systems biology*, 11(6):817, 2015.

[49] Scott L Friedman, Brent A Neuschwander-Tetri, Mary Rinella, and Arun J Sanyal. Mechanisms of nafld development and therapeutic strategies. *Nature medicine*, 24(7):908–922, 2018.

[50] Uwe Sauer. Metabolic networks in motion: 13c-based flux analysis. *Molecular systems biology*, 2(1):62, 2006.

[51] David C Swinney and Jason Anthony. How were new medicines discovered? *Nature reviews Drug discovery*, 10(7):507, 2011.

[52] Andrew L Hopkins. Network pharmacology: the next paradigm in drug discovery. *Nature chemical biology*, 4(11):682, 2008.

[53] Brian P Zambrowicz, C Alexander Turner, and Arthur T Sands. Predicting drug efficacy: knockouts model pipeline drugs of the pharmaceutical industry. *Current opinion in pharmacology*, 3(5):563–570, 2003.

[54] Brian P Zambrowicz and Arthur T Sands. Modeling drug action in the mouse with knockouts and rna interference. *Drug Discovery Today: TARGETS*, 3(5):198–207, 2004.

[55] Kanu Wahi and Jeff Holst. Asct2: a potential cancer drug target. *Expert opinion on therapeutic targets*, pages 1–4, 2019.

[56] Xiaochun Chen, Curtis R Chong, Lirong Shi, Tadashi Yoshimoto, David J Sullivan, and Jun O Liu. Inhibitors of plasmodium falciparum methionine aminopeptidase 1b possess antimalarial activity. *Proceedings of the National Academy of Sciences*, 103(39):14548–14553, 2006.

[57] Curtis R Chong, Xiaochun Chen, Lirong Shi, Jun O Liu, and David J Sullivan Jr. A clinical drug library screen identifies astemizole as an antimalarial agent. *Nature chemical biology*, 2(8):415, 2006.

[58] Wei Zheng, Natasha Thorne, and John C McKew. Phenotypic screens as a renewed approach for drug discovery. *Drug discovery today*, 18(21-22):1067–1073, 2013.

[59] Vineela Parvathaneni, Nishant S Kulkarni, Aaron Muth, and Vivek Gupta. Drug repurposing: a promising tool to accelerate the drug discovery process. *Drug discovery today*, 2019.

[60] Anja Karlstädt, Daniela Fliegner, Georgios Kararigas, Hugo Sanchez Ruderisch, Vera Regitz-Zagrosek, and Hermann-Georg Holzhütter. Cardionet: a human metabolic network suited for the study of cardiomyocyte metabolism. *BMC Systems Biology*, 6(1):1–20, 2012.

[61] STR Moolamalla and PK Vinod. Genome-scale metabolic modelling predicts biomarkers and therapeutic targets for neuropsychiatric disorders. *Computers in Biology and Medicine*, 125:103994, 2020.

[62] Adil Mardinoglu, Rasmus Agren, Caroline Kampf, Anna Asplund, Mathias Uhlen, and Jens Nielsen. Genome-scale metabolic modelling of hepatocytes reveals serine deficiency in patients with non-alcoholic fatty liver disease. *Nature Communications*, 5(1):1–11, 2014.

[63] Ori Folger, Livnat Jerby, Christian Frezza, Eyal Gottlieb, Eytan Ruppin, and Tomer Shlomi. Predicting selective drug targets in cancer through metabolic networks. *Molecular systems biology*, 7(1):501, 2011.

[64] Tomer Shlomi, Moran N Cabili, and Eytan Ruppin. Predicting metabolic biomarkers of human inborn errors of metabolism. *Molecular Systems Biology*, 5(1):263, 2009.

[65] Keren Yizhak, Sylvia E Le Dévédec, Vasiliki Maria Rogkoti, Franziska Baenke, Vincent C de Boer, Christian Frezza, Almut Schulze, Bob van de Water, and Eytan Ruppin. A computational study of the warburg effect identifies metabolic targets inhibiting cancer migration. *Molecular systems biology*, 10(8):744, 2014.

[66] Rasmus Agren, Adil Mardinoglu, Anna Asplund, Caroline Kampf, Mathias Uhlen, and Jens Nielsen. Identification of anticancer drugs for hepatocellular carcinoma through personalized genome-scale metabolic modeling. *Molecular systems biology*, 10(3):721, 2014.

[67] Adil Mardinoglu, Elias Bjornson, Cheng Zhang, Martina Klevstig, Sanni Söderlund, Marcus Ståhlman, Martin Adiels, Antti Hakkarainen, Nina Lundbom, Murat Kilicarslan, et al. Personal model-assisted identification of nad+ and glutathione metabolism as intervention target in nafld. *Molecular Systems Biology*, 13(3):916, 2017.

[68] Beste Turanli, Cheng Zhang, Woonghee Kim, Rui Benfeitas, Mathias Uhlen, Kazim Yalcin Arga, and Adil Mardinoglu. Discovery of therapeutic agents for prostate cancer using genome-scale metabolic modeling and drug repositioning. *EBioMedicine*, 42:386–396, 2019.

[69] Vytautas Raškevičius, Valeryia Mikalayeva, Ieva Antanavičiūtė, Ieva Ceslevičienė, Vytenis Arvydas Skeberdis, Visvaldas Kairys, and Sergio Bordel. Genome scale metabolic models as tools for drug design and personalized medicine. *PloS one*, 13(1):e0190636, 2018.

[70] Peter Kohl, Denis Noble, Raimond L Winslow, and Peter J Hunter. Computational modelling of biological systems: tools and visions. *Philosophical Transactions of the Royal Society of London. Series A: Mathematical, Physical and Engineering Sciences*, 358(1766):579–610, 2000.

[71] Edda Klipp, Wolfram Liebermeister, Christoph Wierling, and Axel Kowald. *Systems biology: a textbook*. John Wiley & Sons, 2016.

[72] Nicolai N Vorobiev. *Fibonacci numbers*. Springer Science & Business Media, 2002.

[73] Daniel Bernoulli and Sally Blower. An attempt at a new analysis of the mortality caused by smallpox and of the advantages of inoculation to prevent it. *Reviews in medical virology*, 14(5):275, 2004.

[74] Thomas Robert Malthus, Donald Winch, and Patricia James. *Malthus:'An Essay on the Principle of Population'*. Cambridge university press, 1992.

[75] Jan Salomon Cramer. The origins of logistic regression. 2002.

[76] Leonor Michaelis, Maud L Menten, et al. Die kinetik der invertinwirkung. *Biochem. z*, 49(333-369):352, 1913.

[77] Bernhard Ø Palsson. *Systems biology: properties of reconstructed networks*. Cambridge university press, 2006.

[78] Haluk Resat, Linda Petzold, and Michel F Pettigrew. Kinetic modeling of biological systems. *Computational systems biology*, pages 311–335, 2009.

[79] Haluk Resat, Michelle N Costa, and Harish Shankaran. Spatial aspects in biological system simulations. In *Methods in enzymology*, volume 487, pages 485–511. Elsevier, 2011.

[80] Barbara M Bakker, Karen van Eunen, Jeroen AL Jeneson, Natal AW van Riel, Frank J Bruggeman, and Bas Teusink. Systems biology from micro-organisms to human metabolic diseases: the role of detailed kinetic models. *Biochemical Society Transactions*, 38(5):1294–1301, 2010.

[81] I-Der Lee and BO Palsson. A comprehensive model of human erythrocyte metabolism: extensions to include ph effects. *Biomedica biochimica acta*, 49(8-9):771–789, 1990.

[82] Cato M Guldberg and Peter Waage. Studies concerning affinity. *CM Forhandlinger: Videnskabs-Selskabet i Christiana*, 35(1864):1864, 1864.

[83] Hiroyuki Kurata, Kazuhiro Maeda, and Yu Matsuoka. Dynamic modeling of metabolic and gene regulatory systems toward developing virtual microbes. *Journal of Chemical Engineering of Japan*, 47(1):1–9, 2014.

[84] Yu Matsuoka and Kazuyuki Shimizu. Current status and future perspectives of kinetic modeling for the cell metabolism with incorporation of the metabolic regulation mechanism. *Bioresources and Bioprocessing*, 2(1):1–19, 2015.

[85] Benno Hess and Arnold Boiteux. Mechanism of glycolytic oscillation in yeast, i. aerobic and anaerobic growth conditions for obtaining glycolytic oscillation. 1968.

[86] Evgenij E SEL'KOV. Stabilization of energy charge, generation of oscillations and multiple steady states in energy metabolism as a result of purely stoichiometric regulation. *European Journal of Biochemistry*, 59(1):151–157, 1975.

[87] ARNOLD BoITEUX, Albert Goldbeter, and Benno Hess. Control of oscillating glycolysis of yeast by stochastic, periodic, and steady source of substrate: a model and experimental study. *Proceedings of the National Academy of Sciences*, 72(10):3829–3833, 1975.

[88] Peter H Richter and John Ross. Oscillations and efficiency in glycolysis. *Biophysical chemistry*, 12(3-4):285–297, 1980.

[89] Arnold Boiteux and Heinrich-Gustav Busse. Circuit analysis of the oscillatory state in glycolysis. *Biosystems*, 22(3):231–240, 1989.

[90] Ron Grosz and Gregory Stephanopoulos. Physiological, biochemical, and mathematical studies of micro-aerobic continuous ethanol fermentation by saccharomyces cerevisiae. i: Hysteresis, oscillations, and maximum specific ethanol productivities in chemostat culture. *Biotechnology and bioengineering*, 36(10):1006–1019, 1990.

[91] Finn Hynne, Sune Danø, and Preben G Sørensen. Full-scale model of glycolysis in saccharomyces cerevisiae. *Biophysical chemistry*, 94(1-2):121–163, 2001.

[92] Franco B du Preez, David D van Niekerk, Bob Kooi, Johann M Rohwer, and Jacky L Snoep. From steady-state to synchronized yeast glycolytic oscillations i: model construction. *The FEBS journal*, 279(16):2810–2822, 2012.

[93] Manfred Rizzi, Michael Baltes, Uwe Theobald, and Matthias Reuss. In vivo analysis of metabolic dynamics in saccharomyces cerevisiae: Ii. mathematical model. *Biotechnology and bioengineering*, 55(4):592–608, 1997.

[94] Uwe Theobald, Werner Mailinger, Michael Baltes, Manfred Rizzi, and Matthias Reuss. In vivo analysis of metabolic dynamics in saccharomyces cerevisiae: I. experimental observations. *Biotechnology and bioengineering*, 55(2):305–316, 1997.

[95] Javier Delgado, Jorge Meruane, and James C Liao. Experimental determination of flux control distribution in biochemical systems: In vitro model to analyze transient metabolite concentrations. *Biotechnology and bioengineering*, 41(11):1121–1128, 1993.

[96] Manfred Rizzi, Michael Baltes, Werner Mailinger, Uwe Theobald, and Matthias Reuss. Modelling of short term crabtree-effect in baker's yeast. *IFAC Proceedings Volumes*, 28(3):124–129, 1995.

[97] Bas Teusink, Jutta Passarge, Corinne A Reijenga, Eugenia Esgalhado, Coen C Van der Weijden, Mike Schepper, Michael C Walsh, Barbara M Bakker, Karel Van Dam, Hans V Westerhoff, et al. Can yeast glycolysis be understood in terms of in vitro kinetics of the constituent enzymes? testing biochemistry. *European Journal of Biochemistry*, 267(17):5313–5329, 2000.

[98] Karen van Eunen, Jose AL Kiewiet, Hans V Westerhoff, and Barbara M Bakker. Testing biochemistry revisited: how in vivo metabolism can be understood from in vitro enzyme kinetics. *PLoS computational biology*, 8(4):e1002483, 2012.

[99] Kieran Smallbone, Hanan L Messiha, Kathleen M Carroll, Catherine L Winder, Naglis Malys, Warwick B Dunn, Ettore Murabito, Neil Swainston, Joseph O Dada, Farid Khan, et al. A model of yeast glycolysis based on a consistent kinetic characterisation of all its enzymes. *FEBS letters*, 587(17):2832–2841, 2013.

[100] Johan H van Heerden, Meike T Wortel, Frank J Bruggeman, Joseph J Heijnen, Yves JM Bollen, Robert Planqué, Josephus Hulshof, Tom G O'Toole, S Aljoscha Wahl, and Bas Teusink. Lost in transition: start-up of glycolysis yields subpopulations of nongrowing cells. *Science*, 343(6174):1245114, 2014.

[101] Christophe Chassagnole, Naruemol Noisommit-Rizzi, Joachim W Schmid, Klaus Mauch, and Matthias Reuss. Dynamic modeling of the central carbon metabolism of escherichia coli. *Biotechnology and bioengineering*, 79(1):53–73, 2002.

[102] Tuty Asmawaty Abdul Kadir, Ahmad A Mannan, Andrzej M Kierzek, Johnjoe McFadden, and Kazuyuki Shimizu. Modeling and simulation of the main metabolism in escherichia coli and its several single-gene knockout mutants with experimental verification. *Microbial cell factories*, 9(1):1–21, 2010.

[103] Kirill Peskov, Ekaterina Mogilevskaya, and Oleg Demin. Kinetic modelling of central carbon metabolism in escherichia coli. *The FEBS journal*, 279(18):3374–3385, 2012.

[104] Barbara M Bakker, Paul AM Michels, Fred R Opperdoes, and Hans V Westerhoff. Glycolysis in bloodstream form trypanosoma brucei can be understood in terms of the kinetics of the glycolytic enzymes. *Journal of Biological Chemistry*, 272(6):3207–3215, 1997.

[105] Barbara M Bakker, Paul AM Michels, Fred R Opperdoes, and Hans V Westerhoff. What controls glycolysis in bloodstream form trypanosoma brucei? *Journal of Biological Chemistry*, 274(21):14551–14559, 1999.

[106] Robert Eisenthal and Athel Cornish-Bowden. Prospects for antiparasitic drugs: the case of trypanosoma brucei, the causative agent of african sleeping sickness. *Journal of Biological Chemistry*, 273(10):5500–5505, 1998.

[107] Vivek Kumar Singh and Indira Ghosh. Kinetic modeling of tricarboxylic acid cycle and glyoxylate bypass in mycobacterium tuberculosis, and its application to assessment of drug targets. *Theoretical Biology and Medical Modelling*, 3(1):1–11, 2006.

[108] Jurgen R Haanstra, Albert Gerding, Amalia M Dolga, Freek JH Sorgdrager, Manon Buist-Homan, Francois Du Toit, Klaas Nico Faber, Hermann-Georg Holzhütter, Balázs Szöör, Keith R Matthews, et al. Targeting pathogen metabolism without collateral damage to the host. *Scientific reports*, 7(1):1–15, 2017.

[109] Richard Bertram, Leslie Satin, Min Zhang, Paul Smolen, and Arthur Sherman. Calcium and glycolysis mediate multiple bursting modes in pancreatic islets. *Biophysical Journal*, 87(5):3074–3087, 2004.

[110] S Tiveci, A Akın, T Çakır, H Saybaşılı, and K Ülgen. Modelling of calcium dynamics in brain energy metabolism and alzheimer's disease. *Computational biology and chemistry*, 29(2):151–162, 2005.

[111] Nan Jiang, Roger D Cox, and John M Hancock. A kinetic core model of the glucose-stimulated insulin secretion network of pancreatic β cells. *Mammalian Genome*, 18(6):508–520, 2007.

[112] Christine Nazaret and Jean-Pierre Mazat. An old paper revisited:"a mathematical model of carbohydrate energy metabolism. interaction between glycolysis, the krebs cycle and the h-transporting shuttles at varying atpases load" by vv dynnik, r. heinrich and ee sel'kov. *Journal of theoretical biology*, 252(3):520–529, 2008.

[113] Christine Nazaret, Margit Heiske, Kevin Thurley, and Jean-Pierre Mazat. Mitochondrial energetic metabolism: a simplified model of tca cycle with atp production. *Journal of theoretical biology*, 258(3):455–464, 2009.

[114] Matthias König, Sascha Bulik, and Hermann-Georg Holzhütter. Quantifying the contribution of the liver to glucose homeostasis: a detailed kinetic model of human hepatic glucose metabolism. *PLoS computational biology*, 8(6):e1002577, 2012.

[115] Chiara Dalla Man, Robert A Rizza, and Claudio Cobelli. Meal simulation model of the glucose-insulin system. *IEEE Transactions on biomedical engineering*, 54(10):1740–1749, 2007.

[116] Mark T Mc Auley, Darren J Wilkinson, Janette JL Jones, and Thomas BL Kirkwood. A whole-body mathematical model of cholesterol metabolism and its age-associated dysregulation. *BMC systems biology*, 6(1):1–21, 2012.

[117] Adrian C Pratt, Jonathan AD Wattis, and Andrew M Salter. Mathematical modelling of hepatic lipid metabolism. *Mathematical Biosciences*, 262:167–181, 2015.

[118] Maxime Durot, Pierre-Yves Bourguignon, and Vincent Schachter. Genome-scale models of bacterial metabolism: reconstruction and applications. *FEMS microbiology reviews*, 33(1):164–190, 2008.

[119] Peter D Karp, Monica Riley, Milton Saier, Ian T Paulsen, Julio Collado-Vides, Suzanne M Paley, Alida Pellegrini-Toole, César Bonavides, and Socorro Gama-Castro. The ecocyc database. *Nucleic acids research*, 30(1):56–58, 2002.

[120] Amit Varma and Bernhard O Palsson. Stoichiometric flux balance models quantitatively predict growth and metabolic by-product secretion in wild-type escherichia coli w3110. *Applied and environmental microbiology*, 60(10):3724–3731, 1994.

[121] Matthew A Oberhardt, Arvind K Chavali, and Jason A Papin. Flux balance analysis: interrogating genome-scale metabolic networks. In *Systems Biology*, pages 61–80. Springer, 2009.

[122] Jeffrey D Orth, Ines Thiele, and Bernhard Ø Palsson. What is flux balance analysis? *Nature Biotechnology*, 28(3):245–248, 2010.

[123] Christophe H Schilling, David Letscher, and Bernhard Ø Palsson. Theory for the systemic definition of metabolic pathways and their use in interpreting metabolic function from a pathway-oriented perspective. *Journal of theoretical biology*, 203(3):229–248, 2000.

[124] Stefan Schuster, Thomas Dandekar, and David A Fell. Detection of elementary flux modes in biochemical networks: a promising tool for pathway analysis and metabolic engineering. *Trends in biotechnology*, 17(2):53–60, 1999.

[125] Stefan Schuster and Claus Hilgetag. On elementary flux modes in biochemical reaction systems at steady state. *Journal of Biological Systems*, 2(02):165–182, 1994.

[126] Frederick C Neidhardt. Escherichia coli and salmonella typhimurium. *Cellular and molecular biology*, 1:1225, 1996.

[127] RA Majewski and MM Domach. Simple constrained-optimization view of acetate overflow in e. coli. *Biotechnology and bioengineering*, 35(7):732–738, 1990.

[128] Amit Varma, Brian W Boesch, and Bernhard O Palsson. Stoichiometric interpretation of escherichia coli glucose catabolism under various oxygenation rates. *Applied and environmental microbiology*, 59(8):2465–2473, 1993.

[129] J Pramanik and JD Keasling. Stoichiometric model of escherichia coli metabolism: Incorporation of growth-rate dependent biomass composition and mechanistic energy requirements. *Biotechnology and bioengineering*, 56(4):398–421, 1997.

[130] J Pramanik and JD Keasling. Effect of escherichia coli biomass composition on central metabolic fluxes predicted by a stoichiometric model. *Biotechnology and bioengineering*, 60(2):230–238, 1998.

[131] Jennifer L Reed and Bernhard Ø Palsson. Thirteen years of building constraint-based in silico models of escherichia coli. *Journal of bacteriology*, 185(9):2692–2699, 2003.

[132] Iman Famili, Jochen Förster, Jens Nielsen, and Bernhard O Palsson. Saccharomyces cerevisiae phenotypes can be predicted by using constraint-based analysis of a genome-scale reconstructed metabolic network. *Proceedings of the National Academy of Sciences*, 100(23):13134–13139, 2003.

[133] Jochen Förster, Iman Famili, Patrick Fu, Bernhard Ø Palsson, and Jens Nielsen. Genome-scale reconstruction of the saccharomyces cerevisiae metabolic network. *Genome research*, 13(2):244–253, 2003.

[134] Natalie C Duarte, Markus J Herrgård, and Bernhard Ø Palsson. Reconstruction and validation of saccharomyces cerevisiae ind750, a fully compartmentalized genome-scale metabolic model. *Genome research*, 14(7):1298–1309, 2004.

[135] Fernando Alvarez-Vasquez, Carlos González-Alcón, and Néstor V Torres. Metabolism of citric acid production by aspergillus niger: Model definition, steady-state analysis and constrained optimization of citric acid production rate. *Biotechnology and Bioengineering*, 70(1):82–108, 2000.

[136] Daniel V Guebel and Néstor V Torres Darias. Optimization of the citric acid production by aspergillus niger through a metabolic flux balance model. *Electronic Journal of Biotechnology*, 4(1):7–8, 2001.

[137] Helga David, Mats Åkesson, and Jens Nielsen. Reconstruction of the central carbon metabolism of aspergillus niger. *European Journal of Biochemistry*, 270(21):4243–4253, 2003.

[138] Jeremy S Edwards and Bernhard O Palsson. Systems properties of the haemophilus influenzaerd metabolic genotype. *Journal of Biological Chemistry*, 274(25):17410–17416, 1999.

[139] Robert D Fleischmann, Mark D Adams, Owen White, Rebecca A Clayton, Ewen F Kirkness, Anthony R Kerlavage, Carol J Bult, Jean-Francois Tomb, Brian A Dougherty, Joseph M Merrick, et al. Whole-genome random sequencing and assembly of haemophilus influenzae rd. *Science*, 269(5223):496–512, 1995.

[140] Irina Borodina, Kanchana R Kildegaard, Niels B Jensen, Thomas H Blicher, Jérôme Maury, Svetlana Sherstyk, Konstantin Schneider, Pedro Lamosa, Markus J Herrgård, Inger Rosenstand, et al. Establishing a synthetic pathway for high-level production of 3-hydroxypropionic acid in saccharomyces cerevisiae via β-alanine. *Metabolic engineering*, 27:57–64, 2015.

[141] Jung Eun Yang, Si Jae Park, Won Jun Kim, Hyeong Jun Kim, Bumjoon J Kim, Hyuk Lee, Jihoon Shin, and Sang Yup Lee. One-step fermentative production of aromatic polyesters from glucose by metabolically engineered escherichia coli strains. *Nature communications*, 9(1):1–10, 2018.

[142] Pranjul Mishra, Na-Rae Lee, Meiyappan Lakshmanan, Minsuk Kim, Byung-Gee Kim, and Dong-Yup Lee. Genome-scale model-driven strain design for dicarboxylic acid production in yarrowia lipolytica. *BMC systems biology*, 12(2):9–20, 2018.

[143] Dany JV Beste, Tracy Hooper, Graham Stewart, Bhushan Bonde, Claudio Avignone-Rossa, Michael E Bushell, Paul Wheeler, Steffen Klamt, Andrzej M Kierzek, and Johnjoe McFadden. Gsmn-tb: a web-based genome-scale network model of mycobacterium tuberculosismetabolism. *Genome biology*, 8(5):1–18, 2007.

[144] Gunnar Sigurdsson, Ronan MT Fleming, Almut Heinken, and Ines Thiele. A systems biology approach to drug targets in pseudomonas aeruginosa biofilm. *PLoS One*, 7(4):e34337, 2012.

[145] Alyaa M Abdel-Haleem, Hooman Hefzi, Katsuhiko Mineta, Xin Gao, Takashi Gojobori, Bernhard O Palsson, Nathan E Lewis, and Neema Jamshidi. Functional interrogation of plasmodium genus metabolism identifies species-and stage-specific differences in nutrient essentiality and drug targeting. *PLoS computational biology*, 14(1):e1005895, 2018.

[146] Kenji Nakahigashi, Yoshihiro Toya, Nobuyoshi Ishii, Tomoyoshi Soga, Miki Hasegawa, Hisami Watanabe, Yuki Takai, Masayuki Honma, Hirotada Mori, and Masaru Tomita. Systematic phenome analysis of escherichia coli multiple-knockout mutants reveals hidden reactions in central carbon metabolism. *Molecular systems biology*, 5(1):306, 2009.

[147] Balázs Szappanos, Károly Kovács, Béla Szamecz, Frantisek Honti, Michael Costanzo, Anastasia Baryshnikova, Gabriel Gelius-Dietrich, Martin J Lercher, Márk Jelasity, Chad L Myers, et al. An integrated approach to characterize genetic interaction networks in yeast metabolism. *Nature genetics*, 43(7):656–662, 2011.

[148] Edward J O'Brien, Jonathan M Monk, and Bernhard O Palsson. Using genome-scale models to predict biological capabilities. *Cell*, 161(5):971–987, 2015.

[149] Anu Raghunathan, Jennifer Reed, Sookil Shin, Bernhard Palsson, and Simon Daefler. Constraint-based analysis of metabolic capacity of salmonella typhimurium during host-pathogen interaction. *BMC systems biology*, 3(1):1–16, 2009.

[150] Aarash Bordbar, Nathan E Lewis, Jan Schellenberger, Bernhard Ø Palsson, and Neema Jamshidi. Insight into human alveolar macrophage and m. tuberculosis interactions via metabolic reconstructions. *Molecular systems biology*, 6(1):422, 2010.

[151] Anu Raghunathan, Sookil Shin, and Simon Daefler. Systems approach to investigating host-pathogen interactions in infections with the biothreat agent francisella. constraints-based model of francisella tularensis. *BMC systems biology*, 4(1):1–19, 2010.

[152] Rienk A Rienksma, Peter J Schaap, Vitor AP Martins dos Santos, and Maria Suarez-Diez. Modeling the metabolic state of mycobacterium tuberculosis upon infection. *Frontiers in cellular and infection microbiology*, 8:264, 2018.

[153] Rienk A Rienksma, Peter J Schaap, Vitor AP Martins dos Santos, and Maria Suarez-Diez. Modeling host-pathogen interaction to elucidate the metabolic drug response of intracellular mycobacterium tuberculosis. *Frontiers in cellular and infection microbiology*, 9:144, 2019.

[154] Mustafa Sertbas and Kutlu O Ulgen. Genome-scale metabolic modeling for unraveling molecular mechanisms of high threat pathogens. *Frontiers in Cell and Developmental Biology*, 8:566702, 2020.

[155] Changdai Gu, Gi Bae Kim, Won Jun Kim, Hyun Uk Kim, and Sang Yup Lee. Current status and applications of genome-scale metabolic models. *Genome biology*, 20(1):1–18, 2019.

[156] Sharon J Wiback and Bernhard O Palsson. Extreme pathway analysis of human red blood cell metabolism. *Biophysical journal*, 83(2):808–818, 2002.

[157] Aristotle Chatziioannou, Georgios Palaiologos, and Fragiskos N Kolisis. Metabolic flux analysis as a tool for the elucidation of the metabolism of neurotransmitter glutamate. *Metabolic engineering*, 5(3):201–210, 2003.

[158] Thuy D Vo, Harvey J Greenberg, and Bernhard O Palsson. Reconstruction and functional characterization of the human mitochondrial metabolic network based on proteomic and biochemical data. *Journal of Biological Chemistry*, 279(38):39532–39540, 2004.

[159] Natalie C Duarte, Scott A Becker, Neema Jamshidi, Ines Thiele, Monica L Mo, Thuy D Vo, Rohith Srivas, and Bernhard Ø Palsson. Global reconstruction of the human metabolic network based on genomic and bibliomic data. *Proceedings of the National Academy of Sciences*, 104(6):1777–1782, 2007.

[160] Hongwu Ma, Anatoly Sorokin, Alexander Mazein, Alex Selkov, Evgeni Selkov, Oleg Demin, and Igor Goryanin. The edinburgh human metabolic network reconstruction and its functional analysis. *Molecular systems biology*, 3(1):135, 2007.

[161] Ines Thiele, Neil Swainston, Ronan MT Fleming, Andreas Hoppe, Swagatika Sahoo, Maike K Aurich, Hulda Haraldsdottir, Monica L Mo, Ottar Rolfsson, Miranda D Stobbe, et al. A community-driven global reconstruction of human metabolism. *Nature biotechnology*, 31(5):419–425, 2013.

[162] Neil Swainston, Kieran Smallbone, Hooman Hefzi, Paul D Dobson, Judy Brewer, Michael Hanscho, Daniel C Zielinski, Kok Siong Ang, Natalie J Gardiner, Jahir M Gutierrez, et al. Recon 2.2: from reconstruction to model of human metabolism. *Metabolomics*, 12(7):1–7, 2016.

[163] Jae Yong Ryu, Hyun Uk Kim, and Sang Yup Lee. Framework and resource for more than 11,000 gene-transcript-protein-reaction associations in human metabolism. *Proceedings of the National Academy of Sciences*, 114(45):E9740–E9749, 2017.

[164] Elizabeth Brunk, Swagatika Sahoo, Daniel C Zielinski, Ali Altunkaya, Andreas Dräger, Nathan Mih, Francesco Gatto, Avlant Nilsson, German Andres Preciat Gonzalez, Maike Kathrin Aurich, et al. Recon3d enables a three-dimensional view of gene variation in human metabolism. *Nature biotechnology*, 36(3):272–281, 2018.

[165] Aleksej Zelezniak, Tune H Pers, Simão Soares, Mary Elizabeth Patti, and Kiran Raosaheb Patil. Metabolic network topology reveals transcriptional regulatory signatures of type 2 diabetes. *PLoS computational biology*, 6(4):e1000729, 2010.

[166] Tomer Shlomi, Tomer Benyamini, Eyal Gottlieb, Roded Sharan, and Eytan Ruppin. Genome-scale metabolic modeling elucidates the role of proliferative adaptation in causing the warburg effect. *PLoS computational biology*, 7(3):e1002018, 2011.

[167] Nathan E Lewis and Alyaa M Abdel-Haleem. The evolution of genome-scale models of cancer metabolism. *Frontiers in physiology*, 4:237, 2013.

[168] Livnat Jerby, Tomer Shlomi, and Eytan Ruppin. Computational reconstruction of tissue-specific metabolic models: application to human liver metabolism. *Molecular systems biology*, 6(1):401, 2010.

[169] Christoph Gille, Christian Bölling, Andreas Hoppe, Sascha Bulik, Sabrina Hoffmann, Katrin Hübner, Anja Karlstädt, Ramanan Ganeshan, Matthias König, Kristian Rother, et al. Hepatonet1: a comprehensive metabolic reconstruction of the human hepatocyte for the analysis of liver physiology. *Molecular systems biology*, 6(1):411, 2010.

[170] Roger L Chang, Li Xie, Lei Xie, Philip E Bourne, and Bernhard Ø Palsson. Drug off-target effects predicted using structural analysis in the context of a metabolic network model. *PLoS computational biology*, 6(9):e1000938, 2010.

[171] Nathan E Lewis, Gunnar Schramm, Aarash Bordbar, Jan Schellenberger, Michael P Andersen, Jeffrey K Cheng, Nilam Patel, Alex Yee, Randall A Lewis, Roland Eils, et al. Large-scale in silico modeling of metabolic interactions between cell types in the human brain. *Nature biotechnology*, 28(12):1279–1285, 2010.

[172] Swagatika Sahoo and Ines Thiele. Predicting the impact of diet and enzymopathies on human small intestinal epithelial cells. *Human molecular genetics*, 22(13):2705–2722, 2013.

[173] Rasmus Agren, Sergio Bordel, Adil Mardinoglu, Natapol Pornputtapong, Intawat Nookaew, and Jens Nielsen. Reconstruction of genome-scale active metabolic networks for 69 human cell types and 16 cancer types using init. *PLoS computational biology*, 8(5):e1002518, 2012.

[174] Pedro Romero, Jonathan Wagg, Michelle L Green, Dale Kaiser, Markus Krummenacker, and Peter D Karp. Computational prediction of human metabolic pathways from the complete human genome. *Genome biology*, 6(1):1–17, 2005.

[175] Minoru Kanehisa, Michihiro Araki, Susumu Goto, Masahiro Hattori, Mika Hirakawa, Masumi Itoh, Toshiaki Katayama, Shuichi Kawashima, Shujiro Okuda, Toshiaki Tokimatsu, et al. Kegg for linking genomes to life and the environment. *Nucleic acids research*, 36(suppl_1):D480–D484, 2007.

[176] Adil Mardinoglu, Rasmus Agren, Caroline Kampf, Anna Asplund, Intawat Nookaew, Peter Jacobson, Andrew J Walley, Philippe Froguel, Lena M Carlsson, Mathias Uhlen, et al. Integration of clinical data with a genome-scale metabolic model of the human adipocyte. *Molecular systems biology*, 9(1):649, 2013.

[177] Leif Väremo, Camilla Scheele, Christa Broholm, Adil Mardinoglu, Caroline Kampf, Anna Asplund, Intawat Nookaew, Mathias Uhlén, Bente Klarlund Pedersen, and Jens Nielsen. Proteome-and transcriptome-driven reconstruction of the human myocyte metabolic network and its use for identification of markers for diabetes. *Cell reports*, 11(6):921–933, 2015.

[178] Jonathan L Robinson, Pınar Kocabaş, Hao Wang, Pierre-Etienne Cholley, Daniel Cook, Avlant Nilsson, Mihail Anton, Raphael Ferreira, Iván Domenzain, Virinchi Billa, et al. An atlas of human metabolism. *Science signaling*, 13(624):eaaz1482, 2020.

[179] Simeone Marino, Ian B Hogue, Christian J Ray, and Denise E Kirschner. A methodology for performing global uncertainty and sensitivity analysis in systems biology. *Journal of theoretical biology*, 254(1):178–196, 2008.

[180] Jon C Helton and Freddie Joe Davis. Latin hypercube sampling and the propagation of uncertainty in analyses of complex systems. *Reliability Engineering & System Safety*, 81(1):23–69, 2003.

[181] MD McKay and WJ Conover. Rj beckman a comparison of three methods for selecting values of input variables in the analysis of output from a computer code. *Technometrics*, 21:239–245, 1979.

[182] James T Wassell. Sensitivity analysis in practice, andrea saltelli, 2005.

[183] Andrea Saltelli and J Marivoet. Non-parametric statistics in sensitivity analysis for model output: a comparison of selected techniques. *Reliability Engineering & System Safety*, 28(2):229–253, 1990.

[184] Andrea Saltelli, Stefano Tarantola, Francesca Campolongo, Marco Ratto, et al. Sensitivity analysis in practice: a guide to assessing scientific models. *Chichester, England*, 2004.

[185] Jennifer L Reed, Iman Famili, Ines Thiele, and Bernhard O Palsson. Towards multidimensional genome annotation. *Nature Reviews Genetics*, 7(2):130–141, 2006.

[186] Scott A Becker and Bernhard O Palsson. Context-specific metabolic networks are consistent with experiments. *PLoS computational biology*, 4(5):e1000082, 2008.

[187] Semidán Robaina Estévez and Zoran Nikoloski. Generalized framework for context-specific metabolic model extraction methods. *Frontiers in plant science*, 5:491, 2014.

[188] Sjoerd Opdam, Anne Richelle, Benjamin Kellman, Shanzhong Li, Daniel C Zielinski, and Nathan E Lewis. A systematic evaluation of methods for tailoring genome-scale metabolic models. *Cell systems*, 4(3):318–329, 2017.

[189] Tomer Shlomi, Moran N Cabili, Markus J Herrgård, Bernhard Ø Palsson, and Eytan Ruppin. Network-based prediction of human tissue-specific metabolism. *Nature biotechnology*, 26(9):1003, 2008.

[190] Hadas Zur, Eytan Ruppin, and Tomer Shlomi. imat: an integrative metabolic analysis tool. *Bioinformatics*, 26(24):3140–3142, 2010.

[191] Yuliang Wang, James A Eddy, and Nathan D Price. Reconstruction of genome-scale metabolic models for 126 human tissues using mcadre. *BMC systems biology*, 6(1):1–16, 2012.

[192] Nikos Vlassis, Maria Pires Pacheco, and Thomas Sauter. Fast reconstruction of compact context-specific metabolic network models. *PLoS computational biology*, 10(1):e1003424, 2014.

[193] Caroline Colijn, Aaron Brandes, Jeremy Zucker, Desmond S Lun, Brian Weiner, Maha R Farhat, Tan-Yun Cheng, D Branch Moody, Megan Murray, and James E Galagan. Interpreting expression data with metabolic flux models: predicting mycobacterium tuberculosis mycolic acid production. *PLoS Computational Biology*, 5(8):e1000489, 2009.

[194] Sangbum Lee, Chan Phalakornkule, Michael M Domach, and Ignacio E Grossmann. Recursive milp model for finding all the alternate optima in lp models for metabolic networks. *Computers & Chemical Engineering*, 24(2-7):711–716, 2000.

[195] JL Reed, TD Vo, CH Schilling, and B Palsson. Escherichia coli ijr904: an expanded genome-scale model of e. coli k-12. *Genome Biol*, 4:R54, 2003.

[196] Radhakrishnan Mahadevan and Chrisophe H Schilling. The effects of alternate optimal solutions in constraint-based genome-scale metabolic models. *Metabolic engineering*, 5(4):264–276, 2003.

[197] Nathan D Price, Jan Schellenberger, and Bernhard O Palsson. Uniform sampling of steady-state flux spaces: means to design experiments and to interpret enzymopathies. *Biophysical journal*, 87(4):2172–2186, 2004.

[198] Jan Schellenberger and Bernhard Ø Palsson. Use of randomized sampling for analysis of metabolic networks. *Journal of biological chemistry*, 284(9):5457–5461, 2009.

[199] Sergio Bordel, Rasmus Agren, and Jens Nielsen. Sampling the solution space in genome-scale metabolic networks reveals transcriptional regulation in key enzymes. *PLoS computational biology*, 6(7):e1000859, 2010.

[200] Helena A Herrmann, Beth C Dyson, Lucy Vass, Giles N Johnson, and Jean-Marc Schwartz. Flux sampling is a powerful tool to study metabolism under changing environmental conditions. *NPJ systems biology and applications*, 5(1):1–8, 2019.

[201] Sharon J Wiback, Iman Famili, Harvey J Greenberg, and Bernhard Ø Palsson. Monte carlo sampling can be used to determine the size and shape of the steady-state flux space. *Journal of theoretical biology*, 228(4):437–447, 2004.

[202] Robert L Smith. Efficient monte carlo procedures for generating points uniformly distributed over bounded regions. *Operations Research*, 32(6):1296–1308, 1984.

[203] David E Kaufman and Robert L Smith. Direction choice for accelerated convergence in hit-and-run sampling. *Operations Research*, 46(1):84–95, 1998.

[204] Hulda S Haraldsdóttir, Ben Cousins, Ines Thiele, Ronan MT Fleming, and Santosh Vempala. Chrr: coordinate hit-and-run with rounding for uniform sampling of constraint-based models. *Bioinformatics*, 33(11):1741–1743, 2017.

[205] Jan Schellenberger, Richard Que, Ronan MT Fleming, Ines Thiele, Jeffrey D Orth, Adam M Feist, Daniel C Zielinski, Aarash Bordbar, Nathan E Lewis, Sorena Rahmanian, et al. Quantitative prediction of cellular metabolism with constraint-based models: the cobra toolbox v2. 0. *Nature protocols*, 6(9):1290, 2011.

[206] Jeremy S Edwards and Bernhard O Palsson. The escherichia coli mg1655 in silico metabolic genotype: its definition, characteristics, and capabilities. *Proceedings of the National Academy of Sciences*, 97(10):5528–5533, 2000.

[207] Daniel Segre, Dennis Vitkup, and George M Church. Analysis of optimality in natural and perturbed metabolic networks. *Proceedings of the National Academy of Sciences*, 99(23):15112–15117, 2002.

[208] Tomer Shlomi, Omer Berkman, and Eytan Ruppin. Regulatory on/off minimization of metabolic flux changes after genetic perturbations. *Proceedings of the national academy of sciences*, 102(21):7695–7700, 2005.

[209] Keren Yizhak, Orshay Gabay, Haim Cohen, and Eytan Ruppin. Model-based identification of drug targets that revert disrupted metabolism and its application to ageing. *Nature Communications*, 4(1):1–11, 2013.

[210] Adil Mardinoglu, Francesco Gatto, and Jens Nielsen. Genome-scale modeling of human metabolism–a systems biology approach. *Biotechnology Journal*, 8(9):985–996, 2013.

[211] Rhys Evans and Keith N Frayn. Human metabolism: a regulatory perspective. 2019.

[212] Beste Calimlioglu, Kubra Karagoz, Tuba Sevimoglu, Elif Kilic, Esra Gov, and Kazim Yalcin Arga. Tissue-specific molecular biomarker signatures of type 2 diabetes: an integrative analysis of transcriptomics and protein–protein interaction data. *Omics: a Journal of Integrative Biology*, 19(9):563–573, 2015.

[213] Zhuo Fu, Elizabeth R Gilbert, and Dongmin Liu. Regulation of insulin synthesis and secretion and pancreatic beta-cell dysfunction in diabetes. *Current diabetes reviews*, 9(1):25–53, 2013.

[214] Michael G White, James AM Shaw, and Roy Taylor. Type 2 diabetes: the pathologic basis of reversible β-cell dysfunction. *Diabetes care*, 39(11):2080–2088, 2016.

[215] Yoo Jin Park and Minna Woo. Pancreatic β cells: gatekeepers of type 2 diabetes. *Journal of Cell Biology*, 218(4):1094–1095, 2019.

[216] Gordon C Weir. Glucolipotoxicity, β-cells, and diabetes: the emperor has no clothes. *Diabetes*, 69(3):273–278, 2020.

[217] Md Habibur Rahman, Silong Peng, Xiyuan Hu, Chen Chen, Shahadat Uddin, Julian MW Quinn, and Mohammad Ali Moni. Bioinformatics methodologies to identify interactions between type 2 diabetes and neurological comorbidities. *IEEE Access*, 7:183948–183970, 2019.

[218] Phyu-Phyu Khin, Jong-Han Lee, and Hee-Sook Jun. A brief review of the mechanisms of β-cell dedifferentiation in type 2 diabetes. *Nutrients*, 13(5):1593, 2021.

[219] Gordon C Weir, Jason Gaglia, and Susan Bonner-Weir. Inadequate β-cell mass is essential for the pathogenesis of type 2 diabetes. *The Lancet Diabetes & Endocrinology*, 8(3):249–256, 2020.

[220] Jonathan E Campbell and Christopher B Newgard. Mechanisms controlling pancreatic islet cell function in insulin secretion. *Nature reviews Molecular cell biology*, 22(2):142–158, 2021.

[221] Pierre Maechler and Claes B Wollheim. Mitochondrial function in normal and diabetic β-cells. *Nature*, 414(6865):807–812, 2001.

[222] Philippe A Halban, Kenneth S Polonsky, Donald W Bowden, Meredith A Hawkins, Charlotte Ling, Kieren J Mather, Alvin C Powers, Christopher J Rhodes, Lori Sussel, and Gordon C Weir. β-cell failure in type 2 diabetes: postulated mechanisms and prospects for prevention and treatment. *The Journal of Clinical Endocrinology & Metabolism*, 99(6):1983–1992, 2014.

[223] Milagros Rocha, Nadezda Apostolova, Ruben Diaz-Rua, Jordi Muntane, and Victor M Victor. Mitochondria and t2d: role of autophagy, er stress, and inflammasome. *Trends in Endocrinology & Metabolism*, 31(10):725–741, 2020.

[224] Kenichi Otani, Rohit N Kulkarni, Aaron C Baldwin, Jan Krutzfeldt, Kohjiro Ueki, Markus Stoffel, C Ronald Kahn, and Kenneth S Polonsky. Reduced β-cell mass and altered glucose sensing impair insulin-secretory function in βirko mice. *American journal of physiology-endocrinology and metabolism*, 286(1):E41–E49, 2004.

[225] Rohit N Kulkarni. New insights into the roles of insulin/igf-i in the development and maintenance of β-cell mass. *Reviews in Endocrine and Metabolic Disorders*, 6(3):199–210, 2005.

[226] Rebeca Fernandez-Ruiz, Elaine Vieira, Pablo M Garcia-Roves, and Ramon Gomis. Protein tyrosine phosphatase-1b modulates pancreatic β-cell mass. *PLoS One*, 9(2):e90344, 2014.

[227] Jake A Kushner, Fawaz G Haj, Lori D Klaman, Matthew A Dow, Barbara B Kahn, Benjamin G Neel, and Morris F White. Islet-sparing effects of protein tyrosine phosphatase-1b deficiency delays onset of diabetes in irs2 knockout mice. *Diabetes*, 53(1):61–66, 2004.

[228] Bylgja Hilmarsdottir, Eirikur Briem, Skarphedinn Halldorsson, Jennifer Kricker, Sævar Ingthorsson, Sigrun Gustafsdottir, Gunhild M Mælandsmo, Magnus K Magnusson, and Thorarinn Gudjonsson. Inhibition of ptp1b disrupts cell–cell adhesion and induces anoikis in breast epithelial cells. *Cell death & disease*, 8(5):e2769–e2769, 2017.

[229] Melissa F Brereton, Maria Rohm, Kenju Shimomura, Christian Holland, Sharona Tornovsky-Babeay, Daniela Dadon, Michaela Iberl, Margarita V Chibalina, Sheena Lee, Benjamin Glaser, et al. Hyperglycaemia induces metabolic dysfunction and glycogen accumulation in pancreatic β-cells. *Nature Communications*, 7(1):1–15, 2016.

[230] Julie Adam, Reshma Ramracheya, Margarita V Chibalina, Nicola Ternette, Alexander Hamilton, Andrei I Tarasov, Quan Zhang, Eduardo Rebelato, Nils JG Rorsman, Rafael Martín-del Río, et al. Fumarate hydratase deletion in pancreatic β cells leads to progressive diabetes. *Cell Reports*, 20(13):3135–3148, 2017.

[231] Michaela Aichler, Daniela Borgmann, Jan Krumsiek, Achim Buck, Patrick E MacDonald, Jocelyn E Manning Fox, James Lyon, Peter E Light, Susanne Keipert, Martin Jastroch, et al. N-acyl taurines and acylcarnitines cause an imbalance in insulin synthesis and secretion provoking β cell dysfunction in type 2 diabetes. *Cell Metabolism*, 25(6):1334–1347, 2017.

[232] Isabel Göhring, Vladimir V Sharoyko, Siri Malmgren, Lotta E Andersson, Peter Spégel, David G Nicholls, and Hindrik Mulder. Chronic high glucose and pyruvate levels differentially affect mitochondrial bioenergetics and fuel-stimulated insulin secretion from clonal ins-1 832/13 cells. *Journal of Biological Chemistry*, 289(6):3786–3798, 2014.

[233] Céline Fernandez, Ulrika Fransson, Elna Hallgard, Peter Spégel, Cecilia Holm, Morten Krogh, Kristofer Wårell, Peter James, and Hindrik Mulder. Metabolomic and proteomic analysis of a clonal insulin-producing β-cell line (ins-1 832/13). *Journal of Proteome Research*, 7(01):400–411, 2008.

[234] Guo-Fang Zhang, Mette V Jensen, Sarah M Gray, Kimberley El, You Wang, Danhong Lu, Thomas C Becker, Jonathan E Campbell, and Christopher B Newgard. Reductive tca cycle metabolism fuels glutamine-and glucose-stimulated insulin secretion. *Cell metabolism*, 33(4):804–817, 2021.

[235] Bjoern A Menge, Henning Schrader, Peter R Ritter, Mark Ellrichmann, Waldemar Uhl, Wolfgang E Schmidt, and Juris J Meier. Selective amino acid deficiency in patients with impaired glucose tolerance and type 2 diabetes. *Regulatory Peptides*, 160(1-3):75–80, 2010.

[236] Lorella Marselli, Jeffrey Thorne, Sonika Dahiya, Dennis C Sgroi, Arun Sharma, Susan Bonner-Weir, Piero Marchetti, and Gordon C Weir. Gene expression profiles of beta-cell enriched tissue obtained by laser capture microdissection from subjects with type 2 diabetes. *PloS One*, 5(7):e11499, 2010.

[237] Peter Langfelder and Steve Horvath. Wgcna: an r package for weighted correlation network analysis. *BMC Bioinformatics*, 9(1):1–13, 2008.

[238] Bin Zhang and Steve Horvath. A general framework for weighted gene co-expression network analysis. *Statistical Applications in Genetics and Molecular Biology*, 4(1), 2005.

[239] Peter Langfelder, Bin Zhang, and Steve Horvath. Defining clusters from a hierarchical cluster tree: the dynamic tree cut package for r. *Bioinformatics*, 24(5):719–720, 2008.

[240] Maxim V Kuleshov, Matthew R Jones, Andrew D Rouillard, Nicolas F Fernandez, Qiaonan Duan, Zichen Wang, Simon Koplev, Sherry L Jenkins, Kathleen M Jagodnik, Alexander Lachmann, et al. Enrichr: a comprehensive gene set enrichment analysis web server 2016 update. *Nucleic Acids Research*, 44(W1):W90–W97, 2016.

[241] Kiran Raosaheb Patil and Jens Nielsen. Uncovering transcriptional regulation of metabolism by using metabolic network topology. *Proceedings of the National Academy of Sciences*, 102(8):2685–2689, 2005.

[242] Markus Stoffel and Stephen A Duncan. The maturity-onset diabetes of the young (mody1) transcription factor hnf4α regulates expression of genes required for glucose transport and metabolism. *Proceedings of the National Academy of Sciences*, 94(24):13209–13214, 1997.

[243] Ben Z Stanger. Hnf4a and diabetes: injury before insult? *Diabetes*, 57(6):1461–1462, 2008.

[244] Suresh Chandran, Victor Samuel Rajadurai, Wai Han Hoi, Sarah E Flanagan, Khalid Hussain, and Fabian Yap. A novel hnf4a mutation causing three phenotypic forms of glucose dysregulation in a family. *Frontiers in Pediatrics*, 8, 2020.

[245] Masaki Miura, Takeshi Miyatsuka, Takehiro Katahira, Shugo Sasaki, Luka Suzuki, Miwa Himuro, Yuya Nishida, Yoshio Fujitani, Taka-aki Matsuoka, and Hirotaka Watada. Suppression of stat3 signaling promotes cellular reprogramming into insulin-producing cells induced by defined transcription factors. *EBioMedicine*, 36:358–366, 2018.

[246] Nathan W Zammit, Ying Ying Wong, Stacey Walters, Joanna Warren, Simon C Barry, and Shane T Grey. Rela governs a network of islet-specific metabolic genes necessary for beta-cell function. *Available at SSRN 3733072*.

[247] Joseph P Tiano and Franck Mauvais-Jarvis. Selective estrogen receptor modulation in pancreatic β-cells and the prevention of type 2 diabetes. *Islets*, 4(2):173–176, 2012.

[248] Hend Al-Jaber, Layla Al-Mansoori, and Mohamed A Elrayess. Gata-3 as a potential therapeutic target for insulin resistance and type 2 diabetes mellitus. *Current Diabetes Reviews*, 2020.

[249] Alexander M Efanov, Sabine Sewing, Krister Bokvist, and Jesper Gromada. Liver x receptor activation stimulates insulin secretion via modulation of glucose and lipid metabolism in pancreatic beta-cells. *Diabetes*, 53(suppl 3):S75–S78, 2004.

[250] Dawn Belt Davis, Jeremy A Lavine, Joshua I Suhonen, Kimberly A Krautkramer, Mary E Rabaglia, Jamie M Sperger, Luis A Fernandez, Brian S Yandell, Mark P Keller, I-Ming Wang, et al. Foxm1 is up-regulated by obesity and stimulates β-cell proliferation. *Molecular Endocrinology*, 24(9):1822–1834, 2010.

[251] Huei-Min Lin, Ji-Hyeon Lee, Hariom Yadav, Anil K Kamaraju, Eric Liu, Duan Zhigang, Anthony Vieira, Seong-Jin Kim, Heather Collins, Franz Matschinsky, et al. Transforming growth factor-β/smad3 signaling regulates insulin gene transcription and pancreatic islet β-cell function. *Journal of Biological Chemistry*, 284(18):12246–12257, 2009.

[252] Masatoshi Nomura, Hai-Lei Zhu, Lixiang Wang, Hidetaka Morinaga, Ryoichi Takayanagi, and Noriyoshi Teramoto. Smad2 disruption in mouse pancreatic beta cells leads to islet hyperplasia and impaired insulin secretion due to the attenuation of atp-sensitive k+ channel activity. *Diabetologia*, 57(1):157–166, 2014.

[253] Matteo G Levisetti and Kenneth S Polonsky. Diabetic pancreatic β cells arnt all they should be. *Cell Metabolism*, 2(2):78–80, 2005.

[254] R Lupi, R Mancarella, S Del Guerra, M Bugliani, Stefano Del Prato, Ugo Boggi, F Mosca, Franco Filipponi, and Piero Marchetti. Effects of exendin-4 on islets from type 2 diabetes patients. *Diabetes, Obesity and Metabolism*, 10(6):515–519, 2008.

[255] Frédérik Oger, Cyril Bourouh, Xavier Gromada, Maeva Moreno, Charlene Carney, Emilie Courty, Nabil Rabhi, Emmanuelle Durand, Souhila Amanzougarene, Lionel Berberian, et al. Pancreatic β-cell specific loss of e2f1 impairs insulin secretion and β-cell identity through the epigenetic repression of non β-cell programs. *bioRxiv*, 2020.

[256] J Lee, K Ma, M Moulik, and V Yechoor. Untimely oxidative stress in β-cells leads to diabetes–role of circadian clock in β-cell function. *Free Radical Biology and Medicine*, 119:69–74, 2018.

[257] Ines Thiele, Swagatika Sahoo, Almut Heinken, Johannes Hertel, Laurent Heirendt, Maike K Aurich, and Ronan MT Fleming. Personalized whole-body models integrate metabolism, physiology, and the gut microbiome. *Molecular systems biology*, 16(5):e8982, 2020.

[258] Anne Richelle, Austin WT Chiang, Chih-Chung Kuo, and Nathan E Lewis. Increasing consensus of context-specific metabolic models by integrating data-inferred cell functions. *PLoS computational biology*, 15(4):e1006867, 2019.

[259] Roqia Bashary, Manish Vyas, Surendra K Nayak, Ashish Suttee, Surajpal Verma, Rakesh Narang, and Gopal L Khatik. An insight of alpha-amylase inhibitors as a valuable tool in the management of type 2 diabetes mellitus. *Current Diabetes Reviews*, 16(2):117–136, 2020.

[260] Ebru Boslem, Peter J Meikle, and Trevor J Biden. Roles of ceramide and sphingolipids in pancreatic β-cell function and dysfunction. *Islets*, 4(3):177–187, 2012.

[261] Julien Véret, Lara Bellini, Paola Giussani, Carl Ng, Christophe Magnan, and Hervé Le Stunff. Roles of sphingolipid metabolism in pancreatic β cell dysfunction induced by lipotoxicity. *Journal of Clinical Medicine*, 3(2):646–662, 2014.

[262] Josefa Fernandez-Alvarez, Ignacio Conget, Joanne Rasschaert, Abdullah Sener, Ramon Gomis, and WJ Malaisse. Enzymatic, metabolic and secretory patterns in human islets of type 2 (non-insulin-dependent) diabetic patients. *Diabetologia*, 37(2):177–181, 1994.

[263] K Ueda, Y Tanizawa, H Ishihara, N Kizuki, Y Ohta, A Matsutani, and Y Oka. Overexpression of mitochondrial fad-linked glycerol-3-phosphate dehydrogenase does not correct glucose-stimulated insulin secretion from diabetic gk rat pancreatic islets. *Diabetologia*, 41(6):649–653, 1998.

[264] Lin Shi, Carl Brunius, Marko Lehtonen, Seppo Auriola, Ingvar A Bergdahl, Olov Rolandsson, Kati Hanhineva, and Rikard Landberg. Plasma metabolites associated with type 2 diabetes in a swedish population: a case–control study nested in a prospective cohort. *Diabetologia*, 61(4):849–861, 2018.

[265] Peter J Meikle, Gerard Wong, Christopher K Barlow, Jacquelyn M Weir, Melissa A Greeve, Gemma L MacIntosh, Laura Almasy, Anthony G Comuzzie, Michael C Mahaney, Adam Kowalczyk, et al. Plasma lipid profiling shows similar associations with prediabetes and type 2 diabetes. *PloS One*, 8(9):e74341, 2013.

[266] ROBERT E CARRAWAY, SANKAR P MITRA, GERHARD E FEURLE, and WALTER H HACKI. Presence of neurotensin and neuromedin-n within a common precursor from a human pancreatic neuroendocrine tumor. *The Journal of Clinical Endocrinology & Metabolism*, 66(6):1323–1328, 1988.

[267] Alberto Noronha, Jennifer Modamio, Yohan Jarosz, Elisabeth Guerard, Nicolas Sompairac, German Preciat, Anna Dröfn Daníelsdóttir, Max Krecke, Diane Merten, Hulda S Haraldsdóttir, et al. The virtual metabolic human database: integrating human and gut microbiome metabolism with nutrition and disease. *Nucleic Acids Research*, 47(D1):D614–D624, 2019.

[268] Xuan Liu, Xiuqing Gao, Rui Zhang, Ziyan Liu, Na Shen, Yanbo Di, Tao Fang, Huanming Li, and Fengshi Tian. Discovery and comparison of serum biomarkers for diabetes mellitus and metabolic syndrome based on uplc-q-tof/ms. *Clinical Biochemistry*, 2020.

[269] MA Barradas, DS Gill, VA Fonseca, DP Mikhailidis, and P Dandona. Intraplatelet serotonin in patients with diabetes mellitus and peripheral vascular disease. *European Journal of Clinical Investigation*, 18(4):399–404, 1988.

[270] J Malyszko, T Urano, R Knofler, A Taminato, T Yoshimi, Y Takada, and A Takada. Daily variations of platelet aggregation in relation to blood and plasma serotonin in diabetes. *Thrombosis Research*, 75(5):569–576, 1994.

[271] Andreas Wiederkehr and Claes B Wollheim. Minireview: implication of mitochondria in insulin secretion and action. *Endocrinology*, 147(6):2643–2649, 2006.

[272] S Jitrapakdee, A Wutthisathapornchai, JC Wallace, and MJ MacDonald. Regulation of insulin secretion: role of mitochondrial signalling. *Diabetologia*, 53(6):1019–1032, 2010.

[273] Malin Fex, Lisa M Nicholas, Neelanjan Vishnu, Anya Medina, Vladimir V Sharoyko, David G Nicholls, Peter Spégel, and Hindrik Mulder. The pathogenetic role of β-cell mitochondria in type 2 diabetes. *Journal of Endocrinology*, 236(3):R145–R159, 2018.

[274] Tetsuro Kobayashi, Koji Nakanishi, Hirofumi Nakase, Hiroshi Kajio, Minoru Okubo, Toshio Murase, and Kinori Kosaka. In situ characterization of islets in diabetes with a mitochondrial dna mutation at nucleotide position 3243. *Diabetes*, 46(10):1567–1571, 1997.

[275] Hongfang Lu, Vasilij Koshkin, Emma M Allister, Armen V Gyulkhandanyan, and Michael B Wheeler. Molecular and metabolic evidence for mitochondrial defects associated with β-cell dysfunction in a mouse model of type 2 diabetes. *Diabetes*, 59(2):448–459, 2010.

[276] Zuheng Ma, Tina Wiström, LA Håkan Borg, Gerd Larsson-Nyrén, Ingrid Hals, John Bondo-Hansen, Valdemar Grill, and Anneli Björklund. Diabetes reduces β-cell mitochondria and induces distinct morphological abnormalities, which are reproducible by high glucose in vitro with attendant dysfunction. *Islets*, 4(3):233–242, 2012.

[277] Simona Cernea and Minodora Dobreanu. Diabetes and beta cell function: from mechanisms to evaluation and clinical implications. *Biochemia Medica*, 23(3):266–280, 2013.

[278] Matthias Elsner, Wiebke Gehrmann, and Sigurd Lenzen. Peroxisome-generated hydrogen peroxide as important mediator of lipotoxicity in insulin-producing cells. *Diabetes*, 60(1):200–208, 2011.

[279] Toshiaki Sawatani, Yukiko K Kaneko, and Tomohisa Ishikawa. Dual effect of reduced type i diacylglycerol kinase activity on insulin secretion from min6 β-cells. *Journal of Pharmacological Sciences*, 140(2):178–186, 2019.

[280] Yukiko K Kaneko and Tomohisa Ishikawa. Diacylglycerol signaling pathway in pancreatic β-cells: An essential role of diacylglycerol kinase in the regulation of insulin secretion. *Biological and Pharmaceutical Bulletin*, 38(5):669–673, 2015.

[281] Cristina Espinosa-Diez, Verónica Miguel, Daniela Mennerich, Thomas Kietzmann, Patricia Sánchez-Pérez, Susana Cadenas, and Santiago Lamas. Antioxidant responses and cellular adjustments to oxidative stress. *Redox biology*, 6:183–197, 2015.

[282] Jeanette M Dypbukt, Maria Ankarcrona, Mark Burkitt, Å Sjöholm, K Ström, Sten Orrenius, and Pierluigi Nicotera. Different prooxidant levels stimulate growth, trigger apoptosis, or produce necrosis of insulin-secreting rinm5f cells. the role of intracellular polyamines. *Journal of Biological Chemistry*, 269(48):30553–30560, 1994.

[283] P Christian Schulze, Konstantinos Drosatos, and Ira J Goldberg. Lipid use and misuse by the heart. *Circulation Research*, 118(11):1736–1751, 2016.

[284] Michael Lever, Peter M George, Sandy Slow, David Bellamy, Joanna M Young, Markus Ho, Christopher J McEntyre, Jane L Elmslie, Wendy Atkinson, Sarah L Molyneux, et al. Betaine and trimethylamine-n-oxide as predictors of cardiovascular outcomes show different patterns in diabetes mellitus: an observational study. *PloS One*, 9(12), 2014.

[285] Ahmed M Selim, Nitasha Sarswat, Iosif Kelesidis, Muhammad Iqbal, Ramesh Chandra, and Ronald Zolty. Plasma serotonin in heart failure: possible marker and potential treatment target. *Heart, Lung and Circulation*, 26(5):442–449, 2017.

[286] William H Frishman and Pam Grewall. Serotonin and the heart. *Annals of Medicine*, 32(3):195–209, 2000.

[287] Yoshiyuki Ban, Takuya Watanabe, Akira Miyazaki, Yasuko Nakano, Takashi Tobe, Tsunenori Idei, Takashi Iguchi, Yoshio Ban, and Takashi Katagiri. Impact of increased plasma serotonin levels and carotid atherosclerosis on vascular dementia. *Atherosclerosis*, 195(1):153–159, 2007.

[288] Kjell Vikenes, Mikael Farstad, and Jan Erik Nordrehaug. Serotonin is associated with coronary artery disease and cardiac events. *Circulation*, 100(5):483–489, 1999.

[289] EK Van den Berg, JM Schmitz, CR Benedict, CR Malloy, JT Willerson, and GJ Dehmer. Transcardiac serotonin concentration is increased in selected patients with limiting angina and complex coronary lesion morphology. *Circulation*, 79(1):116–124, 1989.

[290] Mazher Mohammed, Catalin Filipeanu, and Eric Lazartigues. Kinetensin increases blood pressure by activation of angiotensin-ii type 1 receptors, in isoflurane anesthetized male mice. *The FASEB Journal*, 35, 2021.

[291] Paul R Dobner, Diane L Barber, Lydia Villa-Komaroff, and Colleen McKiernan. Cloning and sequence analysis of cdna for the canine neurotensin/neuromedin n precursor. *Proceedings of the National Academy of Sciences*, 84(10):3516–3520, 1987.

[292] Olle Melander, Alan S Maisel, Peter Almgren, Jonas Manjer, Mattias Belting, Bo Hedblad, Gunnar Engström, Ute Kilger, Peter Nilsson, Andreas Bergmann, et al. Plasma proneurotensin and incidence of diabetes, cardiovascular disease, breast cancer, and mortality. *Jama*, 308(14):1469–1475, 2012.

[293] Frederick J King, Douglas W Selinger, Felipa A Mapa, Jeff Janes, Hua Wu, Timothy R Smith, Qing-Yin Wang, Pornwaratt Niyomrattanakitand, Daniel G Sipes, Achim Brinker, et al. Pathway reporter assays reveal small molecule mechanisms of action. *JALA: Journal of the Association for Laboratory Automation*, 14(6):374–382, 2009.

[294] Andrew G Reaume. Drug repurposing through nonhypothesis driven phenotypic screening. *Drug Discovery Today: Therapeutic Strategies*, 8(3-4):85–88, 2011.

[295] Scott J Warchal, Asier Unciti-Broceta, and Neil O Carragher. Next-generation phenotypic screening. *Future medicinal chemistry*, 8(11):1331–1347, 2016.

[296] Matthew A Oberhardt, Keren Yizhak, and Eytan Ruppin. Metabolically re-modeling the drug pipeline. *Current opinion in pharmacology*, 13(5):778–785, 2013.

[297] Douglas B Kell. Systems biology, metabolic modelling and metabolomics in drug discovery and development. *Drug discovery today*, 11(23-24):1085–1092, 2006.

[298] Jens Nielsen. Systems biology of metabolism: a driver for developing personalized and precision medicine. *Cell metabolism*, 25(3):572–579, 2017.

[299] Keren Yizhak, Edoardo Gaude, Sylvia Le Dévédec, Yedael Y Waldman, Gideon Y Stein, Bob van de Water, Christian Frezza, and Eytan Ruppin. Phenotype-based cell-specific metabolic modeling reveals metabolic liabilities of cancer. *Elife*, 3:e03641, 2014.

[300] Jorrit J Hornberg, Frank J Bruggeman, Hans V Westerhoff, and Jan Lankelma. Cancer: a systems biology disease. *Biosystems*, 83(2-3):81–90, 2006.

[301] Rebecca L Siegel, Kimberly D Miller, and Ahmedin Jemal. Cancer statistics, 2018. *CA: a cancer journal for clinicians*, 68(1):7–30, 2018.

[302] Christina Fitzmaurice, Christine Allen, Ryan M Barber, Lars Barregard, Zulfiqar A Bhutta, Hermann Brenner, Daniel J Dicker, Odgerel Chimed-Orchir, Rakhi Dandona, Lalit Dandona, et al. Global, regional, and national cancer incidence, mortality, years of life lost, years lived with disability, and disability-adjusted life-years for 32 cancer groups, 1990 to 2015: a systematic analysis for the global burden of disease study. *JAMA oncology*, 3(4):524–548, 2017.

[303] Mahiben Maruthappu, Michael G Head, Charlie D Zhou, Barnabas J Gilbert, Majd A El-Harasis, Rosalind Raine, Joseph R Fitchett, and Rifat Atun. Investments in cancer research awarded to uk institutions and the global burden of cancer 2000–2013: a systematic analysis. *BMJ open*, 7(4):e013936, 2017.

[304] Scott A Becker, Adam M Feist, Monica L Mo, Gregory Hannum, Bernhard Ø Palsson, and Markus J Herrgard. Quantitative prediction of cellular metabolism with constraint-based models: the cobra toolbox. *Nature protocols*, 2(3):727–738, 2007.

[305] Ziwei Dai, Shiyu Yang, Liyan Xu, Hongrong Hu, Kun Liao, Jianghuang Wang, Qian Wang, Shuaishi Gao, Bo Li, and Luhua Lai. Identification of cancer–associated metabolic vulnerabilities by modeling multi-objective optimality in metabolism. *Cell Communication and Signaling*, 17(1):1–15, 2019.

[306] Jochen Förster, Iman Famili, Bernhard Ø Palsson, and Jens Nielsen. Large-scale evaluation of in silico gene deletions in saccharomyces cerevisiae. *OMICS A Journal of Integrative Biology*, 7(2):193–202, 2003.

[307] Aviad Tsherniak, Francisca Vazquez, Phil G Montgomery, Barbara A Weir, Gregory Kryukov, Glenn S Cowley, Stanley Gill, William F Harrington, Sasha Pantel, John M Krill-Burger, et al. Defining a cancer dependency map. *Cell*, 170(3):564–576, 2017.

[308] Vivian Law, Craig Knox, Yannick Djoumbou, Tim Jewison, An Chi Guo, Yifeng Liu, Adam Maciejewski, David Arndt, Michael Wilson, Vanessa Neveu, et al. Drugbank 4.0: shedding new light on drug metabolism. *Nucleic acids research*, 42(D1):D1091–D1097, 2013.

[309] Robert H Shoemaker. The nci60 human tumour cell line anticancer drug screen. *Nature Reviews Cancer*, 6(10):813, 2006.

[310] Huijun Wang, Jonathan Klinginsmith, Xiao Dong, Adam C Lee, Rajarshi Guha, Yuqing Wu, Gordon M Crippen, and David J Wild. Chemical data mining of the nci human tumor cell line database. *Journal of chemical information and modeling*, 47(6):2063–2076, 2007.

[311] Adam C Lee, Kerby Shedden, Gustavo R Rosania, and Gordon M Crippen. Data mining the nci60 to predict generalized cytotoxicity. *Journal of chemical information and modeling*, 48(7):1379–1388, 2008.

[312] Jae K Lee, Dmytro M Havaleshko, HyungJun Cho, John N Weinstein, Eric P Kaldjian, John Karpovich, Andrew Grimshaw, and Dan Theodorescu. A strategy for predicting the chemosensitivity of human cancers and its application to drug discovery. *Proceedings of the National Academy of Sciences*, 104(32):13086–13091, 2007.

[313] Nathan E Lewis, Kim K Hixson, Tom M Conrad, Joshua A Lerman, Pep Charusanti, Ashoka D Polpitiya, Joshua N Adkins, Gunnar Schramm, Samuel O Purvine, Daniel Lopez-Ferrer, et al. Omic data from evolved e. coli are consistent with computed optimal growth from genome-scale models. *Molecular systems biology*, 6(1):390, 2010.

[314] Laurent Heirendt, Sylvain Arreckx, Thomas Pfau, Sebastián N Mendoza, Anne Richelle, Almut Heinken, Hulda S Haraldsdóttir, Jacek Wachowiak, Sarah M Keating, Vanja Vlasov, et al. Creation and analysis of biochemical constraint-based models using the cobra toolbox v. 3.0. *Nature protocols*, 14(3):639–702, 2019.

[315] Mathias Uhlen, Per Oksvold, Linn Fagerberg, Emma Lundberg, Kalle Jonasson, Mattias Forsberg, Martin Zwahlen, Caroline Kampf, Kenneth Wester, Sophia Hober, et al. Towards a knowledge-based human protein atlas. *Nature biotechnology*, 28(12):1248, 2010.

[316] Ulrich Brandt and Bernard Trumpower. The protonmotive q cycle in mitochondria and bacteria. *Critical reviews in biochemistry and molecular biology*, 29(3):165–197, 1994.

[317] Antony R Crofts. The cytochrome bc 1 complex: function in the context of structure. *Annu. Rev. Physiol.*, 66:689–733, 2004.

[318] Silviu Sbiera, Ellen Leich, Gerhard Liebisch, Iuliu Sbiera, Andreas Schirbel, Laura Wiemer, Silke Matysik, Carolin Eckhardt, Felix Gardill, Annemarie Gehl, et al. Mitotane inhibits sterol-o-acyl transferase 1 triggering lipid-mediated endoplasmic reticulum stress and apoptosis in adrenocortical carcinoma cells. *Endocrinology*, 156(11):3895–3908, 2015.

[319] G Von Jagow, Per O Ljungdahl, P Graf, T Ohnishi, and BL Trumpower. An inhibitor of mitochondrial respiration which binds to cytochrome b and displaces quinone from the iron-sulfur protein of the cytochrome bc1 complex. *Journal of Biological Chemistry*, 259(10):6318–6326, 1984.

[320] Pouyan Ghaffari, Adil Mardinoglu, Anna Asplund, Saeed Shoaie, Caroline Kampf, Mathias Uhlen, and Jens Nielsen. Identifying anti-growth factors for human cancer cell lines through genome-scale metabolic modeling. *Scientific reports*, 5(1):1–10, 2015.

[321] Justin Lamb, Emily D Crawford, David Peck, Joshua W Modell, Irene C Blat, Matthew J Wrobel, Jim Lerner, Jean-Philippe Brunet, Aravind Subramanian, Kenneth N Ross, et al. The connectivity map: using gene-expression signatures to connect small molecules, genes, and disease. *science*, 313(5795):1929–1935, 2006.

[322] Christos E Zois, Elena Favaro, and Adrian L Harris. Glycogen metabolism in cancer. *Biochemical pharmacology*, 92(1):3–11, 2014.

[323] Monique Rousset, Hervé Paris, Guillemette Chevalier, Blandine Terrain, Jean-Claude Murat, and Alain Zweibaum. Growth-related enzymatic control of glycogen metabolism in cultured human tumor cells. *Cancer research*, 44(1):154–160, 1984.

[324] Marion Curtis, Hilary A Kenny, Bradley Ashcroft, Abir Mukherjee, Alyssa Johnson, Yilin Zhang, Ynes Helou, Raquel Batlle, Xiaojing Liu, Nuria Gutierrez, et al. Fibroblasts mobilize tumor cell glycogen to promote proliferation and metastasis. *Cell metabolism*, 29(1):141–155, 2019.

[325] Joffrey Pelletier, Grégory Bellot, Pierre Gounon, Sandra Lacas-Gervais, Jacques Pouysségur, and Nathalie M Mazure. Glycogen synthesis is induced in hypoxia by the hypoxia-inducible factor and promotes cancer cell survival. *Frontiers in oncology*, 2:18, 2012.

[326] Katsuyoshi Miyashita, Mitsutoshi Nakada, Abbas Shakoori, Yasuhito Ishigaki, Takeo Shimasaki, Yoshiharu Motoo, Kazuyuki Kawakami, and Toshinari Minamoto. An emerging strategy for cancer treatment targeting aberrant glycogen synthase kinase 3β. *Anti-Cancer Agents in Medicinal Chemistry (Formerly Current Medicinal Chemistry-Anti-Cancer Agents)*, 9(10):1114–1122, 2009.

[327] Vikas V Dukhande, Shrikant Barot, Suemaya Husein, and Christian Palaguachi. Inhibition of glycogen metabolism as a potential strategy for anticancer therapy. *The FASEB Journal*, 31(1_supplement):942–10, 2017.

[328] Shrikant Barot, Ehab M Abo-Ali, Daisy L Zhou, Christian Palaguachi, and Vikas V Dukhande. Inhibition of glycogen catabolism induces intrinsic apoptosis and augments multikinase inhibitors in hepatocellular carcinoma cells. *Experimental cell research*, 2019.

[329] Stefanie Hahner and Martin Fassnacht. Mitotane for adrenocortical carcinoma treatment. *Current opinion in investigational drugs (London, England: 2000)*, 6(4):386–394, 2005.

[330] Massimo Terzolo, Alberto Angeli, Martin Fassnacht, Fulvia Daffara, Libuse Tauchmanova, Pier Antonio Conton, Ruth Rossetto, Lisa Buci, Paola Sperone, Erika Grossrubatscher, et al. Adjuvant mitotane treatment for adrenocortical carcinoma. *New England Journal of Medicine*, 356(23):2372–2380, 2007.

[331] Camille Baudry, Joël Coste, Roula Bou Khalil, Stéphane Silvera, Laurence Guignat, Jean Guibourdenche, Halim Abbas, Paul Legmann, Xavier Bertagna, and Jérôme Bertherat. Efficiency and tolerance of mitotane in cushing's disease in 76 patients from a single center. *European Journal of Endocrinology*, 167(4):473–481, 2012.

[332] Feng Geng, Xiang Cheng, Xiaoning Wu, Ji Young Yoo, Chunming Cheng, Jeffrey Yunhua Guo, Xiaokui Mo, Peng Ru, Brian Hurwitz, Sung-Hak Kim, et al. Inhibition of soat1 suppresses glioblastoma growth via blocking srebp-1–mediated lipogenesis. *Clinical Cancer Research*, 22(21):5337–5348, 2016.

[333] Tobiloba E Oni, Giulia Biffi, Lindsey A Baker, Yuan Hao, Claudia Tonelli, Tim DD Somerville, Astrid Deschênes, Pascal Belleau, Chang-il Hwang, Francisco J Sánchez-Rivera, et al. Soat1 promotes mevalonate pathway dependency in pancreatic cancer. *Journal of Experimental Medicine*, 217(9), 2020.

[334] Marco Fiorillo, Rebecca Lamb, Herbert B Tanowitz, Luciano Mutti, Marija Krstic-Demonacos, Anna Rita Cappello, Ubaldo E Martinez-Outschoorn, Federica Sotgia, and Michael P Lisanti. Repurposing atovaquone: targeting mitochondrial complex iii and oxphos to eradicate cancer stem cells. *Oncotarget*, 7(23):34084, 2016.

[335] Mitchell Fry and Mary Pudney. Site of action of the antimalarial hydroxynaphthoquinone, 2-[trans-4-(4'-chlorophenyl) cyclohexyl]-3-hydroxy-1, 4-naphthoquinone (566c80). *Biochemical pharmacology*, 43(7):1545–1553, 1992.

[336] Indresh K Srivastava, Hagai Rottenberg, and Akhil B Vaidya. Atovaquone, a broad spectrum antiparasitic drug, collapses mitochondrial membrane potential in a malarial parasite. *Journal of Biological Chemistry*, 272(7):3961–3966, 1997.

[337] Shenglan Tian, Heng Chen, and Wei Tan. Targeting mitochondrial respiration as a therapeutic strategy for cervical cancer. *Biochemical and biophysical research communications*, 499(4):1019–1024, 2018.

[338] Jing Zhou, Lei Duan, Huaming Chen, Xiaomei Ren, Zhang Zhang, Fengtao Zhou, Jinsong Liu, Duanqing Pei, and Ke Ding. Atovaquone derivatives as potent cytotoxic and apoptosis inducing agents. *Bioorganic & medicinal chemistry letters*, 19(17):5091–5094, 2009.

[339] Hye Jin Jung, Yonghyo Kim, Junghwa Chang, Sang Won Kang, Jeong Hun Kim, and Ho Jeong Kwon. Mitochondrial uqcrb regulates vegfr2 signaling in endothelial cells. *Journal of Molecular Medicine*, 91(9):1117–1128, 2013.

[340] Narae Jung, Ho Jeong Kwon, and Hye Jin Jung. Downregulation of mitochondrial uqcrb inhibits cancer stem cell-like properties in glioblastoma. *International journal of oncology*, 52(1):241–251, 2018.

[341] Yingyan Han, Shujuan Sun, Meisong Zhao, Zeyu Zhang, Song Gong, Peipei Gao, Jia Liu, Jianfeng Zhou, Ding Ma, Qinglei Gao, et al. Cyc1 predicts poor prognosis in patients with breast cancer. *Disease markers*, 2016, 2016.

[342] Guodong Li, Dong Fu, Wenqing Liang, Lin Fan, Kai Chen, Liancheng Shan, Shuo Hu, Xiaojun Ma, Ke Zhou, and Biao Cheng. Cyc1 silencing sensitizes osteosarcoma cells to trail-induced apoptosis. *Cellular physiology and biochemistry*, 34(6):2070–2080, 2014.

[343] Kyong Hwa Jun, Su Young Kim, Jung Hwan Yoon, Jae Hwi Song, and Won Sang Park. Amplification of the uqcrfs1 gene in gastric cancers. *Journal of gastric cancer*, 12(2):73–80, 2012.

[344] Yoko Ohashi, Saori J Kaneko, Tommy E Cupples, and S Robert Young. Ubiquinol cytochrome c reductase (uqcrfs1) gene amplification in primary breast cancer core biopsy samples. *Gynecologic oncology*, 93(1):54–58, 2004.

[345] Yuanyuan Shang, Fang Zhang, Dehui Li, Chang Li, Hongbo Li, Yingjian Jiang, and Dianliang Zhang. Overexpression of uqcrc2 is correlated with tumor progression and poor prognosis in colorectal cancer. *Pathology-Research and Practice*, 214(10):1613–1620, 2018.

[346] Koen Brusselmans, Ellen De Schrijver, Guido Verhoeven, and Johannes V Swinnen. Rna interference–mediated silencing of the acetyl-coa-carboxylase-α gene induces growth inhibition and apoptosis of prostate cancer cells. *Cancer research*, 65(15):6719–6725, 2005.

[347] Véronique Chajès, Marie Cambot, Karen Moreau, Gilbert M Lenoir, and Virginie Joulin. Acetyl-coa carboxylase α is essential to breast cancer cell survival. *Cancer research*, 66(10):5287–5294, 2006.

[348] Zhenglong Gu, Lars M Steinmetz, Xun Gu, Curt Scharfe, Ronald W Davis, and Wen-Hsiung Li. Role of duplicate genes in genetic robustness against null mutations. *Nature*, 421(6918):63–66, 2003.

[349] David Deutscher, Isaac Meilijson, Stefan Schuster, and Eytan Ruppin. Can single knockouts accurately single out gene functions? *BMC Systems Biology*, 2(1):50, 2008.

[350] David Deutscher, Isaac Meilijson, Martin Kupiec, and Eytan Ruppin. Multiple knockout analysis of genetic robustness in the yeast metabolic network. *Nature genetics*, 38(9):993–998, 2006.

[351] Tomer Shlomi, Markus Herrgard, Vasiliy Portnoy, Efrat Naim, Bernhard Ø Palsson, Roded Sharan, and Eytan Ruppin. Systematic condition-dependent annotation of metabolic genes. *Genome research*, 17(11):1626–1633, 2007.

[352] Lars Kuepfer, Uwe Sauer, and Lars M Blank. Metabolic functions of duplicate genes in saccharomyces cerevisiae. *Genome research*, 15(10):1421–1430, 2005.

[353] Jörn Behre, Thomas Wilhelm, Axel von Kamp, Eytan Ruppin, and Stefan Schuster. Structural robustness of metabolic networks with respect to multiple knockouts. *Journal of Theoretical Biology*, 252(3):433–441, 2008.

[354] Nir Yosef, Alon Kaufman, and Eytan Ruppin. Inferring functional pathways from multi-perturbation data. *Bioinformatics*, 22(14):e539–e546, 2006.

[355] Malte P Suppli, Kristoffer TG Rigbolt, Sanne S Veidal, Sara Heebøll, Peter Lykke Eriksen, Mia Demant, Jonatan I Bagger, Jens Christian Nielsen, Denise Oró, Sebastian W Thrane, et al. Hepatic transcriptome signatures in patients with varying degrees of non-alcoholic fatty liver disease compared with healthy normal-weight individuals. *American Journal of Physiology-Gastrointestinal and Liver Physiology*, 316(4):G462–G472, 2019.

[356] Kai K Kummer, Theodora Kalpachidou, Michaela Kress, and Michiel Langeslag. Signatures of altered gene expression in dorsal root ganglia of a fabry disease mouse model. *Frontiers in Molecular Neuroscience*, 10:449, 2018.

[357] Yazdan Asgari, Pegah Khosravi, Zahra Zabihinpour, and Mahnaz Habibi. Exploring candidate biomarkers for lung and prostate cancers using gene expression and flux variability analysis. *Integrative Biology*, 10(2):113–120, 2018.

[358] Mingmei Shao, Zixiang Ye, Yanhong Qin, and Tao Wu. Abnormal metabolic processes involved in the pathogenesis of non-alcoholic fatty liver disease. *Experimental and Therapeutic Medicine*, 20(5):1–1, 2020.

[359] Edith Lubos, Joseph Loscalzo, and Diane E Handy. Glutathione peroxidase-1 in health and disease: from molecular mechanisms to therapeutic opportunities. *Antioxidants & redox signaling*, 15(7):1957–1997, 2011.

[360] Dipanka Tanu Sarmah, Abhijit Paul, Umang Berry, Milan Surjit, Nandadulal Bairagi, and Samrat Chatterjee. Integrating protein-protein interaction network with metabolic model reveals novel targets for nash. *(submitted)*.

[361] Blanca Herrera, Annalisa Addante, and Aránzazu Sánchez. Bmp signalling at the crossroad of liver fibrosis and regeneration. *International journal of molecular sciences*, 19(1):39, 2017.

[362] Timothy E Thayer, Christian L Lino Cardenas, Trejeeve Martyn, Christopher J Nicholson, Lisa Traeger, Florian Wunderer, Charles Slocum, Haakon Sigurslid, Hannah R Shakartzi, Caitlin O'Rourke, et al. The role of bone morphogenetic protein signaling in non-alcoholic fatty liver disease. *Scientific reports*, 10(1):1–13, 2020.

[363] Matthias Ocker. Fibroblast growth factor signaling in non-alcoholic fatty liver disease and non-alcoholic steatohepatitis: Paving the way to hepatocellular carcinoma. *World Journal of Gastroenterology*, 26(3):279, 2020.

[364] Nicole Paland, Aviva Gamliel-Lazarovich, Raymond Coleman, and Bianca Fuhrman. Urokinase-type plasminogen activator (upa) stimulates triglyceride synthesis in huh7 hepatoma cells via p38-dependent upregulation of dgat2. *Atherosclerosis*, 237(1):200–207, 2014.

[365] Srinivas Pittala, Idan Levy, Soumasree De, Swaroop Kumar Pandey, Nataly Melnikov, Tehila Hyman, and Varda Shoshan-Barmatz. The vdac1-based r-tf-d-lp4 peptide as a potential treatment for diabetes mellitus. *Cells*, 9(2):481, 2020.

[366] Adam C Sheka, Oyedele Adeyi, Julie Thompson, Bilal Hameed, Peter A Crawford, and Sayeed Ikramuddin. Nonalcoholic steatohepatitis: a review. *Jama*, 323(12):1175–1183, 2020.

[367] Claire H Wilson and Sharad Kumar. Caspases in metabolic disease and their therapeutic potential. *Cell Death & Differentiation*, 25(6):1010–1024, 2018.

[368] Samjhana Thapaliya, Alexander Wree, Davide Povero, Maria Eugenia Inzaugarat, Michael Berk, Laura Dixon, Bettina G Papouchado, and Ariel E Feldstein. Caspase 3 inactivation protects against hepatic cell death and ameliorates fibrogenesis in a diet-induced nash model. *Digestive diseases and sciences*, 59(6):1197–1206, 2014.

[369] Theodoros Eleftheriadis, Georgios Pissas, Vassilios Liakopoulos, and Ioannis Stefanidis. Cytochrome c as a potentially clinical useful marker of mitochondrial and cellular damage. *Frontiers in immunology*, 7:279, 2016.

[370] Tara Hessa, Ajay Sharma, Malaiyalam Mariappan, Heather D Eshleman, Erik Gutierrez, and Ramanujan S Hegde. Protein targeting and degradation are coupled for elimination of mislocalized proteins. *Nature*, 475(7356):394–397, 2011.

[371] Fernando G Osorio, Clara Soria-Valles, Olaya Santiago-Fernández, Teresa Bernal, María Mittelbrunn, Enrique Colado, Francisco Rodriguez, Elena Bonzon-Kulichenko, Jesús Vázquez, Montserrat Porta-de-la Riva, et al. Loss of the proteostasis factor airapl causes myeloid transformation by deregulating igf-1 signaling. *Nature medicine*, 22(1):91–96, 2016.

[372] Toru Sasaki, Eugene C Gan, Andrew Wakeham, Sally Kornbluth, Tak W Mak, and Hitoshi Okada. Hla-b-associated transcript 3 (bat3)/scythe is essential for p300-mediated acetylation of p53. *Genes & development*, 21(7):848–861, 2007.

[373] Janina Binici and Joachim Koch. Bag-6, a jack of all trades in health and disease. *Cellular and molecular life sciences*, 71(10):1829–1837, 2014.

[374] Enming Zhang, Israa Mohammed Al-Amily, Sarheed Mohammed, Cheng Luan, Olof Asplund, Meftun Ahmed, Yingying Ye, Danya Ben-Hail, Arvind Soni, Neelanjan Vishnu, et al. Preserving insulin secretion in diabetes by inhibiting vdac1 overexpression and surface translocation in β cells. *Cell metabolism*, 29(1):64–77, 2019.

[375] Vanita R Aroda, William C Knowler, Jill P Crandall, Leigh Perreault, Sharon L Edelstein, Susan L Jeffries, Mark E Molitch, Xavier Pi-Sunyer, Christine Darwin, Brandy M Heckman-Stoddard, et al. Metformin for diabetes prevention: insights gained from the diabetes prevention program/diabetes prevention program outcomes study. *Diabetologia*, 60(9):1601–1611, 2017.

[376] Symen Ligthart, Thijs TW van Herpt, Maarten JG Leening, Maryam Kavousi, Albert Hofman, Bruno HC Stricker, Mandy van Hoek, Eric JG Sijbrands, Oscar H Franco, and Abbas Dehghan. Lifetime risk of developing impaired glucose metabolism and eventual progression from prediabetes to type 2 diabetes: a prospective cohort study. *The lancet Diabetes & endocrinology*, 4(1):44–51, 2016.

[377] Gordon C Weir and Susan Bonner-Weir. Five stages of evolving beta-cell dysfunction during progression to diabetes. *Diabetes*, 53(suppl 3):S16–S21, 2004.

[378] Bernardo L Wajchenberg. β-cell failure in diabetes and preservation by clinical treatment. *Endocrine reviews*, 28(2):187–218, 2007.

[379] Lorella Marselli, Mara Suleiman, Matilde Masini, Daniela Campani, Marco Bugliani, Farooq Syed, Luisa Martino, Daniele Focosi, Fabrizio Scatena, Francesco Olimpico, et al. Are we overestimating the loss of beta cells in type 2 diabetes? *Diabetologia*, 57(2):362–365, 2014.

[380] Juris J Meier and Riccardo C Bonadonna. Role of reduced β-cell mass versus impaired β-cell function in the pathogenesis of type 2 diabetes. *Diabetes care*, 36(Supplement_2):S113–S119, 2013.

[381] GUENTHER Boden, JOSE Ruiz, CJ Kim, and XINHUA Chen. Effects of prolonged glucose infusion on insulin secretion, clearance, and action in normal subjects. *American Journal of Physiology-Endocrinology And Metabolism*, 270(2):E251–E258, 1996.

[382] Matilde Masini, M Anello, Marco Bugliani, Lorella Marselli, Franco Filipponi, Ugo Boggi, F Purrello, Margherita Occhipinti, Luisa Martino, Piero Marchetti, et al. Prevention by metformin of alterations induced by chronic exposure to high glucose in human islet beta cells is associated with preserved atp/adp ratio. *Diabetes research and clinical practice*, 104(1):163–170, 2014.

[383] MJ MacDonald, MJ Longacre, E-C Langberg, A Tibell, MA Kendrick, T Fukao, and C-G Ostenson. Decreased levels of metabolic enzymes in pancreatic islets of patients with type 2 diabetes. *Diabetologia*, 52(6):1087–1091, 2009.

[384] Nicolai M Doliba, Wei Qin, Habiba Najafi, Chengyang Liu, Carol W Buettger, Johanna Sotiris, Heather W Collins, Changhong Li, Charles A Stanley, David F Wilson, et al. Glucokinase activation repairs defective bioenergetics of islets of langerhans isolated from type 2 diabetics. *American Journal of Physiology-Endocrinology and Metabolism*, 302(1):E87–E102, 2012.

[385] Eric D Berglund, Candice Y Li, Greg Poffenberger, Julio E Ayala, Patrick T Fueger, Shannon E Willis, Marybeth M Jewell, Alvin C Powers, and David H Wasserman. Glucose metabolism in vivo in four commonly used inbred mouse strains. *Diabetes*, 57(7):1790–1799, 2008.

[386] VJ Csernus, T Hammer, D Peschke, and E Peschke. Dynamic insulin secretion from perifused rat pancreatic islets. *Cellular and Molecular Life Sciences CMLS*, 54(7):733–743, 1998.

[387] Andrea Mari, Andrea Tura, Eleonora Grespan, and Roberto Bizzotto. Mathematical modeling for the physiological and clinical investigation of glucose homeostasis and diabetes. *Frontiers in Physiology*, 11:1548, 2020.

[388] Pasquale Palumbo, Susanne Ditlevsen, Alessandro Bertuzzi, and Andrea De Gaetano. Mathematical modeling of the glucose–insulin system: A review. *Mathematical biosciences*, 244(2):69–81, 2013.

[389] Athena Makroglou, Jiaxu Li, and Yang Kuang. Mathematical models and software tools for the glucose-insulin regulatory system and diabetes: an overview. *Applied numerical mathematics*, 56(3-4):559–573, 2006.

[390] A Boutayeb and A Chetouani. A critical review of mathematical models and data used in diabetology. *Biomedical engineering online*, 5(1):1–9, 2006.

[391] Franz M Matschinsky, Benjamin Glaser, and Mark A Magnuson. Pancreatic beta-cell glucokinase: closing the gap between theoretical concepts and experimental realities. *Diabetes*, 47(3):307–315, 1998.

[392] Gilberto Velho and Philippe Froguel. Genetic, metabolic and clinical characteristics of maturity onset diabetes of the young. *European journal of endocrinology*, 138(3):233–239, 1998.

[393] Michele Giugliano, Marco Bove, and Massimo Grattarola. Insulin release at the molecular level: metabolic-electrophysiological modeling of the pancreatic beta-cells. *IEEE transactions on biomedical engineering*, 47(5):611–623, 2000.

[394] Carl Jørgen Hedeskov. Mechanism of glucose-induced insulin secretion. *Physiological reviews*, 60(2):442–509, 1980.

[395] Mitsuhisa Komatsu, Masahiro Takei, Hiroaki Ishii, and Yoshihiko Sato. Glucose-stimulated insulin secretion: A newer perspective. *Journal of diabetes investigation*, 4(6):511–516, 2013.

[396] CLAES B Wollheim and GW Sharp. Regulation of insulin release by calcium. *Physiological reviews*, 61(4):914–973, 1981.

[397] C Ammälä, L Eliasson, K Bokvist, O Larsson, FM Ashcroft, and P Rorsman. Exocytosis elicited by action potentials and voltage-clamp calcium currents in individual mouse pancreatic b-cells. *The Journal of physiology*, 472(1):665–688, 1993.

[398] Ishan Ajmera, Maciej Swat, Camille Laibe, Nicolas Le Novere, and Vijayalakshmi Chelliah. The impact of mathematical modeling on the understanding of diabetes and related complications. *CPT: pharmacometrics & systems pharmacology*, 2(7):1–14, 2013.

[399] Gerardo J Félix-Martínez and J Rafael Godínez-Fernández. Mathematical models of electrical activity of the pancreatic β-cell: A physiological review. *Islets*, 6(3):e949195, 2014.

[400] Richard Bertram, Leslie S Satin, and Arthur S Sherman. Closing in on the mechanisms of pulsatile insulin secretion. *Diabetes*, 67(3):351–359, 2018.

[401] Joseph P McKenna, Raghuram Dhumpa, Nikita Mukhitov, Michael G Roper, and Richard Bertram. Glucose oscillations can activate an endogenous oscillator in pancreatic islets. *PLoS computational biology*, 12(10):e1005143, 2016.

[402] Phonindra Nath Das, Suvankar Halder, Nandadulal Bairagi, and Samrat Chatterjee. Delay in atp-dependent calcium inflow may affect insulin secretion from pancreatic beta-cell. *Applied Mathematical Modelling*, 84:202–221, 2020.

[403] Chen-Yu Zhang, György Baffy, Pascale Perret, Stefan Krauss, Odile Peroni, Danica Grujic, Thilo Hagen, Antonio J Vidal-Puig, Olivier Boss, Young-Bum Kim, et al. Uncoupling protein-2 negatively regulates insulin secretion and is a major link between obesity, β cell dysfunction, and type 2 diabetes. *Cell*, 105(6):745–755, 2001.

[404] Xiaoyu Duan, Weijie Sun, Hongwen Sun, and Lianying Zhang. Perfluorooctane sulfonate continual exposure impairs glucose-stimulated insulin secretion via sirt1-induced upregulation of ucp2 expression. *Environmental Pollution*, 278:116840, 2021.

[405] P-J Guillausseau, T Meas, M Virally, M Laloi-Michelin, V Médeau, and J-P Kevorkian. Abnormalities in insulin secretion in type 2 diabetes mellitus. *Diabetes & metabolism*, 34:S43–S48, 2008.

[406] Joseph C Koster, M Alan Permutt, and Colin G Nichols. Diabetes and insulin secretion: the atp-sensitive k+ channel (katp) connection. *Diabetes*, 54(11):3065–3072, 2005.

[407] MICHAEL W Roe, JF Worley 3rd, YOSHIHARIJ Tokuyama, LOUIS H Philipson, JEPPE Sturis, JIPING Tang, IAIN D Dukes, GRAEME I Bell, and KENNETH S Polonsky. Niddm is associated with loss of pancreatic beta-cell l-type ca2+ channel activity. *American Journal of Physiology-Endocrinology and Metabolism*, 270(1):E133–E140, 1996.

[408] Yasunori Iwashima, William Pugh, Alex M Depaoli, Jun Takeda, Susumu Seino, Graeme I Bell, and Kenneth S Polonsky. Expression of calcium channel mrnas in rat pancreatic islets and downregulation after glucose infusion. *Diabetes*, 42(7):948–955, 1993.

[409] GW Sharp. Mechanisms of inhibition of insulin release. *American Journal of Physiology-Cell Physiology*, 271(6):C1781–C1799, 1996.

[410] Shao-Nian Yang and Per-Olof Berggren. The role of voltage-gated calcium channels in pancreatic β-cell physiology and pathophysiology. *Endocrine reviews*, 27(6):621–676, 2006.

[411] Lisa Juntti-Berggren, Olof Larsson, Patrik Rorsman, Carina Ammala, Krister Bokvist, Karin Wahlander, Pierluigi Nicotera, Jeanette Dypbukt, Sten Orrenius, Anders Hallberg, et al. Increased activity of l-type ca2+ channels exposed to serum from patients with type i diabetes. *Science*, 261(5117):86–90, 1993.

[412] Lisa Juntti-Berggren, Essam Refai, Ioulia Appelskog, Mats Andersson, Gabriela Imreh, Nancy Dekki, Sabine Uhles, Lina Yu, William J Griffiths, Sergei Zaitsev, et al. Apolipoprotein ciii promotes ca2+-dependent β cell death in type 1 diabetes. *Proceedings of the National Academy of Sciences*, 101(27):10090–10094, 2004.

[413] Leonid E Fridlyand, Li Ma, and Louis H Philipson. Adenine nucleotide regulation in pancreatic β-cells: modeling of atp/adp-ca2+ interactions. *American Journal of Physiology-Endocrinology and Metabolism*, 289(5):E839–E848, 2005.

[414] Andrea De Gaetano and Ovide Arino. Mathematical modelling of the intravenous glucose tolerance test. *Journal of mathematical biology*, 40(2):136–168, 2000.

[415] Shimon Efrat, Margarita Leiser, Y Jian Wu, David Fusco-DeMane, Obaidullah A Emran, Manju Surana, Thomas L Jetton, Mark A Magnuson, Gordon Weir, and Norman Fleischer. Ribozyme-mediated attenuation of pancreatic beta-cell glucokinase expression in transgenic mice results in impaired glucose-induced insulin secretion. *Proceedings of the National Academy of Sciences*, 91(6):2051–2055, 1994.

[416] EA Davis, A Cuesta-Munoz, M Raoul, C Buettger, I Sweet, M Moates, MA Magnuson, and FM Matschinsky. Mutants of glucokinase cause hypoglycaemia-and hyperglycaemia syndromes and their analysis illuminates fundamental quantitative concepts of glucose homeostasis. *Diabetologia*, 42(10):1175–1186, 1999.

[417] Akinobu Nakamura and Yasuo Terauchi. Present status of clinical deployment of glucokinase activators. *Journal of diabetes investigation*, 6(2):124–132, 2015.

[418] Leonid E Fridlyand and Louis H Philipson. Glucose sensing in the pancreatic beta cell: a computational systems analysis. *Theoretical Biology and Medical Modelling*, 7(1):15, 2010.

[419] Leonid E Fridlyand, Natalia Tamarina, and Louis H Philipson. Modeling of ca2+ flux in pancreatic β-cells: role of the plasma membrane and intracellular stores. *American Journal of Physiology-Endocrinology and Metabolism*, 285(1):E138–E154, 2003.

[420] JG Salway. Metabolism at a glance. 1999.

[421] Teresa Ree Chay. Effects of extracellular calcium on electrical bursting and intracellular and luminal calcium oscillations in insulin secreting pancreatic beta-cells. *Biophysical journal*, 73(3):1673–1688, 1997.

[422] Gérald Houart, Geneviève Dupont, and Albert Goldbeter. Bursting, chaos and birhythmicity originating from self-modulation of the inositol 1, 4, 5-trisphosphate signal in a model for intracellular ca 2+ oscillations. *Bulletin of mathematical biology*, 61(3):507–530, 1999.

[423] Krister Bokvist, Lena Eliasson, C Ammälä, Erik Renström, and Patrik Rorsman. Co-localization of l-type ca2+ channels and insulin-containing secretory granules and its significance for the initiation of exocytosis in mouse pancreatic b-cells. *The EMBO Journal*, 14(1):50–57, 1995.

[424] Kyungreem Han, Hyuk Kang, MY Choi, Jinwoong Kim, and Myung-Shik Lee. Mathematical model of the glucose–insulin regulatory system: From the bursting electrical activity in pancreatic β-cells to the glucose dynamics in the whole body. *Physics Letters A*, 376(45):3150–3157, 2012.

[425] Mitio Nagumo. Über die lage der integralkurven gewöhnlicher differentialgleichungen. *Proceedings of the Physico-Mathematical Society of Japan. 3rd Series*, 24:551–559, 1942.

[426] William T Cefalu. Insulin resistance: cellular and clinical concepts. *Experimental biology and medicine*, 226(1):13–26, 2001.

[427] Barbara B Kahn, Jeffrey S Flier, et al. Obesity and insulin resistance. *The Journal of clinical investigation*, 106(4):473–481, 2000.

[428] American Diabetes Association et al. Screening for diabetes. *Diabetes care*, 25(suppl 1):s21–s24, 2002.

[429] Hironobu Sasaki, Yoshifumi Saisho, Jun Inaishi, Yuusuke Watanabe, Tami Tsuchiya, Masayoshi Makio, Midori Sato, Masaru Nishikawa, Minoru Kitago, Taketo Yamada, et al. Reduced beta cell number rather than size is a major contributor to beta cell loss in type 2 diabetes. *Diabetologia*, pages 1–6, 2021.

[430] KS Polonsky, BD Given, W Pugh, J Licinio-Paixao, JE Thompson, T Karrison, and AH Rubenstein. Calculation of the systemic delivery rate of insulin in normal man. *The Journal of Clinical Endocrinology & Metabolism*, 63(1):113–118, 1986.

[431] N Kaiser, Gil Leibowitz, and Rafael Nesher. Glucotoxicity and β-cell failure in type 2 diabetes mellitus. *Journal of Pediatric Endocrinology and Metabolism*, 16(1):5–22, 2003.

[432] Aleksey V Matveyenko and PC Butler. Relationship between β-cell mass and diabetes onset. *Diabetes, Obesity and Metabolism*, 10:23–31, 2008.

[433] Mark A Atkinson, George S Eisenbarth, and Aaron W Michels. Type 1 diabetes. *The Lancet*, 383(9911):69–82, 2014.

[434] M Löhr and G Klöppel. Residual insulin positivity and pancreatic atrophy in relation to duration of chronic type 1 (insulin-dependent) diabetes mellitus and microangiopathy. *Diabetologia*, 30(10):757–762, 1987.

[435] JJ Meier, A Bhushan, AE Butler, RA Rizza, and PC Butler. Sustained beta cell apoptosis in patients with long-standing type 1 diabetes: indirect evidence for islet regeneration? *Diabetologia*, 48(11):2221–2228, 2005.

[436] Jun Inaishi and Yoshifumi Saisho. Beta-cell mass in obesity and type 2 diabetes, and its relation to pancreas fat: a mini-review. *Nutrients*, 12(12):3846, 2020.

[437] Ananda Basu, Chiara Dalla Man, Rita Basu, Gianna Toffolo, Claudio Cobelli, and Robert A Rizza. Effects of type 2 diabetes on insulin secretion, insulin action, glucose effectiveness, and postprandial glucose metabolism. *Diabetes care*, 32(5):866–872, 2009.

[438] Sally M Blower and Hadi Dowlatabadi. Sensitivity and uncertainty analysis of complex models of disease transmission: an hiv model, as an example. *International Statistical Review/Revue Internationale de Statistique*, pages 229–243, 1994.

[439] Simeone Marino and Denise E Kirschner. A multi-compartment hybrid computational model predicts key roles for dendritic cells in tuberculosis infection. *Computation*, 4(4):39, 2016.

[440] Leszek Szablewski. Glucose homeostasis–mechanism and defects. *Diabetes-Damages and Treatments*, 2, 2011.

[441] Charlotte V BURKE, Carol W BUETTGER, Elizabeth A DAVIS, Steven J MCCLANE, Franz M MATSCHINSKY, and Steven E RAPER. Cell-biological assessment of human glucokinase mutants causing maturity-onset diabetes of the young type 2 (mody-2) or glucokinase-linked hyperinsulinaemia (gk-hi). *Biochemical Journal*, 342(2):345–352, 1999.

[442] R Paul Robertson, Hui-Jian Zhang, Kathryn L Pyzdrowski, Timothy F Walseth, et al. Preservation of insulin mrna levels and insulin secretion in hit cells by avoidance of chronic exposure to high glucose concentrations. *The Journal of clinical investigation*, 90(2):320–325, 1992.

[443] Jamie S Harmon, Roland Stein, and R Paul Robertson. Oxidative stress-mediated, post-translational loss of mafa protein as a contributing mechanism to loss of insulin gene expression in glucotoxic beta cells. *Journal of biological chemistry*, 280(12):11107–11113, 2005.

[444] P Sonksen and J Sonksen. Insulin: understanding its action in health and disease. *British journal of anaesthesia*, 85(1):69–79, 2000.

[445] Steven E Kahn. The importance of the β-cell in the pathogenesis of type 2 diabetes mellitus. *The American journal of medicine*, 108(6):2–8, 2000.

[446] Jennifer A Mayfield. Diagnosis and classification of diabetes mellitus: new criteria. *American family physician*, 58(6):1355, 1998.

[447] Michelle Blanco Lemelman, Lisa Letourneau, and Siri Atma W Greeley. Neonatal diabetes mellitus: an update on diagnosis and management. *Clinics in perinatology*, 45(1):41–59, 2018.

[448] Anna L Gloyn. Glucokinase (gck) mutations in hyper-and hypoglycemia: Maturity-onset diabetes of the young, permanent neonatal diabetes, and hyperinsulinemia of infancy. *Human mutation*, 22(5):353–362, 2003.

[449] David K McCulloch. Initial management of blood glucose in adults with type 2 diabetes mellitus. *UpToDate: UpToDate, Waltham, MA (Accessed July 24, 2016)*, 2016.

[450] S Del Prato, M Aragona, and A Coppelli. Sulfonylureas and hypoglycaemia. *Diabetes, nutrition & metabolism*, 15(6):444–50, 2002.

[451] Kevin SC Hamming, Daniel Soliman, Nicola J Webster, Gavin J Searle, Laura C Matemisz, David A Liknes, Xiao-Qing Dai, Thomas Pulinilkunnil, Michael J Riedel, Jason RB Dyck, et al. Inhibition of β-cell sodium-calcium exchange enhances glucose-dependent elevations in cytoplasmic calcium and insulin secretion. *Diabetes*, 59(7):1686–1693, 2010.

[452] André Herchuelz, Adama Kamagate, Helena Ximenes, and Francoise Van Eylen. Role of na/ca exchange and the plasma membrane ca2+–atpase in β cell function and death. *Annals of the new York Academy of Sciences*, 1099(1):456–467, 2007.

[453] Evrard Nguidjoe, Sophie Sokolow, Serge Bigabwa, Nathalie Pachera, Eva D'Amico, Florent Allagnat, Jean-Marie Vanderwinden, Abdullah Sener, Mario Manto, Marianne

Depreter, et al. Heterozygous inactivation of the na/ca exchanger increases glucose-induced insulin release, β-cell proliferation, and mass. *Diabetes*, 60(8):2076–2085, 2011.

[454] Julien Papin, Francesco Paolo Zummo, Nathalie Pachera, Claudiane Guay, Romano Regazzi, Alessandra K Cardozo, and André Herchuelz. Na+/ca2+ exchanger a druggable target to promote β-cell proliferation and function. *Journal of the Endocrine Society*, 2(7):631–645, 2018.

[455] Nathalie Pachera, Julien Papin, Francesco P Zummo, Jacques Rahier, Jan Mast, Kira Meyerovich, Alessandra K Cardozo, and André Herchuelz. Heterozygous inactivation of plasma membrane ca 2+-atpase in mice increases glucose-induced insulin release and beta cell proliferation, mass and viability. *Diabetologia*, 58(12):2843–2850, 2015.

[456] Leif C Groop, Risto Pelkonen, Saija Koskimies, Gian F Bottazzo, and Deborah Doniach. Secondary failure to treatment with oral antidiabetic agents in non-insulin-dependent diabetes. *Diabetes care*, 9(2):129–133, 1986.

[457] Robert C Turner, Carole A Cull, Valeria Frighi, Rury R Holman, UK Prospective Diabetes Study (UKPDS) Group, UK Prospective Diabetes Study (UKPDS) Group, et al. Glycemic control with diet, sulfonylurea, metformin, or insulin in patients with type 2 diabetes mellitus: progressive requirement for multiple therapies (ukpds 49). *Jama*, 281(21):2005–2012, 1999.

[458] D Pitocco, D Valle, A Rossi, and R Gentilella. Unmet needs among patients with type 2 diabetes and secondary failure to oral anti-diabetic agents. *Journal of endocrinological investigation*, 31(4):371–379, 2008.

[459] Máire E Doyle and Josephine M Egan. Mechanisms of action of glucagon-like peptide 1 in the pancreas. *Pharmacology & therapeutics*, 113(3):546–593, 2007.

[460] Deborah Hinnen. Glucagon-like peptide 1 receptor agonists for type 2 diabetes. *Diabetes Spectrum*, 30(3):202–210, 2017.

[461] Robert A Rizza, Morey W Haymond, Carlos A Verdonk, Lawrence J Mandarino, John M Miles, John E Gerich, et al. Pathogenesis of hypoglycemia in insulinoma patients: suppression of hepatic glucose production by insulin. *Diabetes*, 30(5):377–381, 1981.

[462] Sha Liu, Colleen Croniger, Carmen Arizmendi, Mariko Harada-Shiba, Jianming Ren, Valeria Poli, Richard W Hanson, Jacob E Friedman, et al. Hypoglycemia and impaired hepatic glucose production in mice with a deletion of the c/ebpβ gene. *The Journal of clinical investigation*, 103(2):207–213, 1999.

[463] Gisela Wilcox. Insulin and insulin resistance. *Clinical biochemist reviews*, 26(2):19, 2005.

[464] Yan Yang, Zixin Cai, Zhenhong Pan, Fen Liu, Dandan Li, Yujiao Ji, Jiaxin Zhong, Hairong Luo, Shanbiao Hu, Lei Song, et al. Rheb1 promotes glucose-stimulated insulin secretion in human and mouse β-cells by upregulating glut expression. *Metabolism*, 123:154863, 2021.

[465] Jean-Marc Guettier and Phillip Gorden. Insulin secretion and insulin-producing tumors. *Expert review of endocrinology & metabolism*, 5(2):217–227, 2010.

[466] Jean-Marc Guettier and Phillip Gorden. Hypoglycemia. *Endocrinology and Metabolism Clinics*, 35(4):753–766, 2006.

[467] Donald L Curry, Leslie L Bennett, and Gerold M Grodsky. Dynamics of insulin secretion by the perfused rat pancreas. *Endocrinology*, 83(3):572–584, 1968.

[468] Jean-Claude Henquin, Nobuyoshi Ishiyama, Myriam Nenquin, Magalie A Ravier, and Jean-Christophe Jonas. Signals and pools underlying biphasic insulin secretion. *Diabetes*, 51(suppl_1):S60–S67, 2002.

[469] Zhanxiang Wang and Debbie C Thurmond. Mechanisms of biphasic insulin-granule exocytosis–roles of the cytoskeleton, small gtpases and snare proteins. *Journal of cell science*, 122(7):893–903, 2009.

[470] Jean-Claude Henquin. Triggering and amplifying pathways of regulation of insulin secretion by glucose. *Diabetes*, 49(11):1751–1760, 2000.

[471] Samira Daniel, Mitsuhiko Noda, Susanne G Straub, and GW Sharp. Identification of the docked granule pool responsible for the first phase of glucose-stimulated insulin secretion. *Diabetes*, 48(9):1686–1690, 1999.

[472] Muhmmad Omar-Hmeadi and Olof Idevall-Hagren. Insulin granule biogenesis and exocytosis. *Cellular and Molecular Life Sciences*, 78(5):1957–1970, 2021.

[473] Barton Wicksteed, Cristina Alarcon, Isabelle Briaud, Melissa K Lingohr, and Christopher J Rhodes. Glucose-induced translational control of proinsulin biosynthesis is proportional to preproinsulin mrna levels in islet β-cells but not regulated via a positive feedback of secreted insulin. *Journal of Biological Chemistry*, 278(43):42080–42090, 2003.

[474] Michael Welsh, David A Nielsen, Albert J MacKrell, and Donald F Steiner. Control of insulin gene expression in pancreatic beta-cells and in an insulin-producing cell line, rin-5f cells. ii. regulation of insulin mrna stability. *Journal of Biological Chemistry*, 260(25):13590–13594, 1985.

[475] Kristen E Rohli, Cierra K Boyer, Sandra E Blom, and Samuel B Stephens. Nutrient regulation of pancreatic islet β-cell secretory capacity and insulin production. *Biomolecules*, 12(2):335, 2022.

[476] Abhijit Paul, Phonindra Nath Das, and Samrat Chatterjee. A minimal model of glucose-stimulated insulin secretion process explores factors responsible for the development of type 2 diabetes. *Applied Mathematical Modelling*, 108:408–426, 2022.

[477] Rune V Overgaard, Katarina Jelic, Mats Karlsson, Jan Erik Henriksen, and Henrik Madsen. Mathematical beta cell model for insulin secretion following ivgtt and ogtt. *Annals of biomedical engineering*, 34(8):1343–1354, 2006.

[478] Alessandro Bertuzzi, Serenella Salinari, and Geltrude Mingrone. Insulin granule trafficking in β-cells: mathematical model of glucose-induced insulin secretion. *American Journal of Physiology-Endocrinology and Metabolism*, 293(1):E396–E409, 2007.

[479] Eleonora Grespan, Toni Giorgino, Silva Arslanian, Andrea Natali, Ele Ferrannini, and Andrea Mari. Defective amplifying pathway of β-cell secretory response to glucose in type 2 diabetes: integrated modeling of in vitro and in vivo evidence. *Diabetes*, 67(3):496–506, 2018.

[480] D Melloul, S Marshak, and E Cerasi. Regulation of insulin gene transcription. *Diabetologia*, 45(3):309–326, 2002.

[481] Song-iee Han, Kunio Yasuda, and Kohsuke Kataoka. Atf2 interacts with β-cell-enriched transcription factors, mafa, pdx1, and beta2, and activates insulin gene transcription. *Journal of Biological Chemistry*, 286(12):10449–10456, 2011.

[482] Vincent Poitout, Derek Hagman, Roland Stein, Isabella Artner, R Paul Robertson, and Jamie S Harmon. Regulation of the insulin gene by glucose and fatty acids. *The Journal of nutrition*, 136(4):873–876, 2006.

[483] Michael Weiss, Donald F Steiner, and Louis H Philipson. Insulin biosynthesis, secretion, structure, and structure-activity relationships. 2015.

[484] Garrett Birkhoff and Gian-Carlo Rota. *Ordinary differential equations*. John Wiley & Sons, 1978.

[485] Burak Kutlu, David Burdick, David Baxter, Joanne Rasschaert, Daisy Flamez, Decio L Eizirik, Nils Welsh, Nathan Goodman, and Leroy Hood. Detailed transcriptome atlas of the pancreatic beta cell. *BMC medical genomics*, 2(1):1–11, 2009.

[486] Sebastian Barg, Lena Eliasson, Erik Renstrom, and Patrik Rorsman. A subset of 50 secretory granules in close contact with l-type ca2+ channels accounts for first-phase insulin secretion in mouse β-cells. *Diabetes*, 51(suppl_1):S74–S82, 2002.

[487] Patrik Rorsman and Erik Renström. Insulin granule dynamics in pancreatic beta cells. *Diabetologia*, 46(8):1029–1045, 2003.

[488] Troels Bock, Kirsten Svenstrup, Bente Pakkenberg, and Karsten Buschard. Unbiased estimation of total β-cell number and mean β-cell volume in rodent pancreas. *Apmis*, 107(7-12):791–799, 1999.

[489] Dana Prídavková, Matej Samoš, Roman Kyčina, Katarína Adamicová, Michal Kalman, Margita Belicová, and Marián Mokáň. Insulinoma presenting with postprandial hypoglycemia and a low body mass index: A case report. *World Journal of Clinical Cases*, 8(18):4169, 2020.

[490] Pedro Iglesias and Juan J Díez. Management of endocrine disease: a clinical update on tumor-induced hypoglycemia. *European journal of endocrinology*, 170(4):R147–R157, 2014.

[491] Feng Wang, Margery Herrington, Jörgen Larsson, and Johan Permert. The relationship between diabetes and pancreatic cancer. *Molecular cancer*, 2(1):1–5, 2003.

[492] Christian M Cohrs, Julia K Panzer, Denise M Drotar, Stephen J Enos, Nicole Kipke, Chunguang Chen, Robert Bozsak, Eyke Schöniger, Florian Ehehalt, Marius Distler, et al. Dysfunction of persisting β cells is a key feature of early type 2 diabetes pathogenesis. *Cell reports*, 31(1):107469, 2020.

[493] Yukari Ido Kitamura, Tadahiro Kitamura, Jan-Philipp Kruse, Jeffrey C Raum, Roland Stein, Wei Gu, and Domenico Accili. Foxo1 protects against pancreatic β cell failure through neurod and mafa induction. *Cell metabolism*, 2(3):153–163, 2005.

[494] Melissa F Brereton, Michaela Iberl, Kenju Shimomura, Quan Zhang, Alice E Adriaenssens, Peter Proks, Ioannis I Spiliotis, William Dace, Katia K Mattis, Reshma Ramracheya, et al. Reversible changes in pancreatic islet structure and function produced by elevated blood glucose. *Nature communications*, 5(1):1–11, 2014.

[495] H Siebe Spijker, Heein Song, Johanne H Ellenbroek, Maaike M Roefs, Marten A Engelse, Erik Bos, Abraham J Koster, Ton J Rabelink, Barbara C Hansen, Anne Clark, et al. Loss of β-cell identity occurs in type 2 diabetes and is associated with islet amyloid deposits. *Diabetes*, 64(8):2928–2938, 2015.

[496] Chutima Talchai, Shouhong Xuan, Hua V Lin, Lori Sussel, and Domenico Accili. Pancreatic β cell dedifferentiation as a mechanism of diabetic β cell failure. *Cell*, 150(6):1223–1234, 2012.

[497] Gordon C Weir, Cristina Aguayo-Mazzucato, and Susan Bonner-Weir. β-cell dedifferentiation in diabetes is important, but what is it? *Islets*, 5(5):233–237, 2013.

[498] Sean R Hackett, Vito RT Zanotelli, Wenxin Xu, Jonathan Goya, Junyoung O Park, David H Perlman, Patrick A Gibney, David Botstein, John D Storey, and Joshua D Rabinowitz. Systems-level analysis of mechanisms regulating yeast metabolic flux. *Science*, 354(6311):aaf2786, 2016.

List of publications related to thesis

Published

1. **Paul A**, Anand R, Karmakar SP, Rawat S, Bairagi N, Chatterjee S. "Exploring gene knockout strategies to identify potential drug targets using genome-scale metabolic models". *Scientific Reports*, 11, 213, (2021).

2. **Paul A**, Azhar S, Das PN, Bairagi N, Chatterjee S. "Elucidating the metabolic characteristics of pancreatic β-cells from patients with type 2 diabetes (T2D) using a genome-scale metabolic modeling". *Computers in Biology and Medicine*, 144, 105365, (2022).

3. **Paul A**, Das PN, Chatterjee S. "A minimal model of glucose-stimulated insulin secretion process explores factors responsible for the development of type 2 diabetes". *Applied Mathematical Modelling*, 108, 408-426, (2022).

Communicated

1. Sarmah DT[#], **Paul A**[#], Berry U, Surjit M, Bairagi N, Chatterjee S. "Integrated analysis of metabolic model and protein-protein interaction network captures multilayer perturbations and reveals novel potential targets for NASH". (# Equal Contribution)

2. **Paul A**, Kundu J, Chatterjee S. "A minimal mathematical model to study insulin synthesis and secretion process".

List of Other Publications

Published

1. **Paul A**, Chatterjee S and Bairagi N. "Covid-19 transmission dynamics during the unlock phase and significance of testing". *Journal of Vaccines & Vaccination*, 11(6), 433 (2020).

2. **Paul A**, Kadnur HB, Ray A, Chatterjee S and Wig N. "Seroprevalence and attainment of herd immunity against SARS CoV-2: A modelling study". *Journal of Family Medicine and Primary Care*, 10(11), 4030-4035, (2021).

3. **Paul A**, Chatterjee S and Bairagi N. "Prediction on Covid-19 epidemic for different countries: Focusing on South Asia under various precautionary measures". *medRxiv* (2020).

Communicated

1. Sarmah DT, **Paul A**, Kumar S, Bairagi N, Chatterjee S. "A data-driven multilayer approach for the identification of potential therapeutic targets in non-alcoholic steatohepatitis".

2. Kumar S, Sarmah DT, **Paul A**, Chatterjee S. "Differential co-expression analysis identifies key genes responsible for the aggressiveness of glioblastoma".

Conferences

Poster Presentations

1. **The 106th Indian Science Congress**, January 2019, at Lovely Professional University, Phagwara, Jalandhar. (**Best poster award**)

2. **International conference on Calcium Signaling**, January 2020, at Regional Centre for Biotechnology, Faridabad.